AD NUMBER

AD395708

CLASSIFICATION CHANGES

TO: unclassified

FROM: confidential

LIMITATION CHANGES

TO:

Approved for public release, distribution unlimited

FROM:

Distribution authorized to U.S. Gov't. agencies and their contractors; Administrative/Operational Use; Jan 1969. Other requests shall be referred to AFRPL [RPOR/STINFO], Edwards AFB, CA 93523.

AUTHORITY

Air Force Rocket Propulsion ltr, 15 Mar 1971; Air Force Rocket Propulsion ltr, 5 Feb 1986

[redacted]

[redacted]

[redacted]

[redacted]

[redacted]

[redacted]

[redacted]

[redacted]

PATENT SECRECY NOTICE

[redacted]

[redacted]

"When U. S. Government drawings, specifications, or other data are used for any purpose other than a definitely related Government procurement operation, the Government thereby incurs no responsibility nor any obligation whatsoever, and the fact that the Government may have formulated, furnished, or in any way supplied the said drawings, specifications, or other data, is not to be regarded by implication or otherwise, or in any manner licensing the holder or any other person or corporation, or conveying any rights or permission to manufacture, use, or sell any patented invention that may in any way be related thereto."

This material contains information affecting the national defense of the United States within the meaning of the espionage laws, Title 18, U.S.C., Sec. 793 and 794, the transmission or the revelation of which in any manner to an unauthorized person is prohibited by law.

"In addition to security requirements which must be met, this document is subject to special export controls and each transmittal to foreign governments or foreign nationals may be made only with prior approval of AFRPL (RPOR/STINFO), Edwards, California 93523."

PATENT SECRECY NOTICE

Material in this publication relating to:

LAMINATED CHAMBER COOLING MEANS AND A SLOT TUBE INJECTOR CONCEPT

reveals subject matter contained in U. S. Patent Application Serial No. 319,047 and 725,954 entitled "High Pressure Rocket and Cooling Means" and "Slot Tube Swirler Injector," respectively, which have been placed under Secrecy Orders issued by the Commissioner of Patents. These Secrecy Orders have been modified by a SECURITY REQUIREMENTS PERMIT.

A Secrecy Order prohibits publication or disclosure of the invention, or any material information with respect thereto. It is separate and distinct, and has nothing to do with the classification of Government contracts.

By statute, violation of a Secrecy Order is punishable by a fine not to exceed $10,000 and/or imprisonment for not more than two years.

A SECURITY REQUIREMENTS PERMIT authorizes disclosure of the invention or any material information with respect thereto, to the extent set forth by the security requirements of the Government contract which imposes the highest security classification on the subject matter of the application, except that export is prohibited.

Disclosure of these inventions or any material information with respect thereto is prohibited except by written consent of the Commissioner of Patents or as authorized by the permits.

The foregoing does not in any way lessen responsibility for the security of the subject matter as imposed by any Government contract or the provisions of the existing laws relating to espionage and national security.

CONFIDENTIAL

(UNCLASSIFIED TITLE)

AIR FORCE REUSABLE ROCKET ENGINE PROGRAM

XLR129-P-1

FIRST ANNUAL REPORT

CONFIDENTIAL

SECTION V

TASK 1.2 - COMPONENT DEVELOPMENT

A. PREBURNER INJECTOR

SECTION V
TASK 1.2 - COMPONENT DEVELOPMENT

A. PREBURNER INJECTOR

1. Introduction

(C) The preburner injector uses pump-fed propellants that are metered at a maximum mixture ratio of 1.24 at an engine mixture ratio of 7 and 100% engine thrust. These propellants are burned in the transition case duct. The hot gases are divided and flowed through the oxidizer and fuel pump turbines prior to being discharged into the main burner chamber through the main burner injector. This propellant flow is illustrated in Figure 320. Because the preburner gases are used to drive the fuel and oxidizer pump turbines, the design goal temperature profile was 150°R peak-to-average to permit operating the pump turbines at the maximum allowable average temperature. The preburner injector design was based on the requirements to provide stable and efficient combustion with this temperature profile over the 20% to 100% operating range.

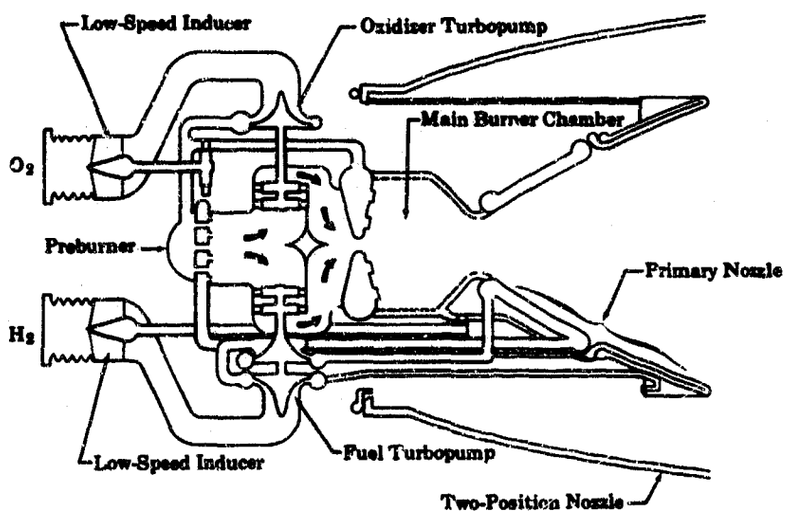

(U) Figure 320. Propellant Flow Schematic FD 25389

2. Summary, Conclusions and Recommendations

(U) The design of the preburner injector for the XLR129-P-1 demonstrator engine was completed. A dual-orifice tangential-entry oxidizer, fixed area fuel injector was selected. Selection of this injector concept was based on test results obtained under the supporting data and analysis subtask discussed in Section IV, Paragraph A.

3. Design Analysis

(U) The design of the preburner injector was based on the data obtained during testing under the supporting data and analysis subtask and during Phase I (Contract AF04(611)-11401). Design studies were conducted on fabrication techniques that would simplify the fabrication and part replacement for the demonstrator engine injector. A removable metering section of the oxidizer element was evaluated as a method for easy matching of the oxidizer flow to the fuel flow at each element location. A removable oxidizer plate between the primary and secondary oxidizer cavities showed potential in aiding fabrication techniques. Two methods of attachment were evaluated. Figure 321 illustrates a one-piece oxidizer element that uses a nut to carry the oxidizer plate pressure loads. Figure 322 illustrates a two-piece design that has a removable cap nut to facilitate oxidizer plate removal. The cap nut has the secondary metering slot machined in it. Because this method would have an axial as well as radial mismatch between the oxidizer element and cap nut, discontinuity tests were conducted to evaluate the effect of this mismatch. These tests indicated that minor mismatch does not adversely affect the stability of the gas core or cone angle. Both configurations required removable seals between the secondary and primary cavities in 253 locations to prevent leakage around the threads. A positive seal would be difficult to attain. A cost analysis of the two configurations indicated both would be more expensive than the one-piece element injector design. Because of the reduced cost and simplicity of design, it was decided to incorporate the brazed one-piece element design in the demonstrator engine preburner injector.

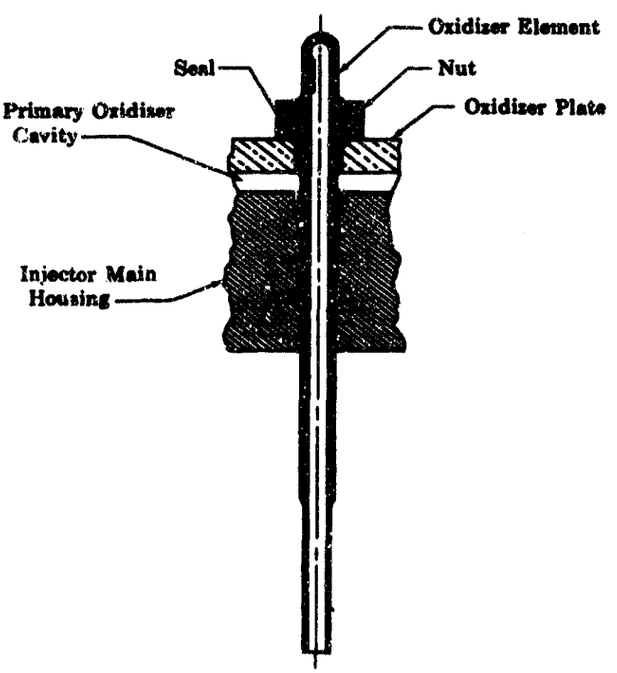

(U) Figure 321. Nut Retained One-Piece Oxidizer Element FD 25382

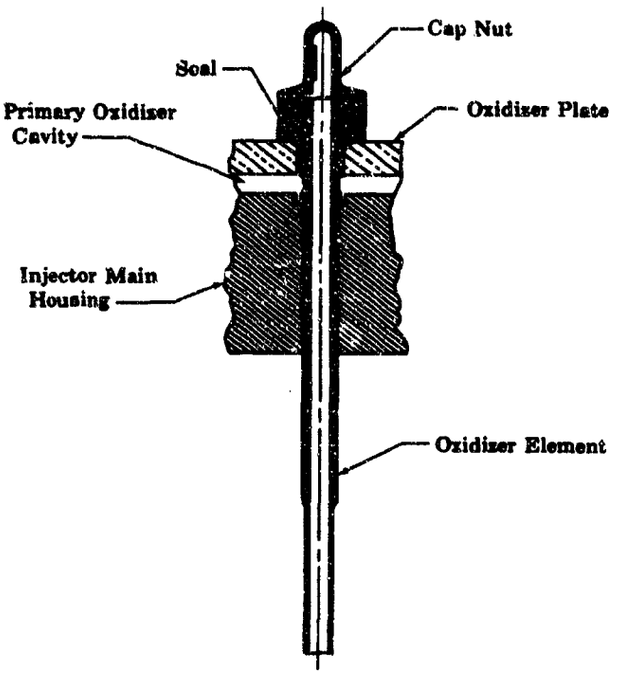

(U) Figure 322. Cap Nut Retained Two-Piece Oxidizer Element FD 25383

(U) Investment casting and diffusion bonding techniques were discussed with vendors as a possible method of fabricating the preburner injector. The oxidizer elements could be cast as an integral part of the oxidizer plate, thereby, providing a diffusion bond joint. However, controlling the element radial location tolerance and the possible collapsing of the orifice holes during casting shrinkage would require extensive development. The caustic contaminates used in removing casting cores necessitate extensive cleaning to eliminate oxidizer incompatibility after the cleaning cycle. This technique was dropped from consideration.

(U) Vendor experience in investment casting the support ribs to the Rigimesh faceplate is limited. Sample castings have completely filled the pores in the Rigimesh material. Extensive development with investment pour temperatures may result in an acceptable method, however, the present state-of-the-art does not include integral casting of ribs to Rigimesh. As a result of the development required, investment casting was not used in the demonstrator engine preburner injector.

(U) Design studies were conducted in an effort to obtain a removable porous faceplate. One method used a porous faceplate supported by a grating-type ribbed section shown in Figure 323. It was necessary, however, to increase the fuel flow cavity area, which increased the overall height of the injector as well as the weight. To reduce the weight of the support system, a honeycomb was considered that had a porous faceplate with a perforated plate on the upstream side. This method required

thicker honeycomb, for the required cell size, than can be produced with present tooling. This method has the same disadvantages as the grate-type ribbed section supports. The design study indicated that this type faceplate support was inferior to the support used for the supporting data and analysis faceplate in which tangs on the faceplate were brazed to the oxidizer elements. Experimentation revealed that the faceplate of the supporting data and analysis preburner injector could be unbrazed without damaging the oxidizer elements. A new faceplate could be readily brazed to the injector with no foreseeable problems. Because the faceplate can be successfully unbrazed, the brazed support was used in the preburner injector design.

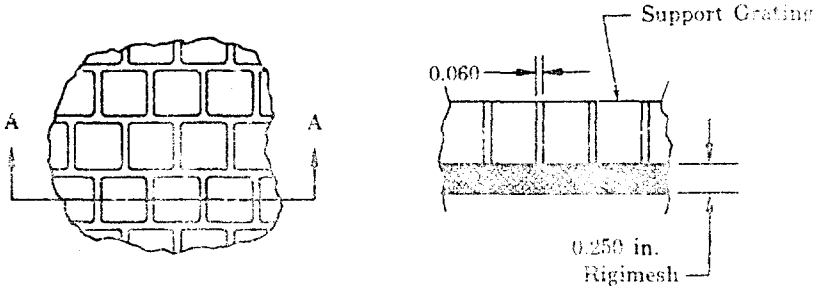

(U) Figure 323. Faceplate Support Grating Concept FD 25384

(U) Local burning on the injector faceplate in the area where the oxidizer elements are brazed to the three tangs was observed during tests with the supporting data and analysis preburner injector. This burning was apparently caused by the phenomena of fuel flow separation around the tangs and the flow remaining separated past the faceplate. This creates a low static pressure downstream of the tang and oxidizer is drawn across the faceplate in this area causing faceplate burning. A design study indicated that for a tang width of 0.040 inch, a fuel slot tang recess of 0.155 to 0.165 inch is required to eliminate the low pressure condition by allowing the flow to rejoin prior to reaching the combustion chamber.

(U) The revised tang recess resulted in a reduction of braze area. To validate the ability of the reduced area braze joint to carry the differential pressure load of the faceplate, samples of the oxidizer element to Rigimesh braze were fabricated and tested. The worst condition tested was one tang completely brazed and the other two only partially brazed. This braze sample failed in shear with a load of 338 pounds. The calculated maximum load was 208 pounds at the outer element.

(U) A transition case with an integral preburner injector fuel manifold was analyzed to determine the feasibility of a reduction of size and weight. The design studied is illustrated in Figure 324. This design was determined unsatisfactory because of the inability to install the transition case liner from the injector side. Complex machining would also

be required if the fuel manifold was designed as an integral part of the transition case. The demonstrator engine preburner injector was designed as a separate removable part independent of the transition case, which will permit the inner liner to be removed from the injector side of the transition case.

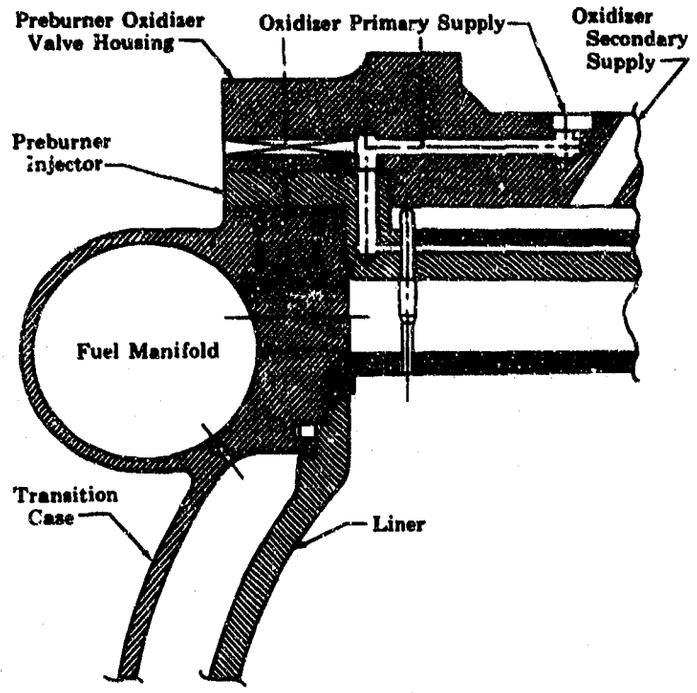

(U) Figure 324. Transition Case Concept With Integral Injector Fuel Manifold FD 25385

4. Injector Design

(U) The XLR129-P-1 demonstrator engine preburner injector design is a dual-orifice, tangential-entry oxidizer and fixed area fuel concept. Data accumulated during Phase I (Contract AF04(611)-11401), the supporting data and analysis task, and analytical design investigations were used as the basis for this design. A cross section of the demonstrator engine preburner injector is shown in Figure 325.

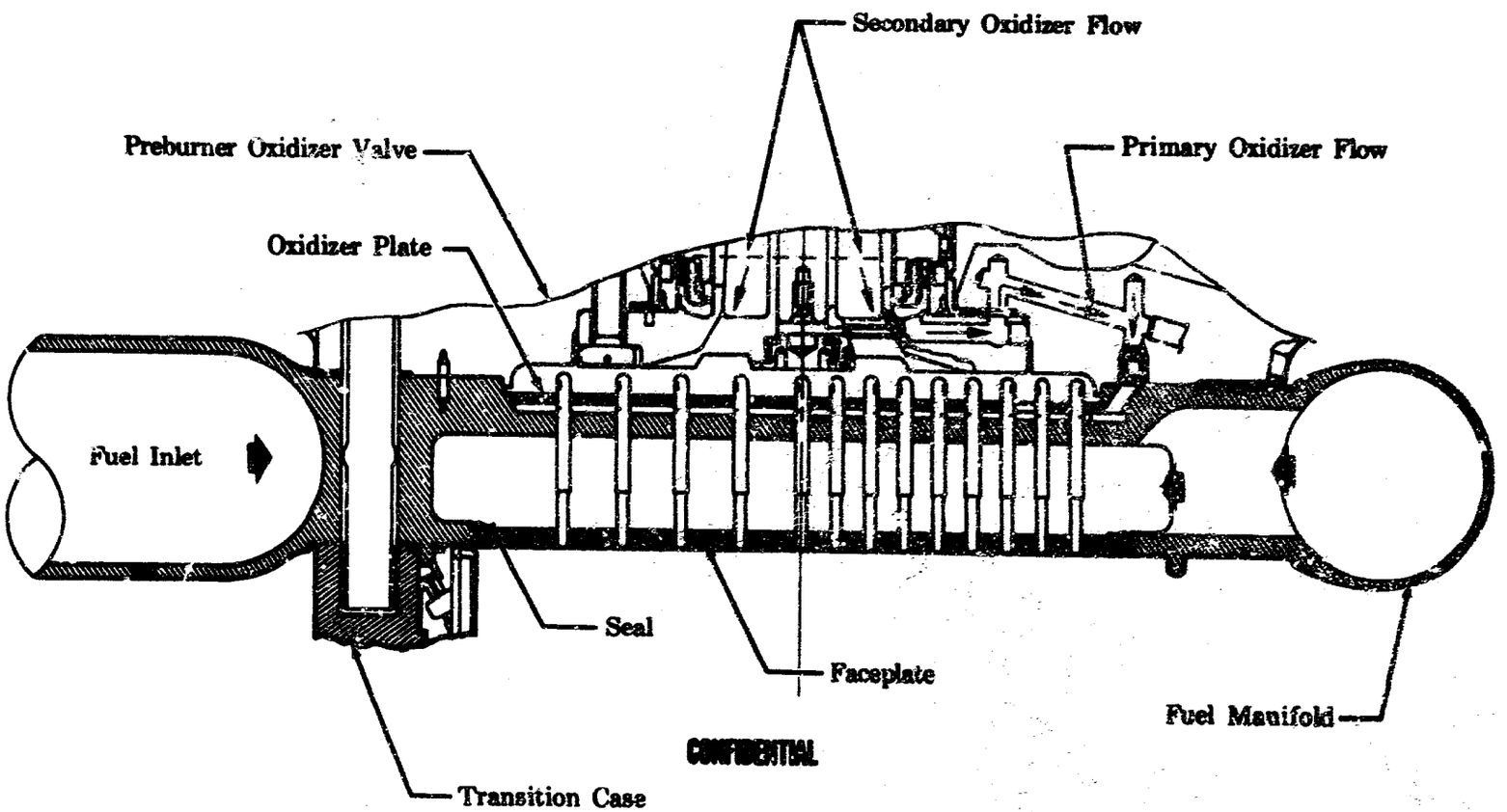

(U) Figure 325. XLR129-P-1 Demonstrator Engine Preburner Injector

FDC 25386

(C) The preburner injector incorporates 253 oxidizer elements arranged in a hexagonal pattern as shown in Figure 326. The oxidizer elements are 0.124-inch inside diameter and have flow entries machined tangentially to the tube ID. The secondary entry is a rectangular slot 0.167 in. by 0.020 in. and the primary entry is a 0.015-inch diameter hole. Both clockwise and counterclockwise rotation induced by the tangential entry are used. The location of the counterclockwise rotating elements is also shown in Figure 326. The element has an A_s/A_p ratio of 0.555 and L/D of 17.3. Each element has an integral collar that rests against the injector main housing for axial positioning prior to brazing the elements to the oxidizer plate.

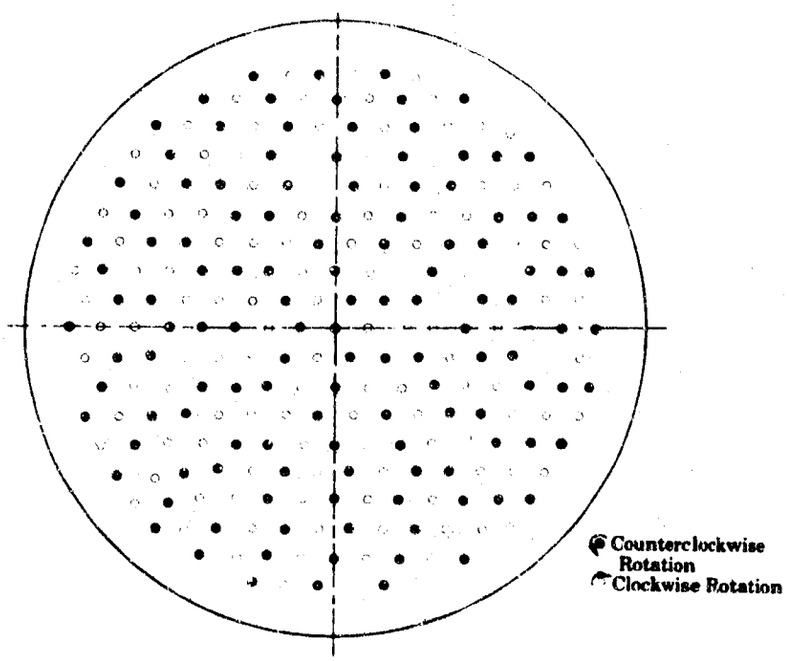

(U) Figure 326. Preburner Injector Face Pattern FD 25387A

(C) An analytical investigation of the combustion instability encountered at the 20% thrust level during the supporting data and analysis tests indicated that the large secondary oxidizer volume contributed significantly to this instability. The secondary oxidizer volume, which includes all the volume downstream of the shutoff at the preburner oxidizer valve and upstream of the orifices on the oxidizer elements, is 27.11 in^3 for the demonstrator engine preburner injector. This is 53.5% of the calculated volume of the supporting data and analysis injector. The primary oxidizer volume is 7.74 in^3, which is 70.5% of the calculated volume of the supporting data and analysis injector. This reduction of the primary and secondary oxidizer volumes will relieve the combustion instability that existed during the supporting data and analysis tests by decreasing the time constant of these cavities.

(C) The secondary oxidizer flow is supplied from the preburner oxidizer valve through three holes in the preburner oxidizer valve housing as shown in Figure 327. The predicted pressure loss is 200 psi at the 100% mixture ratio of 7 flow conditions. The primary oxidizer flow is supplied from the preburner oxidizer valve through six drilled passages in the preburner oxidizer valve housing and the outside diameter of the injector main housing as shown in Figure 325. By routing the primary flow radially inward, a more uniform pressure will be maintained in the primary manifold. A pressure tap is incorporated in the injector main housing to permit measuring the primary cavity pressure during test. A pressure tap is incorporated in the preburner oxidizer valve housing to permit measuring the secondary cavity pressure.

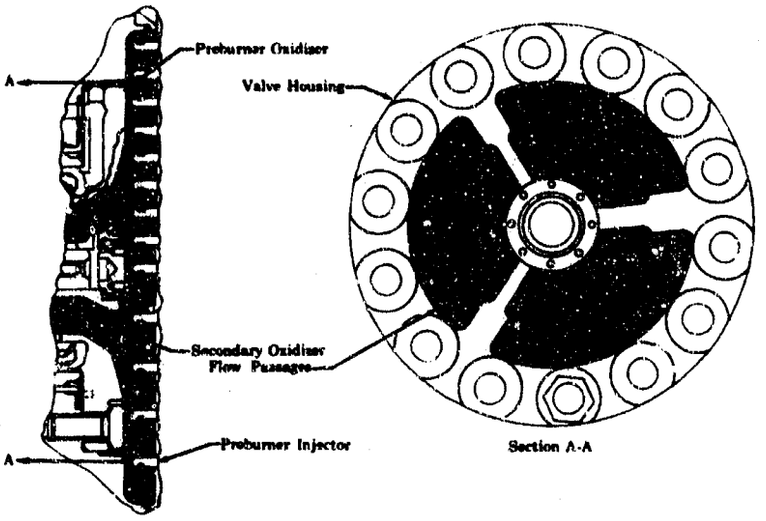

(U) Figure 327. Secondary Oxidizer Flow Passages FD 25388

(U) Fuel flow is supplied to the preburner injector through one inlet into the fuel manifold and is routed around the injector in a 2.84-inch diameter manifold. The fuel is uniformly distributed from this manifold into the fuel cavity through 28 passages. Instrumentation bosses were included in the fuel manifold to measure the fuel manifold pressure and temperature. The fuel manifold inlet flange is designed for 0.002-inch flange defection at the seal location with maximum applied pressure loads and a 5000 in.-lb external bending moment. The external bending moment was assumed to account for plumbing loads.

(C) The porous preburner injector faceplate is fabricated from Rigimesh. The porosity is 40 scfm/ft^2 of air with a ΔP of 2 psi at ambient temperature. The Rigimesh faceplate contains the fixed area fuel annuli, which are centered circumferentially to each oxidizer element by three tangs. The fuel annuli provide a fuel injection area of 4.53 in^2 that creates a 200 psi fuel pressure drop. The faceplate support is provided by brazing the positioning tangs to the oxidizer elements. At the outer circumference of the injector faceplate, a spring seal is provided to prevent fuel

leakage. This seal accounts for 0.003-inch axial deflection because of axial shrinkage of the oxidizer nozzle relative to the main housing when the oxidizer lead signal is initiated. The seal is also capable of allowing a maximum radial shrinkage of 0.011 inch because of instantaneous fuel cooling of the porous faceplate relative to the main housing.

(C) An analysis was conducted to determine if a thermal low cycle fatigue (LCF) life problem could exist in the preburner injector Rigimesh faceplate. This analysis showed that no plastic strain existed for the worst case and, therefore, the Rigimesh is not limited in thermal low cycle fatigue life. In addition to the investigation of the actual worst case possible, it was assumed that a thermal gradient was imposed on the Rigimesh that created plastic strain. It was determined that the allowable temperature gradient was 880 degrees for 300 cycles plastic strain life within the temperature range of 130°R to 1460°R.

(U) The preburner igniter is installed in the transition case just downstream of the preburner injector face. Design of the preburner igniter has not been initiated pending development of an analytical start transient model. Prior to initiation of the hardware design it is necessary to determine the igniter transient mixture ratio, which will set the required propellant flow rate for preburner ignition as well as the coolant flow rate required to ensure hardware durability. The igniter propellant flow rate is the information required to determine the physical size of the igniter.

(U) To permit the design of the transition case without the igniter design, it was assumed that the preburner igniter shape would be basically as shown in Figure 328. Provisions are allowed in the transition case design to permit insertion of the preburner igniter.

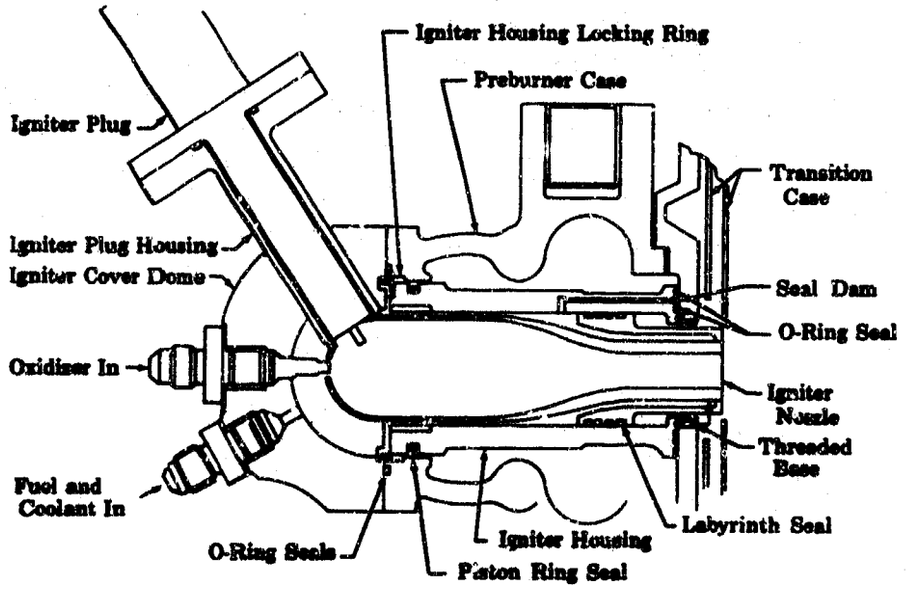

(U) Figure 328. XLR129-P-1 Preburner Igniter FD 25414

B. MAIN BURNER INJECTOR

B. MAIN BURNER INJECTOR

1. Introduction

(U) A design study was conducted on the main burner injector to select the best design concept for the demonstrator engine. To ease fabrication difficulties and improve repairability, prime consideration was given to a multipiece injector design. It was proposed that the injector be built from pie-shaped segments or from individual spraybars brazed or welded into an oxidizer manifold. It was also proposed that an investment cast injector, with the oxidizer injection elements simultaneously diffusion bonded in place, be considered. Consideration was given to fuel faceplate support structure, structure-to-Rigimesh attachment, and faceplate assembly retention. A main burner igniter design study was conducted to analyze various concepts for integrating the main burner igniter into the engine transition case and main burner injector. This study included methods of adapting the igniter fabricated during Phase I (Contract AF04(611)-11401) as well as new concepts that could reduce the complexity of the igniter system.

2. Summary, Conclusions, and Recommendations

(U) 1. Design concepts using the single tapered tube spraybar with an increased flow area are superior in most respects to all other concepts, particularly in weight. This is the concept selected for the demonstrator engine main burner injector.

(U) 2. It was concluded that a straight single tube spraybar, which could either be cast or machined from a forging, is desirable. This type of spraybar is slightly heavier than an angled type of single tube spraybar design. A typical design is shown in Figure 329.

(U) 3. Casting the main burner injector in one single piece is presently beyond the state-of-the-art.

(U) 4. Diffusion bonding the oxidizer injector elements into the cast spraybars is not impractical; however, considerable development would be required.

(U) 5. Pie-shaped segmented construction has the disadvantage of weld shrinkage during assembly that can affect the location of the elements.

(U) 6. Diffusion bonding, during the casting process, of the Rigimesh face support structure is not impractical but development of the process is required.

(U) 7. A one-piece, thick, self-supporting Rigimesh faceplate could be designed if material properties were known.

(U) 8. A fuel faceplate structure to transmit pressure load to the chamber shell during operation is desirable. Retention during assembly can be accomplished with simple non-load-carrying retainers.

(U) 9. The existing Phase I (Contract AF04(611)-11401) igniter hardware cannot be used in the demonstrator engine transition case and injector without modification. The most desirable location to mount the igniter is above the ring connecting the main sphere to the lower sphere. Externally mounted igniter chambers reduce the complexity of the propellant supply probe and spark igniter.

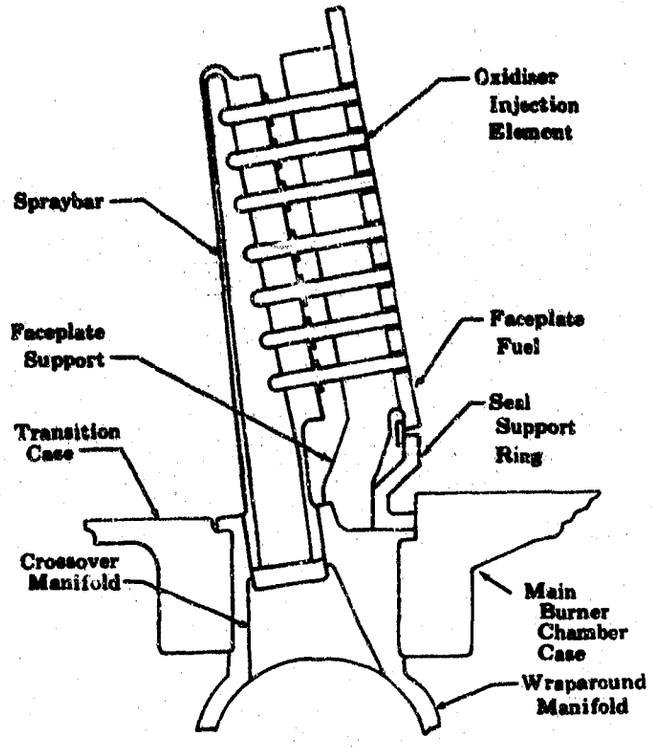

(U) Figure 329. Typical Main Burner Injector Cross Section FD 25360

(U) Two methods of arranging the radial oxidizer manifold area inside the spraybar were studied. One method, shown in Figures 330 through 336, has the radial manifold area composed of numerous small passages stacked axially on top of one another inside the spraybar. The small radial passages are interconnected through internal crossover passages. The stacked radial manifold concept creates a spraybar that is thick in the axial direction but thin in the injector circumferential direction. The distance between the thin spraybars allow enough flow area for the hot gases from the preburner. For the hot gas (fuel) flow area to increase, it requires that the spraybar radial area be made up of smaller diameter, more numerous flow passages, which creates a thicker injector in the axial direction. A thicker injector rapidly increases the weight. The second method of arranging the radial oxidizer manifold inside the spraybar, shown in Figures 337 through 340, consists of forming the total radial flow area required for one spraybar into a single hole. The single hole is tapered to reduce the flow area as the radial oxygen flow rate decreases because of oxygen being discharged through oxidizer elements further upstream. Tapering the radial supply hole allows the outside of the spraybar to be tapered, which increases hot gas flow area and reduces weight of the spraybar. The single hole spraybars can be staggered in two axial planes in the injector housing, which allows a further increase in hot gas flow area around and between the spraybars. The single hole staggered spraybar injector assembly forms the thinnest injector in the axial direction, and therefore, the lightest weight.

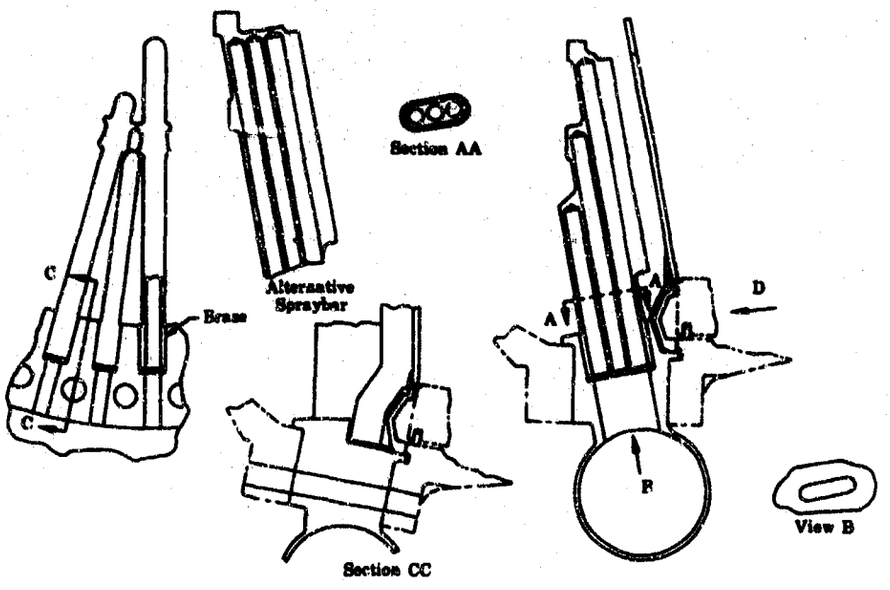

(U) Figure 330. Main Burner Injector Concept No. 1 FD 25361

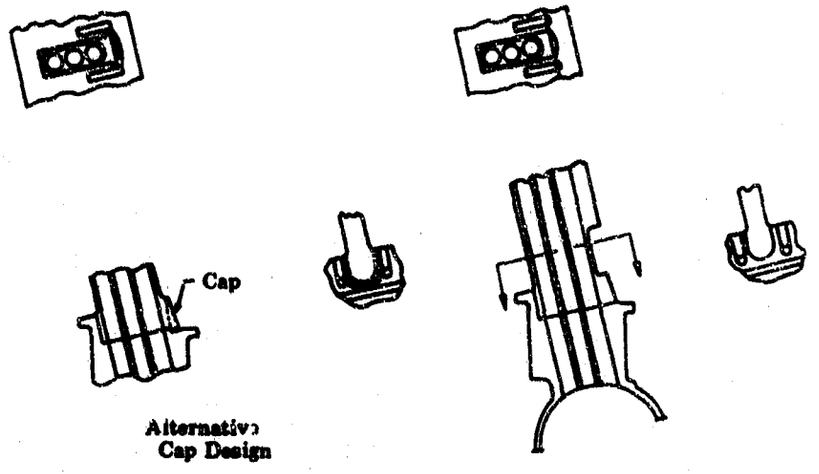

(U) Figure 331. Main Burner Injector Concept No. 2 FD 25362

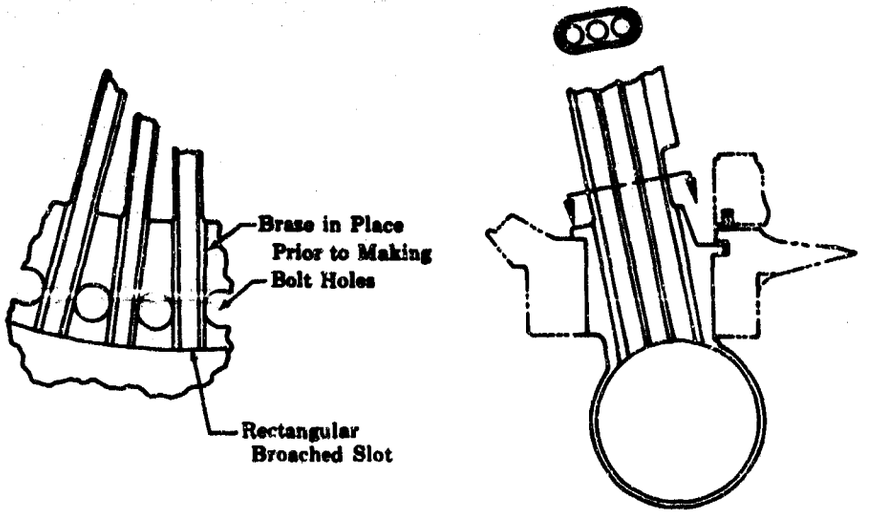

(U) Figure 332. Main Burner Injector Concept No. 3 FD 25363

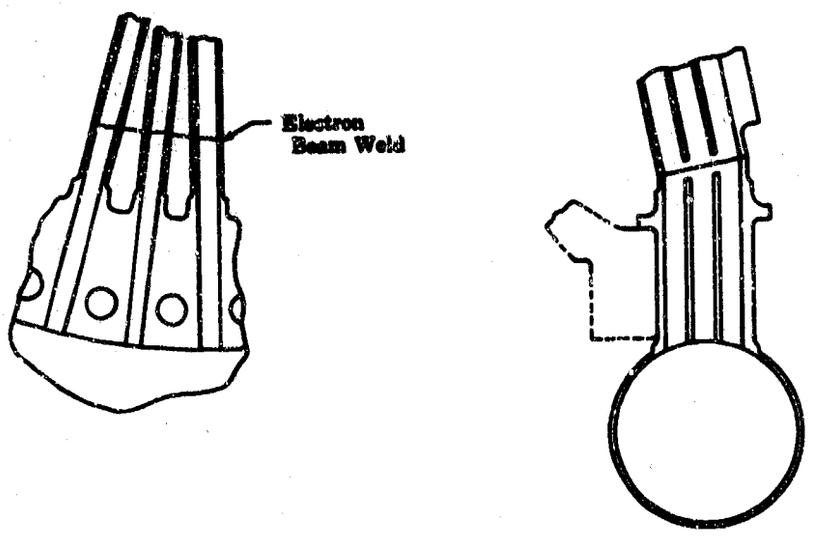

(U) Figure 333. Main Burner Injector Concept No. 4 FD 25364

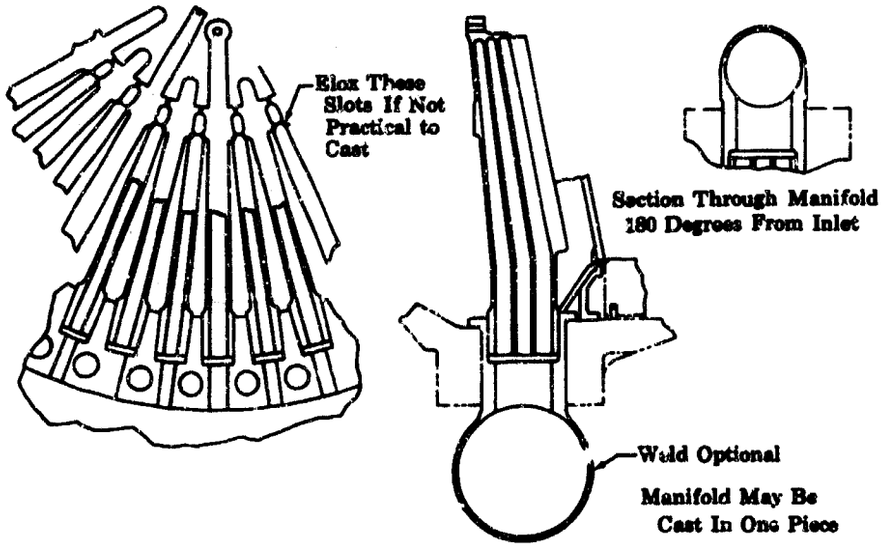

(U) Figure 334. Main Burner Injector Concept No. 5 FD 25365

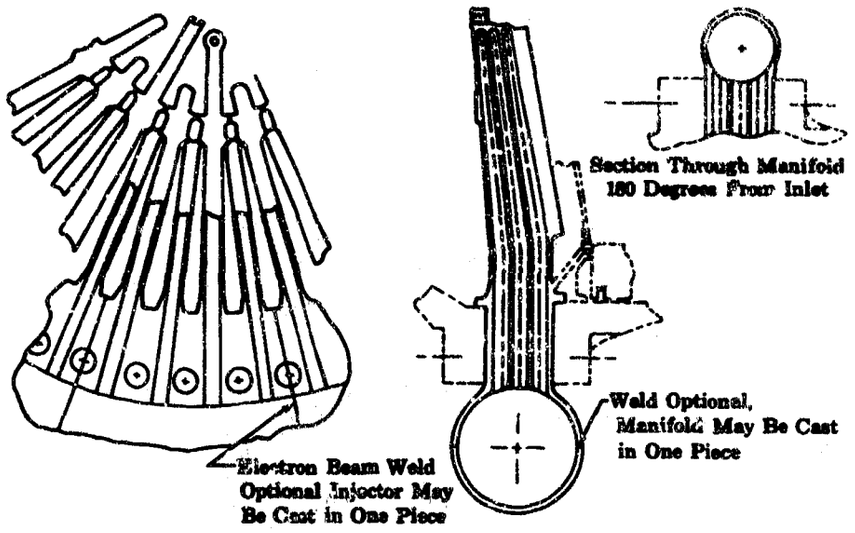

(U) Figure 335. Main Burner Injector Concept No. 6 FD 25366

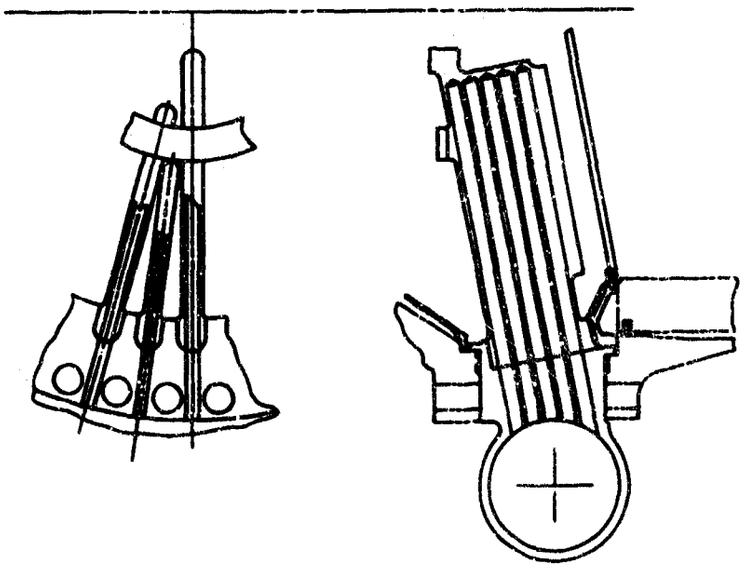

(U) Figure 336. Main Burner Injector Concept No. 11 FD 25371

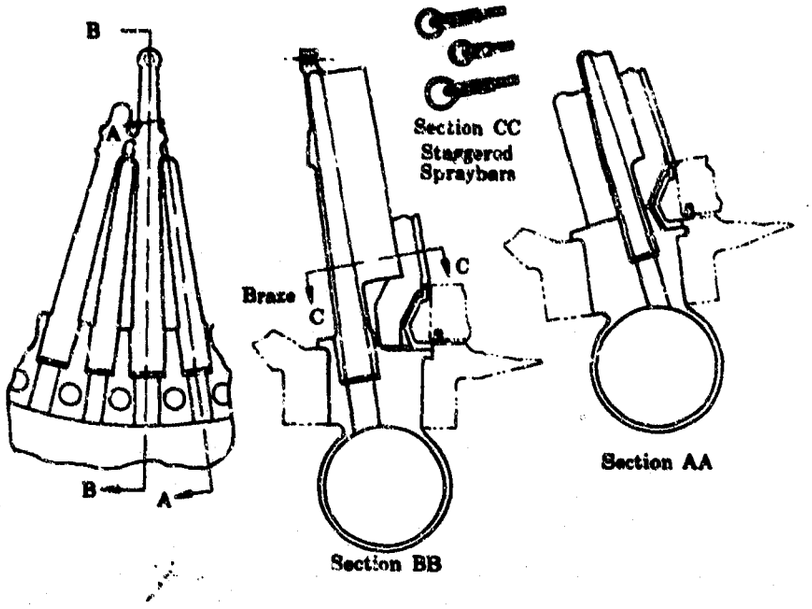

(U) Figure 337. Main Burner Injector Concept No. 7 FD 25367

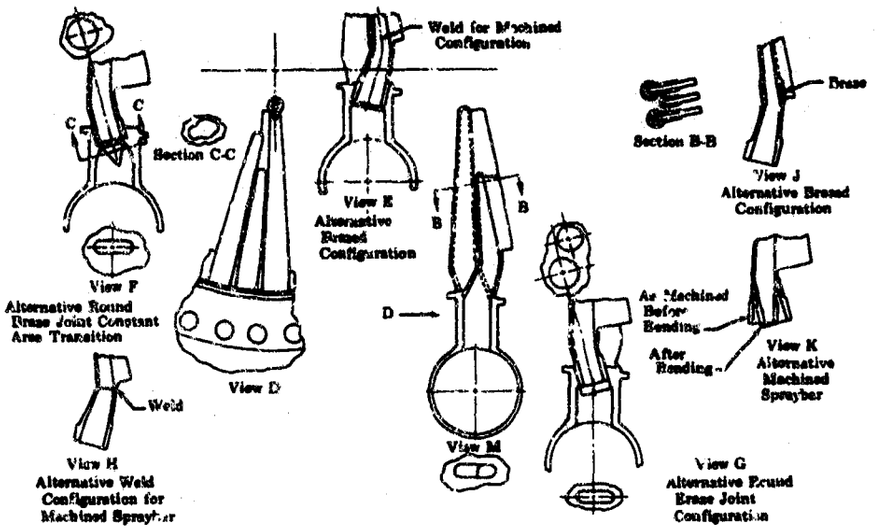

(U) Figure 338. Main Burner Injector Concept No. 9 FD 25369

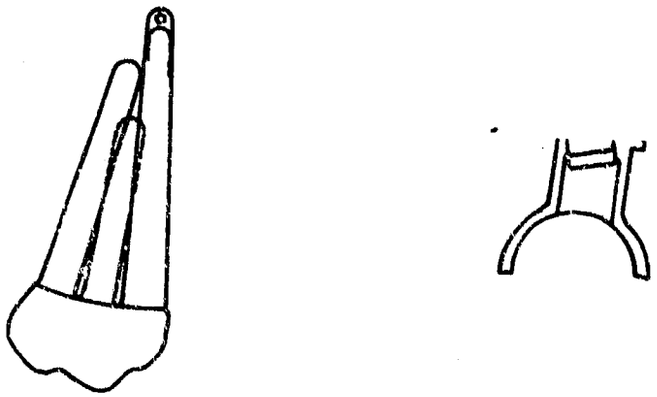

(U) Figure 339. Main Burner Injector Concept No. 10 FD 25370

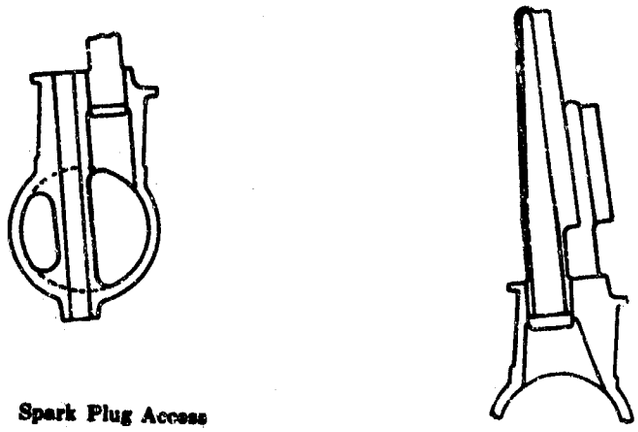

(U) Figure 340. Main Burner Injector Concept No. 15 FD 25375

(U) Fabrication by casting and machining were considered for the individual spraybars. The cast configurations shown in Figures 334 and 335 have a dog-legged radial flow passage which allows the flow passage to be perpendicular to the engine axis at the bolt flange section. This allows the injector to have the smallest axial thickness possible for any particular radial flow area arrangement. The machined fabrication method restricts the radial flow passages to straight cuts, as opposed to angled passages, or to assembling at an angle one or more straight cuts. The machined configurations shown in Figures 330 through 333, 336, 337, 340, and 341 are all applicable to casting techniques but the cast configurations shown in Figures 334, 335, and 339 are not capable of being machined. Figure 338 shows a basic cast design in views M, D, and F with the other views showing ideas of how to attain the angled radial flow passage and still machine the spraybar.

(U) Three methods of making an injector assembly were considered. One by casting the injector in one piece or in the second, by casting large pie-shaped segments and welding the segments together. Both of these

schemes are shown in figure 335. Although casting the injector assembly is within the state-of-the-art, it is not without problems of core removal, core positioning, and tooling. It was concluded in discussion with casting vendors that the limited number of injectors presently to be purchased, it would be uneconomical to attempt fabrication of an injector assembly by casting at this point. The third method of forming an injector assembly is by brazing or welding individual cast or machined spraybars into a main injector housing. These schemes are presented in Figures 328 through 334, 336, 337, 339, and 340. Because of weld shrinkage problems, the welded assemblies do not appear as attractive as the brazed assemblies. From a braze standpoint it is better to braze a round joint than an oblong joint. All single tube spraybars form round joints and all stacked hole spraybars form oblong joints.

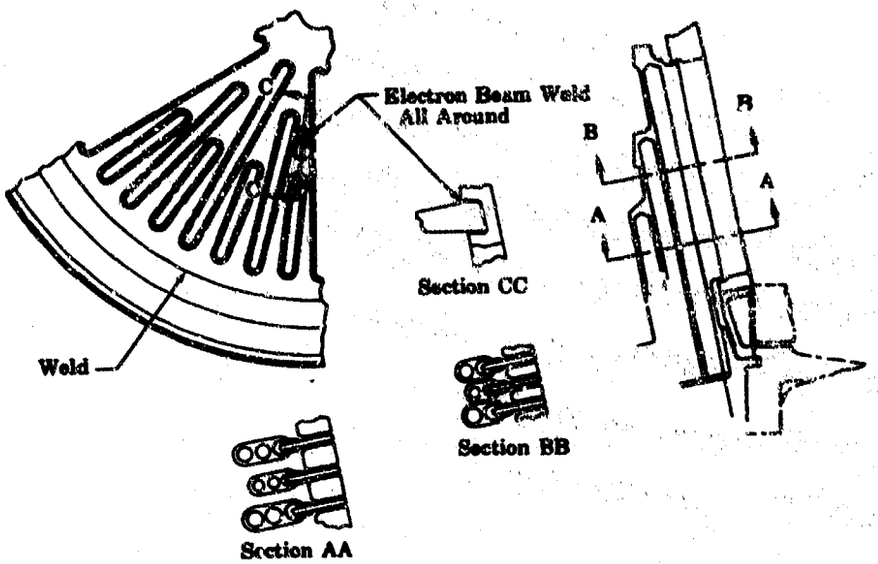

(U) Figure 341. Main Burner Injector Concept No. 14 FD 25374

(U) Two methods of attaching the oxidizer elements into the spraybars were considered. The first method was to support the elements in the core used for forming the radial flow area in a cast spraybar and subsequently form a diffusion bond between the element and spraybar during the casting process. Some work has been done on this type bonding by casting vendors, but it is presently considered outside the state-of-the-art. The second method of attaching the elements in the spraybar is with a furnace braze joint. This method was used on the Phase I (Contract AF04(611)-11401) injector assemblies, and is adaptable to either a cast or machined spraybar.

(U) Several methods of transmitting the fuel faceplate load into the main burner chamber shell are shown in Figure 342. This scheme eliminates the need for 48 bolts and a bolt head retainer, used to transmit the faceplate load back into the injector housing in the Phase I (Contract AF04(611)-11401) design.

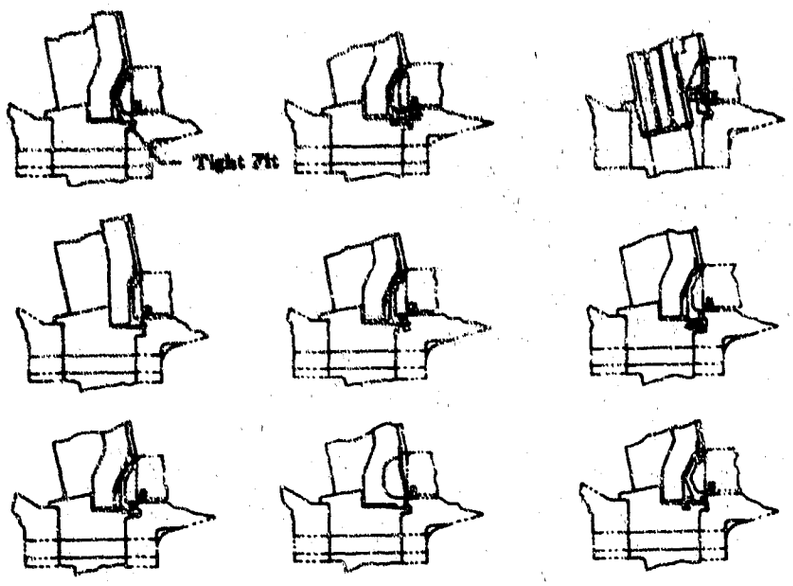

(U) Figure 342. Main Burner Injector Concept No. 13 FD 25373

3. Description of Design Concepts

(U) A typical main burner injector design is shown in Figure 329. The design concepts studied are discussed in the following paragraphs.

a. Concept No. 1

(U) This concept, which is shown in Figure 330, represents a stacked supply tube spraybar design with staggered supply hole depths. An alternative spraybar, with full length supply holes, was also considered. The faceplate support ring is similar to the design tested during Phase I (Contract AF04(611)-11401), except that the seal support ring is trapped between the faceplate support and main burner chamber instead of being bolted to the faceplate support. This injector concept has individual spraybars that are inserted and brazed in slots in the crossover manifold. Oxidizer is supplied from the wraparound outer oxidizer manifold through the crossover manifold to the spraybars. The major part of the injector structure and weight is the crossover manifold, which is a one-piece casting or machined forging. The tie bolts are located between the oxidizer supply holes in the crossover manifold. The straight-side, constant-diameter, stacked supply tube spraybars used in this concept are more suitable for machining from a forging rather than final form casting. Casting this spraybar design would present core support and subsequent core removal problems that would not be present in the single tube design.

b. Concept No. 2

(U) This configuration is shown in Figure 331. The spraybars for this concept are inserted in an axial direction instead of a radial direction. The axial direction of spraybar assembly permits an individual spraybar to be removed from the assembly for repair purposes. The radial direction of spraybar assembly requires that long and medium spraybar be removed in order to remove a short spraybar for repair. An alternative spraybar concept is shown that has a cap on the spraybar.

c. Concept No. 3

(U) Concept No. 3 is shown in Figure 332. This concept has the braze slot for the spraybar extending with constant geometry through the entire crossover manifold, which permits the slot to be broached. Broaching allows lower cost close tolerance control for braze fits at the braze slot.

d. Concept No. 4

(U) This concept, which is shown in Figure 333, has the spraybars welded in place instead of brazed. Welding permits the machined spraybars to be angled, which reduces the flange-to-flange thickness of the crossover manifold. This idea eliminates the need for machining braze slots in the crossover manifold housing. Because the spraybar would be in completely finished form with oxidizer elements brazed in place at the time the weld joint would be made, positioning of the spraybar to allow for weld shrinkage becomes critical.

e. Concept No. 5

(U) This concept, which is shown in Figure 334, represents a multipiece design in which both the spraybars and the manifold are cast. The spraybar stacked supply holes are tapered to allow more hot gas flow area. The spraybars are angled to reduce the flange-to-flange thickness. The combination of these features create the lightest stacked tube design. This design is not suitable for machining from a forging because of the angled spraybar and the tapered stacked tube. This concept has a tapered constant velocity manifold.

f. Concept No. 6

(U) This concept, which is shown in Figure 335, represents a cast injector, which could be cast in one piece or in pie-shaped segments. Casting the entire injector has all the advantages of concept No. 5 plus the advantage of eliminating a braze joint between the spraybar and manifold. But the disadvantages of casting include (1) positioning of a large number of cores to form the flow passages, (2) subsequent removal of the cores, and (3) cleaning the core removal solution from the part to comply with the LO_2 clean requirement.

g. Concept No. 7

(U) This concept, which is shown in Figure 337, has a single supply tube spraybar design. The spraybars are staggered to increase hot gas flow area. The tapered spraybars combined with staggered crossover supply holes provides the highest possible hot gas flow area. The single supply tube is kept straight in this concept to allow the spraybar to be manufactured by conventional machining techniques.

h. Concept No. 8

(U) This concept, which is shown in Figure 343, illustrates a faceplate support system in which the support bolts are secured to a free ring rather than directly to the spraybars. With this arrangement, the free ring can expand with the faceplate as the temperature increases. The bending moment that would result if the bolt was restrained by the cold spraybars is thereby, eliminated. This concept simplifies the spraybar construction because the support pad is less complex and the spraybar can be flat sided.

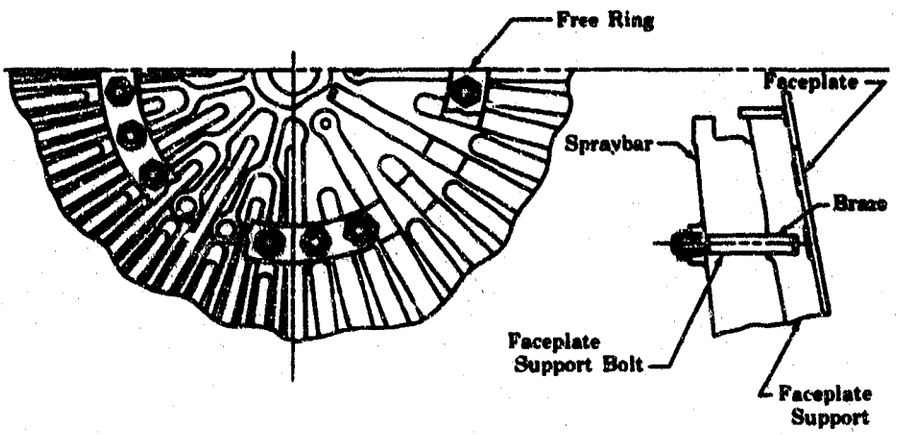

(U) Figure 343. Main Burner Injector Concept No. 8 FD 25368

i. Concept No. 9

(U) This concept, which is shown in Figure 338, offers several variations on the single tube tapered spraybar design of concept No. 7. In this design concept the spraybar oxidizer flow area has been increased in order to meet XLR129-P-1 demonstrator engine cycle pressure loss requirements. A one-piece cast design was also considered as shown in View M. The configurations, represented in Views E, F, G, H, J and K, employ the multipiece concept. View E shows a design where the transition from the slotted hole in the crossover manifold to the round hole in the spraybar is made in the spraybar. View F shows a design where the transition is made smoothly with no area change. In View G, the transition is made

with abrupt changes in area. This concept is suitable for either casting or machining from a forging. Views J, K, H, and E show alternative methods for manufacture of a machined spraybar.

j. Concept No. 10

(U) This concept, which is shown in Figure 339, is a variation on concept No. 9 where the tip inside diameter of the spraybar has been increased to reduce the oxidizer radial pressure loss in the spraybar. The increased tip diameter produces the maximum oxidizer internal flow area at a sacrifice to the hot gas flow area between radial spraybars.

k. Concept No. 11

(U) This concept, which is shown in Figure 336, is a variation on concept No. 2 where the spraybar inlet oxidizer flow area has been increased to comply with the demonstrator engine cycle pressure loss requirements. To obtain the oxidizer flow area required by the cycle, two extra radial supply passages had to be added. This scheme can be compared directly with concept No. 1 except for the increased flow area requirement.

l. Concept No. 12

(U) This concept, which is shown in Figure 344, shows a fuel faceplate design similar to the design tested during Phase I (Contract AF04(611)-11401), except that the rib support structure is fabricated from sheet stock instead of being machined in one piece.

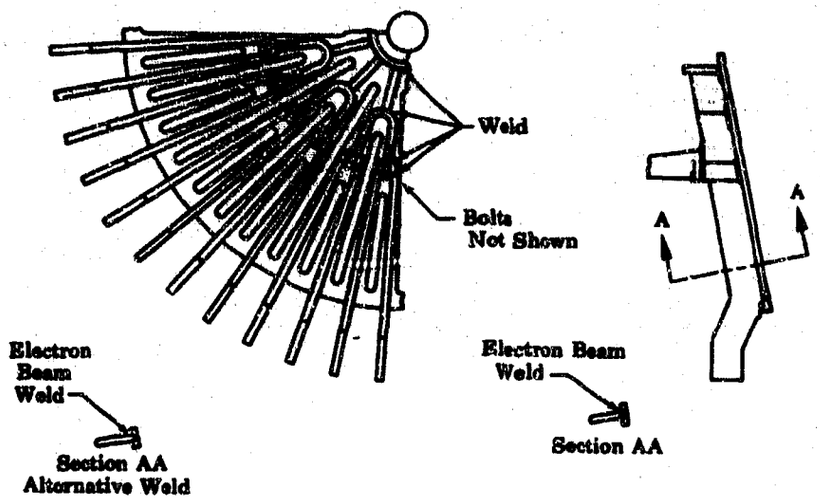

(U) Figure 344. Main Burner Injector Concept No. 12 FD 25372

m. Concept No. 13

(U) These concepts, which are shown in Figure 342, offer a number of methods for retaining the faceplate seal support ring during assembly and disassembly. The type retainers shown consist of either screws,

dowels, tablock, or a press fit. In any case, the retainer is not a load carrying member but it merely retains the faceplate in position during assembly. The load of the faceplate is transmitted into the main chamber case at the outside diameter through the support ring and into the spraybar near the center through bolts as shown in concept No. 8. Transmitting the load into the main chamber case eliminates the set of bolts that attached the faceplate to the injector housing as was done in Phase I.

n. Concept No. 14

(U) This concept, which is shown in Figure 343, has a one-piece solid Rigimesh faceplate and support.

o. Concept No. 15

(U) This concept, which is shown in Figure 340, offers still another variation on concept No. 9. In this design, the spraybars have been straightened to allow the spraybar to be fabricated by conventional machining. Also, the spraybars are arranged so that the injection elements in any one bar are of equal length. View A shows a variation on this design with provisions for access for the main chamber igniter spark plug and the propellant supply lines through the oxidizer manifold.

(U) In this study, two alternative materials were considered for use in the injector designs. Inconel 718 (AMS 5663) was chosen as representative of a good castable high strength material, while stainless steel (AMS 5646) was chosen as representative of a lower strength, less expensive, easier machined, and more ductile material.

4. Design Considerations

(U) Some design considerations reached in a conference with representatives from casting vendors are provided in the following list.

1. Casting of the main burner injector in one piece is presently beyond the state-of-the-art because of the complexity of supporting the cores and subsequent core removal.

2. Diffusion bonding of the oxidizer injection elements into the cast spraybars is not impractical, but some development would be required.

3. Porosity in the casting should be expected internally between the injection elements. Externally, the spraybar would be leak free.

4. Care must be taken in the design of the parts to ensure adequate access for leaching out the core material.

5. The caustic solution used for leaching out the core would be difficult to remove.

6. Core support could be accomplished through the oxidizer injection element holes.

7. Casting the Rigimesh face support directly into the Rigimesh to form a bond and thereby avoid a weld joint is possible, but this requires additional development work.

(U) The following design considerations were made with process planning and fabrication as major factors:

1. The injection elements should be brazed before assembly to permit the spraybars to be individually flow checked.

2. The injection elements can be bent into position at assembly, thus allowing for some deviation from the true position of the elements.

3. The spraybar attachment braze slots for the stacked tube designs will be difficult to machine. The slots should be made as shallow as possible to facilitate manufacture.

4. An axially slotted braze connection is easier to machine than a radially slotted braze connection; however, a through broach design is more desirable than either of these methods.

5. If the injection element holes are cast out of true position, it will be difficult to relocate their center by machining because of tool drift, however, the holes could be eloxed on center. Core support, through the injection element holes, should be held to a minimum or eliminated by supporting from the other side of the spraybar, so that the element holes can be machined on true position.

6. Time would be required to develop the technique required for making the weld required in concept No. 4 without excessive distortion.

7. A round spraybar braze joint, like that required for concepts No. 7, 9, 10, and 15, is the easiest shape to braze.

8. Concept No. 12 is not a satisfactory design, because of weld distortion problems and because of the cost involved in making weld fixtures.

(U) A weight study was made of the representative injector concepts. A summary of these weights is shown in Table XXVII. For the purposes of weight comparison, the spraybar wall thicknesses were assumed to be 0.050 inch, which is a manufacturing limit. The inlet manifold wall

thickness was calculated from the formula S = Pr/t where S = 85% of the 0.2% yield, and P = 1.2 (maximum cycle pressure). All cast designs were assumed to have a tapered manifold, while all machined designs were assumed to have a constant cross section manifold.

(U) Early in the study, the injector schemes were based on the requirements established during Phase I (Contract AF04(611)-11401) It was decided that, for comparison purposes, all designs would use the bolt circle diameter established during Phase I (Contract AF04(611)-11401). The oxidizer spraybar inlet area was held the same as on an earlier cast injector study. The resultant configuration weight, pressure drop, and other parameters were then determined as shown in Table XXVII. The oxidizer pressure drops in concepts No. 1, 5, and 7, are based on the pressure drop requirements established during Phase I (Contract AF04(611)-11401). Later in the study, the demonstrator engine requirements became available and, based on these requirements, a new oxidizer spraybar inlet area was determined. Concepts No. 9, 10, 11, and 15 reflect this change. Concept No. 11 was sized to obtain this oxidizer flow area and at the same time maintain the hot gas flow area established during Phase I (Contract AF04(611)-11401) or greater.

(C)(U) Table XXVII. Injector Selection Criteria

Concept	Weight (lb) SST - Inconel 718 (AMS 5646) (AMS 5663)	Oxidizer Flow Area (in^2)	Fuel Flow[2] Area (in^2)	Oxidizer ΔP (psi)
1	134-96	9.08	58.0	1253
5	96-76	9.08	67.0	1253
7	92-72	9.08	74.0	1253
9[1]	64-44	14.37	71.8	985
10	65-45	14.37	71.8	985
11	156-118	14.37	56.0	985
15	70-50	14.37	71.8	985

(1) Views "E", "F", and "H"

(2) Hot gas flow area around spraybars.

5. Performance Considerations

(U) A study was also made to show the effect of various parameters on injector performance. The parameters that were considered to be influential were oxidizer droplet size, number of injection elements, oxidizer injector pressure drop, pressure loss in a tapered spraybar, effect of spraybar size on fuel injector pressure drop, and contraction ratio.

(U) Table XXVIII shows the magnitude of various influential parameters for the engine cycle. This table in conjunction with the figures explained below can be used to determine the change in injector performance caused by changes in influential parameters.

(C)(U) Table XXVIII. Cycle Values of Influential Parameters

Total Cycle Oxidizer Injector Pressure Drop (psia)	985 psia
Oxidizer Element Pressure Drop (psia)	871 psia
Number of Oxidizer Injection Elements	1080
Total Cycle Fuel Injector Pressure Drop (psia)	120 psia
Fuel Injector Slot Pressure Drop (psia)	96 psia
Throat Diameter (inch)	7.680 inches
Contraction Ratio	3

(U) Figure 345 shows the Sauter mean diameter of the injected liquid oxygen as a function of the pressure drop across the element. Note that the pressure drop across the element is the total cycle injector pressure drop, excluding losses in the supply manifold and spraybar passages. The pressure drop across the elements is 871 psid at 100% thrust and a mixture ratio of 7, which produces a mean drop size of 20 microns.

(U) The effect of the number of oxidizer injection elements on combustion efficiency for lines of fuel injection pressure drop is shown in Figure 346. The fuel pressure drop used is the drop across the fuel slot and does not include the pressure loss experienced while passing around the spraybars. The main burner injector is expected to have approximately 1080 elements, with a fuel injector pressure drop of 96 psia. The increase in combustion efficiency, which is attained by increasing the fuel pressure drop, shows that decreasing the pressure loss around the spraybars is desirable.

(U) Figure 347 shows the effect of oxidizer injection element pressure drop on combustion efficiency.

(U) The pressure loss inside a long single tube tapered spraybar of concept No. 15 is shown in Figure 348 as a function of station numbers associated with the element location. The elements are numbered so that the element closest to the chamber wall is number one. Note that the sharp increase in pressure loss occurs toward the chamber center line. This is the point where the blockage created by the element protruding into the tapering spraybar flow passage becomes a significant portion of the passage area. Lines of spraybar tip inside diameter show the increasing pressure loss down a spraybar as the inside diameter is decreased. The tapered spraybar has a flow gradient associated with the pressure gradient inside the spraybar, but the gradient occurs at a position in the chamber where chamber area at that radius is also making a rapid change. Consequently, the oxidizer weight flow per unit chamber area is not significantly affected by the spraybar flow gradient.

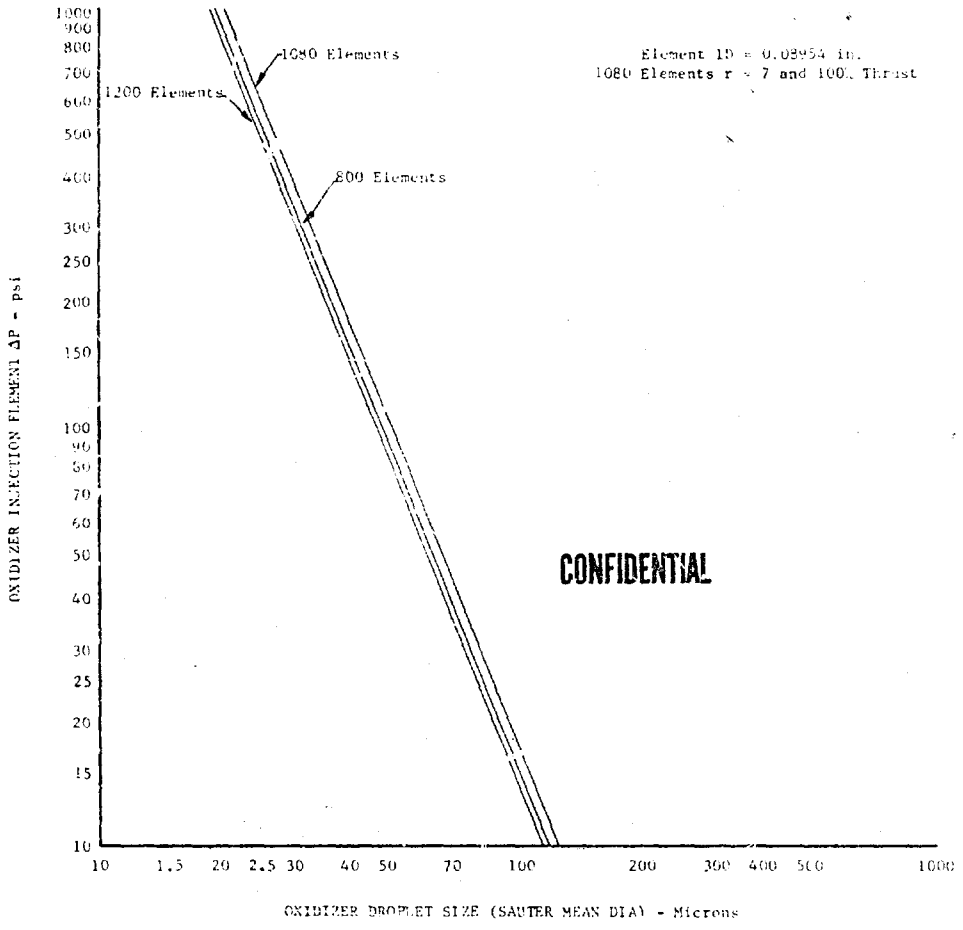

(U) Figure 345. Oxidizer Droplet Size DFC 68800

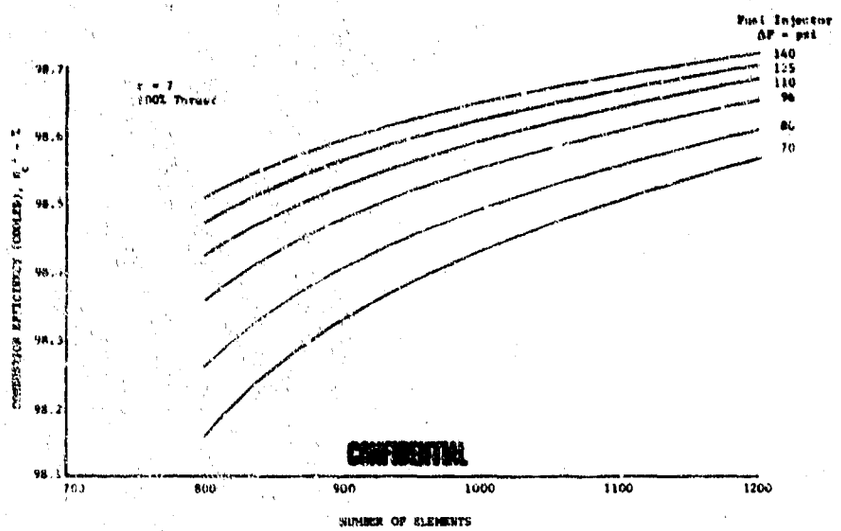

(U) Figure 346. c* Efficiency vs Number of Elements and Fuel Slot ΔP — DFC 68801

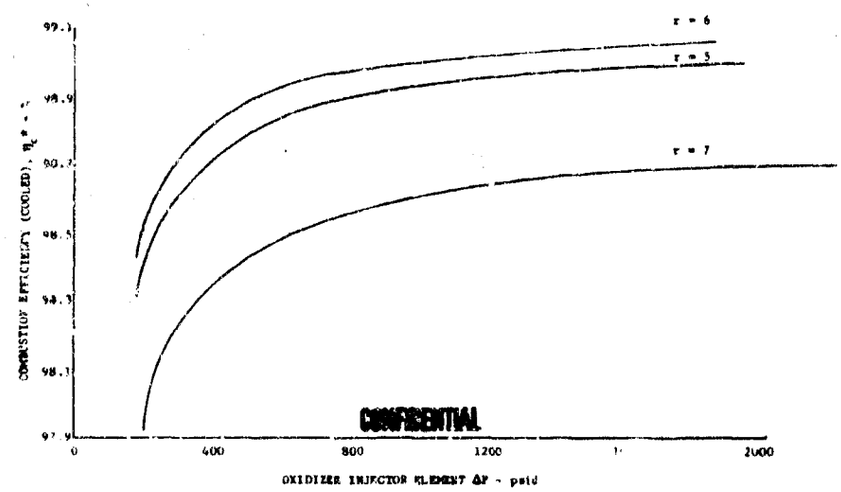

(U) Figure 347. c* Efficiency vs Oxidizer ΔP 100% Thrust — DFC 68802

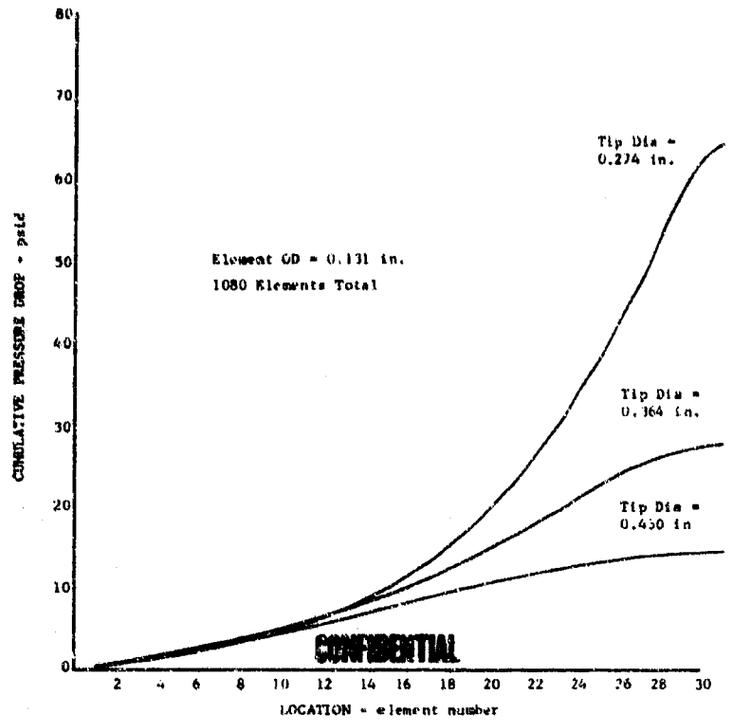

(U) Figure 348. Pressure Loss Inside a Long Single Tube Tapered Spraybar DFC 68803

(U) The spraybar tip diameter has a strong influence on the available fuel flow area around the spraybar. Figure 349 shows fuel flow area as a function of spraybar tip diameter. The fuel pressure loss in passing through the fuel flow area is shown in Figure 350. This pressure loss is subtracted from the total cycle fuel pressure drop to obtain the pressure drop across the fuel slot. By using Figures 346 and 350, a trade can be made between the fuel slot pressure drop and the oxidizer spraybar radial pressure drop.

(C) The current phase throat size is larger than the Phase I (Contract AF04(611)-11401) throat size. If the current phase chamber diameter were held the same as Phase I (Contract AF04(611)-11401), the contraction ratio would decrease from $\epsilon_c = 3$ in Phase I (Contract AF04(611)-11401) to $\epsilon_c = 2.69$ in the current program. Figure 351 shows the influence of contraction ratio on combustion efficiency.

6. Main Burner Igniter

(U) A design study was conducted to determine various concepts of mounting the main burner igniter on the transition case and main burner injector. The investigation included an adaptation of existing hardware in addition to new concepts to reduce the complexity of the igniter systems. The geometry of the coplanar transition case and the single tube tapered spraybar injector prevents the use of existing components. The existing

propellant supply manifold and spark plug are too short for mounting them on the transition case, and the igniter housing is too long for mounting it on the injector. Six alternative locations to provide main burner ignition were investigated for this design study and are divided into two major classes.

(U) Concepts No. 1, 3, 4, and 6 are basically patterned after the previous design. The igniter is centrally located in the main burner injector with the propellant supply and spark plug extending from the center outboard to the exterior of the engine. These concepts do not reduce the size or complexity of the ignition system but they are considered to be within the current state-of-the-art.

(U) Concepts No. 2 and 5 incorporate propellant supply and spark igniter features that are external to the main engine, which requires only one local boss for the igniter housing. These concepts significantly reduce the complexity of the ignition system because the propellant supply would consist of simple fittings, and the spark plug could be a standard automotive type.

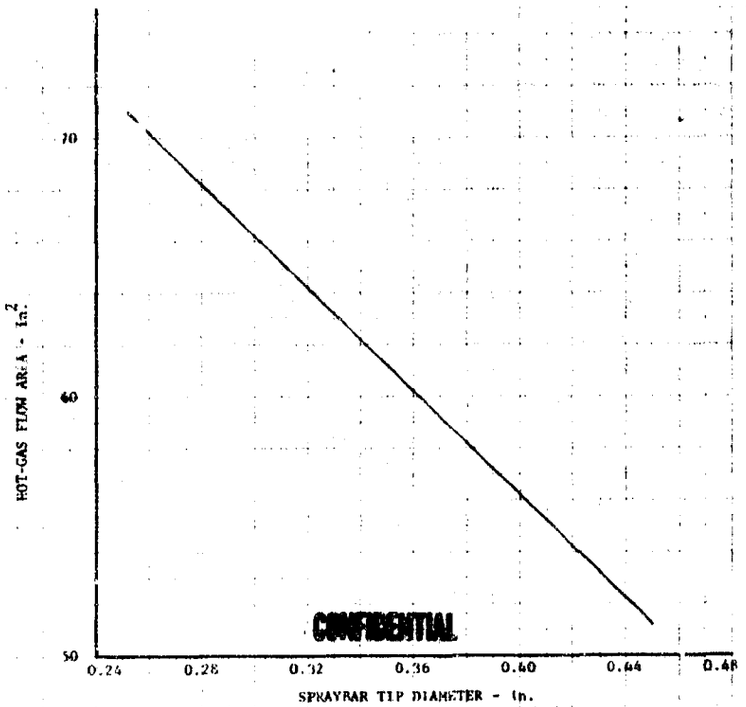

(U) Figure 349. Hot Gas Flow Area vs Spray-bar Tip Diameter DFC 68804

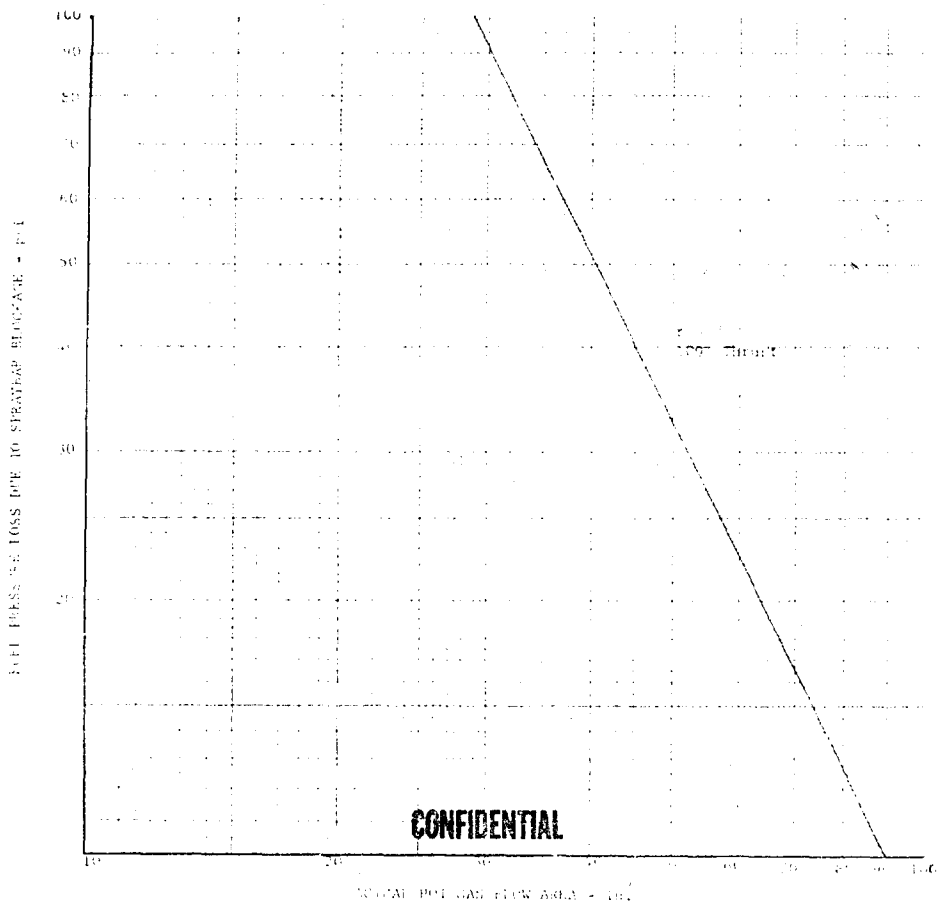

(U) Figure 350. Hot Gas Flow Area vs Fuel Pressure Loss DFC 68806

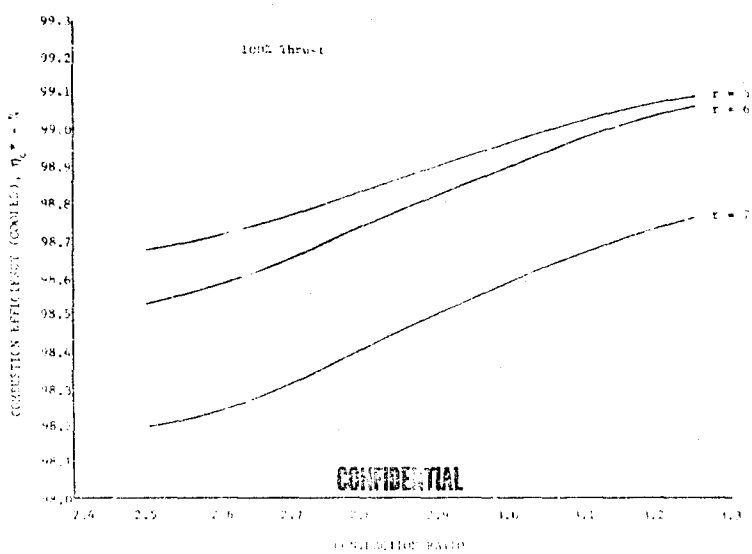

(U) Figure 351. c* Efficiency vs Contraction Ratio DFC 68805

a. Concept No. 1

(U) This concept, which is shown in Figure 352, represents an igniter that is mounted in the center of the injector. The propellant supply and spark plug enter the igniter through local bosses that are integral with the transition case injector flange.

(U) This approach necessitates the removal of a main attaching bolt at each boss location. Structurally, this compromises the transition case flange and sphere intersection point and is considered undesirable. This design also creates an extremely long propellant supply probe and igniter because the mount flange has to extend beyond the oxidizer manifold.

b. Concept No. 2

(U) This concept, which is shown in Figure 353, represents an igniter that is located in the center of the injector, but with the propellant supply and spark plug mounted externally to the main engine. The igniter is made an integral part of the transition case and requires only one local boss on the case flange for mounting.

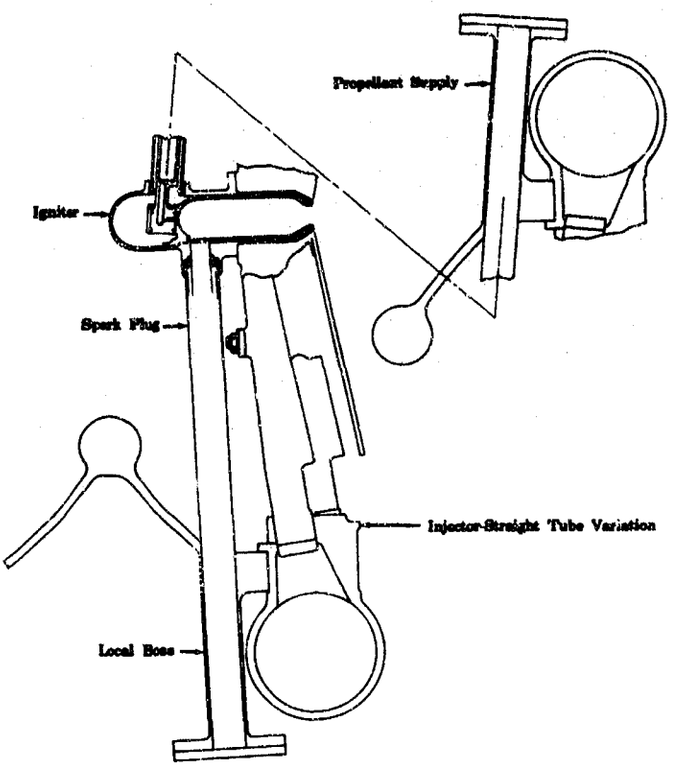

(U) Figure 352. Main Burner Igniter Concept No. 1 FD 25619

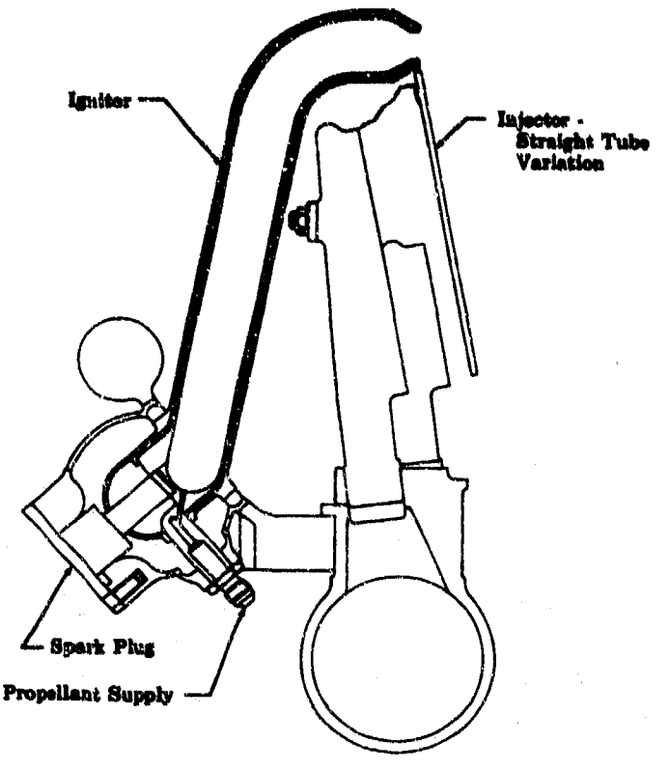

(U) Figure 353. Main Burner Igniter Concept No. 2 FD 25620

(U) The increased chamber length coupled with turning the flame requires cooling requirements above concept No. 1. In addition, the flame temperature drop may require an increase in propellant flow rate because of the higher heat removal requirement of this configuration.

(U) In this concept, either propellant could be used to cool the chamber. The main advantage of using the oxidizer as a coolant is the igniter would ignite its own coolant at the injector face. This would establish a stoichiometric flame temperature to ignite the main injector flow under all flight conditions. Using the oxidizer as a coolant, the igniter flame temperature may be reduced well below the material limits of the liner before the bend and still have sufficient energy to ignite the oxidizer coolant in the main injector.

(U) Mounting the igniter on the lower transition case sphere requires the removal of one injector flange bolt. The same concept could be used with the mount point on the main sphere similar to the mount arrangement shown in concept No. 3. When mounted on the main sphere, the igniter assembly can be removed and therefore does not become an integral part of the transition case.

c. Concept No. 3

(U) This configuration, which is shown in Figure 354, offers a variation on concept No. 1 in which the propellant supply and spark plug access to the igniter are through the main sphere of the transition case. This concept incorporates local spherical segments attached to the main sphere. This location does not necessitate the removal of main attaching bolts.

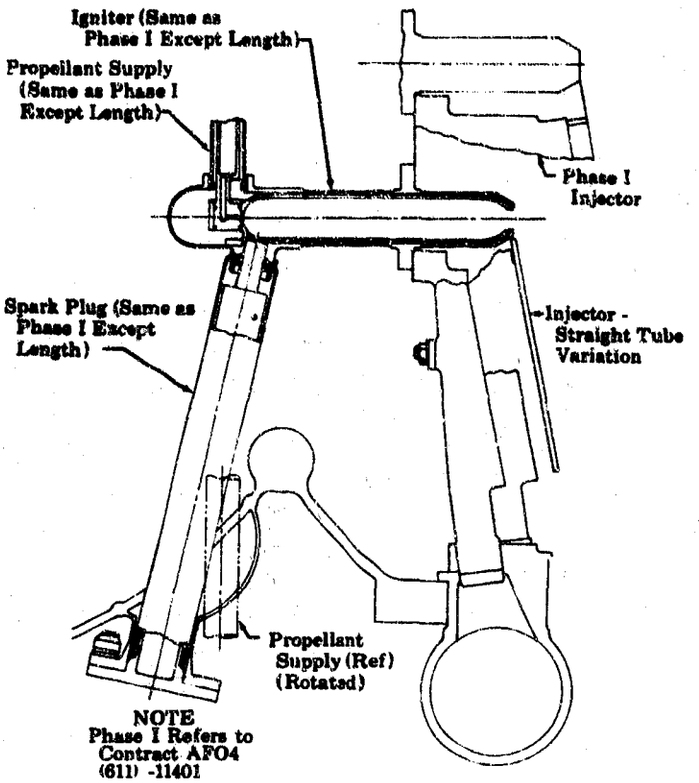

(U) Figure 354. Main Burner Igniter Concept No. 3 FD 25621A

d. Concept No. 4

(U) This configuration, which is shown in Figure 355, offers still another variation on concept No. 1 in which access to the igniter is made downstream of the connector ring. This location requires the removal of a flange bolt at the spark plug and propellant supply probe locations.

(U) This concept adapts the existing hardware with as little rework as possible. Even though the basic shape of the three major pieces of the igniter is the same as Phase I (Contract AF04(611)-11401), all three pieces require extended lengths. The required length extensions are shown labeled as ΔL in Figure 355.

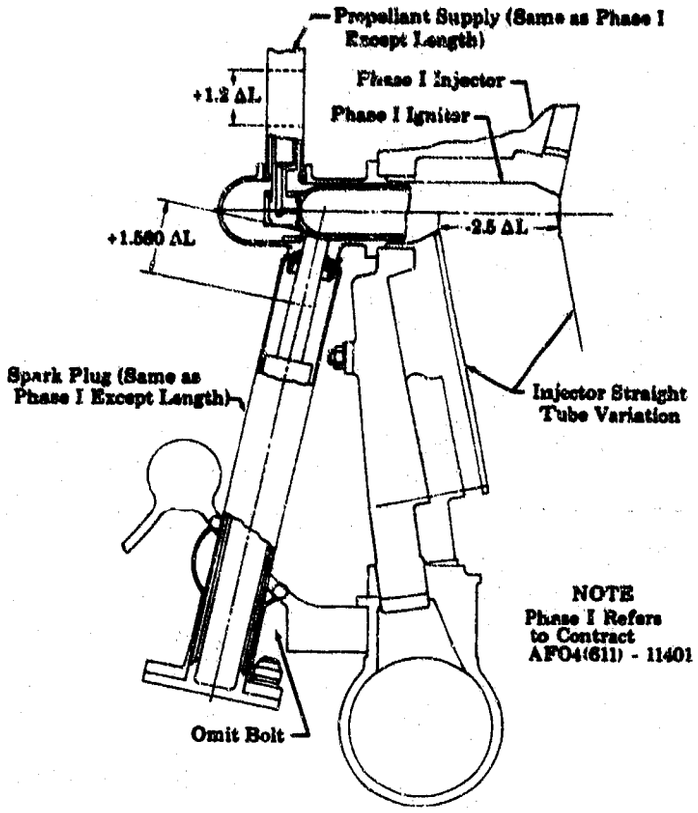

(U) Figure 355. Main Burner Igniter Concept No. 4 FD 25622A

e. Concept No. 5

(U) This concept, which is shown in Figure 356, is a variation on concept No. 2 that incorporates a straight, removable igniter chamber not centrally located. This igniter location compromises the main burner injector and the face plate support structure symmetry. The injector oxidizer mass flow distribution would be affected, but this appears to be reconcilable with a more detailed investigation. The structural capability of the support structure would not be adversely affected by this location.

f. Concept No. 6

(U) This concept, which is shown in Figure 357, shows the mounting of the spark plug through the injector with a centrally located igniter. The injector faceplate support bolt is compromised and would require a new concept in attachment. This location appears to be impractical.

(U) It is concluded that the existing igniter hardware cannot be used in the current program transition case and injector without modification. The most desirable location to mount the igniter is above the ring

connecting the main sphere to the lower sphere. The externally mounted igniter chambers reduce the complexity of the propellant supply probe and spark igniter. For these reasons, the concept No. 2 main burner igniter is recommended.

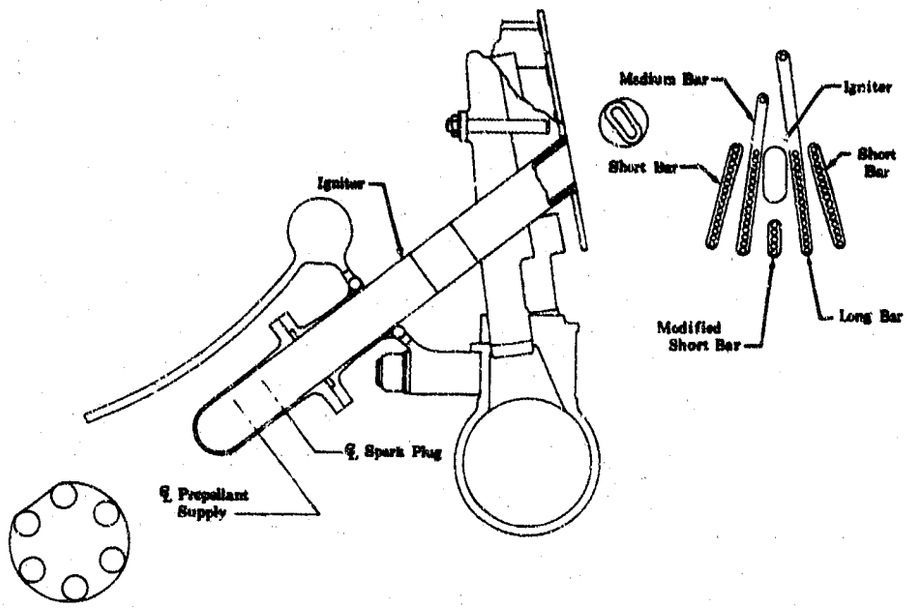

(U) Figure 356. Main Burner Igniter Concept No. 5 FD 25623

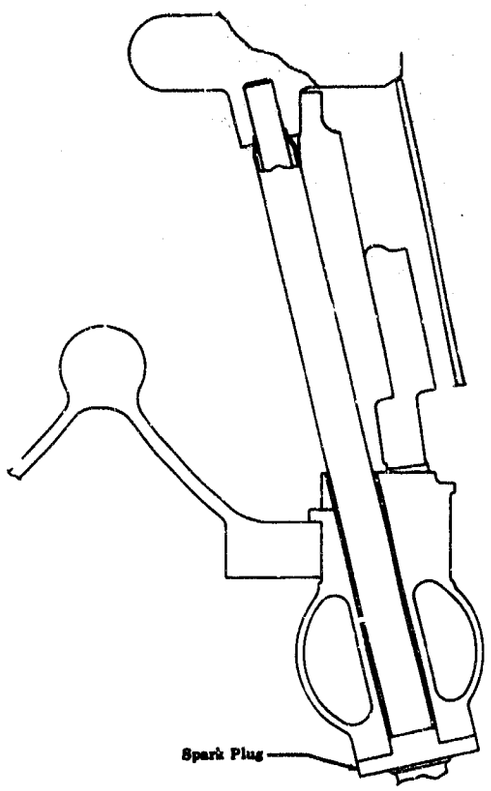

(U) Figure 357. Main Burner Igniter Concept No. 6 FD 25609

C. NOZZLES

C. NOZZLES

1. Introduction

(C) The nozzle assembly for the XLR129-P-1 demonstrator engine will consist of two fixed sections that form the primary nozzle and a translating lightweight section as the two-position nozzle. The primary nozzle attaches to the main burner chamber at an area ratio of 5.3 and extends to an area ratio of 35. The two-position nozzle extends from an area ratio of 35 to an area ratio of 75. The current XLR129-P-1 demonstrator engine nozzle assembly is illustrated in Figure 358. The objective of this subtask is to design and fabricate the primary nozzle, the two-position nozzle, and the two-position nozzle translating mechanism.

2. Summary, Conclusions, and Recommendations

(U) 1. A design study indicates that the primary regeneratively cooled nozzle is mechanically feasible. The recommended primary nozzle design has a single pass heat exchanger at the inlet end and a double pass heat exchanger at the exit end.

(U) 2. The two-position nozzle coolant passages are designed to pass the coolant at a rate that keeps the inner skin of the nozzle at a temperature as high as possible in the axial direction to absorb maximum energy in the flow stream. The skin temperature is limited in the inlet region to avoid low cycle fatigue over the required life of the engine.

(U) 3. The outer skin of the two-position nozzle will have a high circumferential thermal gradient because of the corrugated flow passages and the fin-cooled weld flats. The thermal stresses imposed on the outer skin by the gradient will be taken out in hoop tension.

(U) 4. The outer skin of the two-position nozzle will be smooth, and this has three advantages. The stiffening bands can have an uninterrupted bonding surface, the outer skin thickness is based on strength requirements and not thermal requirements, and the corrugation cannot be constricted by thermal expansion.

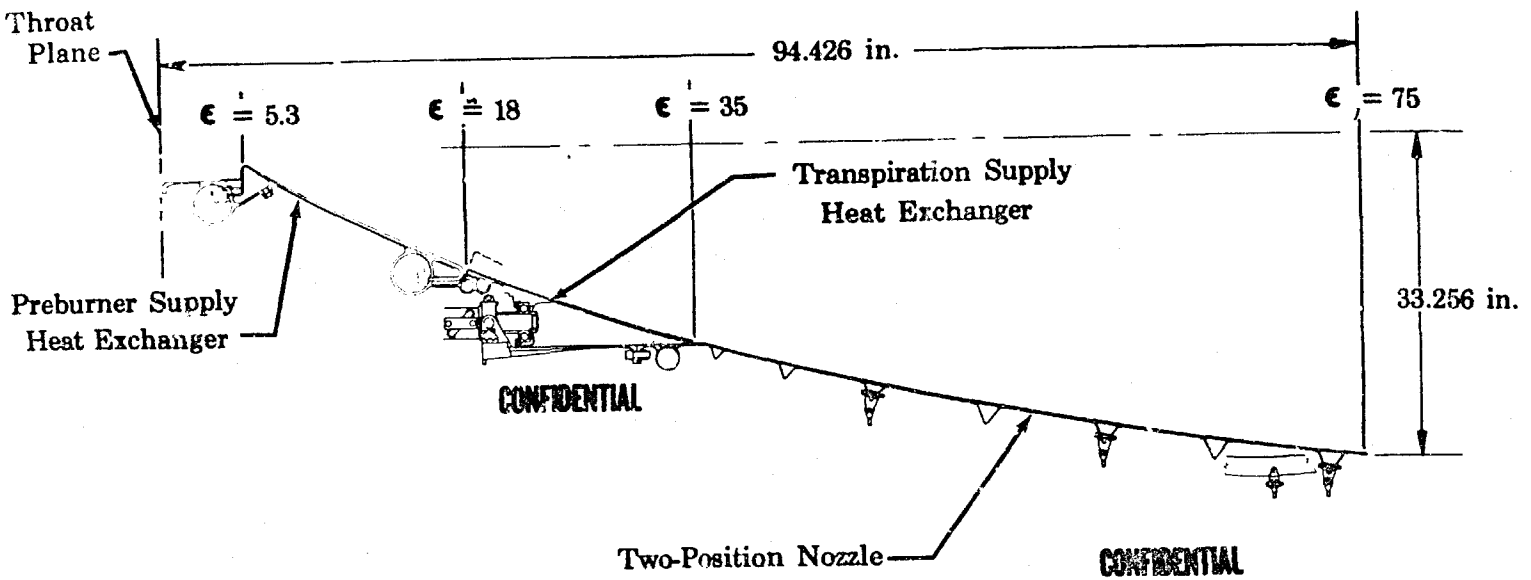

(U) Figure 358. XLR129-P-1 Demonstrator Engine Nozzle Assembly

FDC 25573A

CONFIDENTIAL

3. Design Description

a. Primary Nozzle

(U) The primary nozzle consists of two heat exchangers: a double pass transpiration-supply heat exchanger and a single pass preburner-supply heat exchanger. The locations of the two heat exchangers have been reversed from that of previous studies. By having a double pass at the exit end and single pass at the small end, these advantages were obtained.

1. The weight was reduced 93 pounds with no increase in pressure drop within the manifolds or cooling tubes.

2. All manifolds are forward of the two-position nozzle jackscrew ring gear making possible larger diameter supply lines.

3. The large diameter full flow heat exchanger manifolds are moved in and forward, providing attachment flanges nearer the manifold and making plumbing considerably easier. The nozzle construction is simplified because long supply lines are not permanently attached to the manifolds.

4. The manifolds are much closer to the three translating mechanism jackscrew mounts; this disperses the three loads evenly into the nozzle case in a much shorter distance and results in a lighter-weight case.

5. A turnaround cap, which is the lightest weight turnaround, is possible on the large end of the small tubes, resulting in a lighter nozzle, whereas on the previous designs it was impractical to use.

(C) The primary nozzle configuration shown in Figure 359 is a possible manifolding arrangement. The two regeneratively cooled sections of the primary nozzle will be fabricated using techniques similar to those used on the RL10 rocket engine nozzle. The preburner-supply heat exchanger extends from an area ratio of 5.3 to approximately 18 and the transpiration-supply heat exchanger extends from 18 to 35. This concept weighs approximately 315 pounds. A detailed stress analysis will refine the nozzle case thickness, influencing the weight. The inertial loading of the jackscrew supports, which is an impact load at three points on the nozzle case, is unknown because the time required to stop the translating nozzle has not been defined. Assuming a 17,000-pound load on each support, evenly distributed into the nozzle case, the case thickness was calculated to be approximately 0.065 inch. Case sections that are required to withstand only the internal pressure would be 0.015-inch thick. These calculations assume that the cooling tubes carry none of the case loads.

(U) The material selected for the nozzle cooling tubes is Inconel 625 (AMS 5599). This material can be formed into tapered tubes and easily brazed, although repair brazing is more difficult than with stainless steel (AMS 5646). At elevated temperatures Inconel 625 (AMS 5599) has

an ultimate strength and 0.2% yield strength that is 2.8 times greater than stainless steel (AMS 5646). To keep the materials compatible, the nozzle skirt and manifolds are also of Inconel 625 (AMS 5599). The nozzle cooling tubes were sized by analytical consideration of temperatures and fatigue cycle life requirements.

(U) The suggested manufacturing limitations for the Inconel 625 (AMS 5599) tubes are as follows:

1. Minimum ID = 0.060 inch
2. Minimum tube wall thickness = 0.010 inch
3. Minimum bend radius = 2 times tube OD
4. Double tapered tubes are possible but are more expensive.

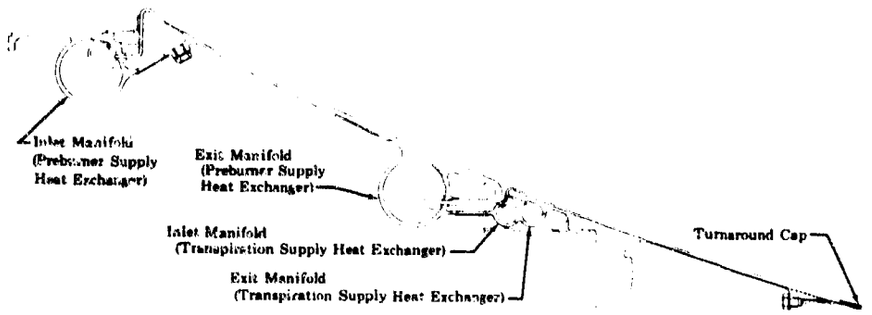

(U) Figure 359. Primary Nozzle FD 25419A

b. Two-Position Nozzle

(U) The two-position nozzle, shown in Figure 360, is a dump-cooled nozzle. The coolant enters the coolant passages through a manifold at the forward end and flows through longitudinal skin passages. The passages are formed sheet metal convolutions that are flared into individual nozzle shapes at the exits. The convolution cross sections are circular arc segments, and the number of convolutions is constant for the entire nozzle length. The convolutions form the inner skin of the nozzle and are seam-welded to the inside surface of the outer skin, which is a smooth single sheet. Vee-shaped loop bands are brazed directly to the outer surface of the outer skin.

(C) The selected shape of the bands transmits maximum stiffness to the nozzle. The coolant passage convolution cross sections are designed to accommodate the required coolant pressure and inner wall temperature of 1450°F. The passages are sized to allow a coolant flowrate that prevents the inner wall temperature from exceeding 1450°F. The two-position nozzle is designed to withstand a maximum axial load of 10 G + thrust pressure load at minimum mixture ratio and 100% thrust, and a maximum transverse load of 6 g + 2000-pound load encountered because of asymmetric

flow in the nozzle. For test firing at simulated altitudes, the nozzle will be in the fully extended position. The hoop bands can be fitted with lugs that attach to the radial suspension cables supporting the nozzle to provide a stabilization against facility induced side loads.

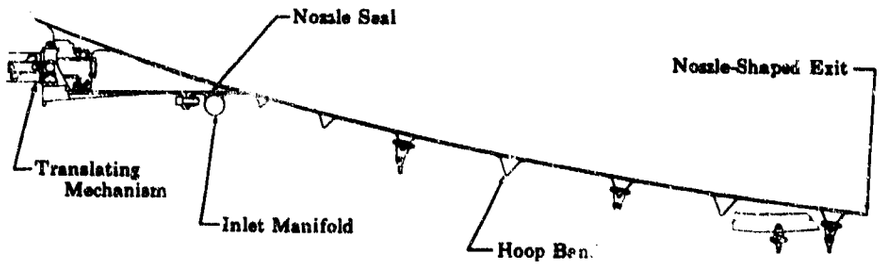

(U) Figure 360. Two-Position Nozzle FD 25420A

(U) The material selected for the inner and outer skin is Inconel 625 (AMS 5599), which exhibits good low cycle fatigue properties at elevated temperatures. The Inconel 625 (AMS 5599) also retains a high rate of ductility at cryogenic temperatures and requires no heat treating after bending or forming. The nozzle coolant passages are designed to pass the coolant at a rate that keeps the inner skin of the nozzle at a temperature as high as possible in the axial direction to absorb as much energy in the coolant as possible. The skin temperature is limited in the inlet region to avoid low cycle fatigue over the required life of the engine. The outer skin will have a high circumferential thermal gradient because of the corrugated inner skin. The thermal stresses imposed on the outer skin by the gradient will be taken in hoop and axial tension. An abrupt change in nozzle contour is encountered at the intersection of the cylindrical portion under the inlet manifold and the true contour.

(U) Bending the corrugations to conform to this contour change may tend to constrict the passage flow areas. A heat transfer analysis shows that constriction will accelerate the coolant flow, thereby increasing the cooling effect in that area. The passage constriction can be held to a minimum by die forming. The exits of the coolant passages are flared on the inner skin to form a nozzle-shape contour. The flaring may be incorporated during the die stumping on the skin panels or on individual passageways after assembly. Area ratios of constriction and expansion are selected to allow the coolant flow to exit at a predetermined Mach number and pressure. This will derive a thrust and performance increment from the coolant.

(U) A shock wave resulting from the crimped convolution nozzle during firing is not anticipated. The predicted thickness of the boundary layer will be sufficient to prevent a shock wave. In the hardware design, the two-position nozzle contour will be drawn to coincide with coordinate points based on room temperature dimensions. Three advantages are realized in selecting the outer skin to be smooth. The stiffening bands can have

an uninterrupted bonding surface; the outer skin thickness is based on strength requirements and not thermal requirements; and the corrugations cannot be constricted by thermal expansion.

(1) Coolant Inlet Manifold

(U) The coolant inlet manifold is situated at the forward end of the nozzle. The base of the manifold is brazed to the outer surface of the outer skin and directly over the area where the coolant passage convolutions begin. Inlet holes for the coolant lead through the base of the manifold and outer skin into the passage convolutions. There is one inlet hole for each coolant passage convolution. The base of the manifold also serves as the forward flange of the nozzle to which the translating mechanism attachment brackets are bolted. The manifold is a constant diameter manifold but flares to a larger diameter in the immediate vicinity of the manifold inlet flange. The neck of the inlet flange has twice the flow area of the constant diameter portion of the manifold. The coolant inlet manifold material size was based on a margin in excess of 1.2 times the operating pressure. The stresses considered are hoop stress resulting from the coolant pressure and bending stresses on the inlet flange.

(U) The material selected for the manifold is Inconel 625 (AMS 5599). The manifold pressure is low and the small hoop stress on the manifold torus wall will permit the use of minimum commercial sheet thicknesses. The mating flanges for the attachement brackets are local in location rather than a continuous circumferential flange. This design results in a substantial weight saving, and it reduces clearance problems during nozzle retraction. The coolant exit holes in the base of the manifold allow the coolant to impinge directly onto the inner wall surfaces of the nozzle passage convolutions, increasing the cooling ability of the coolant flow. The coolant manifold is situated at the beginning of the nozzle coolant passages and directly over and forward of the regenerative nozzle turnaround manifold to allow maximum cooling in the vicinity of the nozzle seal. For simplicity of fabrication and nonstringent flow requirements, the coolant manifold selected is a constant diameter. The low flow rate allows the manifold to serve as a plenum chamber for the nozzle coolant passages. The stress imposed on the inlet flange and neck is based on a bending moment estimate of 425 in.-lb resulting from the friction of a sliding joint coolant supply line. This concept is necessary to supply the nozzle with coolant during translation.

(2) Nozzle Seal

(U) The nozzle seal consists of two concentric, thin, conical sections that are riveted to a support ring located the outer surface of the regenerative nozzle. The support ring is positioned near the turnaround manifold of the regenerative nozzle. The two concentric conical sections are tangent to each other over their respective inner and outer surfaces and are divided into a series of overlapping fingers that act as a flexible circumferential seal against the outer surface of the two-position nozzle as shown in Figure 360. The width and thickness of the fingers may be varied in design concepts to suit alternative stress and deflection ranges.

(U) A possible material selection for the nozzle seal is Inconel 718 (AMS 5596) sheet. This material was used successfully in previously designed jet engine inner skin seals. The ability to seal efficiently with a minimum amount of leakage depends on the overlapping upper and lower fingers remaining in contact over their entire interface surfaces during bending. This contact can be maintained by allowing the aft edge of the fingers to remain unrestrained. The upper and lower fingers will assume a sliding contact and have the advantage of taking radial and axial nozzle joint mismatch. The fingers shown in Figure 360 can deflect approximately 0.15 inch at the ends and remain stressed below 85% of the 0.2% yield strength of the material at 200°F. This is the estimated temperature in the vicinity, and is low enough for the material to retain its elasticity. The support ring to which the seals are riveted is made of Inconel 600 (AMS 5665) and is not subjected to high loading.

c. Translating Mechanism

(1) General

(U) The translating mechanism, shown in Figure 361, is capable of translating the secondary nozzle in 4 to 5 seconds. The drive system consists of three jackscrews and guide tracks. The screws are synchronized and driven by an externally toothed ring gear that serves as the outer race of the primary nozzle-mounted ball bearing. The ring gear is driven by an electrohydraulic drive package at 1500 rpm through a 1:1 offset gearbox. The drive gear and jackscrew drive gears are of the same pitch diameter so that the jackscrews turn at the same speed as the motor. The ball nut of each jackscrew is attached to a two-position nozzle bracket.

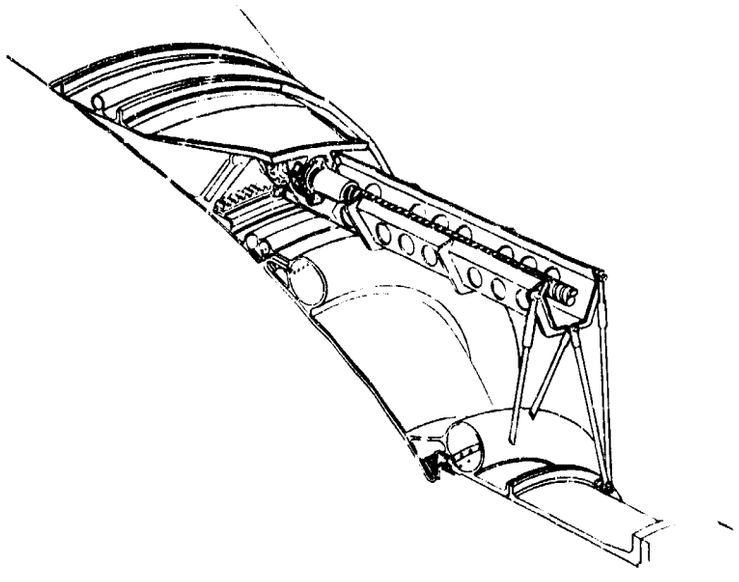

(U) Figure 361. Translating Mechanism FD 25421

(2) Bracket Attachment

(U) Each bracket is a fan-shaped structure in which the wide end is flanged and bolted to the nozzle flange. The narrow end is formed with a lug that is gimbaled to the jackscrew translating nut. The attachment brackets support the nozzle by cantilevering from the jackscrews. The brackets are stressed below the 85% of 0.2% yield strength at room temperature; the load stresses taken into consideration are buckling, shear, and bending from maximum thrust, acceleration, and start transient loads. The bending and shear stresses from the transverse nozzle loads were also considered.

(U) The material selected for the brackets is Inconel 718 (AMS 5663). If the brackets are to be of welded construction, then the heat-treatable Inconel 718 (AMS 5662) version will be used. Inconel 718 has the highest 0.2% yield strength of all the nickel alloys. A second choice of material is titanium (AMS 4966), which is available in bar and forgings and exhibits good weldability. Titanium (AMS 4966) exhibits about two-thirds the strength of Inconel 718 (AMS 5663), but somewhat over half the density. A weight reduction might result if the thinnest possible Inconel 718 (AMS 5663) design were compared with the maximum requirements of the titanium sections.

(U) The brackets are shaped in a curved main panel or web with a gusset or flange running the entire length on both sides. These side gussets join the bolting flange at the end of the bracket; thus, the bracket resembles a tapered box that resists buckling and bending loads. The bending loads can occur in an infinite number of directions because of the gimbaling and transverse spike loads that may be imposed on the nozzle. The bracket is designed on the basis of a cantilevered beam with an end load and end moment. The bracket attachment bolts were sized by determining the total tensile loads imposed by the moments from all of the thrust, impact, and transverse loads applied simultaneously. Calculations indicate that extra ribs across the bracket web are unnecessary and a weight saving can be realized over the design used in the Phase I (Contract AF04(611)-11401) attachment brackets. The nozzle used in the Phase I (Contract AF04(611)-11401) tests was a test rig uncooled nozzle and was considerably heavier than the dump-cooled design.

(3) Jackscrew and Side Deflection Effects

(U) The size of the jackscrew root diameter is based on critical speed, (the smallest diameter giving an acceptable critical speed), but the screw lead is a function of actuation time required and available motor drive speed. As shown in Table XXIX, an actuation time of 2 seconds causes a considerable weight increase because of the increase in horsepower and torque requirements. A translation time of 4.3 seconds requires a smaller screw lead and less horsepower.

(U) Side deflection of the nozzle is a critical factor under translation for the following reasons:

1. Provision of a definite envelope for installation of control and plumbing packages must be provided

2. Large deflections would interfere with ball nut operation

3. Coaxial translation is required to minimize erratic flow attachment.

(U) A comparison of side deflection effects on supported and unsupported jackscrews is presented in Tables XXX and XXXI. This comparison indicates that the track-supported jackscrew is best on a weight versus deflection basis. Material recommended for the track and support hardware is nickel base alloy, such as Inconel 718 (AMS 5596). The track also provides convenient mounting for position-indicating devices (not shown).

(U) Table XXIX. XLR129-P-1 Jackscrew Actuation Time Comparison

1500-1000 SRT Screw (Saginaw Part No.)		
Torque Required*	=	2010 in.-lb
1500 rpm	=	2 sec for 50 in.
Critical Speed	=	2055 rpm for 1.48 sec for 50 in.
Horsepower	=	22.4 required
Screw Lead	=	1.000 in./rev
Transfer G/B Tooth Width		1.750
New Motor Required		20% approximate weight increase 27.9 hp at 1610 rpm 2400 in.-lb stall torque
1500-0473 SRT (Saginaw Part No.)		
Torque Required*	=	1302 in.-lb
1500 rpm	=	4.3 sec for 50 in.
Critical Speed	=	1860 rpm for 3.4 sec for 50 in.
Horsepower	=	12.25 required
Screw Lead	=	0.473 in./rev
Transfer G/B Tooth Width		1.250
Present Moog Motor Acceptable		14.1 hp at 1550 rpm 1600 in.-lb stall torque

*Based on sea level static retraction at 100% flow.

(U) Table XXX. XLR129-P-1 Jackscrew Comparison, Supported vs Unsupported

Comparison Parameters	Track Supported 1.140 Root Diameter Screw	Unsupported Screw Root Diameter 1.140	Unsupported Screw $I_{screw} = I_{track}$ and screw	Unsupported Screw $Defl_{screw} = Defl_{track}$ and screw
Deflection, in.	0.020	1.70	0.150	0.020
Weight, lb	38	24	76	162
Weight/in.	0.695	0.4457	1.390	2.960
Root Diameter, in.	1.140	1.140	2.0644	3.420
Hole Diameter, in.	0.500	0.500	0	0
$I_{bending}$, $in.^4$	0.890	0.0796	0.890	6.750

Assumptions:

1. Each jackscrew supports one-third of total nozzle load.
2. $\rho = 0.288$ lb/$in.^3$ (density)
3. 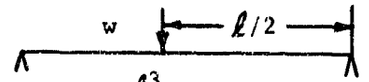

$$y = \frac{1}{48} \frac{w\ell^3}{EI}$$
4. $E = 30 \times 10^6$

(U) Table XXXI. XLR129-P-1 Jackscrew Comparison, Supported vs Unsupported

Comparison Parameters	Track Supported 1.140 Root Diameter	Unsupported Jackscrews Root Diameter 1.140	$I_{screw} = I_{track}$ and screw	$Defl_{screw} = Defl_{track}$ and screw
Deflection, in.	0.020	0.758	0.068	0.020
Weight, lb	38	24	76	105
lb/in.	0.695	0.4457	1.390	2.029
Root Diameter, in.	1.140	1.140	2.0644	2.800
Hole Diameter, in.	0.500	0.500	0	0
$I_{bending}$, in^4	0.890	0.0796	0.890	3.03

Assumptions:

1. Each jackscrew supports one-third of total nozzle load.
2. $\rho = 0.288$ lb/in.^{3}
3. 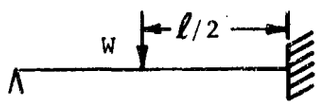

$$y = \frac{0.00932\ W\ell^3}{EI}$$

4. $E = 30 \times 10^6$

(U) Two track shapes are analyzed on a weight versus deflection basis and, as Table XXXII indicates, the hexagonal cross section has a weight advantage over the circular cross section. Fabrication of the circular cross section would be easier, however.

(U) Table XXXII. XLR129-P-1 Translation Mechanism Guide Comparison

	Hexagon	Circle	Circle	Circle
Deflection*, in.	0.020	0.292	0.0385	0.020
Weight, lb/Track	12.250	11.970	13.400	15.260
I_x, $in.^4$	0.890	0.890	0.890	0.890
I_y, $in.^4$	0.0295	0.00217	0.0295	0.172

Assumptions:

1.

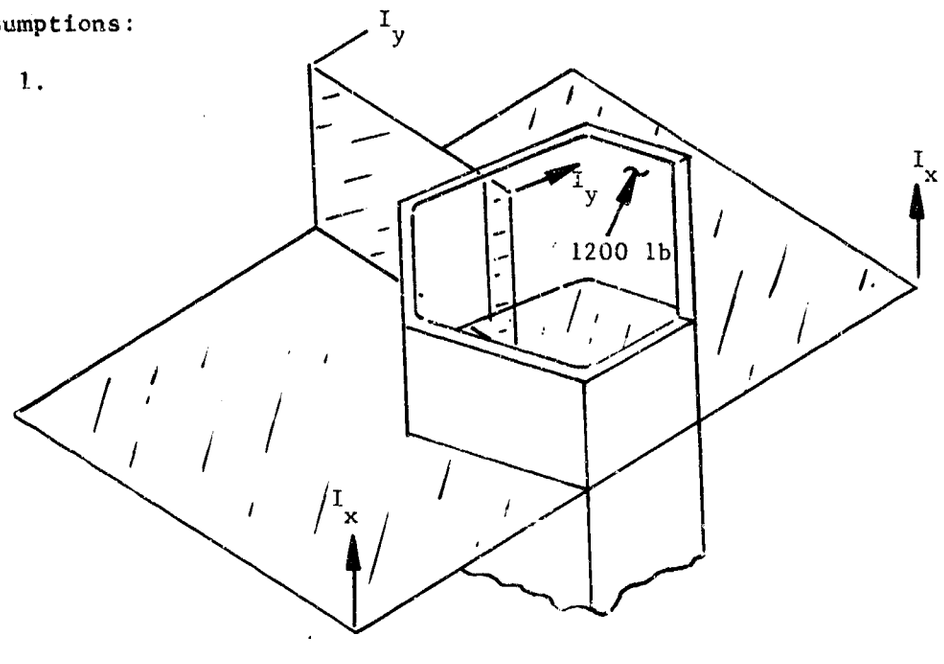

2. Deflection = Total bending of I_x cross section + local bending of I_y cross section.

3. Curved beam analysis * for "Circle" cross section

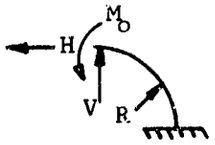

$$A_y = \left[\pi/4\ VR^3 + 1/2\ HR^3 + MoR^2\right]/EI$$

R = Radius

4. $E = 30 \times 10^6$

*Based on unsupported ends

(U) The center track support is the means of limiting side deflection to a minimum and strengthening the track against loads that would tend to open or unfold it. Stiffeners are also welded to the track to minimize this effect. The center support and upper support, which are not shown on the layout because of lack of definition of surrounding hardware, are of the pinned-truss type and have ample provisions for adjustment.

(U) Ball nut to translating nozzle attach point is accomplished by the use of a gimbal or universal joint in place of a spherical ball joint. The gimbal has more load carrying capability than the spherical joint, especially in the axial direction. Control of tolerances to minimize looseness is attained by controlling the fits on the gimbal assemblies. Inconel 718 (AMS 5662) is also recommended for use in the gimbal.

(U) Because an "off-the shelf" ball nut could present a problem in locking the threaded gimbal inner ring to the ball nut, an alternative ball nut with the gimbal inner ring integral with the ball nut housing is also being evaluated. This design eliminates carrying the jackscrew torque through the lock washer if the ball nut jams on the jackscrew.

(U) The transfer gearbox and drive motor mount are design-limited by translation envelope, motor horsepower, and stall torque. The transfer gear pitch diameter is defined by the translation envelope, therefore requiring a wide face width to meet power requirements. The mounting bracket material is Inconel X (AMS 5598).

(U) The 3-piece ring gear ball bearing retainer also serves as the lower mount for the jackscrew track and final travel stop for the nozzle. A 3-piece protective titanium alloy cover is also furnished for the ring gear.

D. MAIN BURNER CHAMBER

D. MAIN BURNER CHAMBER

1. Introduction

(U) The main burner thrust chamber design is based on the copper wafer cooled thrust chamber demonstrated during Phase I (Contract AF04(611)-11401).

(U) A study of the cooled wafer liner was conducted to provide a chamber liner that is not radially pressure loaded in the cylindrical portion and to reduce the bolt circle diameter of the main injector attachment flange for reduced weight. A number of main burner chamber liner configurations were studied for the most advantageous configuration. The selection of the best design will be based on the following considerations: heat transfer and pressure drop, structural and mechanical integrity, and weight.

2. Summary, Conclusions, and Recommendations

(U) Structures and heat transfer studies of conceptual configurations are in process. The final selection will be made after completion of these studies.

(C) Preliminary studies indicate that either a 32-tube or 96-tube design for providing coolant to the wafer liners coolant zones appears to be the most advantageous configuration. This is the configuration being analyzed in complete detail.

3. Analysis

(U) A design analysis of the Phase I (Contract AF04(611)-11401) main burner cooled thrust chamber configuration is in progress for improved mechanical integrity and reduced weight. Figure 362 shows two schemes in the cylindrical portion, Figure 363 shows three schemes in the throat region, and Figure 364 shows two schemes in the diverging section.

(C) The 32-tube design shown as scheme 1 of Figure 362 provides for coolant distribution through tubes brazed into the copper liner with each tube supplying three orifices. All orifices can be changed by removing the liner and removing the plug permitting access to the orifice. The alternative orifice design provides for orifice replacement by unscrewing the orifice. It eliminates the plug and reduces the outside diameter of the liner, the case and the injector mounting flange by 0.200 inch. The two orifice schemes are shown in Figure 365.

(C) The 96-tube design shown in Figure 366 is an extension of the 32-tube design providing coolant flow to each zone at eight points. The orifices are accessible from the rear end after removing the regenerative skirt. This design permits the same 0.200-inch reduction in injector flange bolt circle diameter. In addition, the radial thickness of the heat exchanger is increased from the 32-tube design.

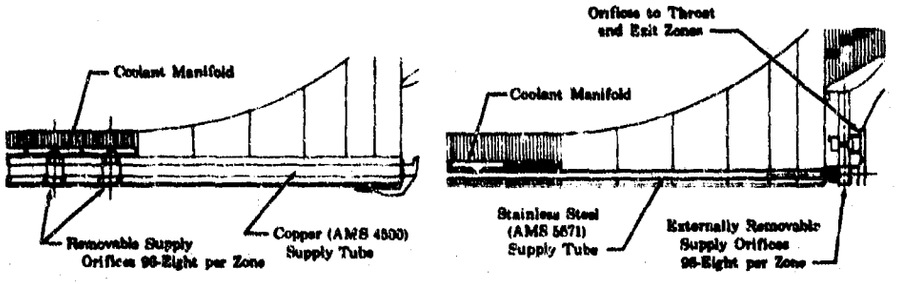

Scheme 1 Scheme 2

CONFIDENTIAL

(U) Figure 362. Main Burner Chamber Liner Cylindrical Schemes FDC 25664A

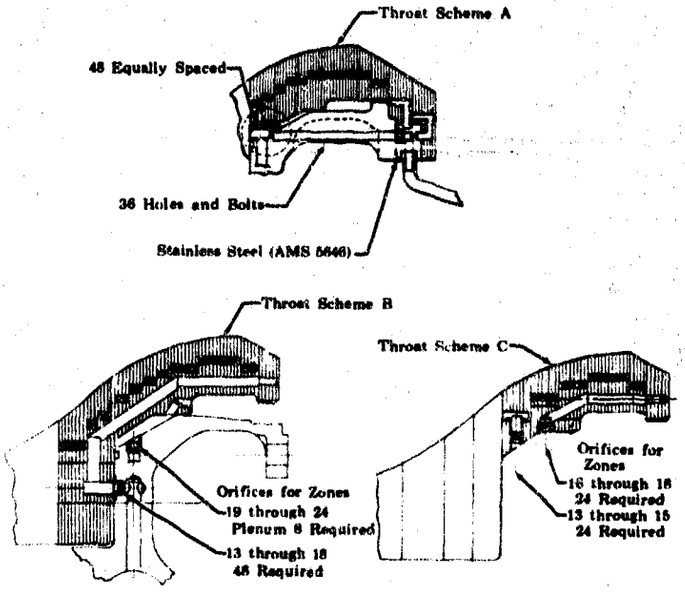

CONFIDENTIAL

(U) Figure 363. Main Burner Chamber Liner Throat Schemes FDC 25679A

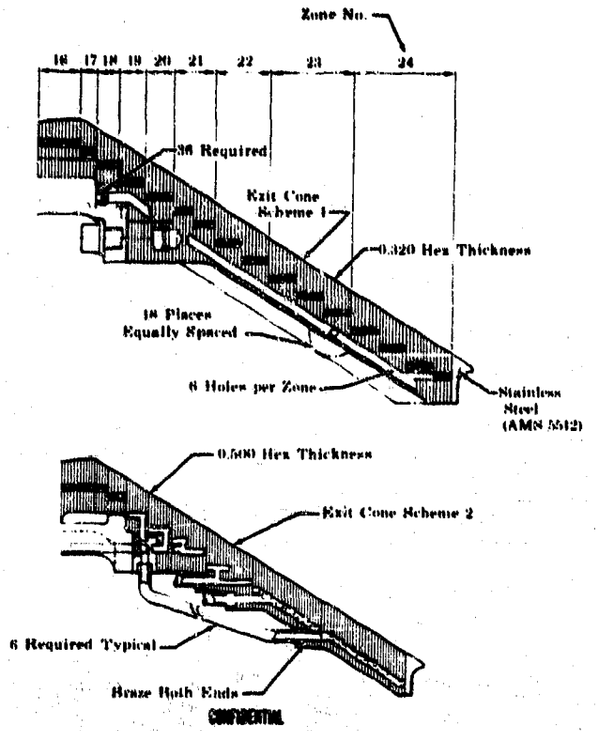

(U) Figure 364. Main Burner Chamber Liner Diverging Section FDC 25680A

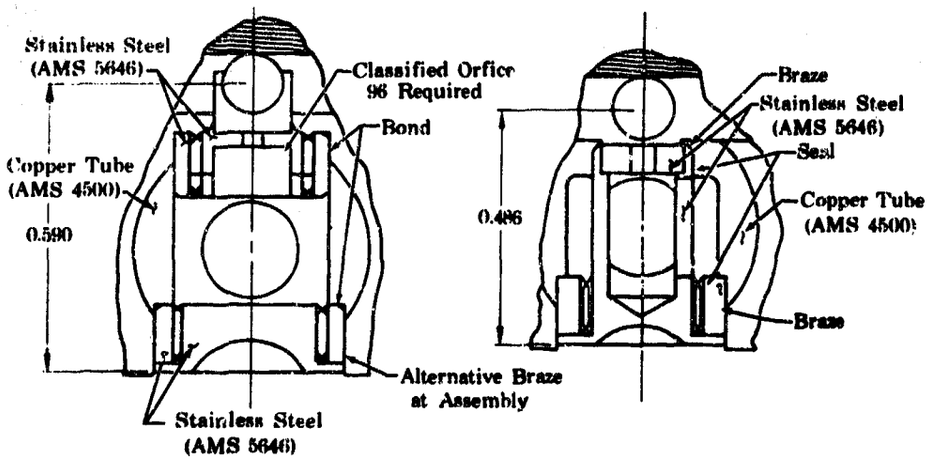

(U) Figure 365. Orifice Schemes FDC 25681A

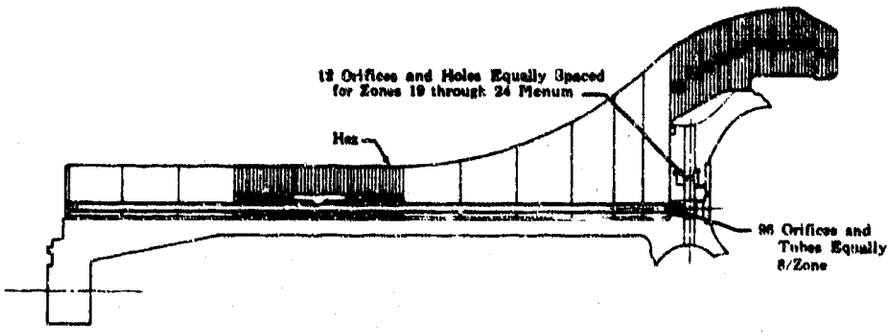

(U) Figure 366. 96-Tube Design FDC 25682

(U) Manifolding in the throat region may be accomplished by flowing high-pressure coolant to an annulus at the outside of the copper throat. From this high-pressure annulus the coolant is supplied to zones 13 through 18 through eight orifices per zone and through eight orifices to a plenum area for zones 19 through 24 as shown in Figure 367.

(U) Another alternative, as shown in Figure 368, shows that zones 13 through 18 can be supplied from the passages drilled in the case and orifices in the case with internal manifolding to eight points in each zone. This approach is similar to Phase I (Contract AF-4(611)-11401) except for the location of the orifices. This does reduce the radial inward load on the chamber liner at the throat.

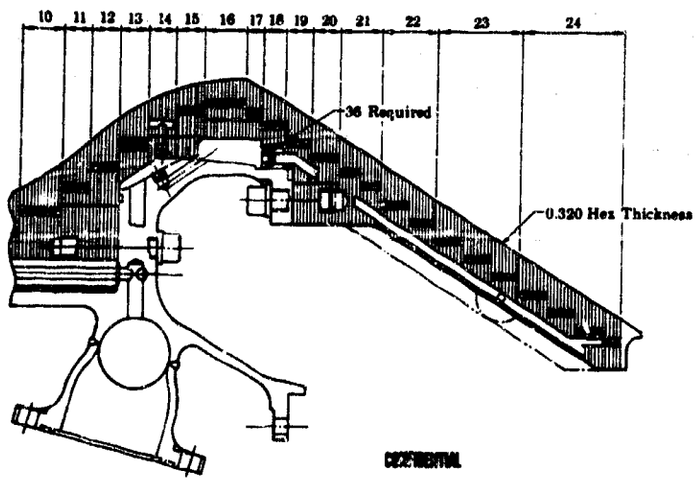

(U) Figure 367. Throat Region Manifolding (Scheme 1) FDC 25683

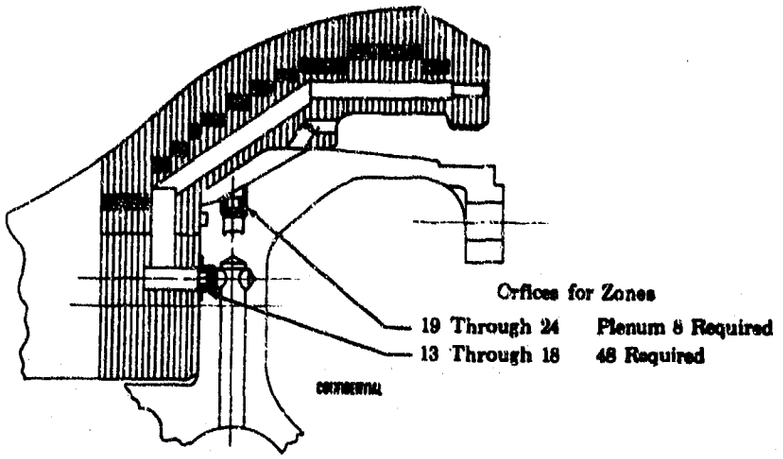

(U) Figure 368. Alternative Throat Region Manifolding (Scheme 2) FDC 25684

(U) A third alternative manifolding scheme, which is shown in Figure 369, involves venting most of the area outside of the chamber liner at the throat to the pressure at the liner separation plane. This scheme could also be manifolded internally for zones 13 through 18 as shown in Figure 369. This eliminates the high-pressure inward load on zone 13. This scheme also involves external manifolds for the diverging section of the liner, as shown in Figure 369, thus permitting a reduction in copper thickness because excess material is unnecessary for internal passages as in Phase I (Contract AF04(611)-11401) hardware.

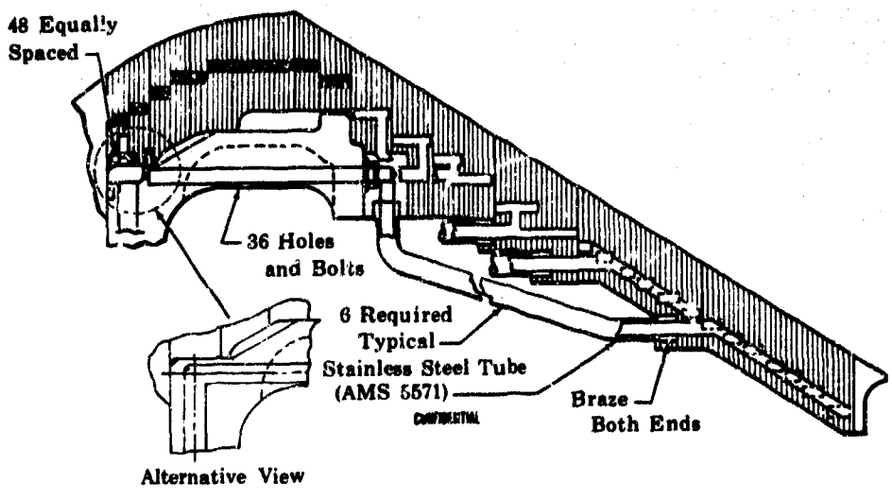

(U) Figure 369. Alternative Throat Region Manifolding (Scheme 3) FDC 25685A

(C) From the heat transfer data produced by a preliminary analysis, all the above discussed schemes are workable with acceptable manifold losses, either as described or with a reasonable variation of the concept. Heat exchanger thicknesses vary, however. The various approaches discussed represent the following percentage of Phase I (Contract AF049611)-11401) heat exchanger thickness:

Scheme	Phase I (Contract AF04(611)-11401) Thickness, %
Cylindrical Selection	
32-Tube Design (main orifice)	45.5
32-Tube - Small Orifice Design (alternative orifice)	45.5
96-Tube Design	86.5
At Exit or Diverging Cone	
Phase I (Contract AF04(611)-11401) Liner (Baseline)	100
Internal Manifold 32- or 96-Tube	45.5
External Manifold 32- or 96-Tube	86.5

(U) In all cases, the configurations shown are not loaded by transpiration coolant supply pressure across the liner from OD to ID as in the Phase I (Contract AF04(611)-11401) hardware. This reduces the structural requirements of the liner by eliminating the coolant differential pressure and allows running the liner at higher average copper temperatures. Reducing the heat exchanger thickness increases average copper liner temperature but not the ID wall temperature. This is shown in the preliminary curves provided as Figures 370 through 372.

(C) The 96-tube chamber scheme offers advantages in allowing the removal of orifices without requiring disassembly of the outer case and chamber liner. In addition, the 96-tube scheme provides the possibility of additional structural support by permitting welding of the stainless steel tubes to the stainless steel end plates.

(C) The comparison provided in Table XXXIII of the Phase I (Contract AF04(611)-11401) and the discussed schemes show the design with an externally manifolded exit cone to be the lightest in weight. This is true for both the 32 and 96-tube chambers.

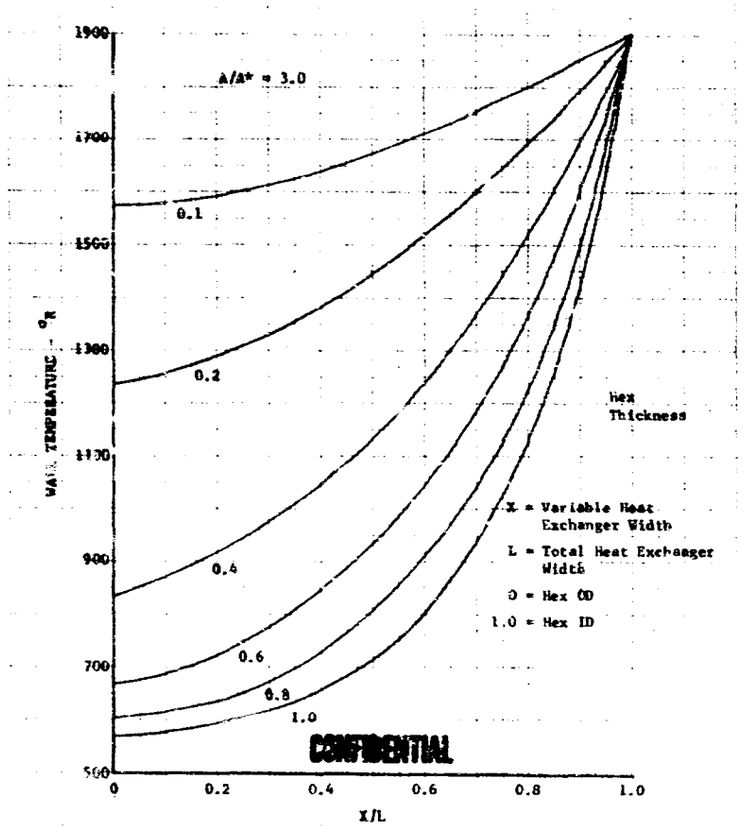

(U) Figure 370. Wall Temperature Variations for Cylindrical Section DFC 68982

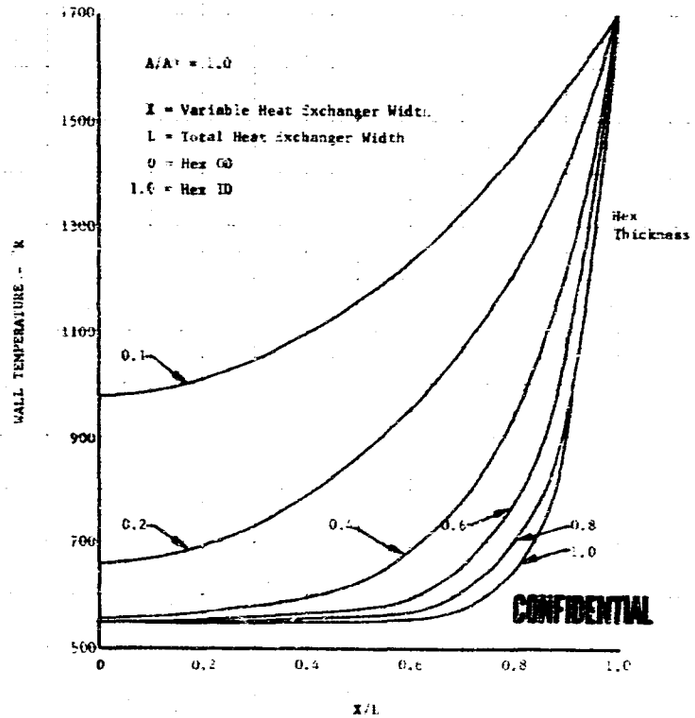

(U) Figure 371. Wall Temperature Variations for Throat Section DFC 68983

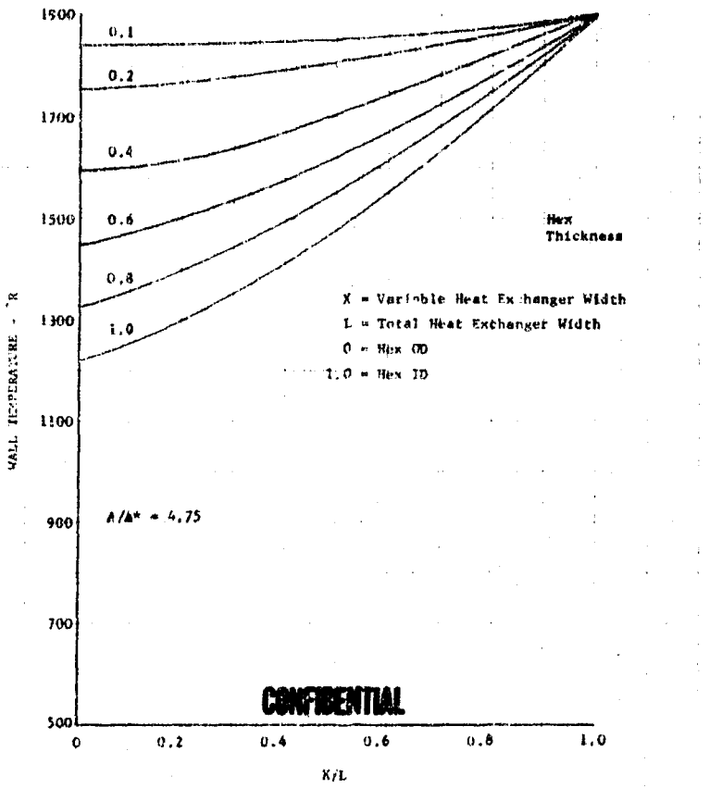

(U) Figure 372. Wall Temperature Variations for Exit Section DFC 68984

(U) Table XXXIII. Comparison of Phase I (Contract AF04(611)-11401) and Current Design Schemes

	Chamber Liner (lb)	Case and Support (lb)	Case (lb)	Total (lb)
Phase I (Contract AF04(611)-11401)	350.5	129.0		542.5
32-Tube Design	319.0	-	131.0	450.0
32-Tube Design*	300.5	-	128.6	429.1
96-Tube Design*	300.5	-	128.6	429.1
32 or 96-Tube Design* and Phase I (Contract AF04(611)-11401) Type (2 piece case)	300.5	173.0	-	473.5
32 or 96-Tube Design* and External Manifolded Exit Cone	288.5	-	130.0	418.5

*Case Bolt Circle Reduced by 0.200 in. Diameter

E. TRANSITION CASE

E. TRANSITION CASE

1. Introduction

(U) The transition case is that component of the engine that acts as the mounting structure for three major engine components; namely, the preburner, oxidizer pump, and fuel pump. It is a pressure vessel that ducts the fuel-rich gases from the preburner through the fuel and oxidizer pump turbines and to the main burner injector. The transition case is designed to split the gas flow to provide adequate gas flow into each of the turbines; the fuel turbine requiring approximately twice the flow needed to drive the oxidizer turbine. A design analysis was initiated to determine the basic design approach for the transition case, gas flow ducts, and coolant liners. The design analysis of the transition case was substantiated by sub-scale transition case model tests that assisted in the evaluation of the selected design.

2. Summary, Conclusions, and Recommendations

(U) A design concept of intersecting segmented spheres is being proposed for the transition case configuration. Because a sphere is inherently a more efficient pressure vessel than a cylinder or cone, this concept will provide the following advantages:

1. Lighter construction because a thinner shell is required to resist pressure; the material is loaded in tension, not bending.

2. Easier construction because intersecting spheres provide circular intersections, where stiffening is required, instead of elliptical intersections for cylinders and cones, where even more stiffening would be required.

3. A decreased bending stress at the flanges and other boundaries because of the radial load component.

(U) Five intersecting sphere configurations were studied initially; namely, three co-planar component designs and two canted component designs. Hand calculations and computer programs were conducted on each of these designs to determine if they could perform under the predicted pressures and stresses. Two of these designs; namely, one canted version and one co-planar version were selected for further study and model testing. In addition, a truncated spherical model was selected that simulated construction and load conditions anticipated for the inner duct center body.

(U) The truncated spherical model was tested under pressure until the proportional limit of the material was reached at local areas. A review of these data indicates good correlation between the test results and the predicted results. The predicted stresses for a complete sphere (Pr/2t) are less by a factor of 2 than those for a cylinder (Pr/t). Test results verify the theoretical tensile stress relationship.

(U) A model, which simulated the intersection of the basic sphere and a sphere segment for the co-planar component design, was tested. The results of these tests show that the loads required to reach the proportional limit of each model was generally higher than predicted because of the biaxial stress field. There were instances where applied loads were limited to lower values than predicted, because of bending concentrations around the ring and shell intersections resulting from weld mismatch.

(U) A thrust structure model, representing the canted component design was also tested. These tests indicated that the load in the shell is lower than the predicted value, and that the rings take a greater portion of the load than the shell because the load was distributed along the stiffest path, which was the intersection of the thrust pad and the three component rings.

(U) Studies were conducted on the internal ducts of the transition case that showed the co-planar concept was lighter than the canted concept, and that the ducts should be cooled.

(U) It was concluded that for the overall design, the co-planar transition case offers the best solutions regarding the inner duct design, cooling, thrust load handling, assembly, and manufacturing.

3. Design Analysis

(U) The design approach for the transition case, which is chiefly a pressure vessel, was to minimize or eliminate discontinuity stresses by endeavoring to take all the loads in membrane. Because the three major engine components, the preburner, oxidizer pump, and fuel pump, are mounted to a common duct, the method of intersecting these major components defines the engine package. Because the ideal pressure vessel is a sphere, the concept of intersecting segments of spheres was the basis for this design instead of intersecting cylinders or cones. At the intersections, a ring is provided to take the combined radial loads imposed by the two intersecting spheres. The cross-sectional area of the ring is sized to match the radial growth of the spheres to limit the stress to that of membrane. Theoretically, the ring area would have to be applied on the intersecting line only (a line area), which is impossible. Therefore, there is some stress discontinuity, but this can be handled by faring the shell into the ring. The thrust load is taken in membrane in the center sphere by intersecting it with an inverted cone containing the gimbal. An effort is made to make the pressure area term enclosed by the intersection circle equal to the thrust load.

(U) The flanges are designed such that the shell (tangential membrane) load passes through the centroid of the flange cross-sectional area. This load path will minimize or eliminate flange twist and pry-up, thereby ensuring better sealing and lower bolt load requirements.

(U) The design approach as outlined above would provide the following advantages:

1. Lighter structure

   a. Thinner shell to resist pressure

      Stress = Pr/t (Cylinder)

      Stress = Pr/2t (Sphere) = 1/2 of cylinder stress

   b. Discontinuity stresses minimized or eliminated

2. Easier construction because intersecting spheres provide circular intersections, where stiffening is required, rather than elliptical intersections created by intersecting cylinders and cones where even more stiffening would be required

3. Less bending stress at flanges and other boundaries because of the radial load component provided by the sphere membrane. This component also causes the flange to grow.

4. More reliable and predictable structure because of pure membrane conditions.

(U) The design criteria used were as follows:

Design Pressure	= 1.2X (operating pressure) (to account for overspeed condition)
Inertia Loads	= 10g maneuver loads + gyroscopic moments
Combined Acceleration	= 10g's axial with 2g's transverse 6.5g's axial with 3g's transverse 3g's axial with 6g's transverse
Case Temperature	= 560°R
Material	= Inconel 718 (AMS 5663)
Allowable Combined Stress Limit	= 85% of 0.2% yield

(U) The center sphere is sized by combining pressure, inertia, and thrust loads and limiting stress to 85% of 0.2% yield. The component spheres are sized to grow at the same rate as the center sphere under pressure. Spheres under equal pressure will grow at the same rate at their intersection in the intersection plane if stress is constant. That is,

$$S_1 = \frac{Pr_1}{2t_1} = \frac{Pr_2}{2t_2} = S_2$$

The component spheres are then checked for a combined stress found by superimposing the axial blow off, because of component pressures, with the pressure stress.

(U) The two basic transition case configurations that were selected for study were the canted configuration and the co-planar configuration. These two configurations are shown in Figure 373. It can be seen that the canted component configuration has the components entering the transition case at an angle, and the co-planar configuration has the components entering perpendicularly, all in the same plane. Engine models were made for the purpose of studying the engine packaging aspects of these two transition case configurations. Figures 374 and 375 show some of the various engine models made with the canted and co-planar transition cases. These engine models showed that insofar as plumbing was concerned the engine packaging envelope was improved; however, the improvement was not significant. From this study, a model testing program evolved that included a truncated sphere model, an intersecting sphere model, and a canted model. These three basic model types are shown schematically in Figure 376.

(U) Comparison of the co-planar and canted versions show that either were prime candidates for selection. For example, the canted version was attractive because of the weight savings; specifically, 263 lb versus 286 lb for the co-planar as shown in Table XXXIV. The co-planar configuration was attractive because of the ease of fabrication, and the elimination of a high internal duct thrust load inherent in the canted component design.

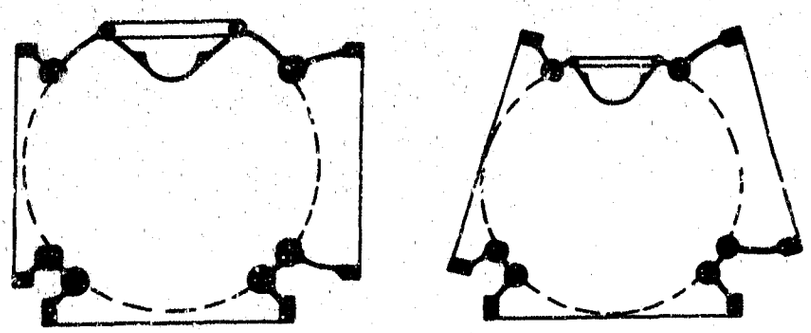

(U) Figure 373. Candidate Transition Case Configurations FD 27632

(U) Figure 374. Component Arrangement Study With Canted Transition Case FD 25762

(U) Figure 375. Component Arrangement Study With Co-Planar Transition Case FD 25763

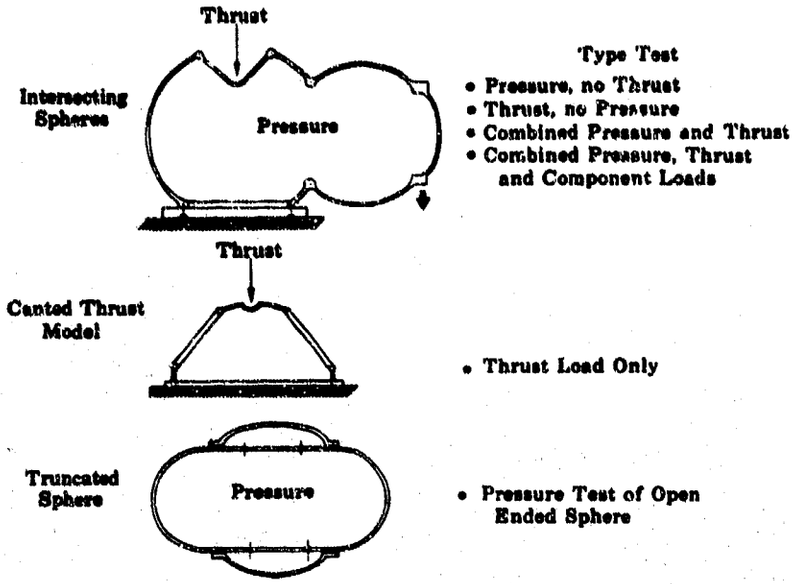

(U) Figure 376. Structural Model Test Program FD 24310A

(U) Table XXXIV. 250K Transition Case Weight Breakdown

	15 degree Canted	Co-Planar
Dome Shell	25	33
Injector Ring	49	49
Fuel Pump Ring	58	64
Preburner Ring	46	46
Oxidizer Ring	78	78
Gimbal	7	16
Total	263 lb	286 lb

(U) Design studies were also conducted on the internal ducts of the transition case, particularly with respect to the effects that the canted and co-planar concepts would have upon the internal ducts. Figure 377 shows a side view of the canted spherical internal duct configuration. In this view, the hot gases are flowing down into the main burner injector, which would be at the bottom of the figure. Figure 378 shows a top view of the co-planar internal duct configuration. In this view, the hot gases are flowing toward the main injector in the center and perpendicularly into the figure. One of the problems encountered with the canted internal ducts was that very large axial loads were induced on the lower center duct towards the main burner injector. For example, a 15-degree canted internal duct produced a 55,800 lb load, and a 27-degree canted internal duct produced a 95,000-lb load. These axial loads were caused by the differences in areas between the upper and lower portions of the ducts; the lower portions having

more area, and therefore, greater pressure loads. This large axial load was one of the disadvantages of the canted transition case configuration. Heat transfer studies were also made regarding cooled and uncooled internal ducts. Table XXXV summarizes the results of these studies, which shows that the cooled internal ducts are definitely lighter than uncooled or insulated ducts. Therefore, the inner ducts will be cooled by using doubled wall liners and having hydrogen coolant pass through the passages of the double wall.

(U) The co-planar configuration was selected, and the final design was initiated.

4. Model Testing

a. General

(U) The purpose of the model test program was to provide a comparison of the measured and calculated stresses and stress distributions in the shell structure. Three different type models were tested; namely, a (1) truncated sphere as shown in Figure 379, (2) an intersecting sphere, a co-planar design, as shown in Figure 380, and (3) a canted ring model as shown in Figure 381. The testing of all models was completed. The general type of structural tests conducted on the models is shown in Figure 376.

(U) A stress-coat was used on all the models to locate the areas of maximum tensile stress. Strain gage rosettes were then applied to models according to the stress-coat patterns. Rosettes were located and oriented to allow separation of membrane and bending stresses. Dial indicators were also used to measure the overall deflection of the model. In addition, the intersecting sphere model had cap and base flange bolts instrumented with uniaxial strain gages to calibrate and measure the assembly load, and to determine the increased bolt load and bending caused by combined test loading.

(U) Pressure tests were conducted with the truncated sphere model, and thrust tests were conducted on the canted ring model. The intersecting sphere model had tests with individual and combined loads of pressure, thrust, and shear.

b. Truncated Sphere Model Tests

(U) The truncated sphere model, shown in Figure 379, was the first model to be tested in the program. This model was designed for a pressure test to evaluate the stress distribution.

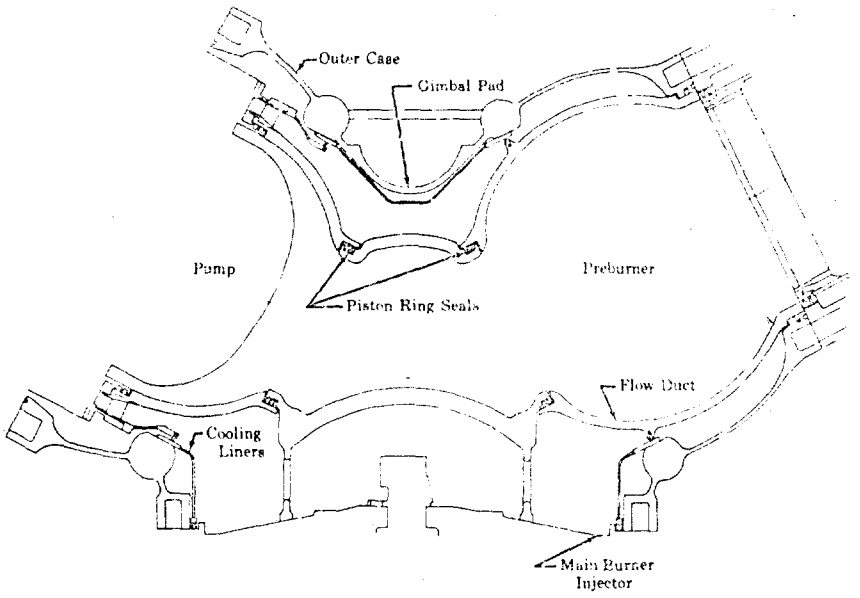

(U) Figure 377. Canted Spherical Internal Duct Configuration FD 24311B

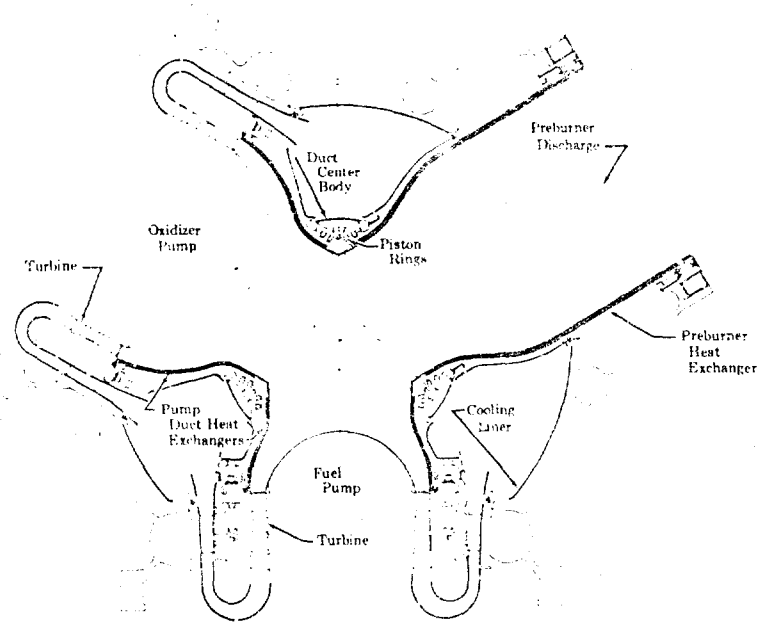

(U) Figure 378. Co-Planar Internal Duct Configuration FD 25764

(U) Table XXXV. Cooled Duct vs Uncooled Duct Weight Study

Material	Temperature (°R)	Design Limit (psi)	Duct Weight (lb)
IN 100 (AMS 5397) Cast	2200 Uninsulated	20,000 LCF Unacceptable	125
Waspaloy (AMS 5544)	2050 Insulated	25,000 1% Creep	130
Waspaloy (AMS 5544)	1100 Cooled	85,000 85% 0.2% Yield	70
Inconel 718 (AMS 5596	1100 Cooled	106,000 85% 0.2% Yield	60

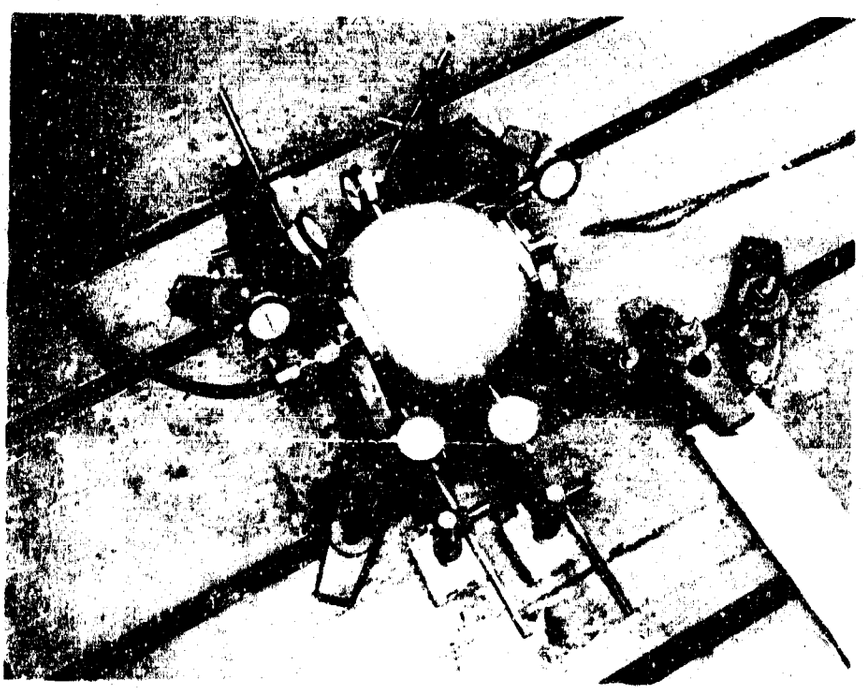

(U) Figure 379. Truncated Sphere Model FD 78157

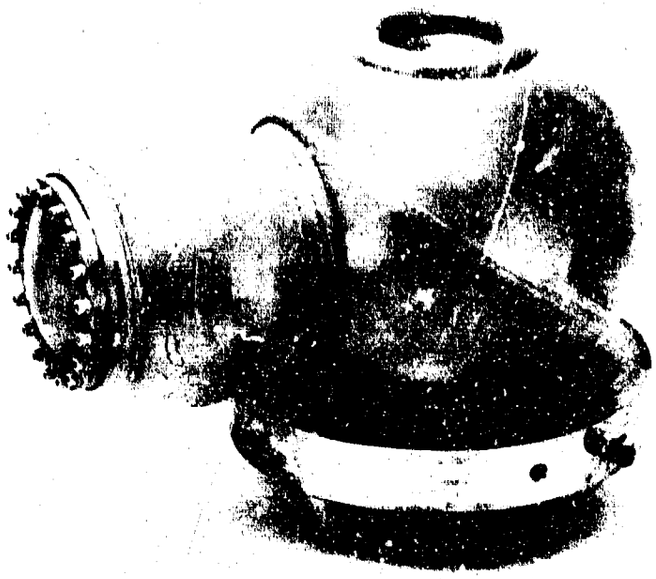

(U) Figure 380. Intersecting Sphere Model FE 79390

(U) Figure 381. Canted Ring Model FE 79193

(U) The truncated sphere model was fabricated of stainless steel (AMS 5647). This model was essential a sphere with a hole in each end, which was pressurized by a cylinder inserted through the holes in order to determine the stress distribution and the deflections of this pressure vessel. This model was also an attempt to simulate the load conditions anticipated for the inner duct center body as indicated in Figure 378. Stress-coat was applied to locate the areas of maximum tensile stress under internal hydraulic pressure as shown in Figure 382. Fourteen two-gage strain gage rosettes were used according to stress-coat patterns and oriented to allow separation of membrane and bending stresses as shown in Figure 379. Six dial indicators were located to measure the overall deflection of model. Internal pressure was hydraulically applied in increments up to 400 psig where strain plots indicated the proportional limit.

(U) Figure 382. Truncated Sphere Model Stress-Coat Test FE 78833

(U) The test results of the strain gage rosette are shown in table XXXVI. The strain gage rosette locations are shown in Figure 383. The correlation of theoretical spherical membrane stresses and actual stresses is shown in Figure 384. The major portion of the hoop stress falls well below that for a cylinder (Pr/t). If a cylinder had been used here instead of a truncated sphere, the hoop stress would have been Pr/t, and the meridian stress would have been zero. Therefore, the induced blow-off load caused by the configuration lowers the hoop stress thereby increasing the meridian stress. This is an advantage as can be seen in a completely closed sphere where the hoop and meridian stresses both

equal Pr/2t, as shown in Figure 385, are exactly half the hoop stress in a cylinder. The test, which was limited to the proportional limit of the material, indicated higher elastic stresses at local areas than yield stress indicated by a uniaxial pull test of the vessel material. Therefore, the advantage of inducing biaxial stress is twofold, first, it reduces the hoop stress, and second the yield point for the material in a biaxial stress field is higher than the uniaxial allowable.

(U) Table XXXVI. Truncated Sphere Stress Data
(400 psig Internal Pressure)

Strain Gage Rosette No.	Directional Stress (psi) Hoop	Axial	Membrane + Bending Stress (psi) Hoop	Axial
1	22,100	5300		
2	22,900	3000	22,500 ± 400	4150 ± 1150
3	25,000	8300		
4	25,000	4700	25,000 ± 0	6500 ± 1800
5	21,700	10,100		
6	21,900	9100	21,800 ± 100	9600 ± 500
7	18,700	7300		
8	18,000	14,500	18,350 ± 350	10,900 ± 3600
9	20,600	9200		
10	21,400	9200	21,000 ± 400	9200 ± 0
11	25,300	9500		
12	24,400	4600	24,900 ± 500	7100 ± 2400
13	22,900	5800		
14	22,000	2500	22,450 ± 450	4200 ± 1600

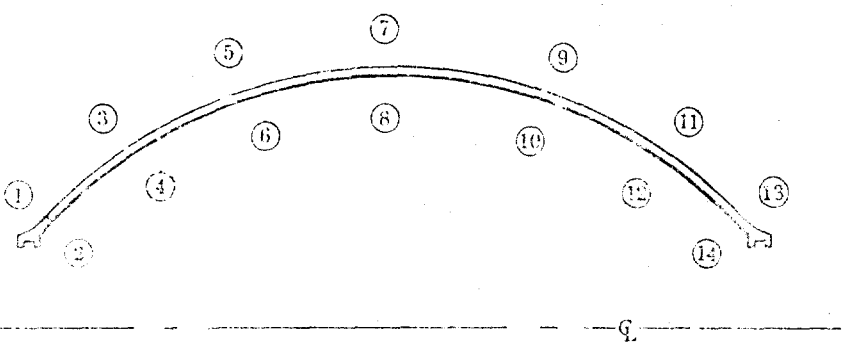

(U) Figure 383. Strain Gage Rosette Locations FD 25765

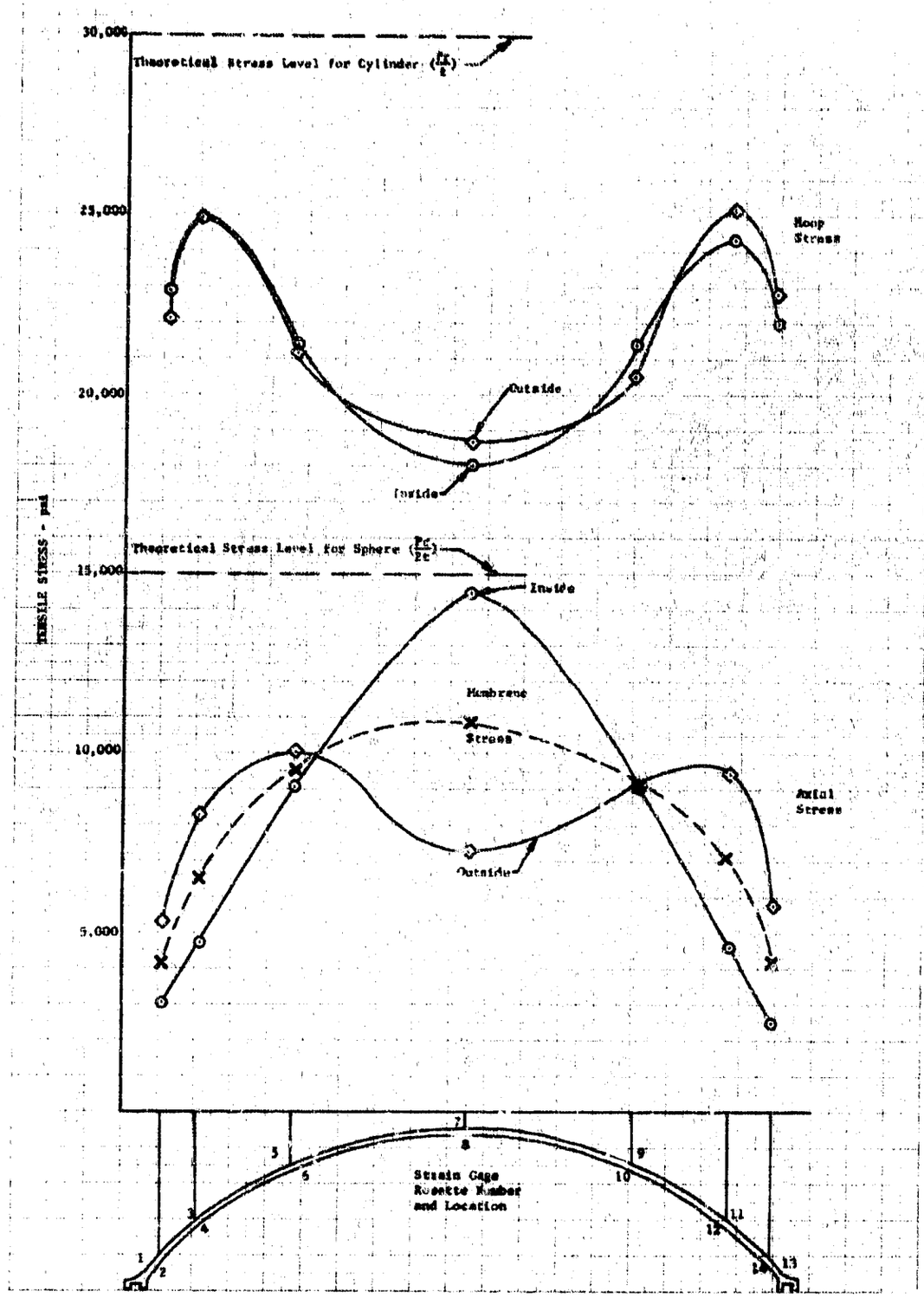

(U) Figure 384. Correlation of Theoretical Spherical Membrane Stresses and Actual Stresses

DF 68975

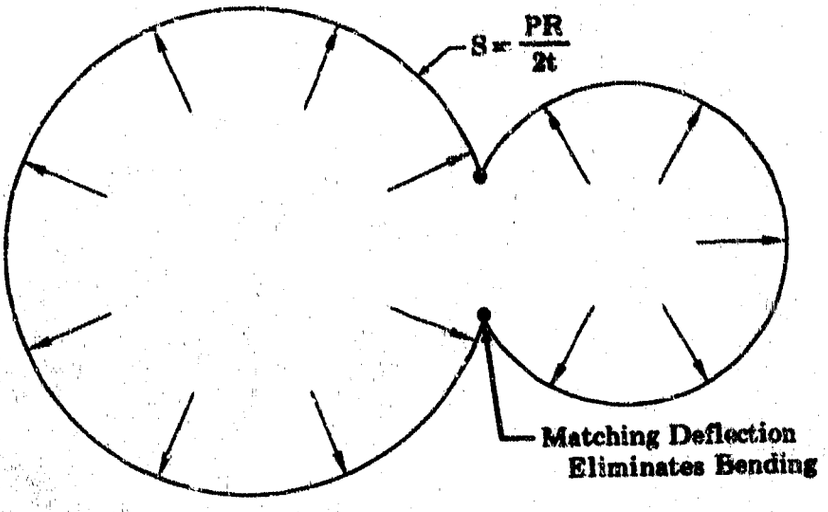

(U) Figure 385. Wall Thickness Is Reduced in Spherical Pressure Vessel FD 23200

c. Intersecting Spheres Model Tests

(U) The intersecting spheres models, one of which is shown being tested in Figure 386, had tests conducted with individual and combined loads of pressure, thrust, and shear. These loads were increased in increments to the point where strain plots indicated that the proportional limit of the model had occurred locally. The test results show that the loads required to reach the proportional limit of each model was generally higher than predicted because of the biaxial stress field. Limitations in loads, because of bending concentrations around the ring and shell intersections, resulted from weld mismatch. As a result of the test program, the design approach of the intersecting spheres concept was modified to decrease the weight and to increase the strength.

(U) A Pressure/Thrust/Shear Model, as shown in Figure 380, consisted of two intersecting spheres with a stiffening ring at the intersection. The ring was sized to grow at the same rate as the two spheres. One sphere was 9.00-inch in diameter with a 0.125-inch thick wall, and the other sphere was 13.00-inch in diameter with a 0.180-inch thick wall. An inverted cone was provided in the larger sphere to take a punch or thrust load simulating the gimbal thrust load of the engine. A mount shear bracket was also provided to be attached to the small sphere flange. This provided a means to simulate the shear moment g loads imposed on the transition case by the components.

(U) Prior to testing, the model was stress-coated. A typical stress-coat after test is shown in Figure 387, which shows the areas of highest stress concentration under the given conditions. This, in turn, indicated

where the strain gages should be applied. The test model described above was tested as follows:

1. Pressure and thrust combined
2. Thrust
3. Pressure
4. Shear load on small sphere
5. Combination of shear, thrust, and pressure

This order was followed to reduce the risk of rupture between tests.

(1) Pressure and Thrust Combined Test

(U) When performing the first test, the thrust-to-pressure ratio was kept at 19.65. That is, for 1 psi pressure, the thrust was 19.65 lb (Thrust = 19.65 P). This ratio results from the area of the thrust cone and sp intersection. $A = \pi \gamma 1.2 = \pi(2.5)^2 = 19.65$. This ratio was maintain until the strain gages indicated the proportional limit of the material had been reached.

(U) The predicted pressure and thrust was:

	Pressure (psi)	Thrust (lb)
Proportional limit (approximately 24,000)	975	19,200
0.2% yield	1220	24,000
Burst - 75,000 psi	3050	60,000

The predicted maximum stress point on the shell was 1.5 to 2.0 inches down from the center of the stiffening ring at the thrust cone.

(2) Thrust Test

(U) The thrust in this test was applied gradually until the strain gages indicated the proportional limit had been reached. The maximum stress points were expected at the cone ring and at the mount ring because of the boundary conditions causing bending in addition to the membrane loads. The predicted maximum thrust was:

Proportional limit (approximately 24,000 psi)	24,000 lb
Buckling load	27,500

The buckling load was below the 0.2% yield value, which would be 30,000 lb. It was determined by the empirical formula

$$\frac{Pr}{Et^3} = \sqrt{0.152\ (\lambda + 74.9)} - 2.88$$

where

$$\lambda = \frac{b^4}{r^2 t^2}$$

$b = r \sin \phi$ (angle at load point)

P = thrust

(U) Figure 386. Testing Intersecting Spheres Model FE 79366

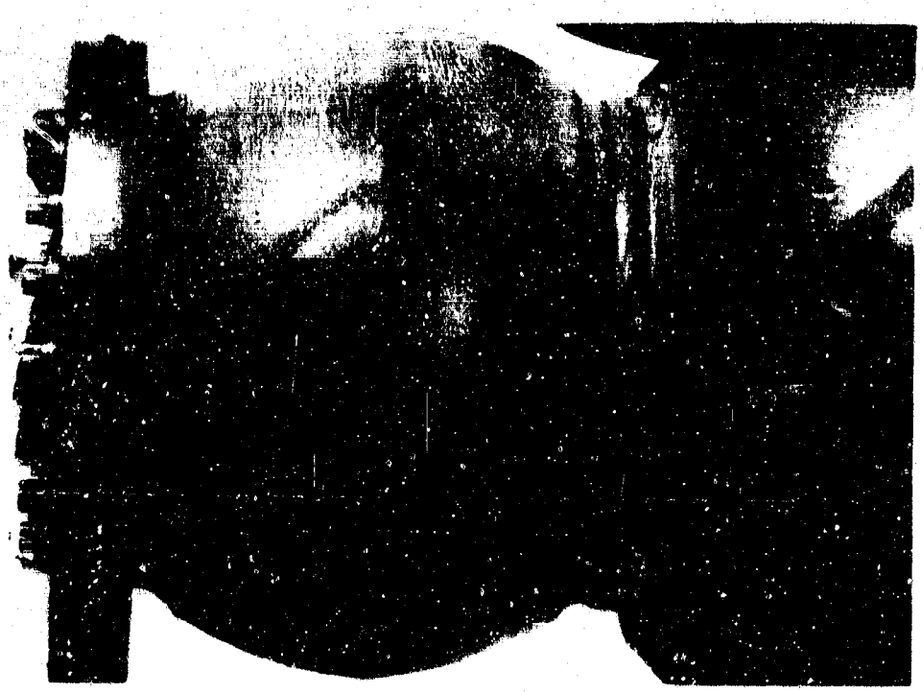

(U) Figure 387. Typical Stress-Coat After Test FE 79416

(3) Pressure Test

(U) The pressure was applied gradually until the proportional limit was reached. The maximum stress was expected in the cone near the stiffening ring. A secondary maximum stress point was expected in the spherical shell near the cone ring and near the mount ring because of bending at these boundaries. The predicted maximum pressure was:

Proportional limit (approximately 24,000 psi)	300 psi
0.2% yield (30,000 psi)	375 psi
Burst (75,000 psi)	562 psi

Calculations also indicated a high bending stress in the cone near the stiffening ring.

(4) Shear Load on Small Sphere Test

(U) Shear was applied gradually by means of the bracket provided until the strain gages indicated the proportional limit had been reached. Care was exercised to observe any indication of buckling on the compression side of the small sphere as well as on the large sphere. The literature does not contain much information regarding the buckling of spherical shells, which makes analytical predictions difficult in this area. The predicted maximum shear was:

	Shear (lb)
Proportional limit (approximately 24,000 psi)	5,800
0.2% yield (30,000 psi)	7,250
Ultimate (75,000 psi)	18,000

Strain gages were placed around the shells near the stiffening ring at the intersection of the two spheres and around the larger shell at the mount ring.

(5) Combination Shear, Thrust, and Pressure

(U) This test was conducted to check super-position of stresses calculated for the preceding cases. The maximum predicted pressure and shear were

	Pressure (psi)	Thrust (lb)	Shear (lb)
Proportional limit	362	7,100	357
0.2% Yield	450	8,850	460
Burst	1,130	2,210	1,145

(6) Test Results

(U) Hand calculations were made using actual load conditions imposed on the model. A comparison of the actual stresses and the calculated stresses is shown in Table XXXVII. The tests were stopped when strain gage plots became nonlinear, indicating that the proportional limit had been reached at some particular point. It should be noted that the limiting stress occurred at boundary planes (shell and ring intersections) and at weld joints. The test data and hand calculations agreed very closely in regions removed from the boundary planes. A very high stress was measured at the weld joints, which inspection by probe-graph showed to have a mismatch of from 50 to 100% of material thickness. These high stresses are made up of membrane and bending stresses. It can be shown that mismatch at joints induces a bending moment proportional to the membrane load and offset, which in turn, induces an additional membrane in both hoop and meridian directions as well as an additional moment in the hoop direction. The induced membrane stress by bending might be as high as 3 to 4 times greater than the bending stress that induced it. This induced membrane is a function of the meridian angle and boundary conditions as well as the moment, and is a result of lateral and meridian restraint of an element in a shell of revolution. Upon first examination of test data, it was thought that the stiffening ring at the intersection of the two spheres was improperly sized. Theoretically there should have been little or no moment at this plane. For purposes of proving this point, the stiffening ring was first considered infinitely stiff and a moment was calculated. The moment calculated from the test data was approximately 6 times greater. Next a moment was calculated using the mismatch offset directly, which is somewhat conservative. This moment compared with the one indicated by strain gage. It should be noted that the predicted proportional limits were considerably higher on the model than those measured by uniaxial pull tests of the shell material. The higher proportional limit is caused by the combination loading, which induces material interaction. It has been shown in tests that when a bar is subjected to combined tensile and bending loads that the proportional limit is increased by a minimum of 1.3 times the uniaxial value. It was also substantiated that there is an increased allowable of 1.25 times the uniaxial data for a biaxially loaded element where the loads have a ratio of 2 to 1 to each other. As noted above, the model tests substantiate these facts. At the flange rings, the geometry is such that flange twist is minimized. Shell membrane loads have been aimed at ring centroids to achieve this; however, some twist did exist because of the difference of shell and ring hoop deflection causing a bending moment in this area. This induced moment will be counteracted in the final design by aiming the shell membrane load off center of the centroid to just compensate for the moment, thereby, achieving a no twist flange ring and lowered bolt requirement.

(U) It was concluded that the limiting loads at which the proportional limit was reached was higher than predicted loads because of the biaxial stress field and interaction allowable stress factors. These factors will be considered in choosing an allowable stress from the uniaxial data for the final design of the inner ducts and transition case. Considerable effort will be exercised to limit the bending at

boundaries so that all of the shell membrane may be worked at a higher stress level. Welds mismatch control is especially important, as indicated by the tests, and should be held to 5% material thickness maximum. The weld bead height is also important, but it appears that its influence in these tests was minor and may be held to weld specifications dimensions.

(U) Weld mismatch appears to have overshadowed all other stresses because it imposes such high bending stresses, which in turn, induce additional membrane stresses in both the hoop and meridian directions.

(U) Additional design studies showed that the canted ring transition case design was potentially the lightest design because the thrust load may be taken as shear between rings and shell allowing a thinner shell and potentially lighter rings. In the co-planar design the rings are directly proportional to the shell thickness, which is not the case in the canted design. However, it was concluded that for the overall design, the co-planar transition case offers the best solutions regarding the inner duct design, cooling, thrust load handling, assembly, and manufacturing.

d. Canted Ring Model Tests

(U) The canted ring (thrust) model shown in Figure 381 was designed in an effort to make the transition case more compact and to improve the engine packaging envelope. The stiffener rings were placed in a plane 120 degrees apart to simulate component spacing and the canting forward of 27 degrees. The thrust load was designed to be transferred by shearing into the stiffening rings through a sheet metal shell. The fabrication material was stainless steel.

(U) Stress-coat was used to locate the areas of maximum tensile stress under the thrust load. The high stress areas, as shown in Figure 388, occur as designed near the stiffness rings. Fifty-one two-gage and nine three-gage rosettes were applied to the model as shown in Figure 389. The location of the strain gages are shown in Figures 390 and 391. All rosettes were located and oriented to allow separation of a membrane and the bending stresses. The thrust loads were applied in increments up to 40,000 lb where strain plots indicated the proportional limits.

(U) The test results are shown in Figures 392 through 397. Comparing the actual hoop and meridian stresses with the theoretical (shell only) stresses, Figure 392 shows that the load in the shell is lower than that predicted by theory. This indicates that the rings take a greater portion of the load than the shell, and that the load did not act in a pure shell fashion. A plot of the meridian stresses around the circumference of the shell at the base (hoop direction), which is shown in Figure 393, indicates a load concentration peaking at the ring center lines. At the thrust ring at the top of the model, the stress concentrations are high at the ring center lines indicating that a great portion of the thrust load goes into the stiffening rings and is taken as shear in the shell. If the load had been taken out in shell fashion, the stress at the gimbal ring would have been uniform.

(U) Table XXXVII. Test Data Correlation

Strain Gage		Pressure (750 psi)				Thrust (25,000 lb)				Pressure (700 psi) and Thrust (13,750 lb)				Shear (7,000 lb)				Pressure (750 psi), Thrust (14,300 lb), and Shear (750 lb)			
		Actual		Theory		Actual		Theory		Actual		Theory		Actual		Theory		Actual		Theory	
		Membrane	Bending	Membrane	Bending	Membrane	Bending	Membrane	Bending	Membrane	Bending	Membrane	Bending	Membrane	Bending	Membrane	Bending (max)	Membrane	Bending	Membrane	Bending
Global Ring																					
Sphere $\alpha = 5°$	1	18,850	+21,650	13,750	-2,540	-9,000	-52,500	-14,700	+5,170	N/A		+5,650	+310	-1,100	-4,200	-	-	11,550	-5,750	-	-
	3	N/A		13,750	-2,540	N/A		-14,700	+5,170	9,900	-4,800	+5,650	+310	500	-900	-	-	N/A		-	-
Intersecting Ring																					
Small Sphere $\alpha = 5°$	35	17,300	+9,900	13,700	0	1,000	-1,100	-	-	17,600	+8,700	-	-	-17,650	-28,650	-9,300	3,000	15,550	+7,250	17,925	300
	37	14,400	+12,800	13,700	0	-650	-250	-	-	12,500	+12,600	-	-	400	-500	0		14,300	+14,400		
	39	13,750	+15,750	13,700	0	N/A		-	-	15,650	+15,550	-	-	N/A		+8,300	3,000	N/A		14,475	300
	41	15,150	+11,150	13,700	0	N/A		-	-	13,500	+9,550	-		N/A		0		N/A			
Large Sphere	43	17,050	+30,650	13,700	0	-4,500	-8,500	-5,370	-50	14,800	+21,700	10,709	-30	-12,000	+31,200	-8,340	3,000	14,350	+29,650	14,800	300
	45	19,550	+9,050	13,700	0	800	+2,300	+6,280	+50	18,500	+9,200	16,240	+42	-900	-3,850	0		19,400	10,600		
	49	16,250	+17,550	13,700	0	1,500	+2,250	+6,280	+50	15,750	+18,050	16,240	+42	700	-1,600	0		17,150	18,750		
Base																					
Machining $\alpha = 5°$	9	14,850	+17,550	14,150	3,350	-2,700	-7,600	-5,900	2,870	8,100	+20,300	10,000	4,700	8,800	+11,600	+7,400	3,000	11,550	+12,850	+19,700	5,000
	11	21,000	+30,600	14,150	3,350	-8,150	-19,750	-5,900	2,870	11,550	+15,650	10,000	4,700	1,700	+2,900			13,150	17,250		
	15	19,150	+23,350	14,150	3,350	-5,700	-11,900	-5,900	2,870	12,500	+14,000	10,000	4,700	-6,850	-16,350	-7,600	3,000	17,050	18,650	9,500	4,600
	19	15,700	+17,650	14,150	3,350	-6,350	-14,950	-5,900	2,870	10,000	+9,100	10,000	4,700	700	+2,100	0		12,200	+10,600		
Shell $\alpha = 7°$	13	N/A			-1,850	N/A		-5,150	0	N/A		9,000	1,000	N/A				N/A			
	17	N/A			-1,850	N/A		-5,150	0	N/A		9,000	1,000	N/A				N/A			
	21	-17,600	-16,000		-1,850	-5,000	+9,900	-5,150	0	12,750	-12,150	9,000	1,000	1,100	-1,400	0		16,300	-13,600		
	47	14,500	+13,100		-1,850	-1,750	+9,750	-5,150	0	12,150	-7,350	9,000	1,000	10,100	+700	+8,340	3,000	14,650	-6,650	10,600	2,100
Cap Flange																					
Machining	27	11,000	+2,000	14,000	Bending Due To Boundary	750	+350	-	-	12,550	+4,650	-	-	-900	-2,100	Negligible	Negligible	13,050	+4,450		
	29	17,550	-1,450	14,000		300	-400	-	-	16,200	-1,600	-	-	-1,050	+450			18,400	-4,500		
	31	12,650	+10,550	14,000		N/A		-	-	12,250	+9,950	-	-	N/A				N/A			
	33	11,050	+11,850	14,000		N/A		-	-	11,150	+12,650	-	-	N/A				N/A			
Center Shell																					
	51	21,450	-6,150	13,650	97	-4,050	-850	-5,370	-40	16,550	-5,050	10,480	53	-750	-150			19,450	-6,700		
	53	15,550	-450	13,700	90			-6,280	80	10,550	-5,050	9,300	130	-1,550	+50			12,300	-700		
	55	13,650	+50	13,650	-375			-6,320	-300	12,300	0	2,300	-527	-2,200	+300			13,600	+400		
	23	N/A		13,700	90	N/A		-6,280	80	N/A		9,300	130	N/A				N/A			
	25	14,600	+4,700	13,700	90	-650	+150	-6,280	80	13,300	-4,700	9,300	130	1,950	-450			14,750	-5,050		

(U) Figure 388. High Stress Areas on Canted Ring Model FD 25766

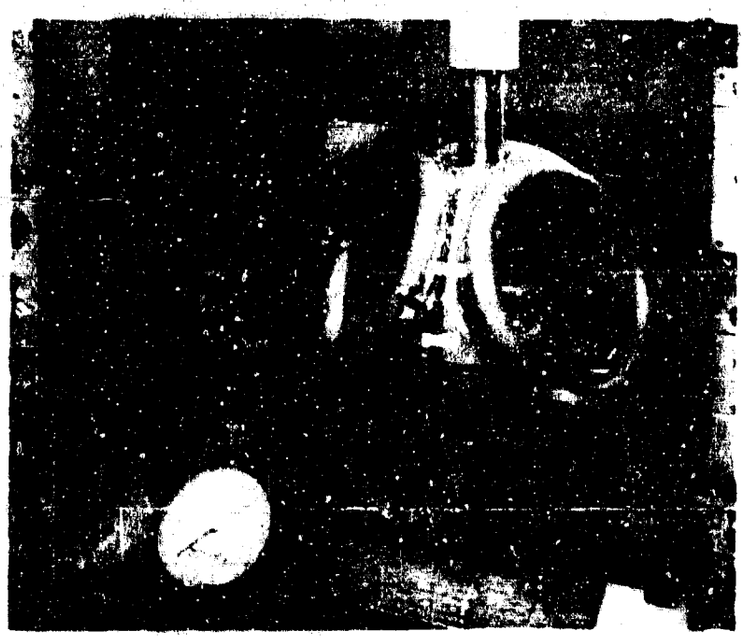

(U) Figure 389. Canted Ring Model Strain Gage Installations FE 80259

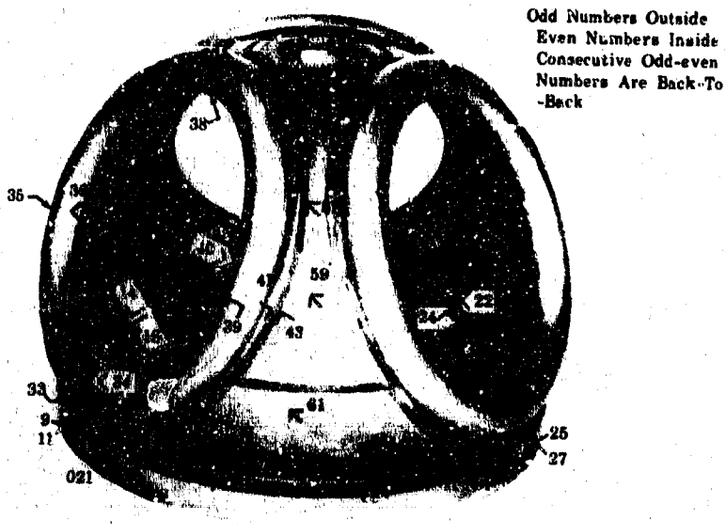

(U) Figure 390. Strain Gage Locations FD 25769

(U) Figure 391. Strain Gage Locations FD 25770

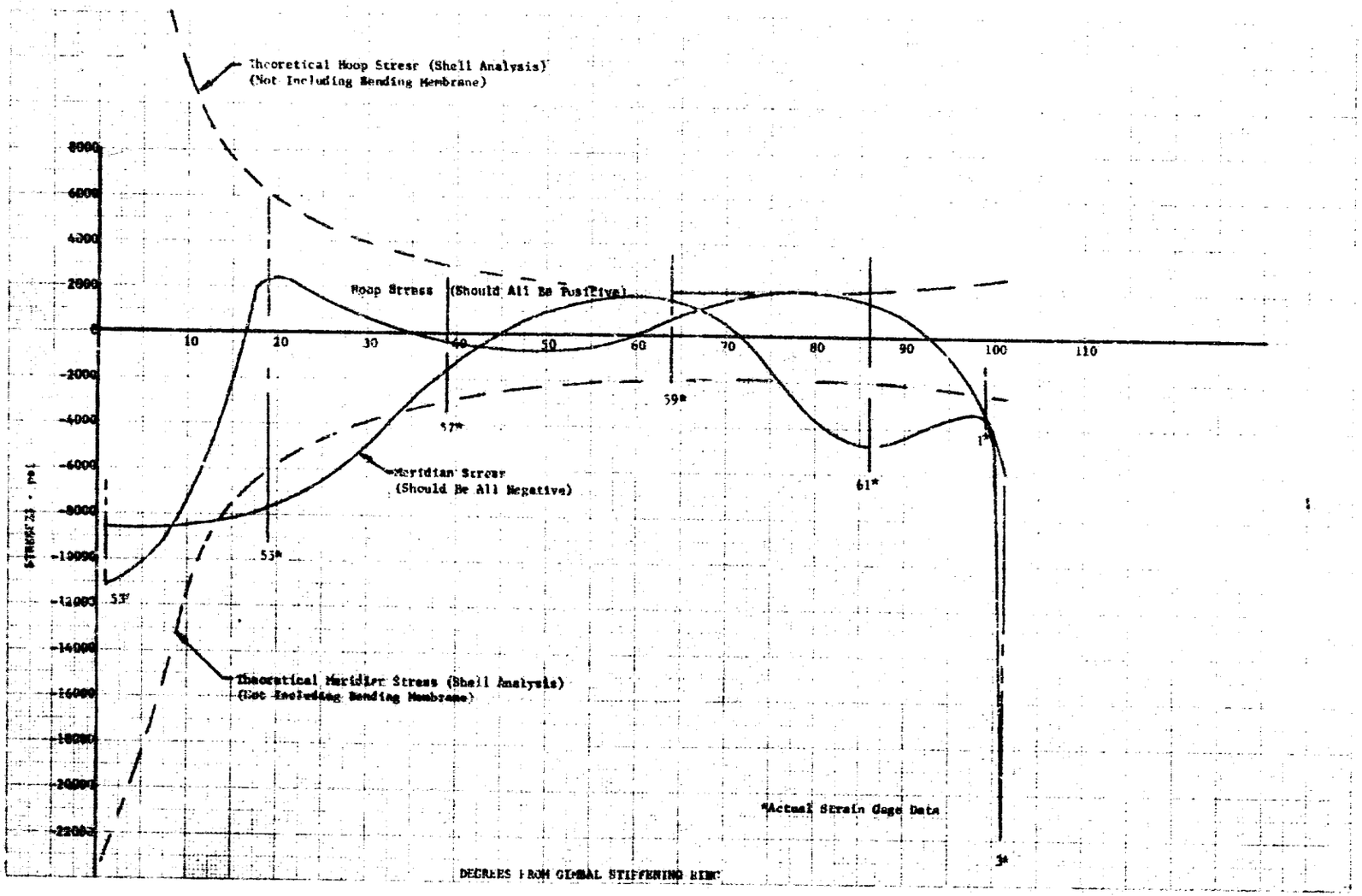

(U) Figure 392. Meridian Plot - Membrane Stress ϕ_o = 16 Degrees

DF 68976

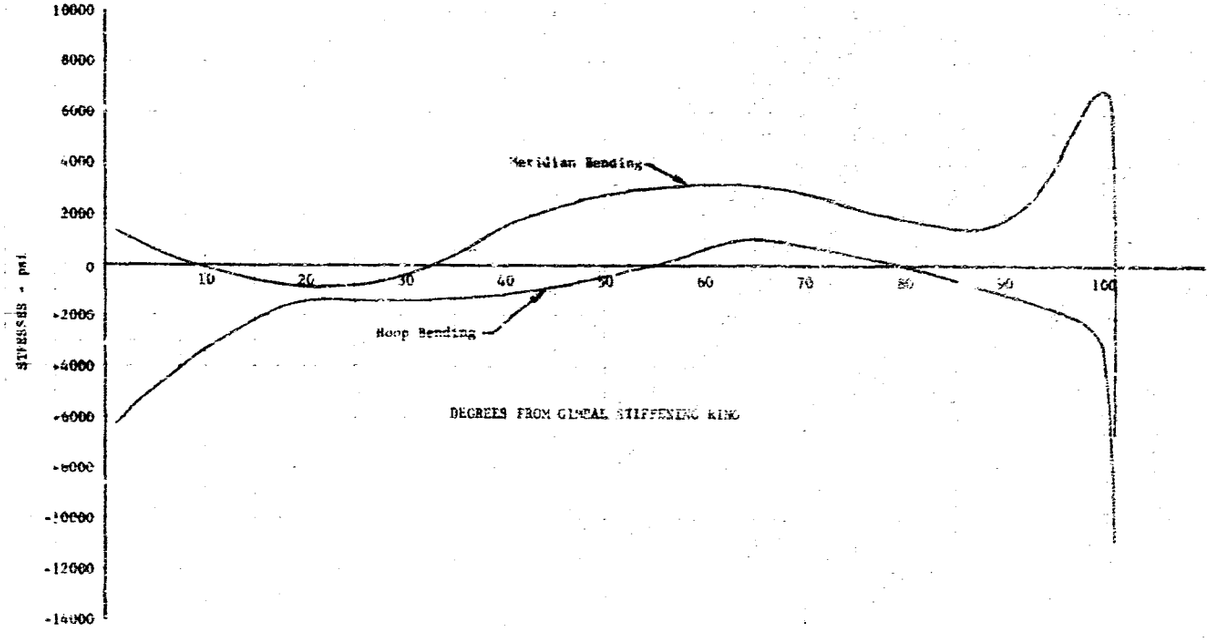

(U) Figure 393. Meridian Plot - Membrane Bending Stress (Outer Surface) ϕ_o = 16 Degrees DF 68977

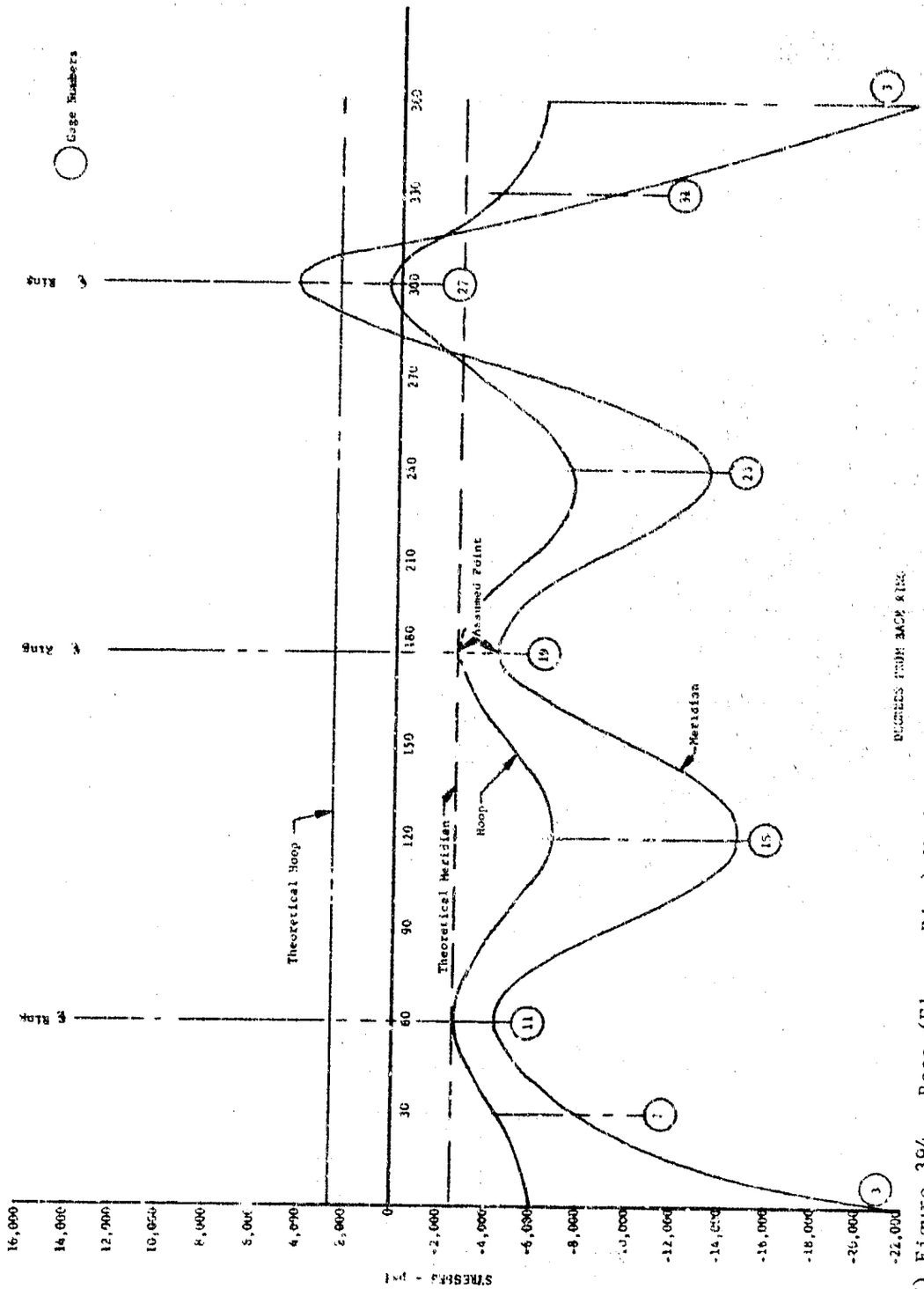

DF 68478

(U) Figure 394. Base (Flange Ring) Membrane Stress Φ = 63 Degrees

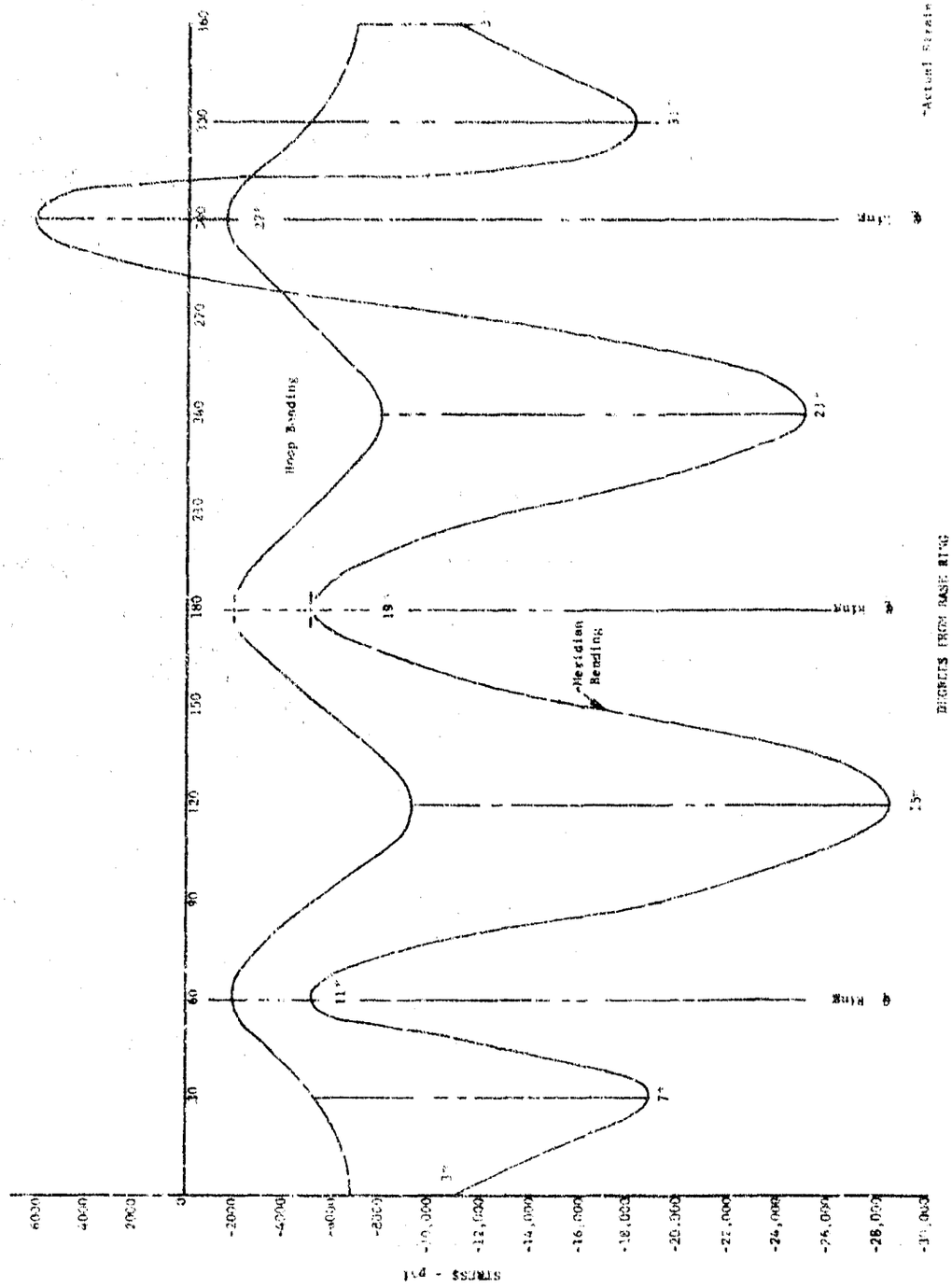

DF 68979

(U) Figure 395. Base (Flange Ring) Bending Stress ϕ = 63 Degrees

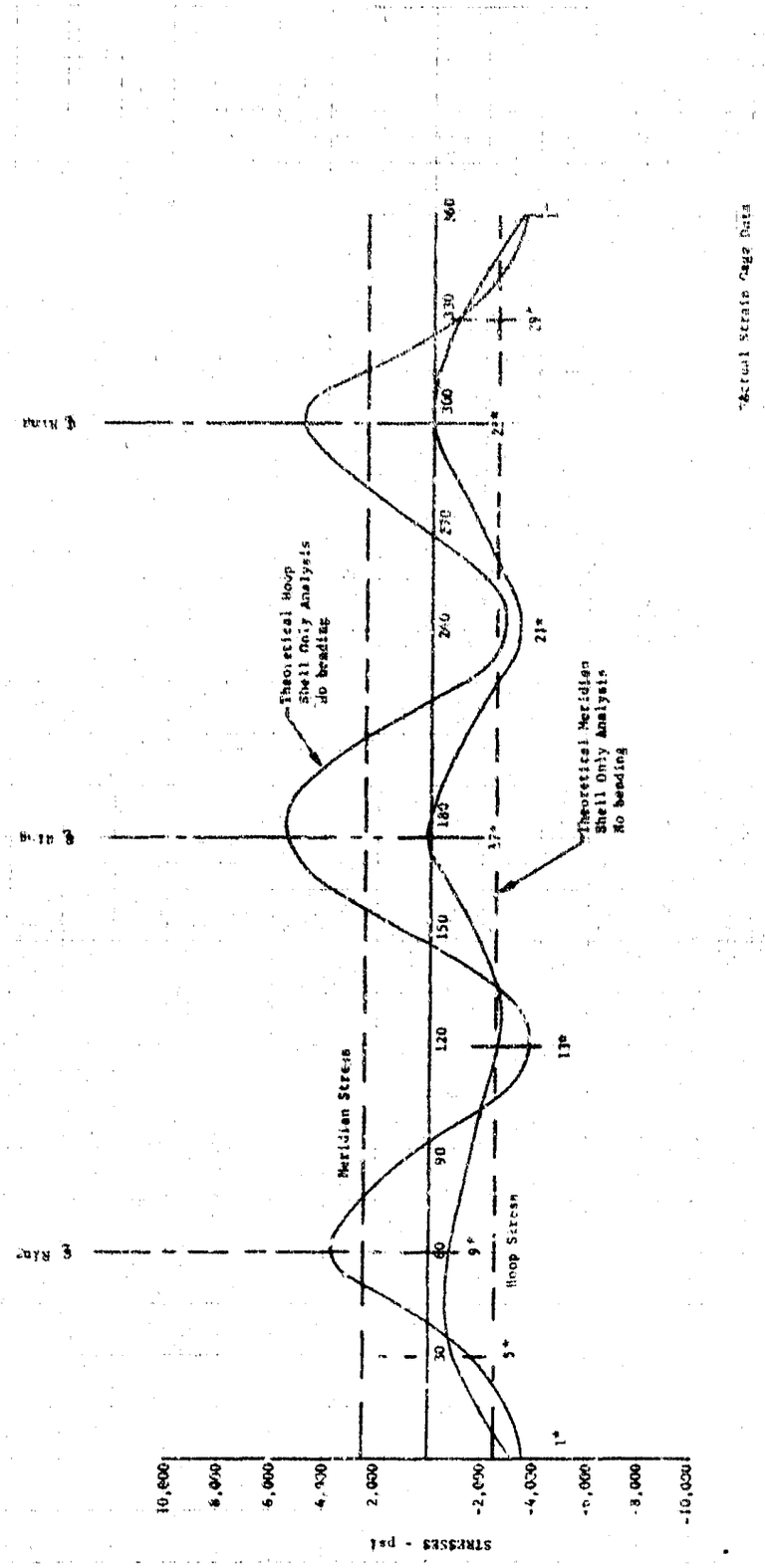

(U) Figure 396. Base (Shell) Membrane Stress (Circunferential Plot) ϕ = 65 Degrees

DF 68581

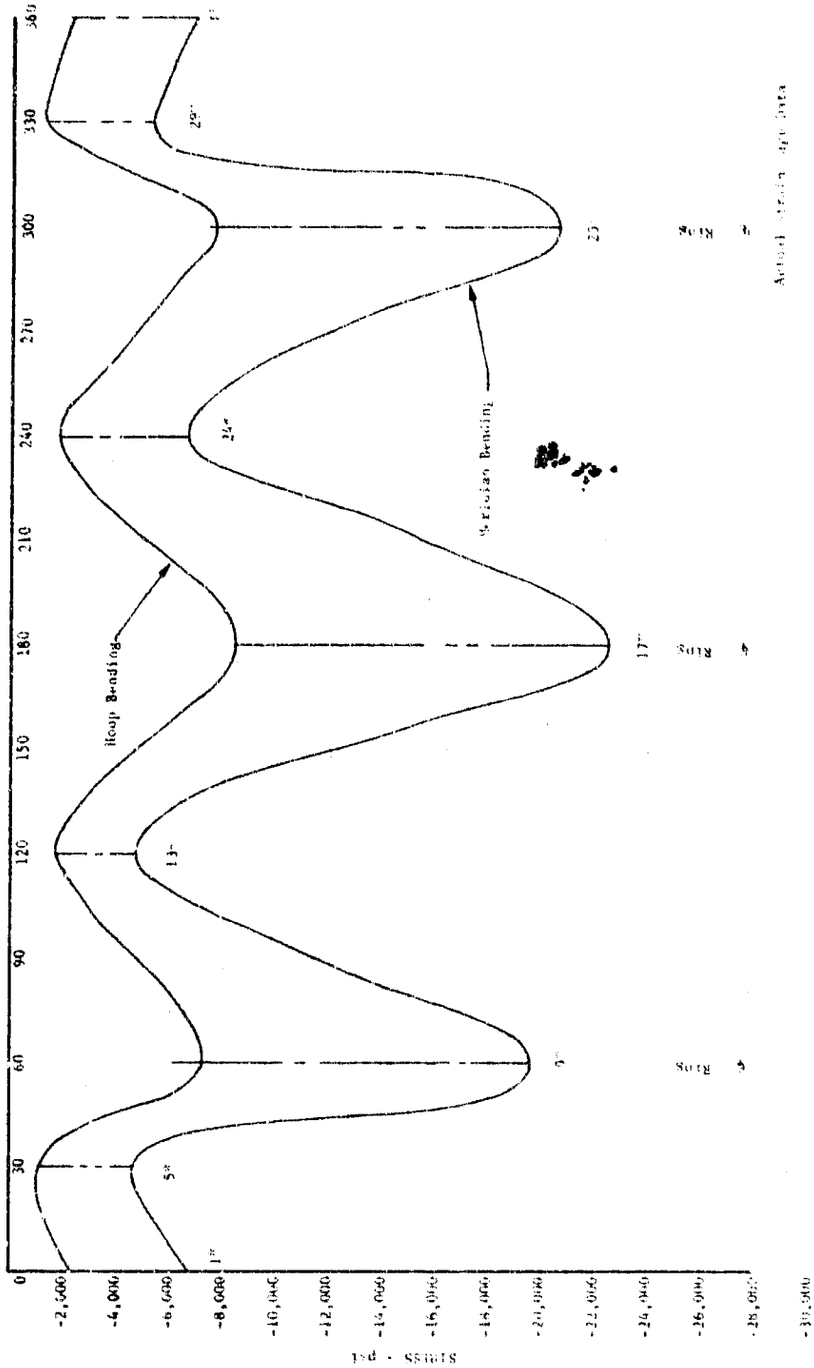

(U) Figure 397. Base (Shell) Bending Stress Φ = 65 Degrees

DF 68980

F. FUEL TURBOPUMP

F. FUEL TURBOPUMP

1. Introduction

(C) The demonstrator engine requires that the fuel turbopump deliver liquid hydrogen at a flow rate of 99.3 lb/sec at a pressure of 5654 psia at its design point (mixture ratio of 5). The two-stage turbine must deliver approximately 49,872 horsepower to the pump and must operate at a minimum inlet temperature of 1986°R and at a maximum inlet temperature of 2292°R at 100% thrust. In addition, the fuel pump must demonstrate satisfactory starting capability and stable operation over the engine operating range of 20 to 100% thrust and mixture ratio of 5 to 7. The turbopump to be tested will be a lightweight compact arrangement with a design weight goal of 355 lb, and with a sufficient safety factor to assure confident operation without undue design refinement or test failures. Life will be based on a 10-hour time between overhaul, 100 reuses, 300 starts, and 600 seconds maximum run duration.

2. Design Concept

(U) The preliminary design configuration for the fuel turbopump is shown in Figure 398. This conceptual design incorporates the following features:

1. Integral high-speed axial-flow inducer
2. Two-stage pump with centrifugal impellers, axial entry and double discharge
3. Double acting hydrostatic thrust balance piston
4. Full-admission, axial-flow, two-stage, pressure-compounded turbine with cooled disks and uncooled airfoils
5. Two antifriction roller bearings.

(U) The design criteria for the fuel turbopump was the same as used for the design of the 350K Breadboard Liquid Hydrogen Pump that was tested successfully on Contract NAS8-11427. The initial design effort has been to evolve a conceptual rotor design that would satisfy critical speed and burst margin requirements, and be compatible with the engine envelope and hydraulic requirements. The conceptual rotor assembly has been designed and preliminary analysis indicates that, with the compact arrangement illustrated in Figure 398, design requirements will be met. Additional refinements to be incorporated during the final detail design should reduce the envelope and improve the fabrication of this turbopump.

(C) The fuel turbopump bearings used in the conceptual pump design are 55 x 96.5 x 21 mm roller bearings. Phase I (Contract AF04(611)-11401) studies indicated that a roller bearing would satisfy the 10-hour design life requirement at the estimated radial loading of 1700 lb and DN value of 2.64×10^6. Preliminary bearing tests indicated that excessive roller end wear was a potential problem. Bearing tests have been conducted during this report period and several bearings have demonstrated a life in excess of 12.6 hours and with negligible roller end wear. These tests are discussed in detail in Section IV.

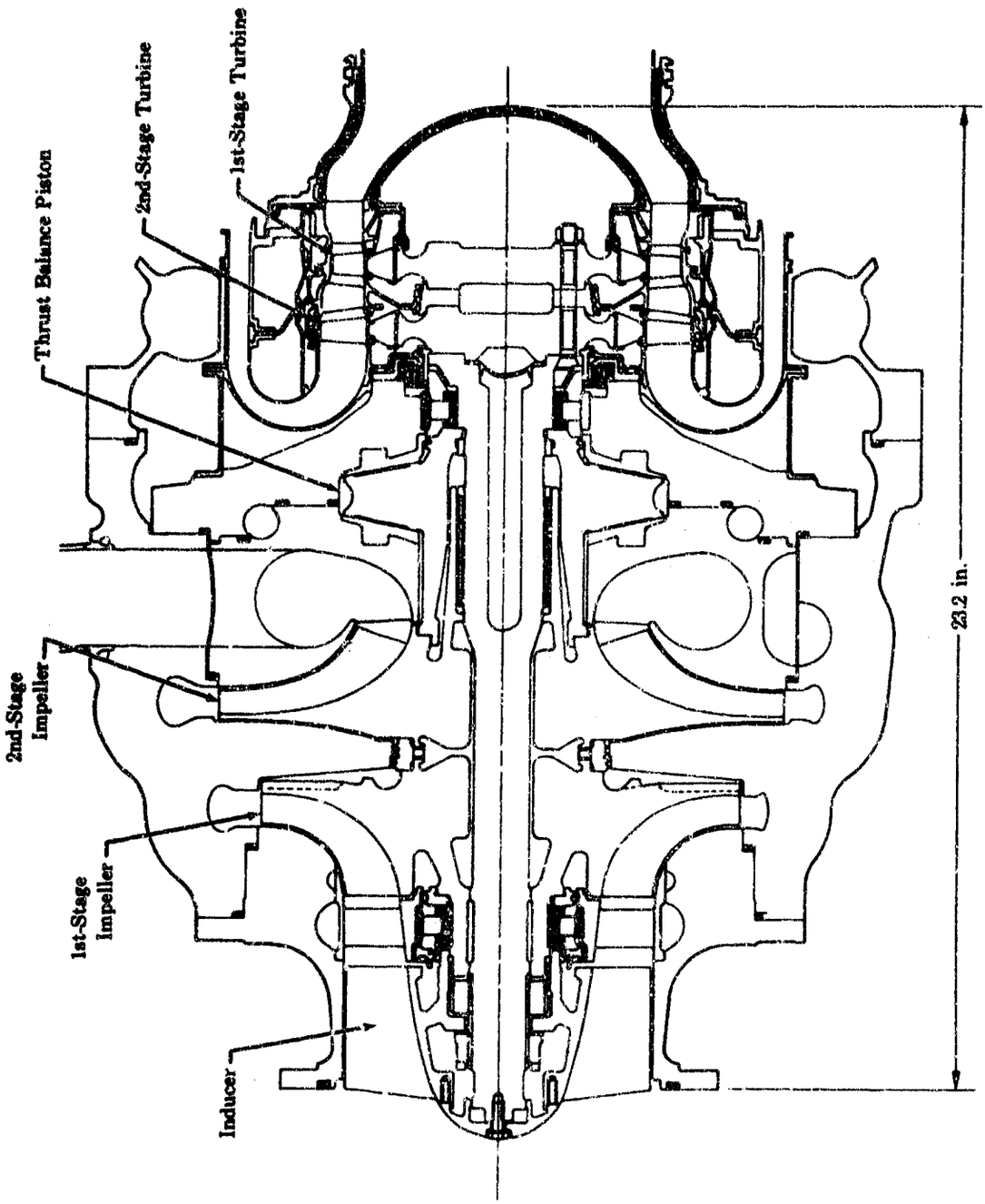

FD 27633

(U) Figure 398. Fuel Turbopump Preliminary Design

(U) A compact fuel pump arrangement is required to satisfy critical speed, engine envelope, and weight considerations. The interstage diaphragm between the two impellers is a deflection limited area and the use of Inconel 718 (AMS 5663) with its high strength and modulus of elasticity allows a narrow spacing in this area. The use of this material for the main housing also allows the interstage plumbing between the two impellers to be welded as an integral part of the housings. This eliminates four flanges and the associated bolts, seals, and potential leak paths.

(U) A turbine disk and blade root cooling arrangement being considered for the fuel pump is fundamentally different than that utilized in the 350K fuel turbopump design. The 350K scheme used front and rear side plates on both disks to subject the disks and blade roots to a "cold" hydrogen environment. To accomplish this, it was necessary to pressurize the turbine inlet bullet cavity with coolant. Because the coolant was at a relatively high density, considerable coolant leakage into the main gas path (ahead of the 1st-stage blade) was unavoidable and an undesirable forward thrust on the rotor was inherent. This radial leakage of cold hydrogen into the primary flow path also results in a turbine aerodynamic performance penalty.

(U) The proposed turbine cooling scheme, shown in Figure 399, avoids these problems by subjecting the disks and blade roots to a lower pressure (and higher temperature) coolant. The radial inflow at the blade root also reduces the aerodynamic performance penalty caused by radial outflow of cooling gas. The coolant is a mixture of main flowpath gas and 2nd-stage pump discharge fuel. This arrangement reduces the penalty to the cycle and improves mechanical design of the turbine. A predetermined amount of flowpath gas is allowed to bleed into the seal chamber (seal location A) ahead of the 1st-stage blade where it is cooled, by the metered addition of fuel, to a temperature that is desirable for disk and blade attachment coolant. This coolant mixture then flows through the labyrinth seal inside the 1st-stage blade platform to surround the disk and blade roots. Natural circulation of this coolant around both stages can be achieved with a proper balance between coolant flow and seal clearances at the various locations. The goal of this design is to maintain adequate coolant pressures at all locations along the flowpath inner wall to ensure outward flow of coolant and preclude inflow of hot flowpath gas. The seals shown at location F are not an essential part of the coolant scheme but were introduced to benefit rotor thrust balance by lowering the pressure inside the bullet. With these seals, the bullet pressure may be vented to a lower pressure area, reducing the gas load acting forward on the 1st-stage turbine disk.

(U) Detail design work has begun to define the high-speed inducer, 1st-stage impeller, 2nd-stage impeller, thrust piston set, 1st- and 2nd-stage turbine blades, 1st-stage turbine vanes, and the main fuel pump housing. Based on the preliminary parts designs, vendor quotes will be requested to determine the parts requiring the longest fabrication lead time. Fabrication information associated with the preliminary designs will also be requested to provide the designers with anticipated fabrication problems that will be evaluated before any design is finalized. Based on the fabrication lead time for each of the parts, design and detailing effort will be planned to assure that the long lead time parts are available for testing in accordance with the development schedule.

399

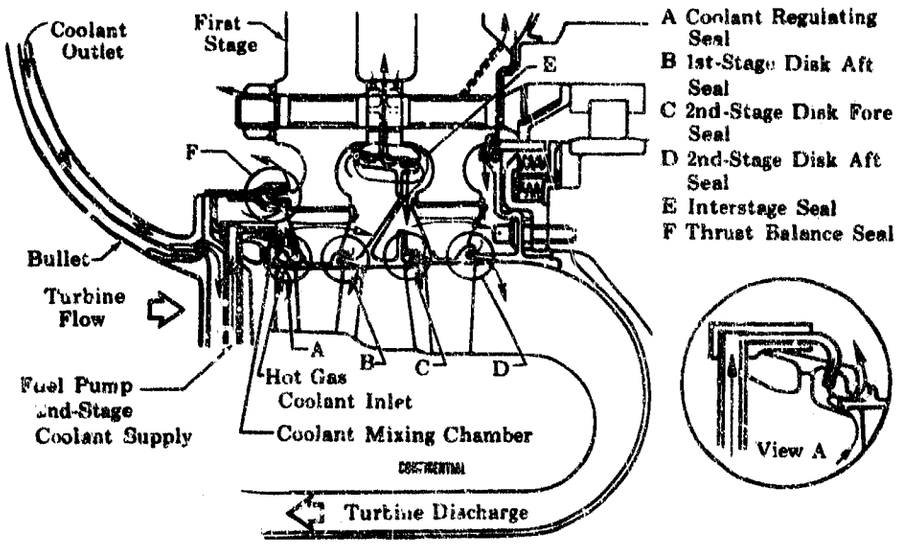

(U) Figure 399. Preliminary XLR129-P-1 Fuel Turbine Coolant and Seal Arrangement FDC 25674

G. OXIDIZER TURBOPUMP

G. OXIDIZER TURBOPUMP

1. Introduction

(C) The demonstrator engine requires that the oxidizer turbopump deliver liquid oxygen at a maximum flow rate of 548 lb/sec with a pressure rise of 4603 psid at its design point (mixture ratio of 7) and a maximum pressure rise of 6785 psid at a mixture ratio of 5. This pressure rise is reduced to 5737 psid at a mixture ratio of 5 by recirculation of approximately 20% of the oxidizer flow back to the pump inlet. The turbine must operate at a minimum inlet temperature of 1986°R and a maximum inlet temperature of 2292°R at 100% thrust. Preliminary analysis indicates that the turbopump must be capable of operating at a maximum speed of 25,925 rpm. In addition, the turbopump must demonstrate satisfactory starting and stable operation over the engine operating range of 20 to 100% thrust and mixture ratio of 5 to 7. The turbopump to be tested will be lightweight and compact with a design goal of 280 lb with a safety factor sufficiently high to assume confident operation without undue design refinement or testing failures. Life will be based on a 10-hour time between overhaul and 100 reuses (300 starts).

2. Design Concept

(U) A design configuration for the oxidizer turbopump, based on preliminary design studies, is shown in Figure 400. This design incorporates the following features:

1. Integral high-speed, axial-flow inducer
2. Single-stage shrouded impeller with axial entry and double discharge
3. Single-acting hydrostatic thrust balance piston
4. Full-admission, axial-flow, two-stage, pressure-compounded turbine with cooled disks and uncooled airfoils
5. Two antifriction ball bearings.

(U) Initial effort has been directed to define hardware with expected long procurement time. Delivery of the antifriction ball bearings is expected to be approximately 40 weeks. Therefore, studies to define the bearings are being performed at the earliest date.

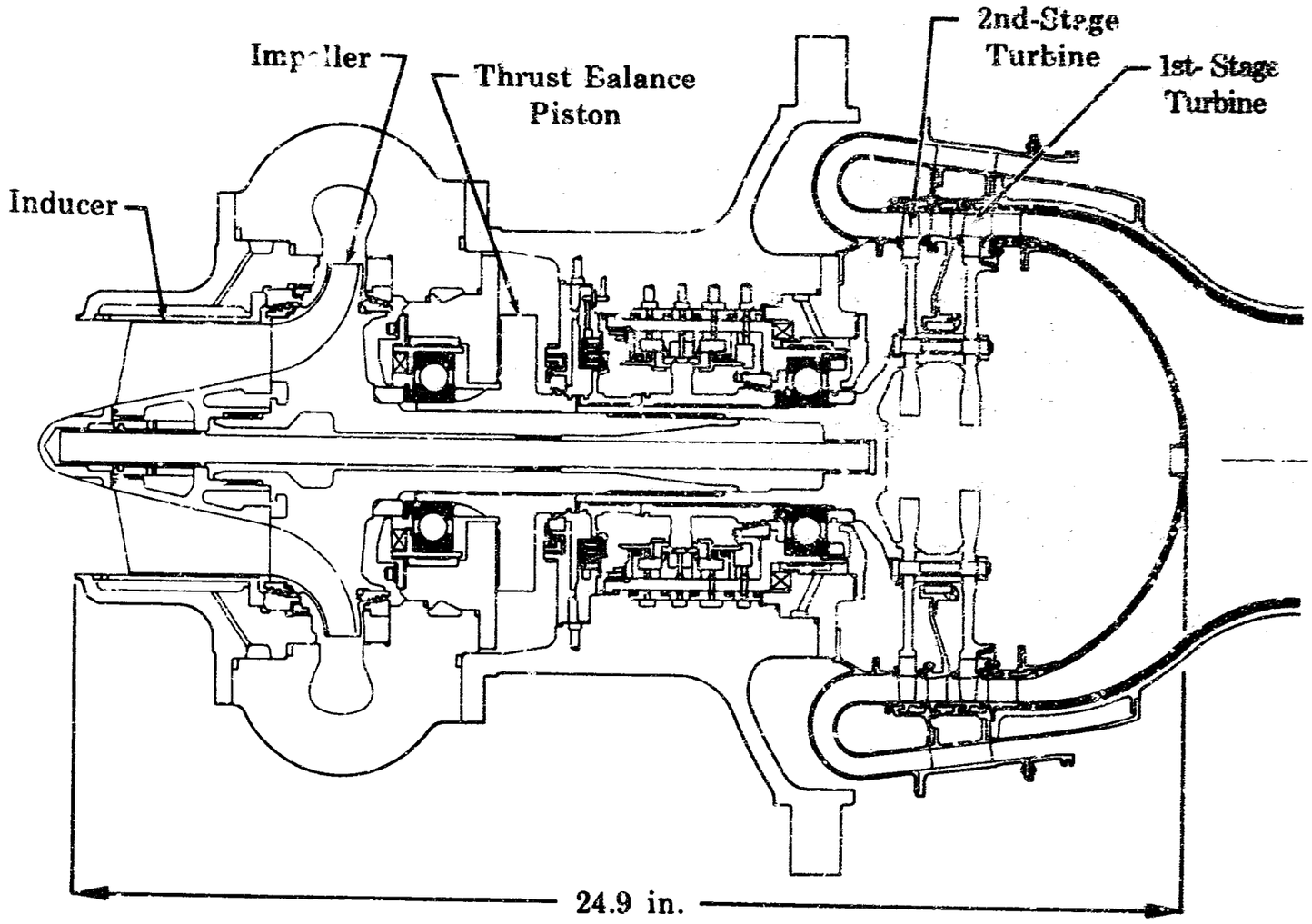

(U) Figure 400. Oxidizer Turbopump Preliminary Design

FD 22382A

(C) Table XXXVIII lists the calculated front and rear bearing loads for the liquid oxygen turbopump preliminary design. Three sets of vehicle load conditions are shown. Estimated hydraulic loading, as well as loading caused by vehicle maneuvers, gyroloading caused by engine gimbal motion, and loading caused by dynamic unbalance are included. An unbalance of 0.01 oz-in. was assumed. This value of unbalance is higher than the 0.005 oz-in. experienced with the 350K liquid oxygen pump on Contract NAS8-20549, but was used to provide for unknowns that may be reduced when experience is accumulated on this turbopump. The loads are taken in planes perpendicular and parallel to the vehicle axis. The vehicle loading, maneuver loading, and gyroloading were summed vectorially. The hydraulic loading and dynamic unbalance loading were then added to this vector to provide the maximum radial loading of the bearings. This vector summation for the case resulting in the greatest radial load is shown in Figure 401. The maximum resultant radial load for the three cases studied was 1433 lb on the front bearing. This load is quite severe and can be obtained only when all loads are considered to be present at the same time and in an additive direction.

(C) The selection of a ball bearing is based on a requirement for 10 hours life at 26,000 rpm with the maximum resultant radial load applied. Experience has shown that load capacity curves may be generated by the standard AFBMA method for oil lubricated bearings, if the life predictions are divided by 2 for bearings operating in liquid oxygen. Therefore 20-hour life curves for varying radial and axial loads were generated to predict 10-hour life capability in liquid oxygen.

(U) The maximum load capacity was sacrificed in all bearing designs analyzed so as to minimize heat generation and provide necessary skid margin. These two items are considered of primary importance in liquid oxygen applications and cryogenics in general. The load capacity of the bearings is further reduced by removing some elements to provide for standard cryogenic cage design and larger than standard ball pocket clearance. These modifications are considered to be necessary to allow for thermals and ball excursion.

(C) The bearings analyzed were of a split inner race, angular contact type of the same general design as used in other PWA-FRDC cryogenic turbopumps. Life curves for various candidate bearings are presented in Figure 401. Bearing A does not provide the desired life with 1433 lb radial load. It is desirable to maintain the thrust load the same as or higher than the radial load to ensure full rolling of the elements with no skidding. Therefore bearing B of Figure 402 would not provide sufficient life at the required radial and axial loads. Bearing C represents the maximum possible ball diameter for a 55 x 110 mm bearing without compromising the strength of the races.

(C)(U) Table XXXVIII. Bearing Load Summary

	Front Bearing			Rear Bearing		
Relation to Vehicle Axis						
Vehicle Loading[1]	80	400		39	186	
Vehicle Loading[2]	120	260		64	117	
Vehicle Loading[3]	240	120		108	54	
Gimbaling Loads[4]	191	64		177	17	
Vehicle Pitch Gyroloads[5]	55	-		55	-	
Vehicle Roll Gyroloads[6]	-	83		-	83	
Total Vehicle Loads[1]	326	547		271	280	
Resultant[1]		637			390	
Total Vehicle Loads[2]	366	407		296	217	
Resultant[2]		547			367	
Total Vehicle Loads[3]	486	267		340	154	
Resultant[3]		555			373	
Hydraulic Loading[7]		785			153	
Unbalance Loading[8]		11			11	
Total Loads (lb)	1433[1]	1343[2]	1351[3]	554[1]	531[2]	537[3]

[1] 10 g Axial and 2 g Transverse

[2] 6.5 g Axial and 3 g Transverse

[3] 3 g Axial and 6 g Transverse

[4] Acceleration 30 rad/sec^2, Velocity 30 deg/sec

[5] Pitch 10 deg/sec

[6] Roll 15 deg/sec

[7] 2% ΔP Static

[8] 0.01 oz-in.

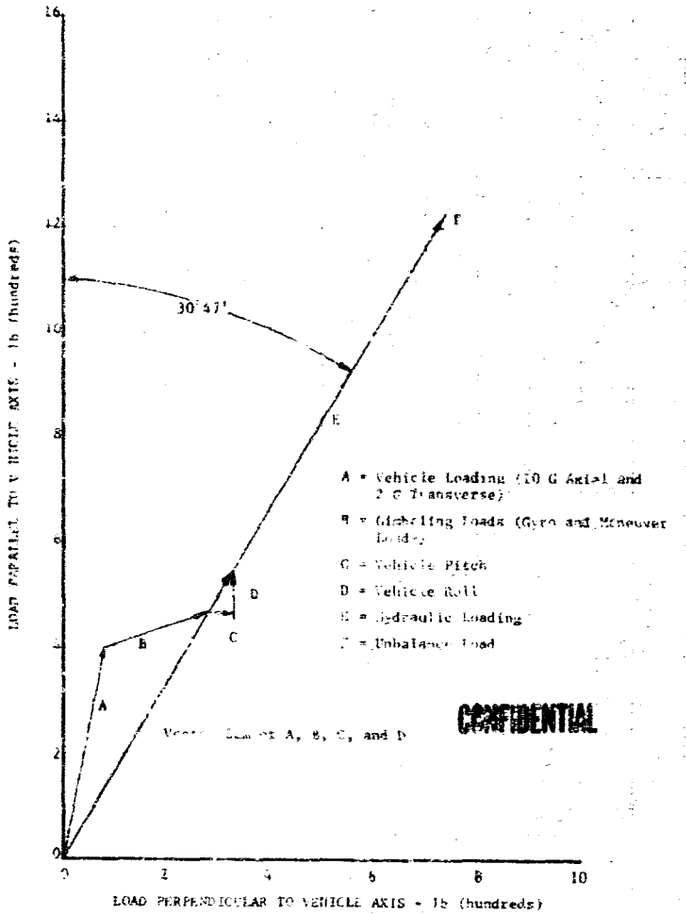

(U) Figure 401. Oxidizer Pump Maximum Radial Loading of Front Bearing Vector Load Diagram DFC 68919

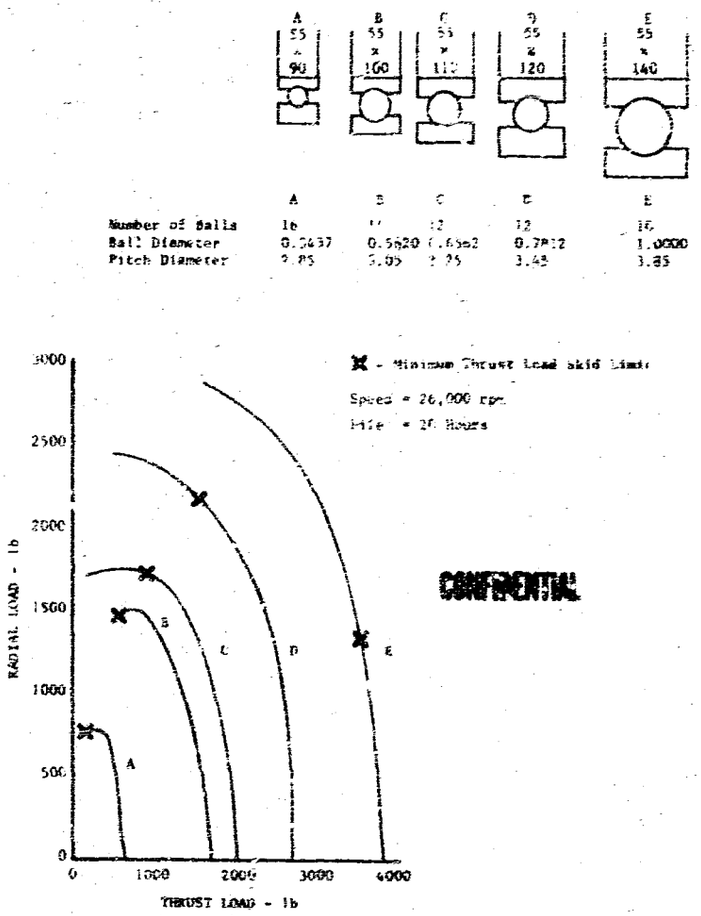

(U) Figure 402. Ball Bearing Load Capacity DFC 68920

(U) Bearings D and E of Figure 402 show increased life but are excessively large and cause severe compromise to the pump envelope requirements. These bearings also show an increase in the minimum thrust load to prevent skidding. Increasing the bearing inner diameter results in increased predicted life. However, a bearing of 6 mm ID increased the DN value above the liquid oxygen experience level and requires higher thrust loads to prevent skidding. Using the life predictions a bearing will be selected for complete system analysis. The system analysis will determine contact angle, curvature, pocket clearance and internal clearance. In analyzing the system, loads speed, deflection, preload, preload spring rate, and bearing geometry are mathematically analyzed as a combined system. The results of the analysis provide information on position and velocity of each element in the bearing.

(U) Because the radial loads are higher than usually used in ball bearing selection a duplexing of ball bearings would theoretically increase the radial load capacity. In practice, however, it is difficult to assure that both units are carrying load. The requirement for outside diameter sliding clearances plus misalignment on the shaft and manufacturing tolerances could cause one bearing to accept greater load, thereby causing the life characteristics to approach those of a single ball bearing. This technique may be considered, however, based on the results of the system analysis.

(C) The liquid hydrogen cooled rear bearing and liquid oxygen cooled front bearing are separated by a low leakage seal package. Because the seal leakage is vented overboard, this leakage must be minimized, in a high performance engine. The factors governing the leakage rate are seal differential pressure and seal clearance. Because of the excessive seal velocity (approximately 400 ft/sec) a rubbing seal of zero clearance is prohibitive with respect to life requirements. Experience indicates that wear rates on rubbing seals at velocities less than 400 ft/sec are a number of magnitudes higher than would be acceptable for a 10-hour life seal. To provide the minimum seal clearance, a limited wear, close clearance seal is being considered as shown in Figure 403. This seal is preloaded with a wave washer to provide contact with the rub face. During the first few seconds of operation approximately 0.002 inch of seal face is removed until the recessed portion of the seal contacts a stop. This provides the minimum noncontact gap for leakage. This gap is maintained by mounting the seal package stationary parts in an extens on of the rear bearing carrier which follows shaft movement as the axial shaft loads vary.

(U) The differential pressure across the seal is minimized by venting the high pressure fuel and oxidizer cavities to the respective fuel and oxidizer turbopump inlets. This provides the lowest reference pressure in the engine and returns the greater portion of the bearing coolant flow to the engine.

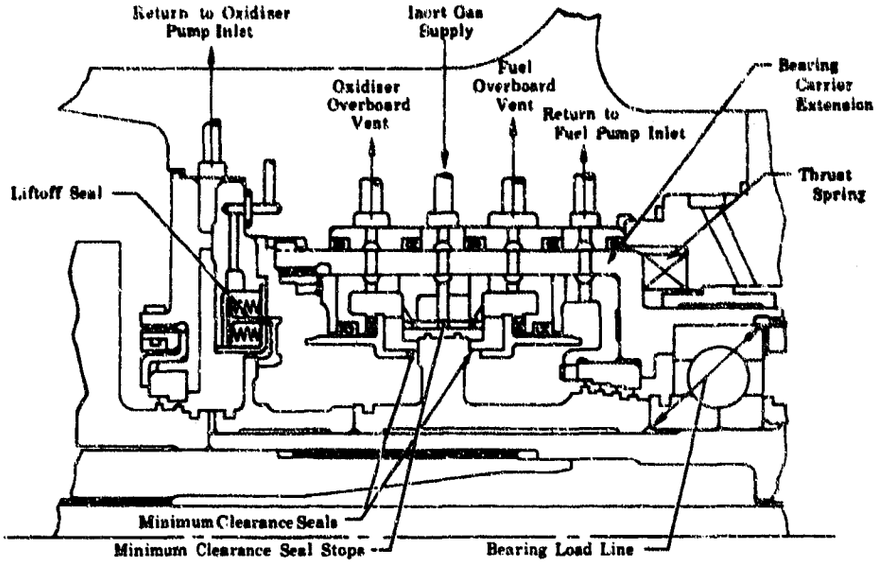

(U) Figure 403. Oxidizer Pump Seal Package FD 25625

(U) An inert gas block of higher pressure is provided between the oxidizer and fuel overboard vent cavities. The labyrinth seal on each side of the inert gas block maintains the higher block pressure and reduces gas consumption.

(U) A pressure actuated liftoff seal is provided in the liquid oxygen section upstream of the minimum clearance seal to further minimize leakage overboard during periods when the shaft is not rotating. This seal is actuated immediately prior to pump rotation to eliminate rubbing contact.

H. FUEL LOW-SPEED INDUCER

H. FUEL LOW-SPEED INDUCER

1. Introduction

(C) The demonstrator engine requires that the fuel low-speed inducer deliver hydrogen to the inlet of the fuel turbopump at conditions that are not detrimental to operation of the fuel turbopump. The inducer must be capable of operating at a minimum NPSH of 60 ft over a hydrogen inlet temperature range from 1 atmosphere boiling temperature to 45°R. The inducer will be designed with a suction specific speed of 46,800 and a maximum pressure rise of 109 psid. The low-speed inducer will be lightweight and compact with a design goal of 90 lb and be capable of stable operation over the engine operating range. It will have a safety factor sufficiently high to assure confident operation without undue design refinement or testing failure. Life will be based on a 10-hour time between overhaul and 100 reuses (300 starts).

2. Design Concept

(U) A preliminary conceptual design of the fuel low-speed inducer has been completed, but detailed analysis of the components has not yet begun. The fuel low-speed inducer fabrication and testing is scheduled after the main fuel turbopump test program and the design effort has been primarily in that area to date. The preliminary design of the fuel low-speed inducer is shown in Figure 404. This conceptual design incorporates the following features:

1. Helical axial flow inducer
2. Single acting, hydrostatic thrust balance piston
3. Two-stage, axial-flow, partial-admission impulse turbine
4. Two antifriction ball bearings.

(C) In this design, the fuel inducer operates at a speed of approximately 19,800 rpm. The inducer will be a helical design, as axial flow is required by the high suction specific speed. It is a three-bladed 12.400-inch diameter aluminum (AMS 4130) inducer, designed assuming 80% of inducer pressure rise occurs across the first complete blade. Aluminum (AMS 4130) has a weight advantage over Inconel 718 (AMS 5663) or other materials for this inducer, because only the 1st-stage blade is highly stressed. This may be improved by decreasing blade thickness uniformly as it progresses along the shaft axis. The inducer discharge and turbine housing collects the flow uniformly and maintains a constant flow velocity. The high pressure in the turbine area favors the use of titanium with its high strength-to-weight ratio. The low expansion coefficient is also compatible with the bearing material.

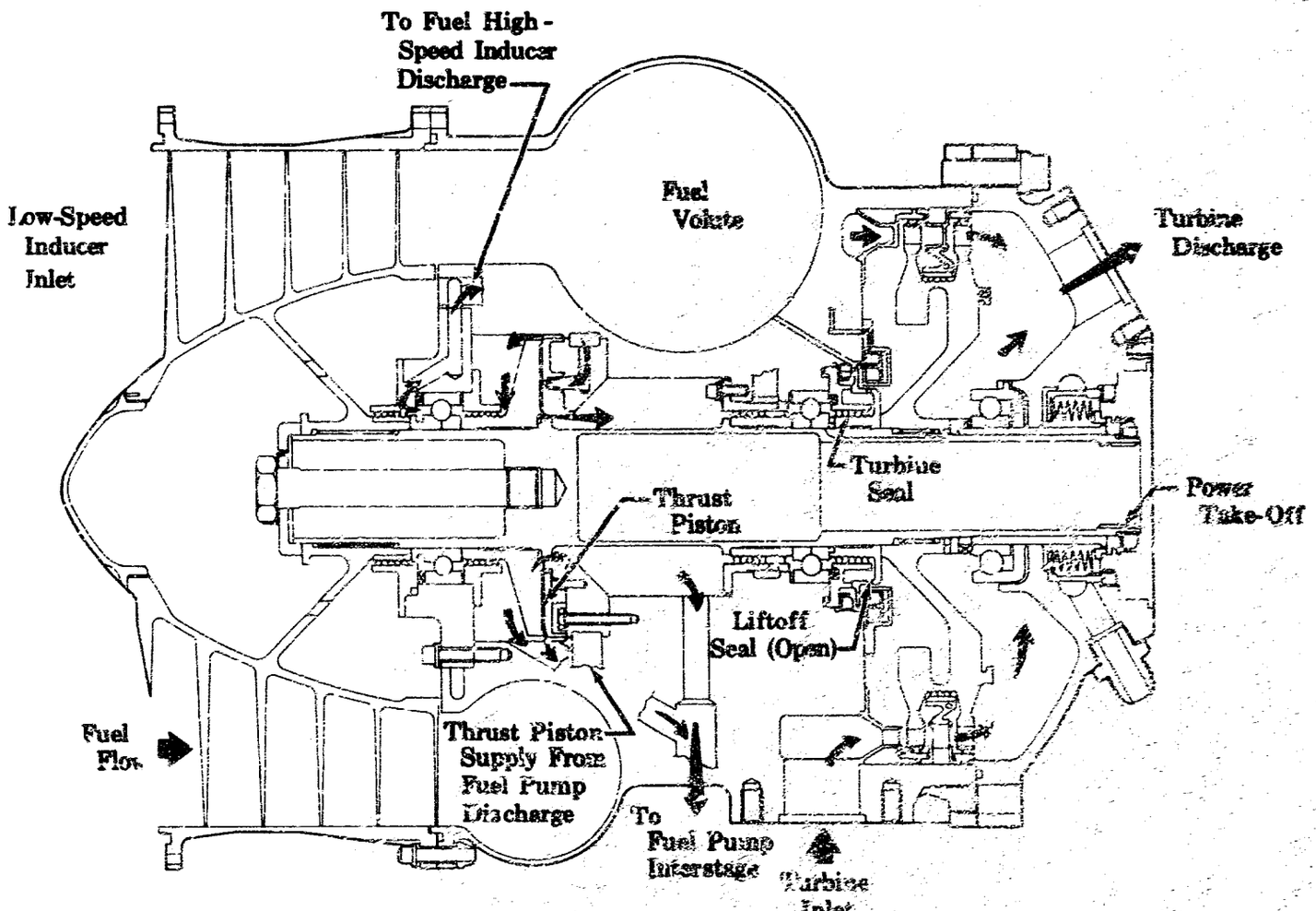

(U) Figure 404. Fuel Low-Speed Inducer Preliminary Design

FD 25542

(U) Incorporation of a single acting thrust balance piston was required because analysis of the preliminary fuel inducer rotor indicated that the range of the unbalanced pressure loads was too high to be carried by a thrust bearing. This was caused by the power takeoff requirements, thrust and mixture ratio variations. The direction and magnitude of the thrust loads was varied by changing the turbine labyrinth seal diameter to arrive at the best conceptual design. Four thrust balance schemes (Figures 405 through 408) were considered. All thrust piston areas were sized for a maximum differential pressure equal to 80% of the available pressure drop. The minimum piston axial clearance was set at 0.001 inch for the liquid piston design supplied from fuel pump discharge. This was increased to 0.002 inch for the turbine gas piston design because of the difficulty in controlling deflection of the turbine disk. The extra flow required to drive the inducer in the power takeoff mode is bypassed around the turbine during normal cycle operation.

(U) In scheme A the smallest cycle penalty was achieved by venting the piston discharge pressure to fuel pump interstage; however, the turbine seal leakage was prohibitive.

(U) Schemes B and C used turbine inlet gas to supply the piston; however, the total flow for the piston and labyrinth seal exceeded the amount available for power takeoff. These schemes would also require additional controls to maintain correct inducer speed and flow to the main chamber due to the varying flow to the piston as thrust fluctuates.

(U) In scheme D, the turbine seal diameter was minimized to reduce the leakage bypass flow to an acceptable value. A detailed comparison with scheme B was then made as to piston supply flow and stability of the gas vs quasi-liquid scheme. Scheme D was found to be more stable in the low thrust range.

(U) Figure 404 is a refinement of scheme D, which had no prohibitive disadvantage, and imposed the least cycle penalty. The suction performance of the main fuel turbopump is very sensitive to warm gas introduced ahead of the high-speed inducer. A vent in front of the forward bearing recirculates most of the bearing coolant to the fuel high-speed inducer discharge where pump operation is least affected. Because of the preliminary nature of the turbine design and ensuing cycle revisions, no attempt was made to provide thrust margin in the piston at this time, although sufficent envelope is available to provide this margin with a minimum of effort by increasing the piston diameter.

(U) Power to drive the inducer will be provided by a two-stage partial admission axial flow impulse turbine. The two-stage turbine is similar to a proven RL10 design using a brazable aluminum (AMS 4127). The turbine is designed with excess power to provide power takeoff capability. The power takeoff provision is by means of an internal spline coupling located on the turbine end of the fuel inducer. The feasibility of using bevel gears and driving the fuel low-speed inducer with the fuel pump turbine was investigated. This was considered impractical due to the large pitch line velocity required (37,700 ft/min) and prec[illegible] requirements for flow meter between the inducer and main pump.

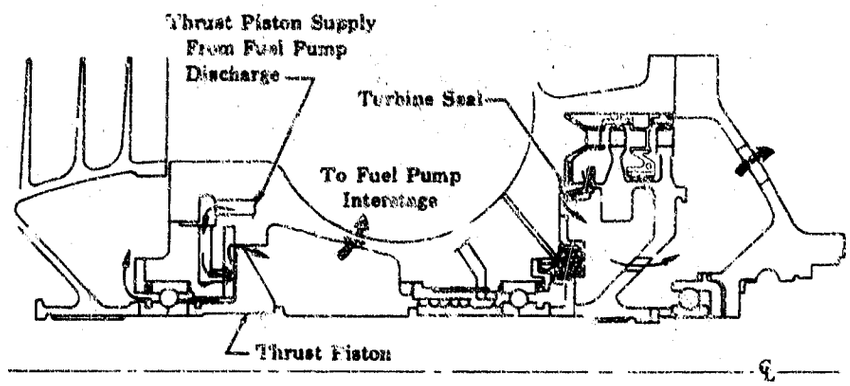

(U) Figure 405. Preliminary Fuel Low-Speed Inducer Liquid Thrust Piston (Scheme A) FD 25675

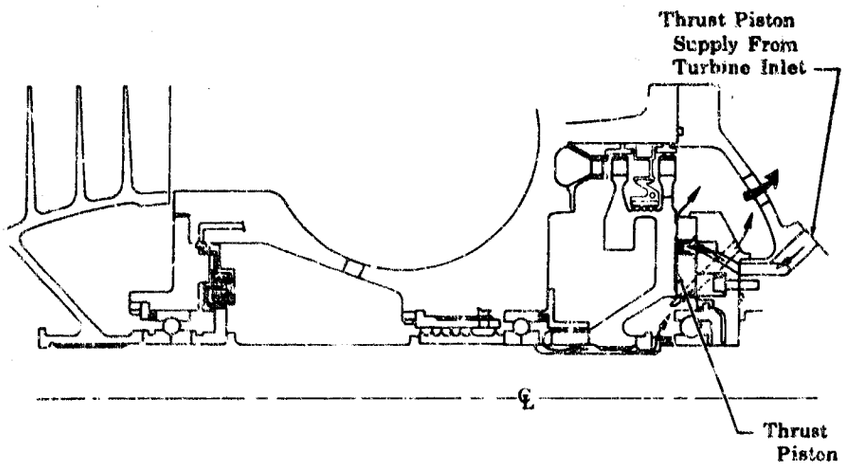

(U) Figure 406. Preliminary Fuel Low-Speed Inducer Gas Thrust Piston (Scheme B) FD 25676

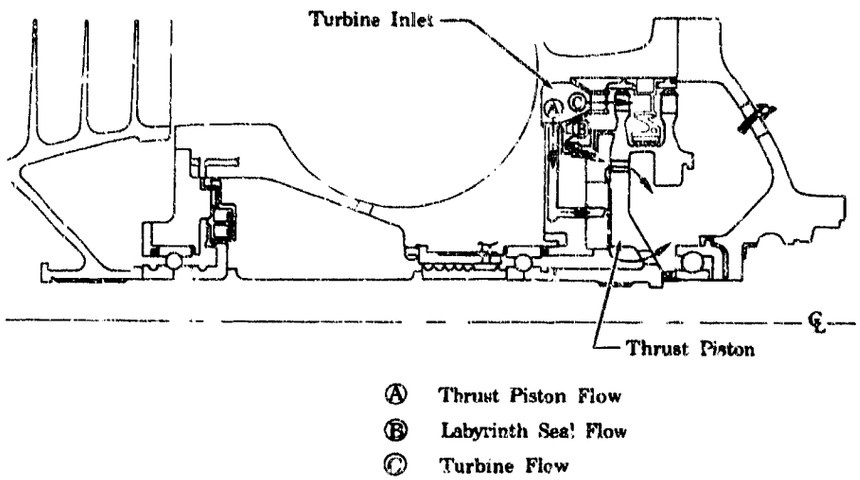

(U) Figure 407. Preliminary Fuel Low-Speed Inducer Gas Thrust Piston (Scheme C) FD 25677

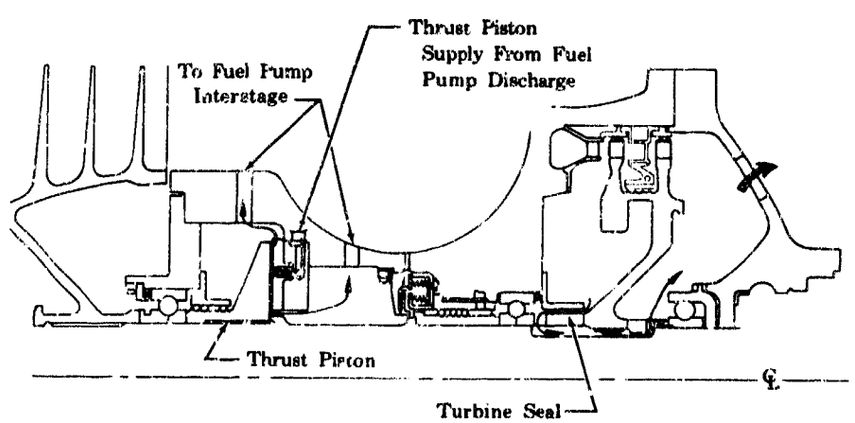

(U) Figure 408. Preliminary Fuel Low-Speed Inducer Liquid Thrust Piston (Scheme D) FD 25678

(U) Because of the power takeoff feature provided on this shaft, an overboard leakage results. This may be held to a minimum by means of a guided ring seal on the turbine end of the shaft. This seal design has been previously evaluated experimentally and based on these results it is calculated that the overboard leakage could be maintained at approximately 0.15 lb/sec with this arrangement.

(U) A liftoff seal is incorporated to prevent liquid hydrogen from flowing into the turbine during the intervals between engine operation. The liftoff seal package is common to the main fuel and oxidizer pumps.

(U) The rotor assembly of the fuel inducer is supported on 55 x 90 mm ball bearings. Because a thrust balance piston was necessary, the bearing axial load was held to only the spring force. Operational experience was accumulated on these bearings during testing of the 350K oxidizer and fuel pumps. During the final design of this component, the same bearings that are qualified for the liquid oxygen turbopump may be incorporated to provide commonality.

I. OXIDIZER LOW-SPEED INDUCER

1. OXIDIZER LOW-SPEED INDUCER

1. Introduction

(C) The demonstrator engine requires that the oxidizer low-speed inducer deliver oxygen to the inlet of the oxidizer turbopump at conditions that are not detrimental to operation of the oxidizer turbopump. The inducer must be capable of operating at a minimum NPSH of 16 ft over an oxygen inlet temperature range from 1 atmosphere boiling temperature to 180°R. The inducer will be designed with a suction specific speed of 40,000 and a maximum pressure rise of 253 psid. The low-speed inducer will be lightweight and compact with a design goal of 125 lb and be capable of stable operation over the engine operating range. The low-speed inducer will have a safety factor sufficiently high to assure confident operation without undue design refinement or testing failure. Life will be based on a 10-hour time between overhaul and 100 reuses (300 starts).

2. Design Concept

(C) A preliminary design of the oxidizer low-speed inducer is shown in Figure 409. In this design, the oxidizer inducer operates at a speed of 5716 rpm. The shaft assembly is located radially by ball bearings that are preloaded axially on the outer races to prevent ball skidding. The inducer bearings will operate well below the limiting bearing DN levels. The DN value for this preliminary design is 0.2×10^6 mm-rpm.

(C) The inducer, having a very high suction specific speed requirement of 40,000 suggests an axial flow as opposed to centrifugal or mixed flow. A complete hydraulic analysis of the inducer has not yet been performed but it is anticipated that a helical axial flow inducer will be incorporated.

(U) A thrust balance piston is required. The radial inflow turbine being a partial reaction device with a large rotor differential pressure as compared to other designs considered provides the least unbalance. The required thrust balance piston flow rate is estimated at 8.0 lb/sec.

(C) Power to drive the oxidizer inducer will be provided by a variable admission hydraulic turbine using liquid oxygen in the main chamber oxidizer line. The preliminary drive turbine selected is a single-stage, radial inflow design. Because the working fluid is a liquid, the pressure drop through a fixed area turbine would vary as a function of the flow rate squared. Therefore, a fixed-area turbine sized at minimum thrust (20% of rated thrust) will require excessive pressure drop at maximum thrust. Similarly, a turbine sized at maximum thrust will have such a small pressure drop at the minimum flow condition that it cannot provide enough power to drive the inducer. A variable-area turbine is an ideal approach to provide variable pressure drop to meet the power requirements of the inducer over the entire operating range of engine.

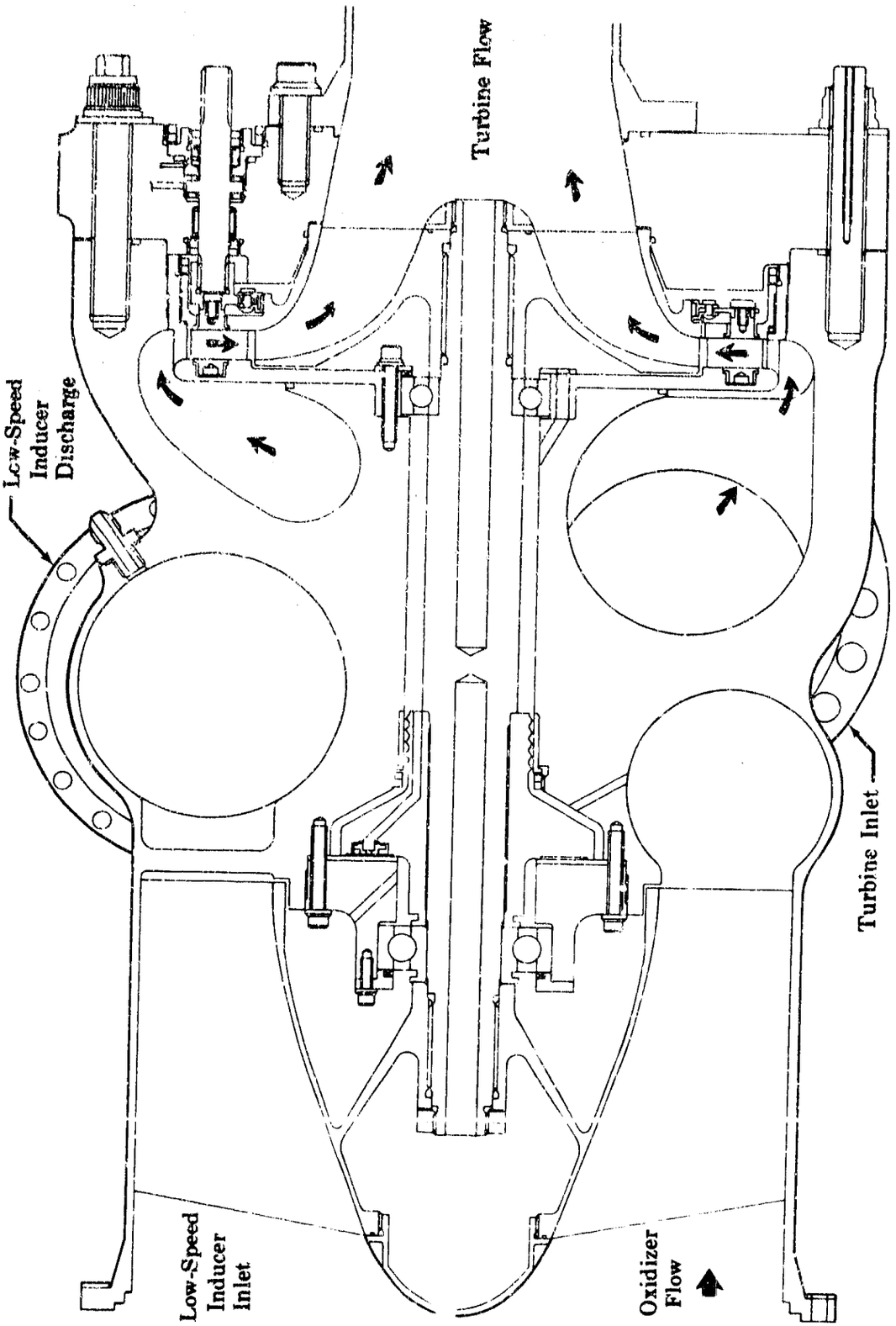

FD 25543

(U) Figure 409. Oxidizer Low-Speed Inducer Preliminary Design

(U) Variable inlet guide vanes applied to the radial inflow turbine provides maximum controllability and leakage is minimized because it is a full admission device and because the vanes operate between two parallel surfaces. This configuration is shown in Figure 409. A partial admission rotating sleeve or variable bypass area are also candidates for control of turbine power. The rotating sleeve configuration requires dividing the radial inflow area into sections that can be partially closed or opened to control power. A variable bypass may be feasible if turbine efficiency is high over the operating range. These schemes will be evaluated during the final detail design.

(U) Mechanically, the pump designed consists basically of aluminum (AMS 4130) housings, inducer, and turbine rotor with an Inconel 718 (AMS 5663) shaft, thrust balance piston, and housing, and control mechanism. The inducer can be made of K01-T6 aluminum with just under the 25% maximum allowable blockage. The potential of rubbing similar materials (i.e., aluminum on aluminum) should be minimal because with the soaked pump there will be no thermal transient and because the rotational growth will be so small. This will represent a 1/3 to 1/2 inducer weight savings as compared to an Inconel 718 (AMS 5663) inducer because much of the inducer is machining limited. Aluminum (AMS 4150) housings represent minimum weight but in the hardware design Inconel 718 (AMS 5663) will be considered. A preliminary analysis was made on the rear coverplate using the spherical design approach of the transition cases. Using Inconel 718 (AMS 5663), it appeared there would be a slight weight advantage but this will require considerable analysis. The inducer discharge horn and the turbine inlet horn are located to facilitate plumbing and to minimize pump length.

(U) An aluminum (AMS 4130) turbine rotor was chosen for weight considerations because the stress level due to rotation and pressure will be small. The Inconel 718 (AMS 5663) shaft is stress limited and the Inconel 718 (AMS 5663) thrust balance piston and housing are deflection limited.

(U) The control mechanism and supports are steel. The front support plate is subjected to turbine stator ΔP and acts as the rear bearing support isolating the aluminum thermal deflection from the bearing. The rear control support plate acts to maintain the impeller running clearance by isolating the rear coverplate pressure deflections from the impeller. Making this plate of Inconel 718 (AMS 5663) gives a dissimilar rub material to the aluminum (AMS 4130) impeller.

J. CONTROL SYSTEM

J. CONTROL SYSTEM

1. Introduction

(U) The XLR129-P-1 high pressure rocket engine uses a staged combustion cycle in which most of the fuel is burned with a portion of the oxygen in a preburner to provide turbopump power before combustion with the remainder of the oxygen in the main burner chamber. A propellant flow schematic illustrating the principal flow paths and functional component arrangement of this engine is shown in Figure 410.

(U) Hydrogen enters at the engine-driven fuel low-speed inducer where sufficient pressure rise is produced to satisfy the main fuel pump NPSH requirements. The low-speed inducer is used to minimize vehicle NPSH (i.e., tank pressure) requirements and allows high-speed main propellant pump operation at high turbopump efficiency. Hydrogen is pumped to the system operating pressure by the main fuel pump. The principal hydrogen flow path from the pump is through the preburner supply heat exchanger, and then into the preburner chamber through the preburner injector. The remainder of the hydrogen flows through the transpiration supply heat exchanger and then through low-speed fuel inducer drive turbine prior to being passed into the main chamber as transpiration coolant. A small amount of hydrogen is bled off at the main fuel pump interstage to provide coolant for the two-position nozzle. This coolant flows to the nozzle through a regulating orifice and a shutoff valve that is provided to stop the flow when the two-position nozzle is in the retracted position.

(U) Oxygen enters at the oxidizer low-speed inducer where enough pressure rise is produced to satisfy the main oxidizer pump NPSH requirements. The oxygen is then pumped to system operating pressure levels by the main oxidizer pump. Pump discharge flow is split between the preburner and the main combustion chamber. The principal oxidizer flow passes through and becomes the working fluid for the oxidizer low-speed inducer turbine before being injected into the main burner chamber. The remainder, a smaller scheduled portion of the oxygen, is ducted to the preburner where it is burned with the hydrogen. The resulting combustion products split through parallel ducts passing through the two main pump turbines, arranged in parallel. The energy required to drive the main pumps is extracted from these combustion products, which then exhaust from the turbines and mix in a common passage of the transition case. These gases then pass through the main burner injector and into the main burner chamber where they mix and burn with the principal oxidizer flow. These combustion gases are then expanded through the bell nozzle to provide thrust.

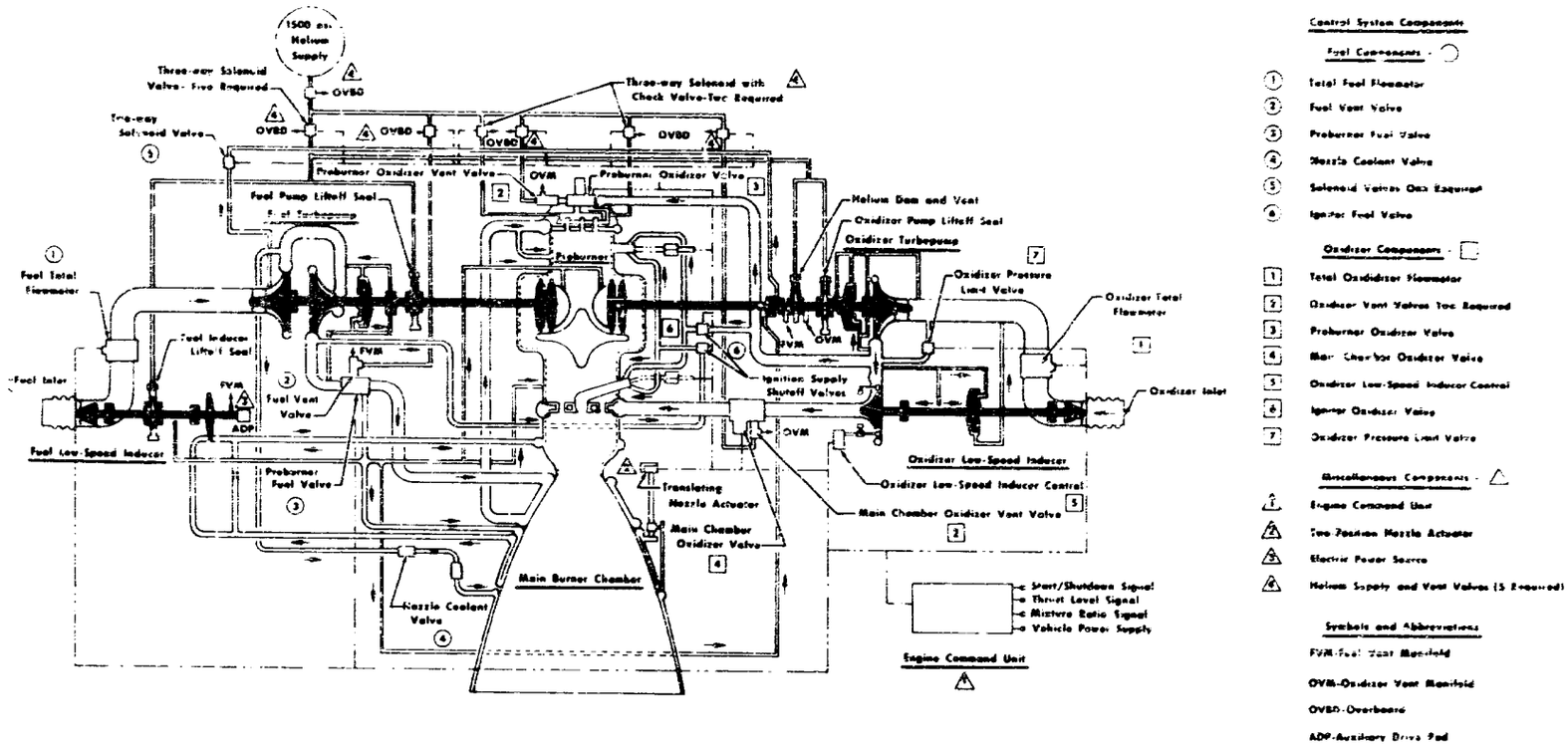

(U) Figure 410. Engine Control System Schematic

FD 25345

(U) Analysis of the XLR129-P-1 rocket engine cycle has established that the following five control points are required for satisfactory steady-state operation:

1. Preburner fuel valve
2. Oxidizer pressure limit valve
3. Preburner oxidizer valve
4. Main chamber oxidizer valve
5. Oxidizer low-speed inducer control.

(U) It is recommended that valve designs for these locations be completed for incorporation into the demonstrator engine.

a. Preburner Fuel Valve

(1) Introduction

(U) The preburner fuel valve is located downstream of the fuel pump in the line to the preburner supply heat exchanger. The function of this valve is to regulate the hydrogen flow to the preburner, and split off transpiration coolant flow for the main chamber. Because this control regulates hydrogen flow, it has a major influence on pump discharge pressure, chamber mixture ratio, and available turbine power. It has only a minor influence on thrust, because fuel flow is a small part of total propellant weight flow. Because the fuel valve influences pump discharge pressure, it affects low-speed inducer drive power (i.e., main fuel pump NPSH) as well as transpiration cooling flow. Further, the fuel valve provides pressure loss to aid fuel system stability and provides the main fuel flow shutoff function.

(2) Conclusions and Recommendations

(U) The valve selection study completed for this control point requirement resulted in selection of a butterfly type valve for this application. Completion of the selected valve design, parts procurement and testing are recommended for the next period.

b. Oxidizer Pressure Limit Valve

(1) Introduction

(C) The oxidizer pressure limit valve limits pump discharge pressure to 6000 psia. When excess oxidizer pump drive horsepower is available (at high thrust and low mixture ratio conditions), the valve opens and regulates oxidizer pump recirculation flow to absorb the excess power and thus limit pump discharge pressure.

(2) Conclusions and Recommendations

(U) A recirculation valve for the oxidizer turbopump will be required to limit the oxidizer turbopump discharge pressure. Completion of a design selection study and a valve design for the demonstrator engine are recommended.

c. Preburner Oxidizer Valve

(1) Introduction

(U) The preburner oxidizer valve regulates the flow split to the primary and secondary oxidizer elements of the preburner injector during engine operation. The resultant variation in primary and secondary flow split controls the velocity of the oxidizer entering the preburner and ensures stable and efficient preburner combustion. This valve has a major influence on available main turbine power and engine thrust, but only a minor influence on overall engine mixture ratio.

(U) The preburner oxidizer valve also shuts off the oxidizer flow to the preburner when the engine is not operating.

(2) Conclusions and Recommendations

(U) A translating sleeve valve with rig tested lip type shaft seals, pressure balanced beryllium cooper piston rings bearing on a precision chrome-coated housing, and a face type TFE Teflon shutoff seal is being designed for the demonstrator engine.

(U) It is recommended that the valve design be completed and parts be procured for demonstrator engine testing.

d. Main Chamber Oxidizer Valve

(1) Introduction

(U) The main chamber oxidizer valve is located in the oxidizer supply line to the main chamber. Because this control regulates the main burner flow, which is a major portion of the total propellant flow, it has a strong influence on both engine mixture ratio and thrust. The main chamber oxidizer valve was designed and fabricated during Phase I (Contract AF04(611)-11401).

(U) The valve is a butterfly type and incorporates a shutoff seal for the oxidizer flow to the main burner injector. To accommodate this shutoff feature, a canted shaft with integral disk was selected so that an uninterrupted disk sealing surface would be provided.

(2) Conclusions and Recommendations

(U) Shaft lip seal and shutoff seal development resulted in satisfactory designs. The designs are recommended for incorporation in the demonstrator engine design.

e. Oxidizer Low-Speed Inducer Control

(1) Introduction

(U) The oxidizer low-speed inducer control schedules the nozzle (admission) area of the oxidizer low-speed inducer turbine. Modulation of this control affects available main oxidizer pump NPSH because the turbine nozzle velocity determines turbine power and, therefore, oxidizer low-speed inducer pressure rise. Because this control is in series with the main chamber oxidizer valve it also has a strong effect on engine mixture ratio and thrust.

(2) Conclusions and Recommendations

(U) No specific design requirements will be available until the low-speed inducer turbine design concept is firm. Design and procurement will be recommended at that time.

2. Preburner Fuel Valve

a. Valve Type Selection

(U) The preburner fuel valve regulates the fuel flow to the preburner injector and provides a positive shutoff seal. A port downstream of the shutoff seal and upstream of the regulated flow area is required for transpiration coolant supply for the main burner chamber.

(C) The preburner fuel valve design selection study requirements specified a maximum effective area of 5.34 in^2 and a turndown ratio of 14.8 to 1. Inlet and exit line sizes were based on 200 ft/sec maximum fuel velocity.

(U) The objective of the selection study was to evaluate various valve types and select one for use in this engine application. The evaluation included definition of the actuation power requirements, weight and packaging studies and general performance characteristics. The various candidates are discussed in the following paragraphs. As a result of this selection study, the butterfly valve candidate was selected for the preburner fuel valve.

(1) Translating Sleeve Valve Candidates

(U) The four translating sleeve valve candidates are illustrated in Figure 411 through 414. Parametric curves for sizing these valves are provided in Figure 415 in which valve diameter is plotted as a function of stroke for various ratios of maximum port width to valve circumference. Experience and minimum envelope requirements dictated the point selection shown.

(U) The sleeve valve candidates illustrated in Figures 411 and 412 have only one shutoff seal. These candidates also have a relatively long clearance path with labyrinth type seal between the sleeve and the housing that is intended to eliminate the requirement for a piston ring secondary seal.

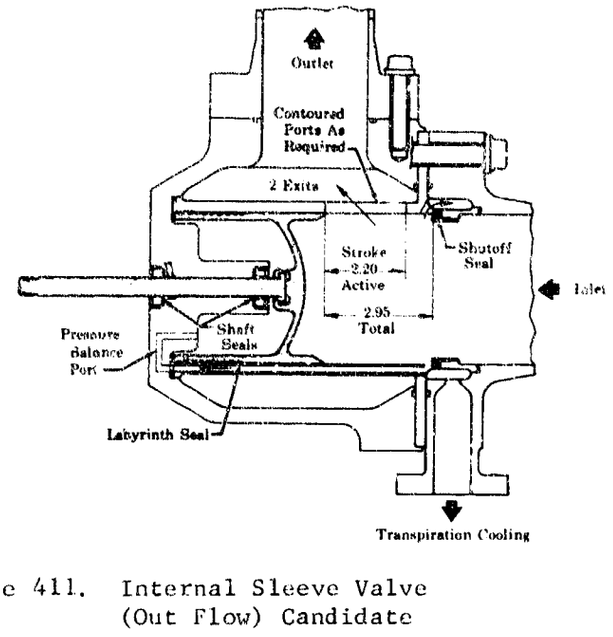

(U) Figure 411. Internal Sleeve Valve (Out Flow) Candidate FD 25346

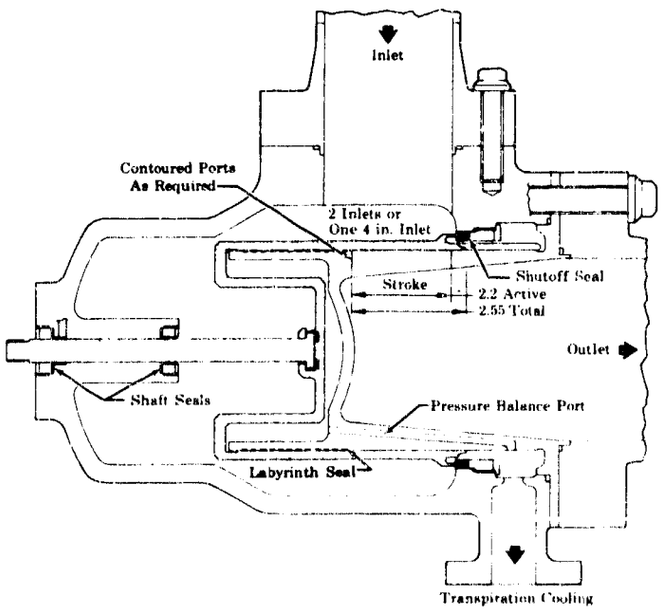

(U) Figure 412. External Sleeve Valve Candidate FD 25347

(This page is Unclassified)

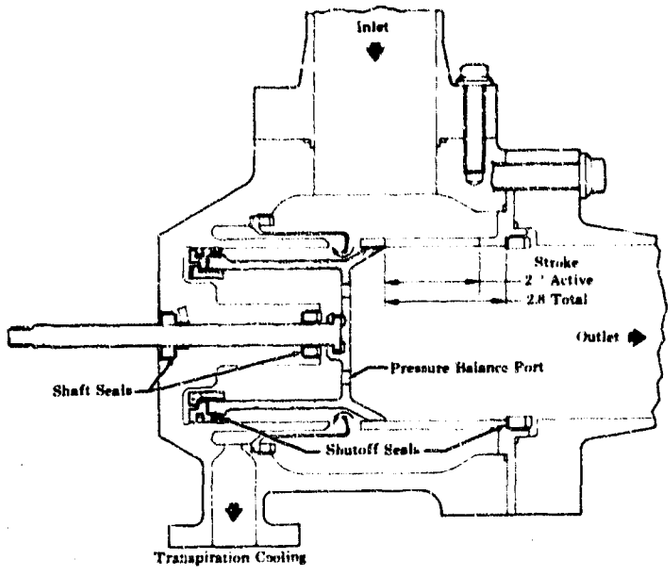

(U) Figure 413. Internal Sleeve Valve (Fixed Ports) Candidate FD 25348

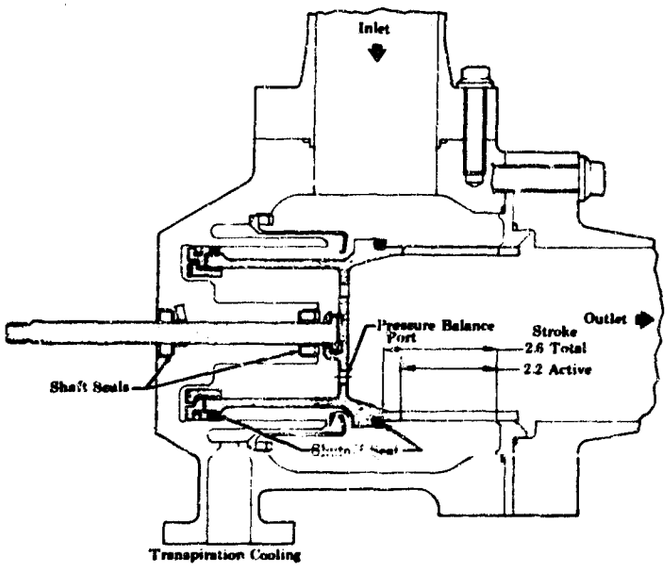

(U) Figure 414. Internal Sleeve Valve (Movable Ports) Candidate FD 25349

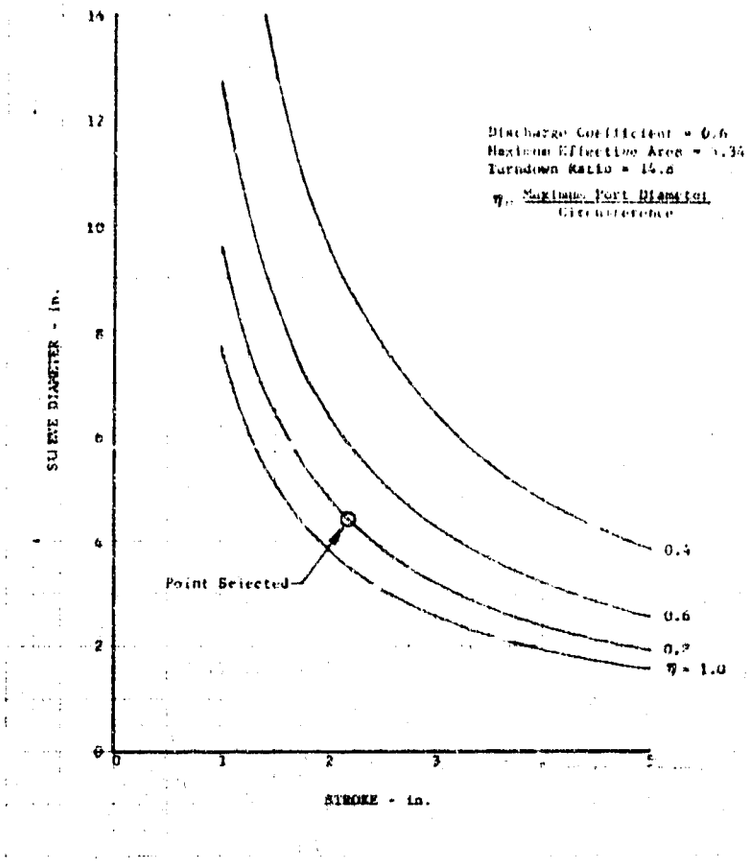

(U) Figure 415. Sleeve Valve Diameter vs Stroke DF 68372

(U) The sleeve valve candidates illustrated in Figures 413 and 414 have two shutoff seals. The second seal shuts off the transpiration chamber coolant flow as well as the secondary leak path around the sleeve. This configuration requires a flexible housing member that deflects and permits both seals to attain adequate sealing pressure. The preburner oxidizer valve program has shown that the face type seal is durable and has low leakage.

(U) The axial flow forces acting on the sleeve valve candidates are shown in Figures 416 through 419. A comparison plot of the maximum force curves for these valves is shown in Figure 420.

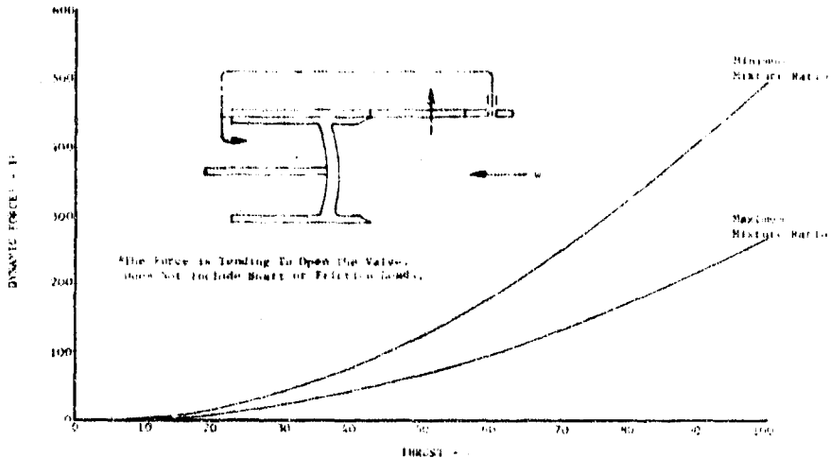

(U) Figure 416. Dynamic Force vs Thrust (Internal Sleeve Valve - Reverse Flow) DF 68373

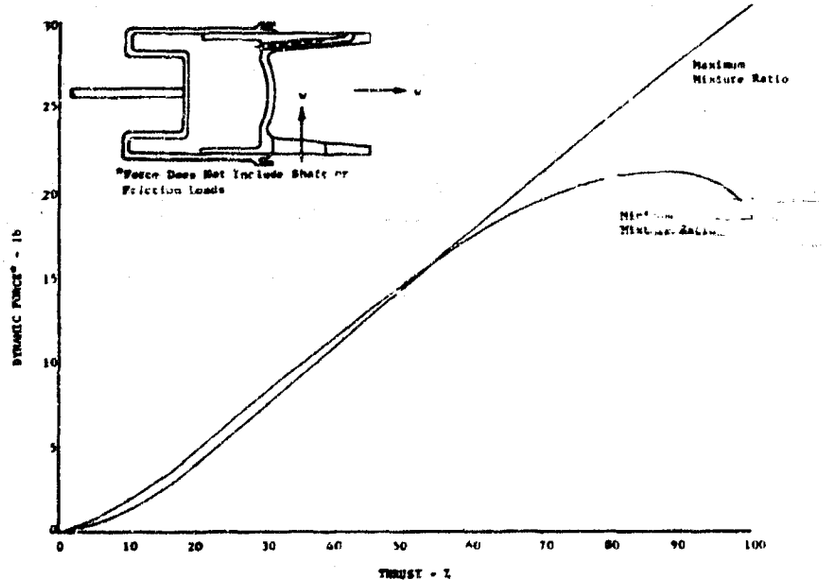

(U) Figure 417. Dynamic Force vs Thrust (External Sleeve Valve) DF 68374

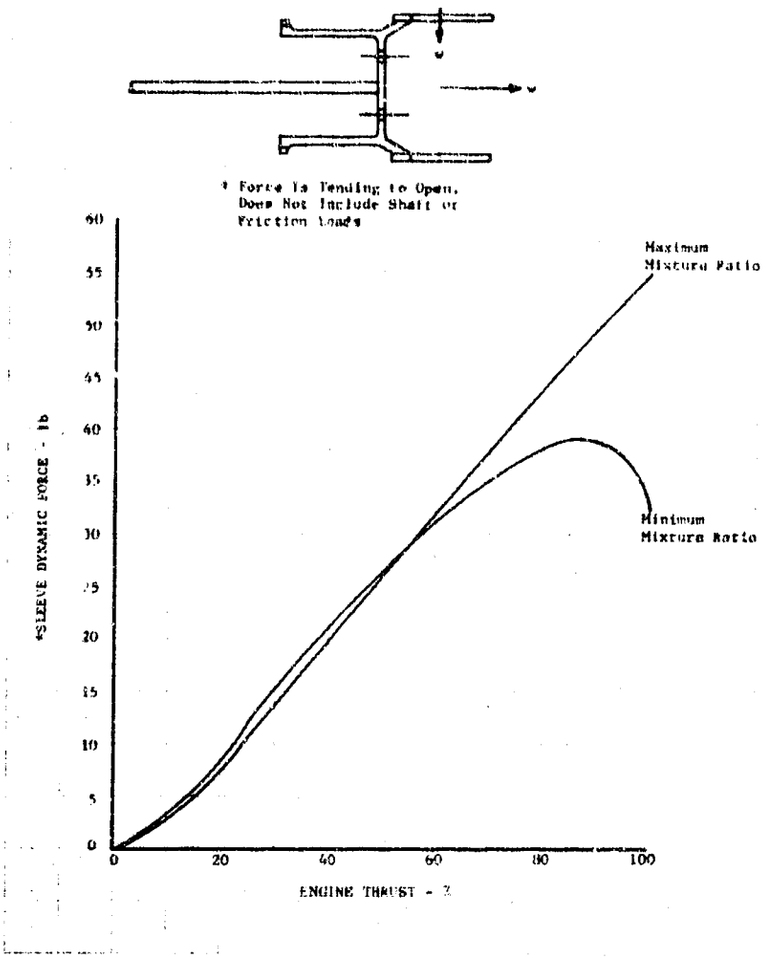

(U) Figure 418. Dynamic Force vs Thrust (Internal Sleeve Valve - Fixed Ports) DF 68375

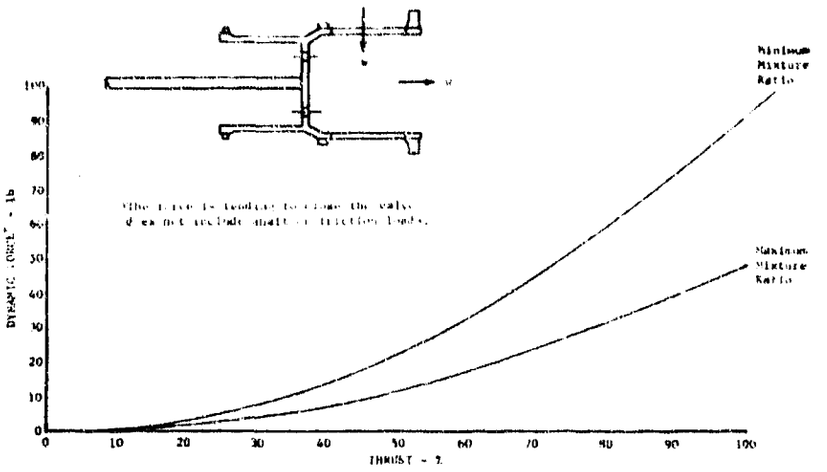

(U) Figure 419. Dynamic Force vs Thrust (Internal Sleeve Valve - Movable Ports) DF 68376

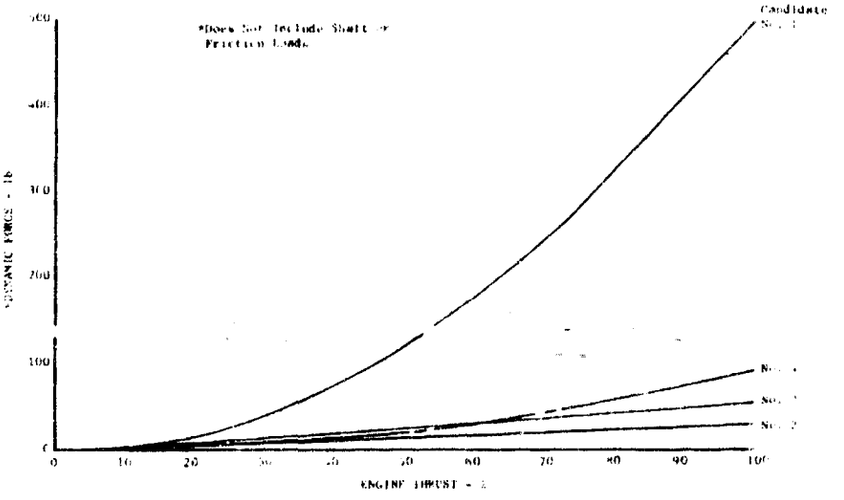

(U) Figure 420. Dynamic Force Comparison of Sleeve Valve Candidates DF 68637

(2) Pintle Valve Candidate

(U) The pintle valve candidate is illustrated in Figure 421. The valve is similar in construction to the sleeve type valve candidate except a contoured pintle is utilized for flow control instead of a sleeve and contoured ports. The inlet port is 90 degrees from the axis of the valve.

The pintle valve candidate also has two shutoff seals; one for primary fuel flow and one for transpiration coolant flow. The pintle valve candidate parametric sizing is shown in Figure 422. The point selected provides the shortest stroke compatible with a reasonable orifice diameter and pintle contour angle. The axial dynamic force acting on the pintle as a function of engine thrust is shown in Figure 423.

(U) Operational and mechanical problems previously experienced with respect to force reversals, parts concentricities, and contamination sensitivity also apply to this application.

(3) Inverted Pintle Valve Candidate

(U) The inverted pintle valve candidate is illustrated in Figure 424. The inverted pintle is similar to the pintle valve candidate except the housing is contoured to produce the effective area versus stroke relationship. This causes the area with a variable pressure profile to be on the housing instead of on the moving part. Two shutoff seals are also required for this candidate.

(U) The throat sizing is illustrated in Figure 425 and the parametric valve sizing curves are illustrated in Figure 426. The points selected allow reasonable package size and low parasitic losses.

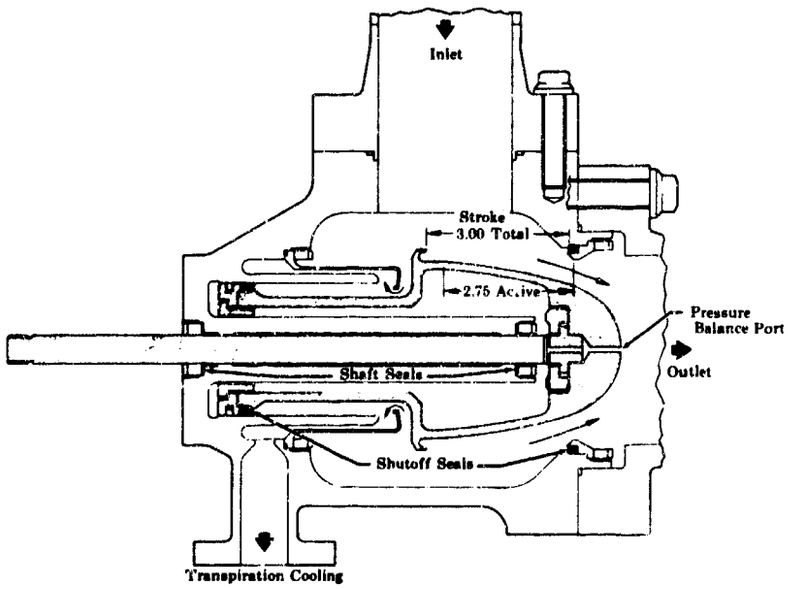

(U) Figure 421. Pintle Valve Candidate FD 25350

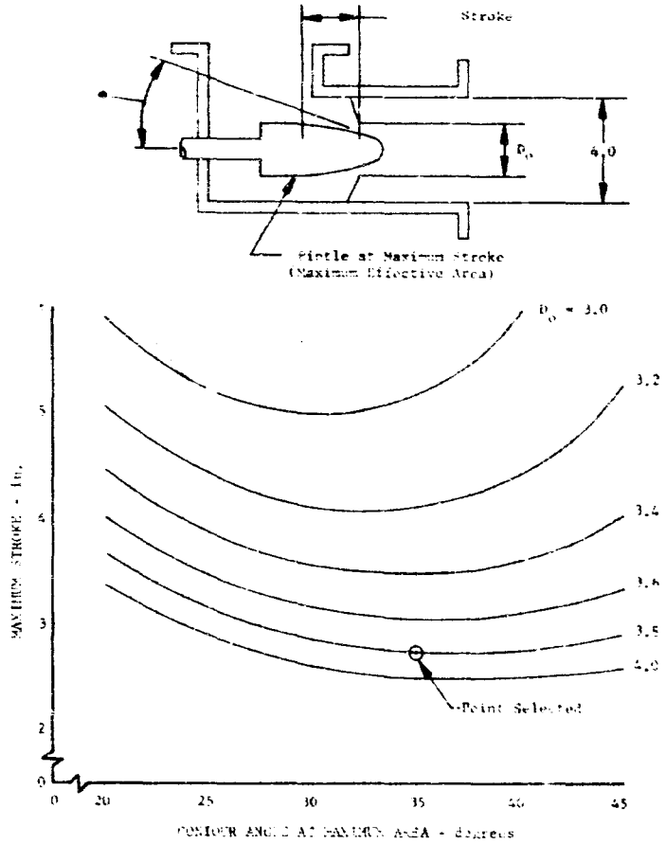

(U) Figure 422. Maximum Stroke vs Contour Angle (Pintle Valve) DF 68377

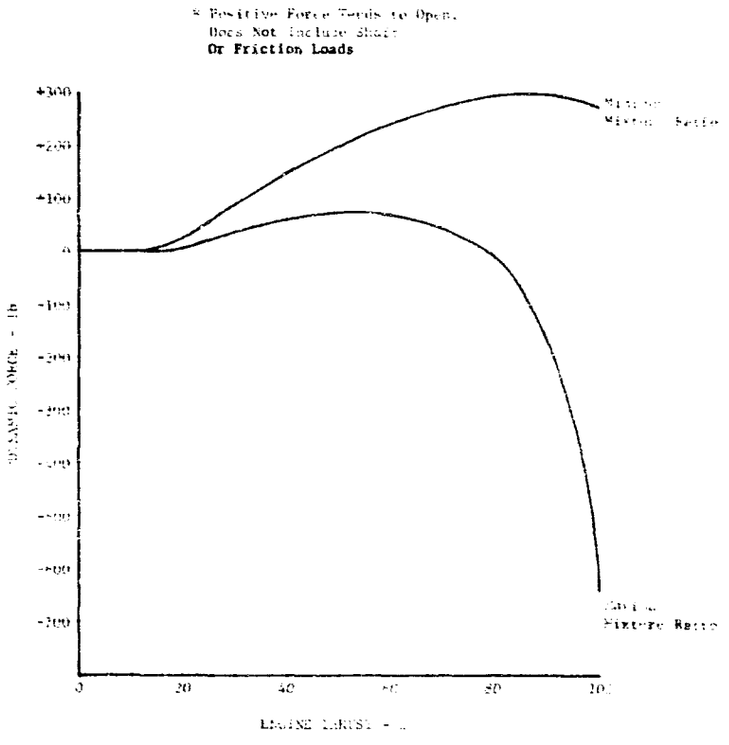

(U) Figure 423. Dynamic Force vs Thrust (Pintle Valve) DF 68378

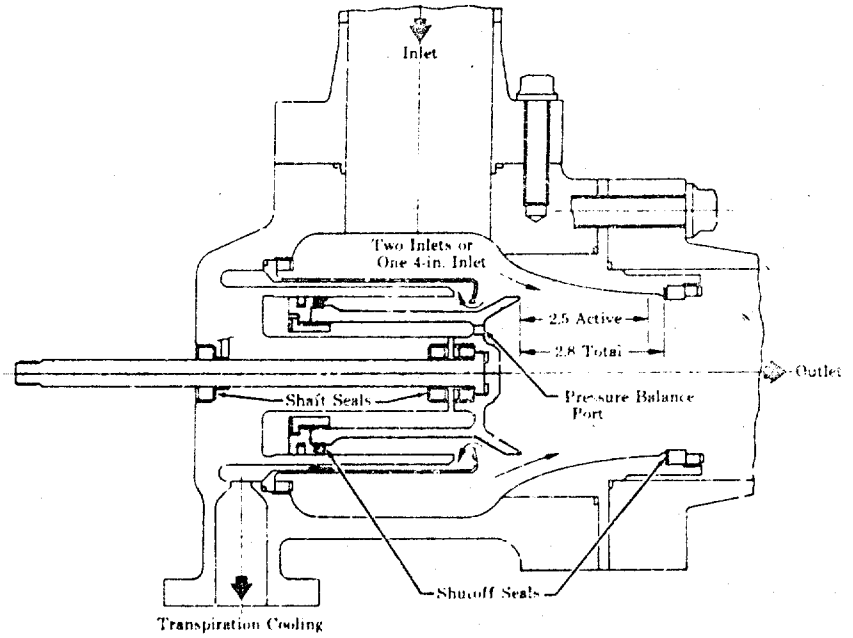

(U) Figure 424. Inverted Pintle Valve Candidate FD 25351

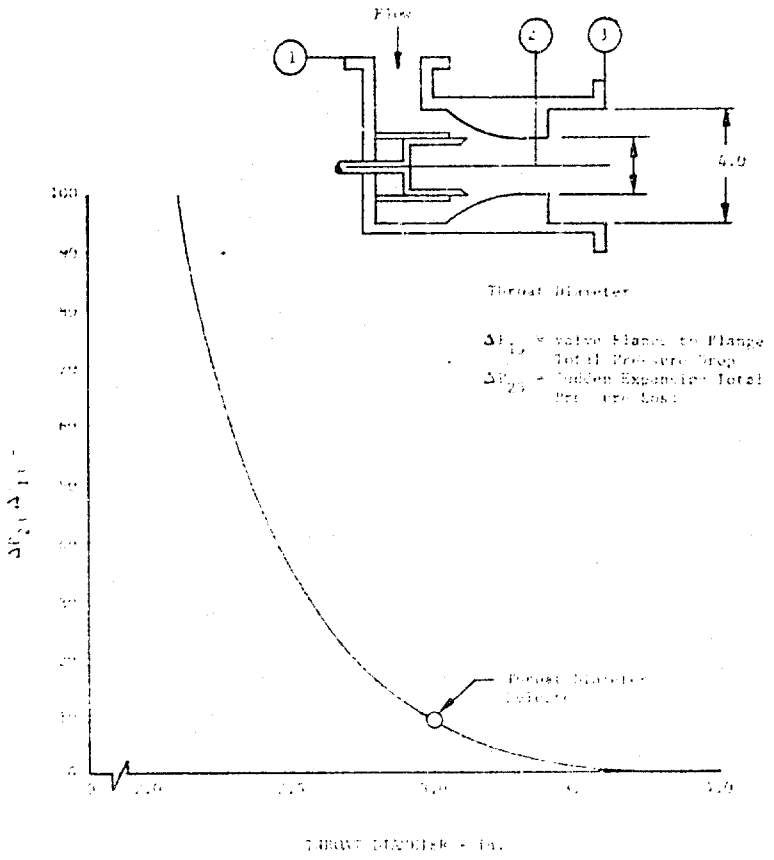

(U) Figure 425. Throat Size Selection DF 68379
(Inverted Pintle)

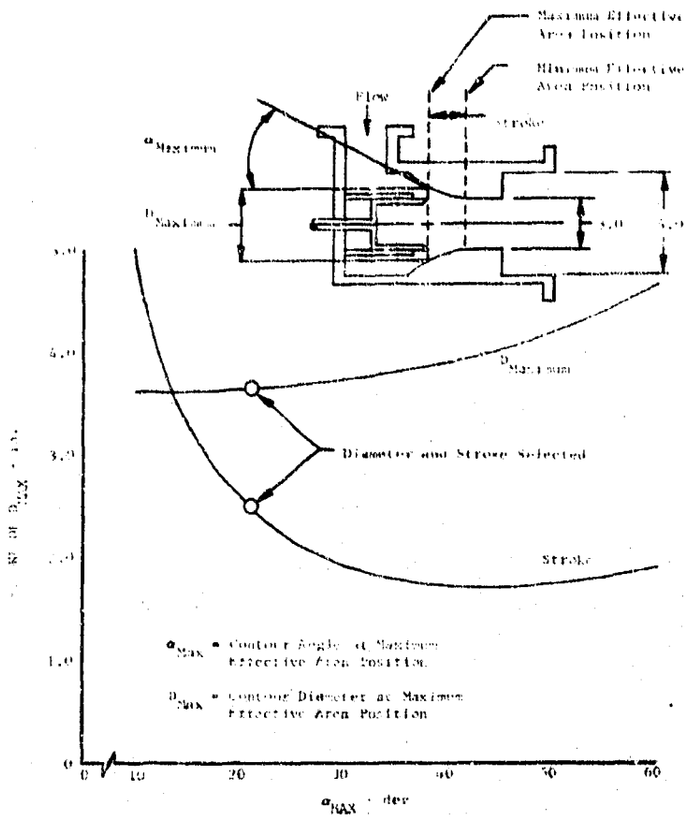

(U) Figure 426. Parametric Sizing for Inverted Pintle DF 68380

(4) Butterfly Valve Candidate

(U) The butterfly valve candidate is illustrated in Figure 427. The trailing edge of this butterfly valve, instead of being streamlined, is rather broad and shaped to cause the flow coefficient to remain low on the trailing edge, as it normally does for the leading edge, over the entire stroke. The throat sizing point illustrated in Figure 428 was selected to provide optimum percentage area characteristics with reasonable area margin.

(U) The flow velocity across the face of the disk is lower than for a standard disk shape, resulting in low dynamic torque as shown in Figure 429. The design also allows a spherical zone on the disk, offset from the shaft centerline, that may be used as the sealing surface. This eliminates the necessity for an inclined shaft and the resulting unbalanced thrust load.

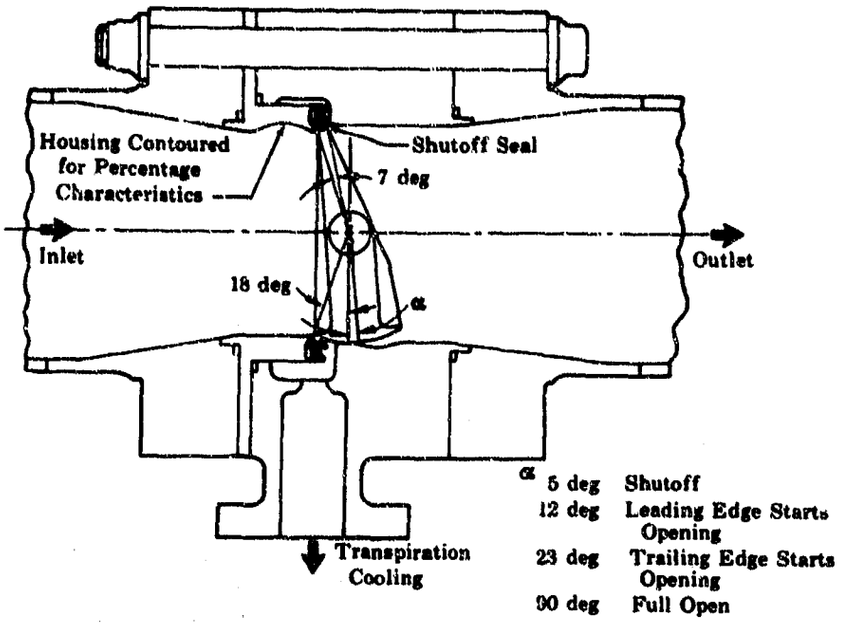

(U) Figure 427. Butterfly Valve Candidate FD 25352A

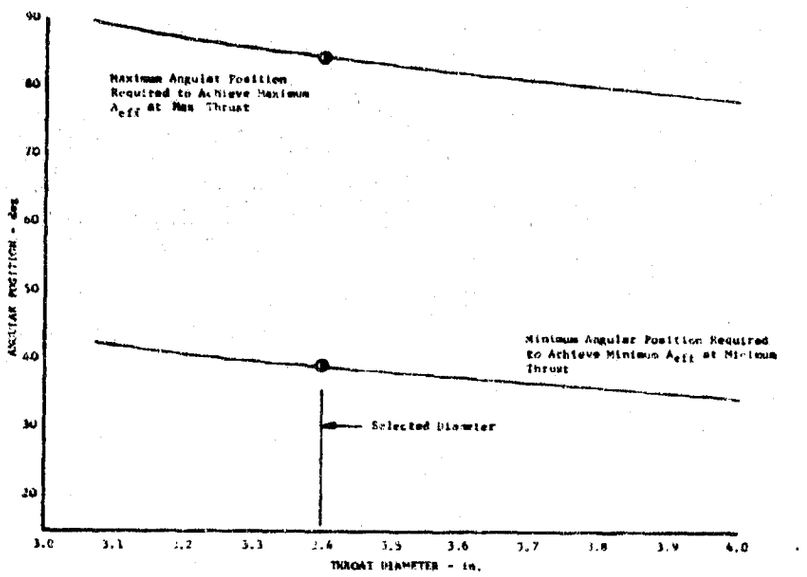

(U) Figure 428. Angular Position vs Throat Diameter (Butterfly Valve) DF 68381

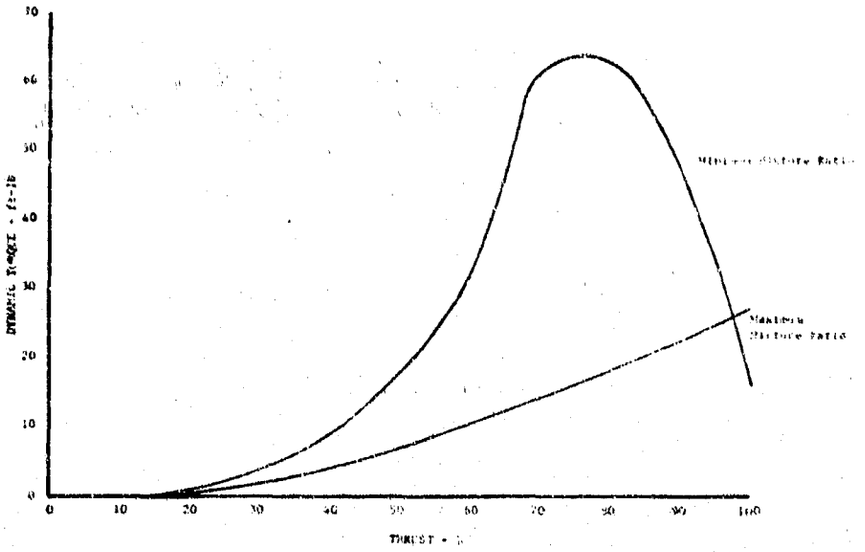

(U) Figure 429. Dynamic Torque vs Thrust (Butterfly Valve) DF 68382

(U) The configuration shown allows an angular travel of 18 degrees from the shutoff position to the position where the trailing edge starts regulating. This travel deadband provides a convenient location to tap off transpiration chamber coolant flow upstream of the regulated area. Figures 430 and 431 show effective area versus stroke and percent error characteristics for this valve with a cylindrical flow path. The housing contour may be modified as shown in Figure 427 to optimize the percentage error characteristics.

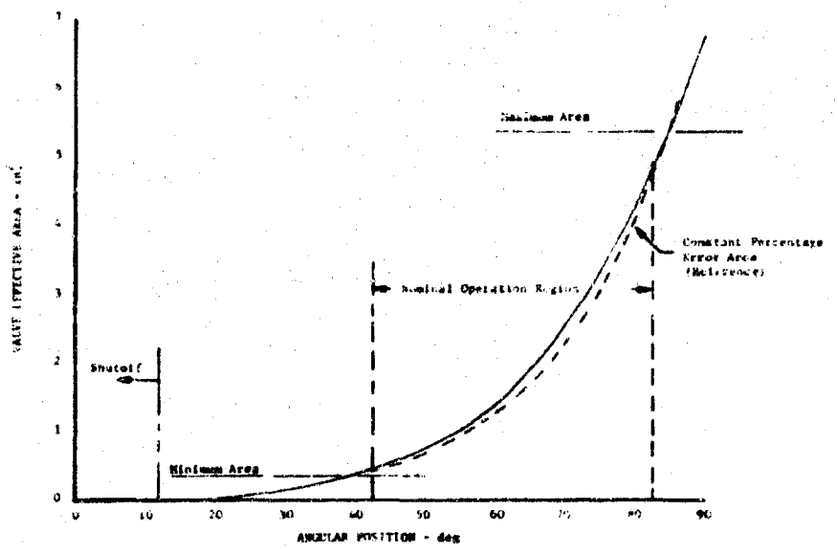

(U) Figure 430. Effective Area vs Angular Position (Butterfly Valve) DF 68383

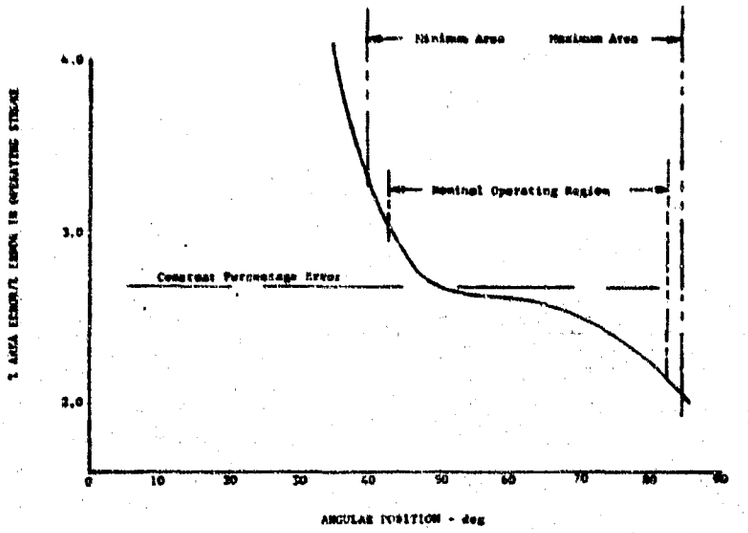

(U) Figure 431. Area Error vs Angular Position (Butterfly Valve) DF 68384

(5) Comparison Summary

(U) Valve and associated system weights for all of the candidates are provided in Table XXXIX, which also includes the power required for each of the candidates. The rating for both were made in the same manner. The dynamic power value is based on the maximum force required for each candidate. The total power includes that required for shaft lip seals and piston ring secondary seals if applicable. The ratings for valve weight are based on the total installation requirements and include the attaching flanges shown shaded in Figure 432.

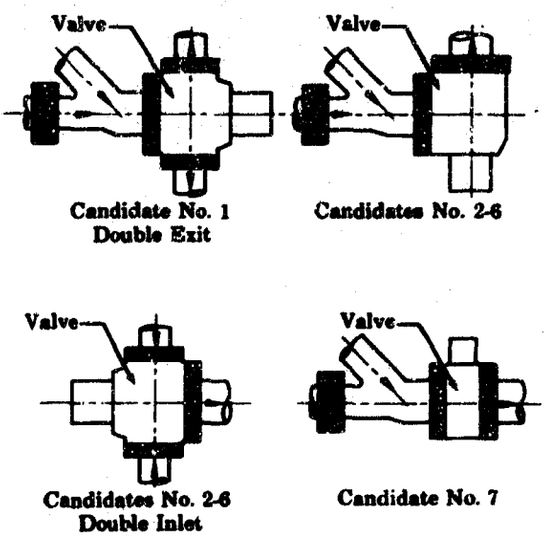

Candidate No.

1. Internal Sleeve Valve (Out Flow)
2. External Sleeve Valve
3. Internal Sleeve Valve (Fixed Ports)
4. Internal Sleeve Valve (Movable Ports)
5. Pintle Valve
6. Inverted Pintle Valve
7. Butterfly Valve

(U) Figure 432. Preburner Fuel Valve Installation Schematic FD 25359

(U) Table XXXIX. Weight and Power

		Internal Sleeve Valve (Out Flow)	External Sleeve Valve	Internal Sleeve Valve (Fixed Ports)	Internal Sleeve Valve (Movable Ports)	Pintle Valve	Inverted Pintle Valve	Butterfly Valve
Valve Weight (lb)		52.9	54.7	52.9	52.9	47.0	51.2	33.3
Valve and Associated Flange Weight (lb)* Single Inlet		92.5	100.9	99.1	99.1	93.2	97.4	69.5
Valve and Associated Flange Weight (lb)* Double Inlet		92.5	81.1	79.3	79.3	73.4	77.6	69.5
Horsepower ** Unbalanced Actuator Rod	Dynamic	43.0	22.4	23.1	17.9	16.6	27.4	5.6
	Shaft Seal	2.2	2.2	2.2	2.2	2.2	2.2	5.9
	Piston Ring			3.2	3.2	3.6	0.4	
Dynamic Includes Pressure on Rod	Total	45.2	24.6	28.5	23.3	22.4	30.0	6.5
	Dynamic	10.0	0.6	1.1	1.1	17.0	0.0	5.6
Horsepower ** Pressure Balanced Actuator Rod	Shaft Seal	4.0	4.0	4.0	4.0	4.0	4.0	0.9
	Piston Ring			3.2	3.2	3.6	2.6	
	Total	14.0	4.6	8.3	8.3	24.6	6.6	6.5

*This weight includes flanges shown shaded in Figure 432.
**Horsepower is based on an arbitrarily selected frequency of 10 cycles per second because the actual required frequency has not been determined.

(U) The relative values of the selection criteria are shown in the first column of Tables XL, XLI, and XLII. The highest rated candidate received the greatest number of points. The ratings in Table XL consider single pipe inlets and unbalanced actuation shafts as shown in the valve configuration sketches. Those in Table XLI assume that the actuator shaft has been fully balanced by addition of opposing pressure areas. Table XLII shows the added advantage gained through the use of two inlet lines for those valve types that would benefit from such an arrangement. The butterfly valve received the highest number of points in each rating. The external sleeve valve received the next highest number of points for two of the three ratings.

(U) Table XL. Valve Rating Based on Single Inlets and Unbalanced Actuation Shafts

Selection Criteria	Maximum No. of Points For Each Category	Internal Sleeve Valve (Out Flow)	External Sleeve Valve	Internal Sleeve Valve (Fixed Ports)	Internal Sleeve Valve (Movable Ports)	Pintle Valve	Inverted Pintle Valve	Butterfly Valve
Weight (Valve and Flanges)	100	75	69	70	70	70	71	100
Shutoff Seal Development Req'd	100	100	100	80	80	80	80	50
Actuator Power	95	14	25	22	28	28	20	95
Reliability	90	70	70	50	50	50	50	70
Low Parasite Pressure Loss	70	50	35	35	35	40	40	70
No. of Dynamic Seals Req'd.	65	65	65	65	65	65	65	65
Packaging	60	60	45	45	45	45	45	55
Percent Error Characteristics	60	60	60	60	60	55	55	60
Manufacturing Ease	55	45	40	35	35	30	30	55
Flexibility	50	40	40	40	40	50	50	35
Complexity	45	40	40	35	35	30	35	45
Total Points	790	619	589	537	543	548	541	700

(U) Table XLI. Valve Rating Based on Single Inlets and Balanced Actuation Shafts

Selection Criteria	Maximum No. of Points For Each Category	Internal Sleeve Valve (Out Flow)	External Sleeve Valve	Internal Sleeve Valve (Fixed Ports)	Internal Sleeve Valve (Movable Ports)	Pintle Valve	Inverted Pintle Valve	Butterfly Valve
Weight (Valve and Flanges)	100	75	69	70	70	75	71	100
Shutoff Seal Development Req'd.	100	100	100	80	80	80	80	50
Actuator Power	95	31	95	53	53	18	66	67
Reliability	90	65	65	45	45	45	55	70
Low Parasite Pressure Loss	70	50	35	35	35	40	40	70
No. of Dynamic Seals Req'd.	65	50	50	50	50	50	50	65
Packaging	60	60	45	45	45	45	45	55
Percent Error Characteristics	60	60	60	60	60	55	55	60
Manufacturing Ease	55	40	35	30	30	25	25	55
Flexibility	50	40	40	40	40	50	50	35
Complexity	45	35	35	30	30	25	30	45
Total Points	790	606	629	538	538	508	567	672

(U) Table XLII. Valve Rating Based on Double Inlets (where applicable) and Balanced Actuation Shafts

Selection Criteria	Maximum No. of Points For Each Criteria	Internal Sleeve Valve (Out Flow)	External Sleeve Valve	Internal Sleeve Valve (Fixed Ports)	Internal Sleeve Valve (Movable Ports)	Pintle Valve	Inverted Pintle Valve	Butterfly Valve
Weight (Valve and Flanges)	100	75	86	88	88	95	90	100
Shutoff Seal Development Req'd.	100	100	100	80	80	80	80	50
Actuator Power	95	31	95	53	53	18	66	67
Reliability	90	65	65	45	45	45	55	70
Low Parasite Pressure Loss	70	50	35	35	35	40	40	70
No. of Dynamic Seals Req'd.	65	50	50	50	50	50	50	65
Packaging	60	60	45	45	45	45	45	55
Percent Error Characteristics	60	60	60	60	60	55	55	60
Manufacturing Ease	55	40	35	30	30	25	25	55
Flexibility	50	40	40	40	40	50	50	35
Complexity	45	35	35	30	30	25	30	45
Total Points	790	606	646	556	556	528	586	672

3. Oxidizer Pressure Limit Valve

a. Introduction

(U) A recirculation valve for the oxidizer turbopump will be required to limit the oxidizer turbopump discharge pressure. The valve will only be required to operate near maximum thrust and minimum mixture ratio. A scheduled valve position as a function of thrust and mixture ratio is the planned control mode.

b. Analysis

(U) The cycle analysis has defined the valve area schedule, however, no design effort on the valve has been started.

4. Preburner Oxidizer Valve

a. Introduction

(U) A valve is required to control the oxidizer flow to the preburner injector. The valve must (1) provide a positive shutoff to the total preburner oxidizer flow, (2) provide primary flow for starting, and (3) modulate the secondary flow over the operating range. Most of the design features of the preburner oxidizer valve now being designed have been evaluated in test rigs or during the flow divider valve test program that was conducted during Phase I (Contract AF04(611)-11401). Lip seals, which were evaluated during the supporting data and analysis program phase, will be used to seal the translating shaft and balance piston. Pressure balanced piston ring designs were tested under the supporting data and analysis subtask. These piston ring designs effectively reduced wear and actuation force; however, it was desired to optimize the piston ring design to minimize the actuation force requirements. A piston ring redesign and actuation force test were conducted in support of the preburner oxidizer valve design.

b. Conclusions and Recommendations

(U) The balanced piston rings as tested will provide acceptable actuator loads for the preburner oxidizer valve.

c. Analysis

(U) The preburner oxidizer valve, which is nearing the layout completion stage is shown in Figure 433. Basic design features differing from the preburner oxidizer valve tested during Phase I (Contract AF04(611)-11401) include incorporating; the preburner dome cover as the valve housing, replaceable trim orifices in the primary flow passages, shaft lip seals, balanced piston rings, improved lower piston ring retainer and reduced overall length.

(U) Design layouts for water flow and cryogenic pressure test blocks are also in process. A revised facility type actuator layout has been completed and is shown in Figure 434.

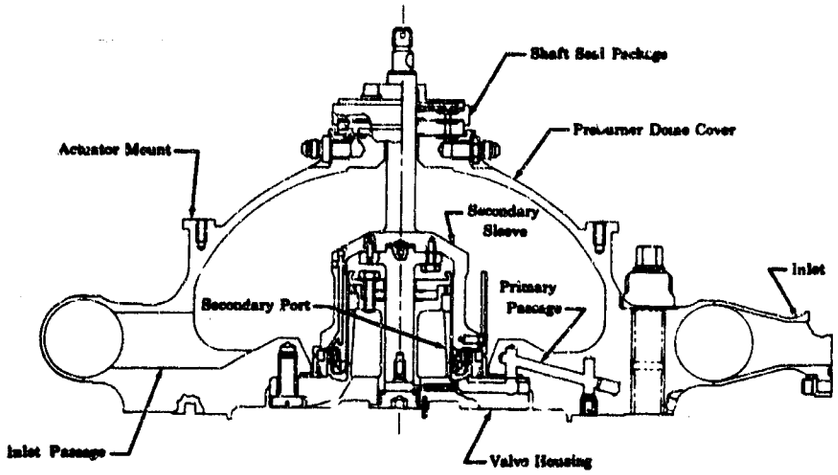

(U) Figure 433. Preburner Oxidizer Valve Layout FD 25595

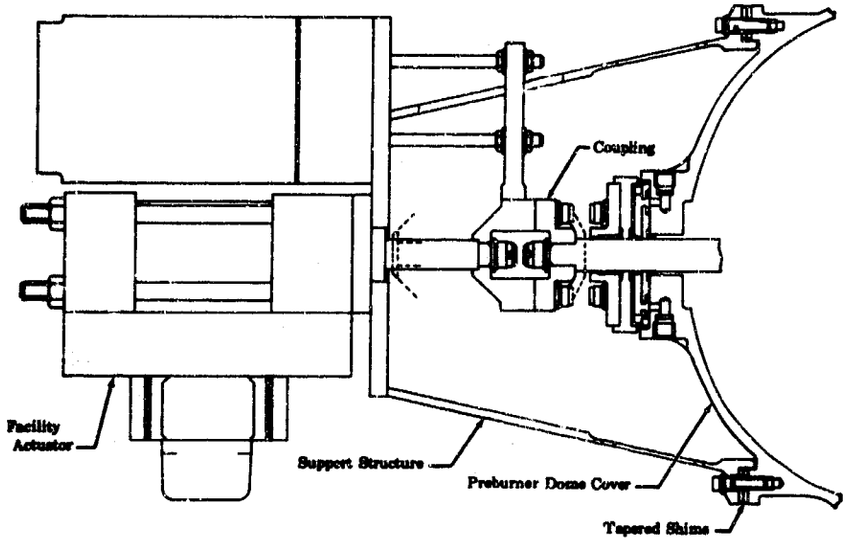

(U) Figure 434. Preburner Oxidizer Valve Actuator Layout FD 25596

(U) A piston ring design analysis task was initiated to reduce the valve actuation drag load that was experienced during the tests that were conducted under the supporting data and analysis subtask. The rig and the valve had two piston rings each: an upper ring attached to the housing and a lower ring attached to the sleeve. Figure 435 compares the four upper rings that were analyzed in this design study and Figure 436 compares the lower rings. All rings were made of Berylco 25, either AMS 4650 or AMS 4532.

(C) Two sets of data were available from previous rig tests. At a pressure differential of 2000 psi, the unbalanced rings had a drag of 1480-lb opening and 4560-lb closing. Under the same conditions, the balanced rings had a drag of 755-lb opening and 1890-lb closing. The difference

between the opening and closing drag loads and the wear patterns on the previously tested piston rings indicated that the rings were twisting and that the corners were possibly digging into the sliding surfaces. These conditions would, therefore, cause the friction factor to vary.

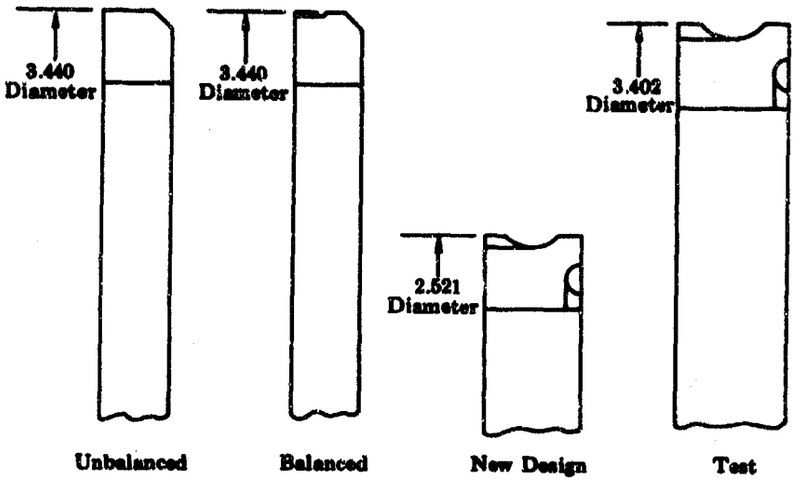

(U) Figure 435. Upper Piston Rings Analyzed FD 25597

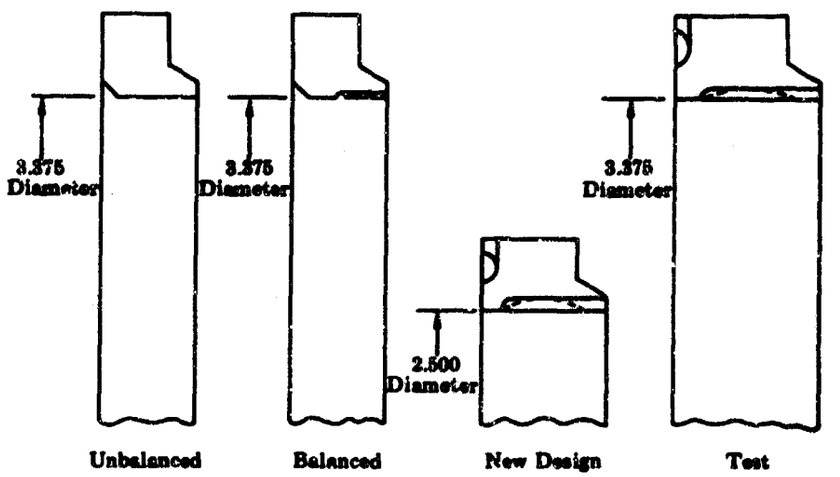

(U) Figure 436. Lower Piston Rings Analyzed FD 25598

(U) The unbalanced and balanced rings were analyzed to determine if the drag loads experienced could be found analytically. Ten different loading cases could be found for each ring when they were allowed to twist. Of these, only three of each could be solved and they gave scattered results, none of which were usable. The unsolvable cases were redundant or impossible loadings. The lower ring solutions even indicated the ring should twist opposite to the direction the wear indicated. The analytical solution for an absolute value of drag was abandoned at this point.

(U) The next method of analysis was to use the data of the two previous tests to estimate the changes in loading required to reduce the drag sufficiently. The percentage changes of several quantities were found between the balanced and unbalanced rings as shown in Table XLIII. The new ring required a reduction of 88% in drag (H_A) over the unbalanced ring. Comparing this to the balanced ring change, the percentage changes required in the other properties were found. This determined the design criteria for the new ring loads.

(U) The radial load per inch of circumference because of pressure unbalance (G_R) was chosen because it is a calculable number and its change should be proportionately related to the change in drag. The radial load per inch of circumference because of wall reaction (F_R) used was found with an appropriate value for the radial load per inch of circumference due to friction forces (H_R) derived from a friction coefficient of 0.25. The change in F_R should also be proportionate to changes in drag. The unit pressure was also approximate because it is derived from F_R; however, it could contribute to drag as well as leakage. It was kept as high as possible to prevent leakage but low enough to reduce drag.

(U) Table XLIII. Percentage Change from Unbalanced Ring

Quantity	Balanced	Required For New Ring	Actual New Ring
Combined Upper and Lower H_A Open	-49.0%	-88.0%	--
Close	-58.5%		
Combined Upper and Lower G_R	-42.0%	-63.2%	-78.0%
Combined Upper and Lower F_R	-55.0%	-82.7%	-82.3%
Average Upper and Lower UP	-48.2%	-72.5%	-76.6%

(U) The results for the unbalanced ring show that the closing drag was reduced more than any of the other quantities. The only explanation found is that the balanced ring had smaller moments because of pressure and friction and thus had less tendency to twist.

(U) Besides the restrictions put on G_R, F_R, and unit pressure on the rubbing surface of the ring (UP), the new rings were designed so that the pressure moment per inch of circumference due to pressure unbalance (M_G) were negligible. The moment of inertia was increased to reduce the ability to twist. In the new designs the upper ring was 6.1 times stiffer than the balanced ring and the lower ring 4.2 times stiffer. The moment caused by friction was decreased about 35%. The combination of the reduced moments and increased stiffness was expected to provide an 88% reduction in twist of the rings.

(C) Other results from the new designs are shown in the last column of Table XLIII and the first column of Table XLIV. If it can be assumed that the percentage change method is a good analysis, then the piston [illegible] will be less than 400 lb in either direction. Because most of the twisting was taken out of the ring, it can be assumed to remain

flat against the rubbing surface. The drag may be estimated using the drag formulas shown in Figure 437. A definition of all terms used is provided in Table XLV. With a coefficient of friction of 0.35 and a pressure differential of 2000 psi, the total drag will be 250 lb using G_R, and 150 lb using F_R. The UP will be 331 psi on the upper ring and 229 psi on the lower ring. The UP on the balanced rings were (upper) 752 psi and (lower) 560 psi.

(U) Table XLIV. Comparison of New and Tested Piston Rings

	New	Test	Scale Factor
Combined G_R	0.0450 P	0.0525 P	1.168
Combined F_R	0.0274 P	0.0320 P	1.168
UP Upper	0.1655 P	0.1625 P	
Lower	0.1145 P	0.1025 P	
Average Circumference	7.85	10.65	1.358

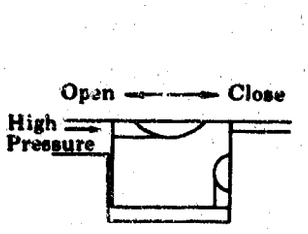

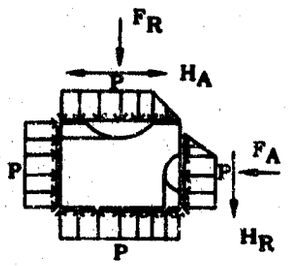

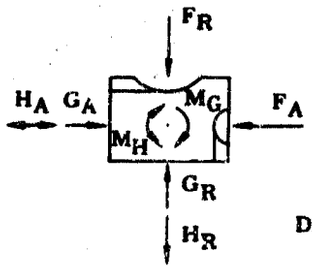

$$F_A = G_A \pm H_A$$

$$F_R = G_R - H_R$$

$$H_A = \mu F_R \qquad \frac{F_A}{F_R} \leq 3$$

$$|H_R| \leq \mu F_A \qquad \frac{G_A}{G_R} \leq 3$$

$$UP = \frac{F_R}{A_R}$$

$$\text{Drag} = 2\pi r \mu (F_R \text{ upper} + F_R \text{ lower})$$

$$= 2\pi r (H_A \text{ upper} + H_A \text{ lower})$$

Approximations: $H_A = \mu G_R$

$H_R = \mu G_A$

(U) Figure 437. Nomenclature Explanation and Definition FD 25599

(U) Table XLV. Nomenclature Definition

P	Differential Pressure Across Ring
G_A	Axial Load Per Inch of Circumference Because of Pressure Unbalance
G_R	Radial Load Per Inch of Circumference Because of Pressure Unbalance
H_A	Axial Load Per Inch of Circumference Because of Friction Forces
H_R	Radial Load Per Inch of Circumference Because of Friction Forces
F_A	Axial Load Per Inch of Circumference Because of Wall Reaction
F_R	Radial Load Per Inch of Circumference Because of Wall Reaction
M_G	Moment Per Inch of Circumference Because of Pressure Unbalance
M_H	Moment Per Inch of Circumference Because of Friction Forces
r	Average Radius of Rubbing Surfaces of Both Rings
μ	Coefficient of Friction
UP	Unit Pressure on Rubbing Surface of Ring
A_R	Rubbing Area Per Inch of Circumference

(U) The balancing grooves on the lower ring were designed so that a minimum amount of leakage would occur through the grooves and into the metering port of the valve. This leakage is kept below 5% of the total flow.

(U) The test rings were designed with the same twisting characteristics as the new design so that twisting would not have to be scaled. By scaling up the ring, the G_R and F_R terms were 16.8% too high. The circumference of the test ring was also 35.8% higher than the new design. Because of the scaling, the measured drag from the test rings had to be multiplied by 0.63 to obtain the estimated drag of the new rings and the measured leakage had to be multiplied by 0.74 to obtain a leakage estimate.

d. Piston Ring Actuation Force Tests

(U) This test program was conducted to evaluate the actuator force requirements for balanced piston rings. These piston rings were scaled from the design planned for the preburner oxidizer valve. The valve sleeve was nickel plated to provide a 0.0115-inch clearance between the housing and sleeve. The sleeve was then precision chrome coated 0.001-inch thick with no subsequent machining.

(C) The upper ring was pressure balanced to a unit bearing load of 325 psi at 2000 psi ΔP, and the lower ring was pressure balanced to a unit bearing load of 205 psi at 2000 psi ΔP. The rig shown mounted in the test block in Figure 438 was subjected to 200 cycles at LN_2 temperatures. A schematic of the valve installation in B-22 test stand is shown in Figure 439.

(C) The valve was cycled 50 cycles at a frequency of three Hertz at a ΔP of 1000, 1500, 1750, and 2000 psi for a total of 200 cycles. Strain gage force measurements were used to indicate piston ring drag.

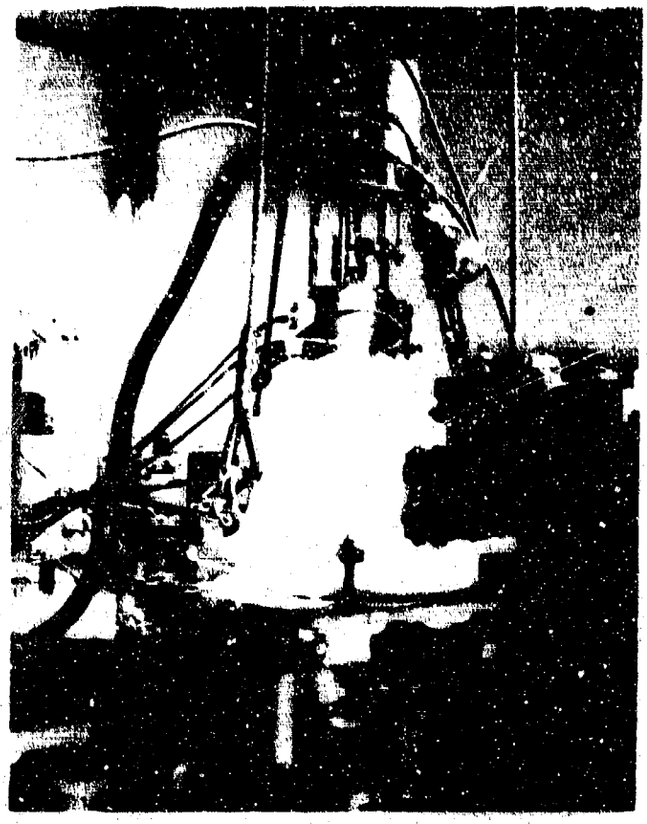

(U) Figure 438. Balanced Piston Ring Test Rig FE 68532

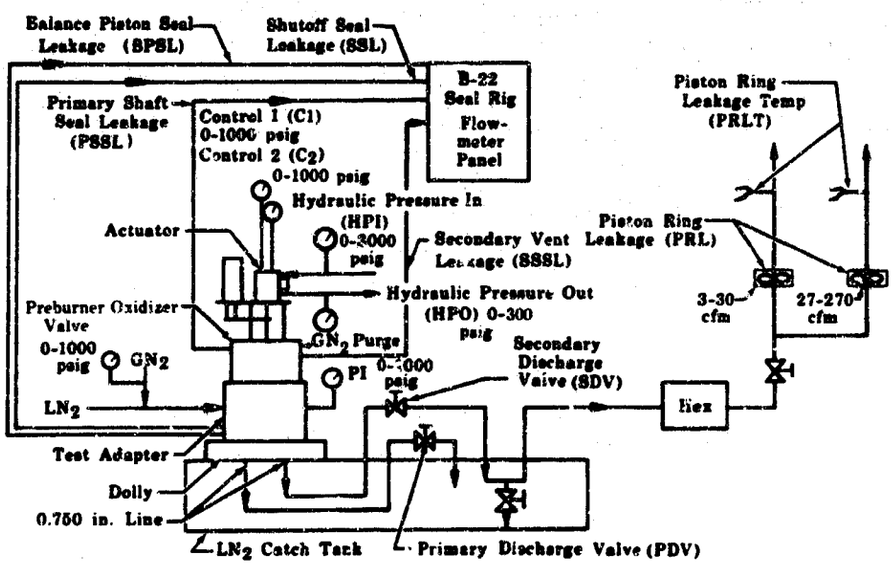

(U) Figure 439. Valve Installation Schematic FD 22151B

(U) The comparison of the pretest and post-test condition is provided by Figures 440 and 441.

(U) The force versus inlet pressure is shown in Figure 442. As shown, the forces recorded on the oscillograph compared favorably with the predicted values. Very little wear of the piston rings or moving surfaces was noted.

(U) The redesigned secondary piston rings were found suitable for use in the preburner oxidizer valve. As shown in Figure 443, the force loading was close to the predicted results and gave a decidedly advantageous reduction in force loading.

5. Main Chamber Oxidizer Valve

a. Introduction

(U) The main chamber oxidizer valve regulates and shuts off the main burner oxidizer flow. The basic valve is a canted shaft butterfly type design accomplished during Phase I (Contract AF04(611)-11401).

(U) Two builds (Rig F-33466-11 and Rig F-35106-8) of the main chamber oxidizer valve were tested under the component development subtask. The primary objectives of these tests were to endurance test the hoop and cam-actuated shutoff seals at cryogenic and ambient temperatures. Secondary objectives were to hydrostatic leak check the seals at 1300 psid, perform valve position versus effective area water flow calibrations, and test the seals at high flow conditions.

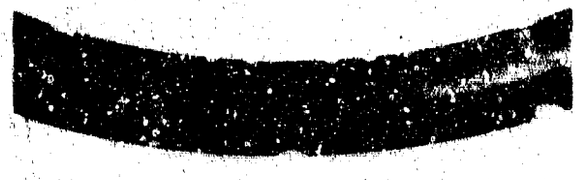

Pretest

Post-Test

(U) Figure 440. Lower Secondary Piston Ring Inside Diameter Pre- and Post-Test FD 25600

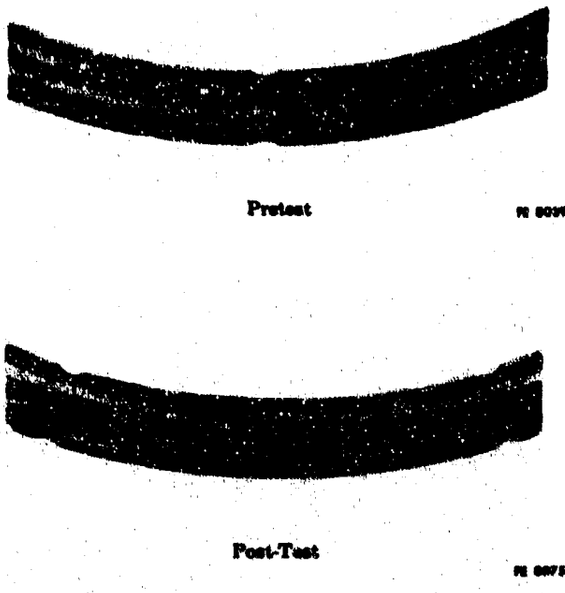

(U) Figure 441. Upper Secondary Piston Ring Outside Diameter Pre- and Post-Test FD 25601

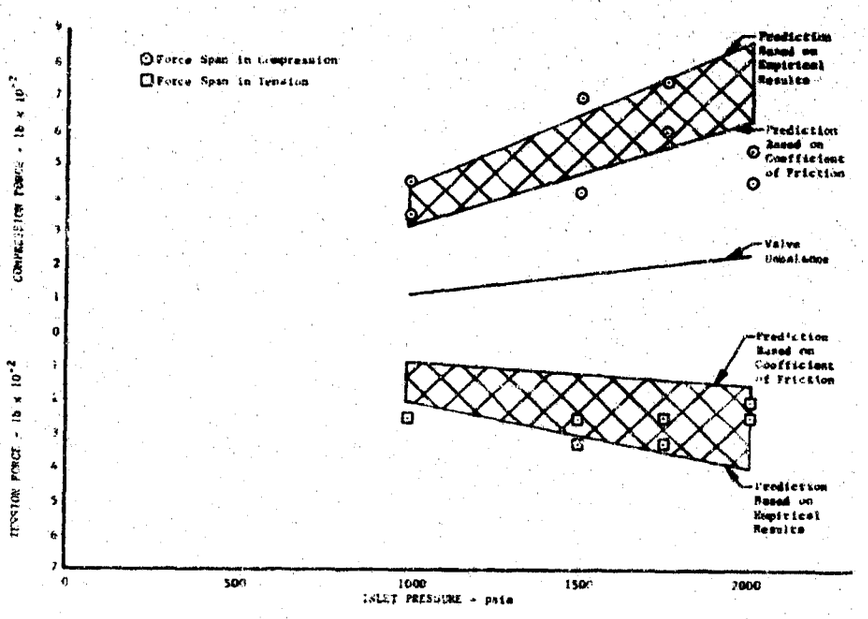

(U) Figure 442. Actuation Force vs Inlet Pressure DF 68893

b. Conclusions and Recommendations

(U) The hoop-type shutoff seal provided the most consistent results, met all of the test goals, and was still serviceable at the end of the test, although the seal element was damaged during the water flow test.

(U) The cam-actuated shutoff seal minimum leakage was less than that of the hoop seal, but the maximum leakage was greater and the seal element was severely damaged during the water flow test.

(U) It is recommended that the silver plated hoop seal be incorporated in the main chamber oxidizer valve design for the demonstrator engine.

c. Hardware Description

(1) Rig F-33466-11

(U) Rig F-33466-11 of the main chamber oxidizer valve used a rotary hydraulic servoactuator and incorporated the following features:

1. A shutoff seal consisting of a silver plated hoop with 0.010-inch tight fit on the disk. Improved silver plating and more access area for cleaning inside the hoop was incorporated. The seal was installed on the disk by heating the seal to approximately 250°F and cooling the disk in LN_2. Figure 443 shows a cross section view of the seal as installed. Figure 444 shows an overall view of the seal and Figure 445 is a closeup of the seal element.

2. An integral shaft and butterfly Inconel 718 (PWA 1010) spherical seal surface chrome plated with an 18 micro-finish.

3. Revised shaft lip seal design (Figure 446).

4. Shaft lip seals of laminated Kapton F (three layers) and FEP Teflon (one layer next to shaft). Total thickness was 0.019 inch.

5. Tufram thrust bearing and silver plated thrust washers.

(2) Rig F-35106-8

(U) Rig F-35106-8 of the main chamber oxidizer valve used a cam-actuated shutoff seal and incorporated the following features:

1. An FEP Teflon seal element contracted against the disk surface by a cam-actuated tapered slip ring. The assembly also included a 0.010-inch thick Inconel X (AMS 5667) seal support. Figure 447 shows a cross section view of the seal and Figure 448 shows the layout of the seal assembly.

2. The disk was chrome plated Inconel 718 (PWA 1010) with a spherical seal surface and a 9.5 micro-finish. The shaft actuating lug was modified from the original configuration

to return the drive cam to the open position during the first few degrees of valve opening.

3. Revised shaft lip seal design (Figure 446)

4. Shaft lip seals of laminated Kapton (three layers) and FEP Teflon (one layer next to shaft). Total thickness was 0.019 inch.

5. Rotary hydraulic servoactuator.

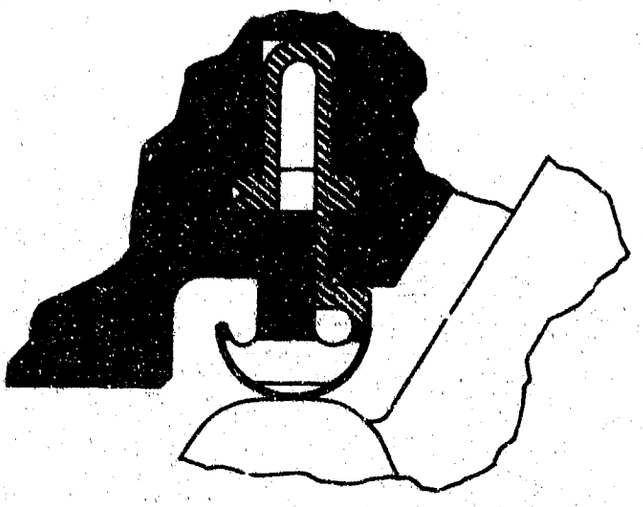

(U) Figure 443. Main Chamber Oxidizer Valve Shutoff Seal Cross Section Rig F-33466-11 FD 25572

(U) Figure 444. Main Chamber Oxidizer Valve Shut-off Seal Overall View Rig F-33466-11 FE 80066

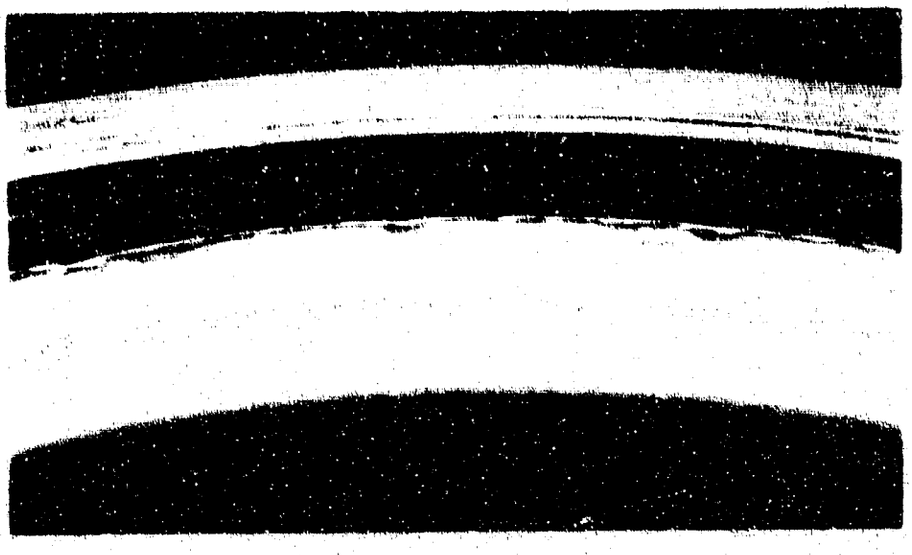

(U) Figure 445. Main Chamber Oxidizer Valve Shutoff Seal Element Rig F-33466-11 FE 80067

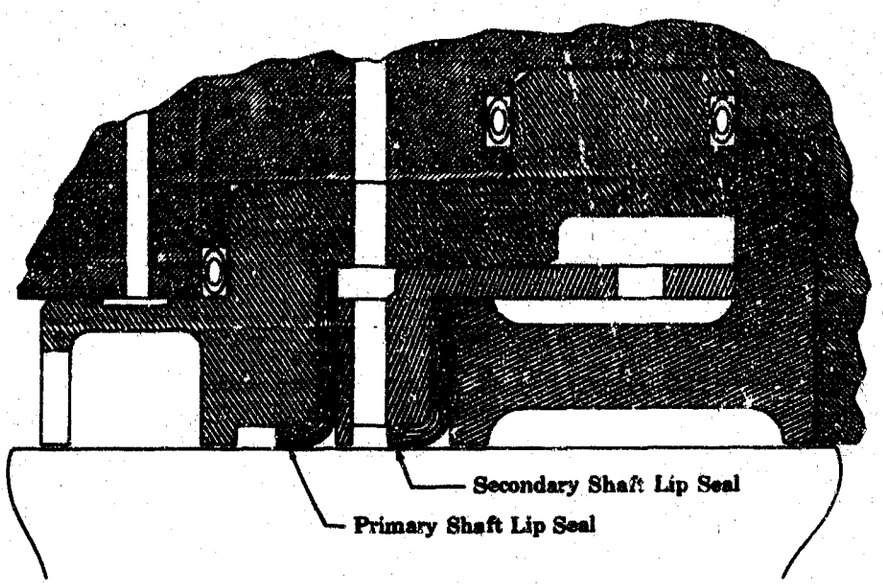

(U) Figure 446. Revised Shaft Lip Seal Design FD 24852

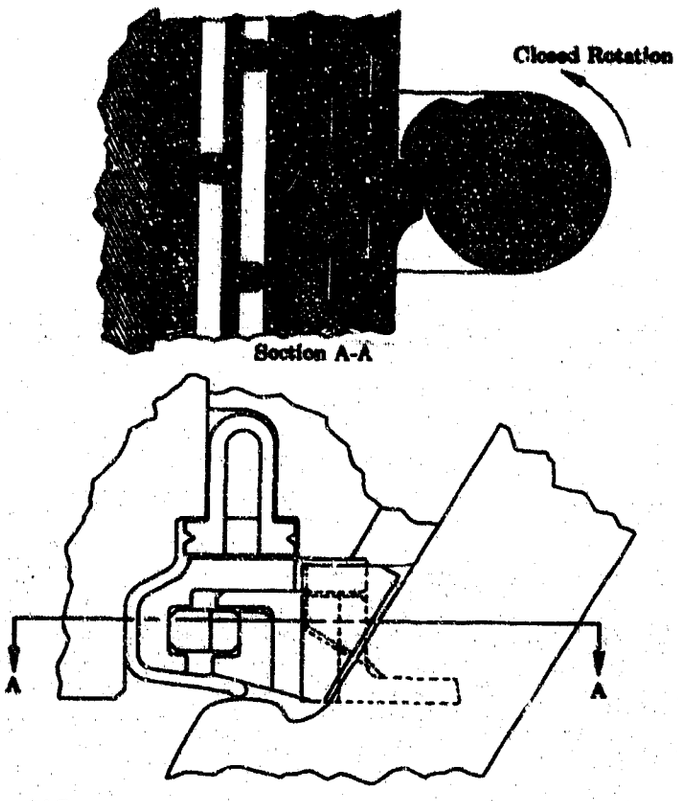

(U) Figure 447. Cam-Actuated Shutoff Seal FD 24991

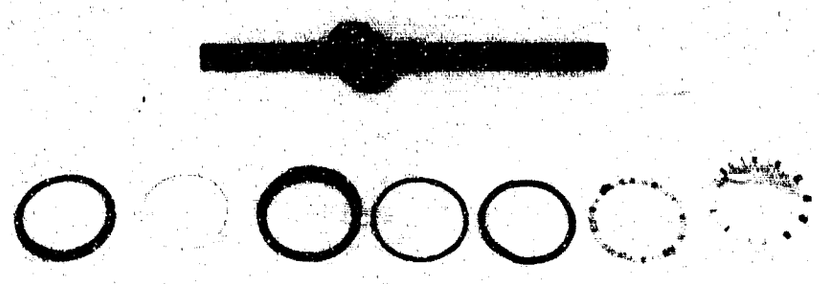

(U) Figure 448. Cam-Actuated Seal Parts Layout FE 80250

d. Testing

(1) Rig F-33466-11

(C) The valve was installed and tested on B-22 stand. No mechanical malfunctions were observed during the tests. Ambient temperature shutoff seal leakage was undetectable prior to cycling the valve at 50 psid GN_2. The torque required to open the valve at liquid Argon temperatures prior to cycling was approximately 400 in.-lb.

(C) The first 25% of the required shutoff cycles were performed with the valve submerged in liquid Argon. The valve was then allowed to warm to ambient temperature and the remaining 75% of the programmed shutoff cycles were completed at ambient temperature. The valve was again submerged in liquid Argon and an additional 100 shutoff cycles were completed. All cycles were performed at one cycle per second and with 50 psid nitrogen pressure across the closed valve disk seal. Shutoff seal leakage measurements at 50 psid were taken periodically during the test.

(C) Shutoff seal leakage during the endurance test is shown in Figure 449. Stable disk seal leakage during the cryogenic testing was observed approximately 15 minutes after the valve was closed. Figure 450 shows typical indicated leakage decay due to boiloff in the discharge housing. The cryogenic leakage values shown in Figure 449 were recorded at least 15 minutes after the valve was closed. Disk seal leakage versus shaft position is shown in Figure 451. Post-test leakage at liquid Argon temperatures at 50 psid GN_2 is shown in Figure 452.

(C) Post-test ambient disk seal leakage at 50 psid GN_2 was 0.03 sccs with the valve at zero degrees. Inspection revealed that the hoop seal wear area was approximately 0.100-inch wide as shown in Figure 453. The disk seal surface was in good condition as shown in Figure 454.

(U) Moisture was found in the inlet housing and on the upstream side of the disk at teardown. No moisture was found elsewhere in the valve. The origin of this contamination was not determined.

(C) The valve was then delivered to the B-21 water flow test stand for hydrostatic leak check and water calibration. A shutoff seal test at 1300-psid water pressure resulted in no visible leakage prior to the water flow calibration. The water calibration results are shown in Figure 455. Post-test shutoff seal leakage at ambient temperature and 1300-psid water pressure was 0.3 sccs.

(C) Teardown inspection revealed that ambient temperature shutoff seal leakage was undetectable at 50 psid GN_2. The hoop sealing surface was in good condition, with some minor scratches in the contact area (Figure 456). The seal fit on the disk measured 0.005-inch tight. The seal element had failed for approximately 0.75 inch along the upstream lip-weld (Figure 457). Seal surface roughness at this point (Figure 458) indicated possible flow cavitation damage. This area and a similar rough area on the seal surface approximately 120 degrees from this point indicated that the valve was at the open position when this occurred. The index of cavitation $(P_{in} - P_{out})/(P_{in} - P_{vapor})$ at 20-degree shaft angle and 1450 psid, and several additional points during the water calibration, was greater than 0.90. The general index of incipient cavitation for a butterfly valve is 0.37. Engine operating conditions are less than the incipient cavitation index of 0.37.

(U) The shaft seal surface was in excellent condition as shown in Figure 459. All other parts were in excellent condition as shown in Figure 460.

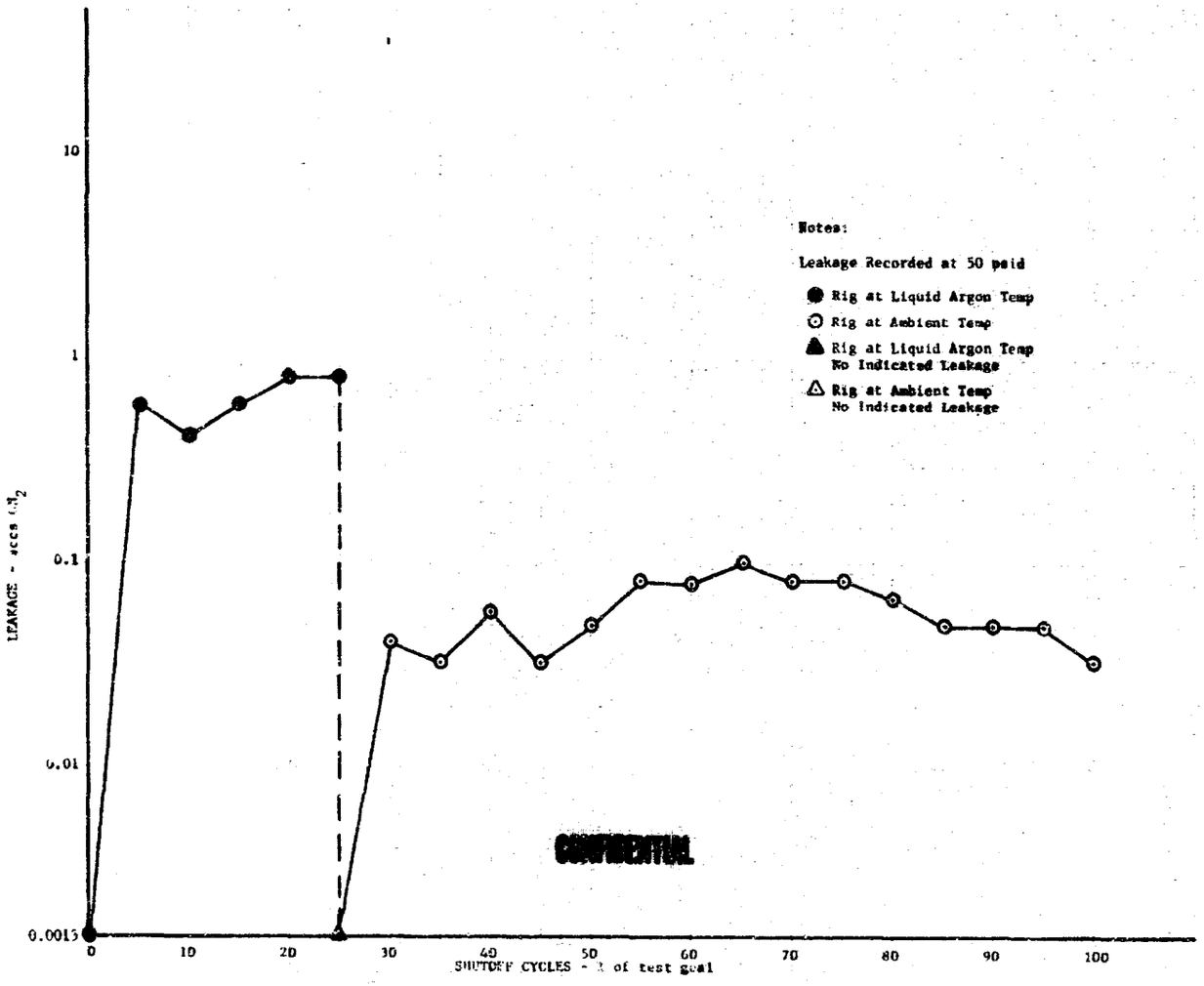

(U) Figure 449. Hoop Seal Leakage vs Percent of Test Goal, Rig F-33466-11

DFC 68892

CONFIDENTIAL

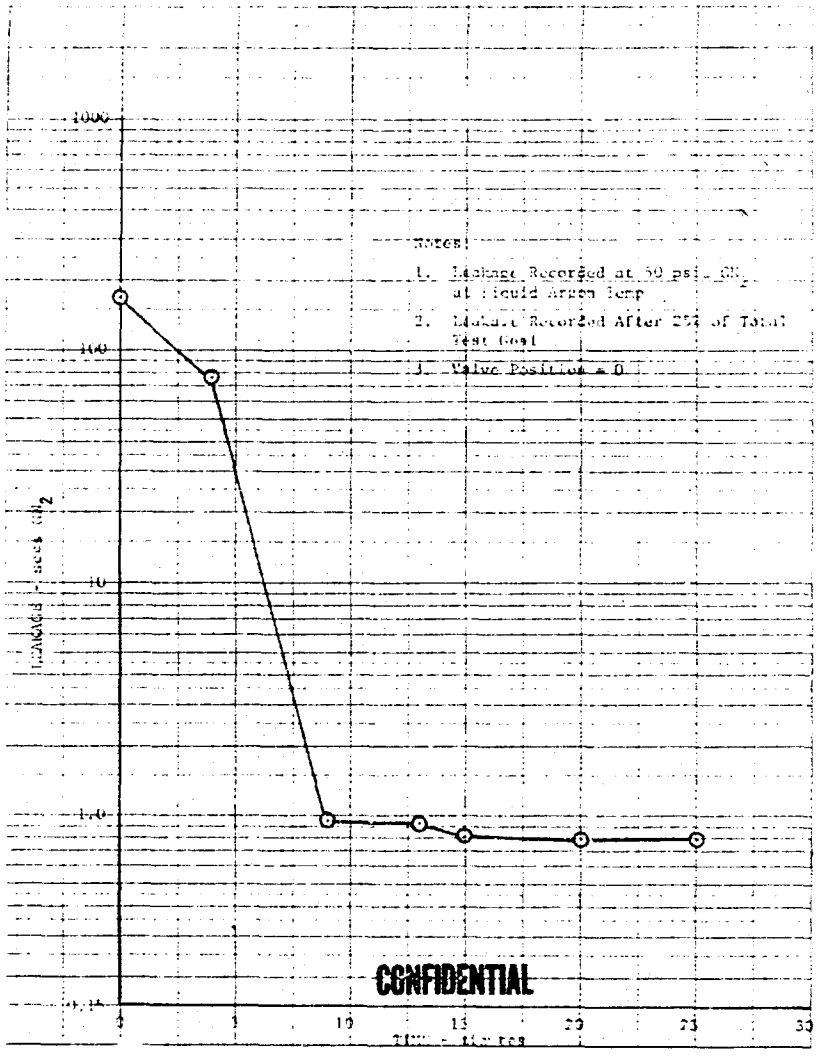

(U) Figure 450. Seal Leakage vs Time, Rig F-33466-11 DFC 68891

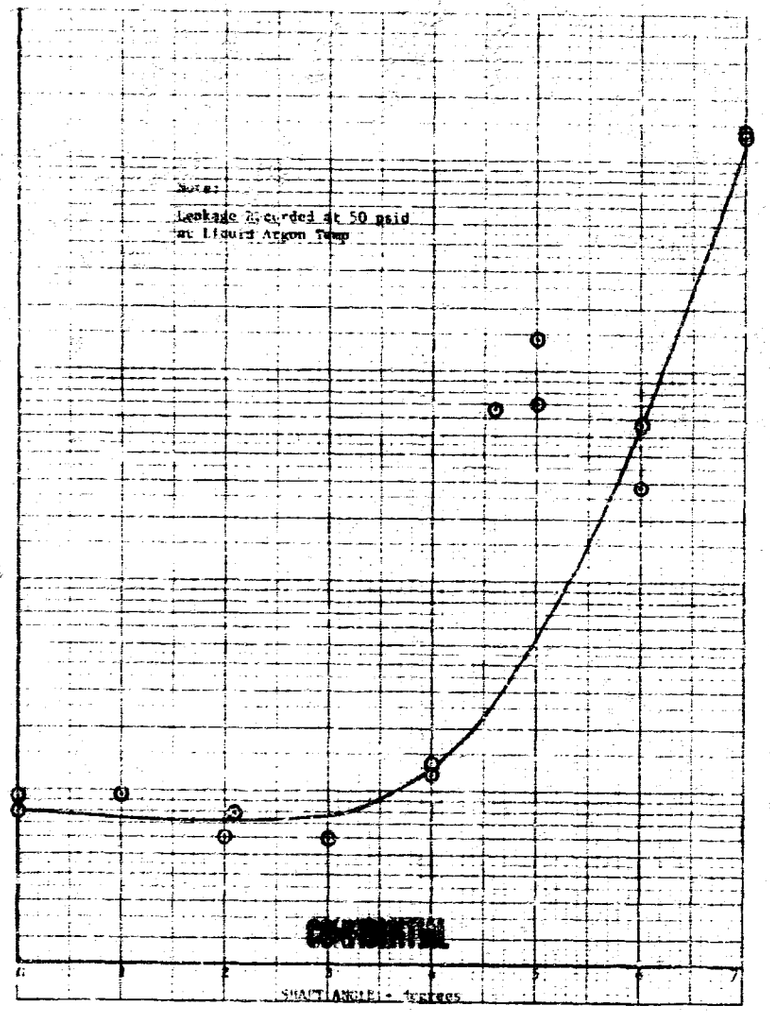

(U) Figure 451. Seal Leakage vs Shaft Angle, Rig F-33466-11 DFC 68890

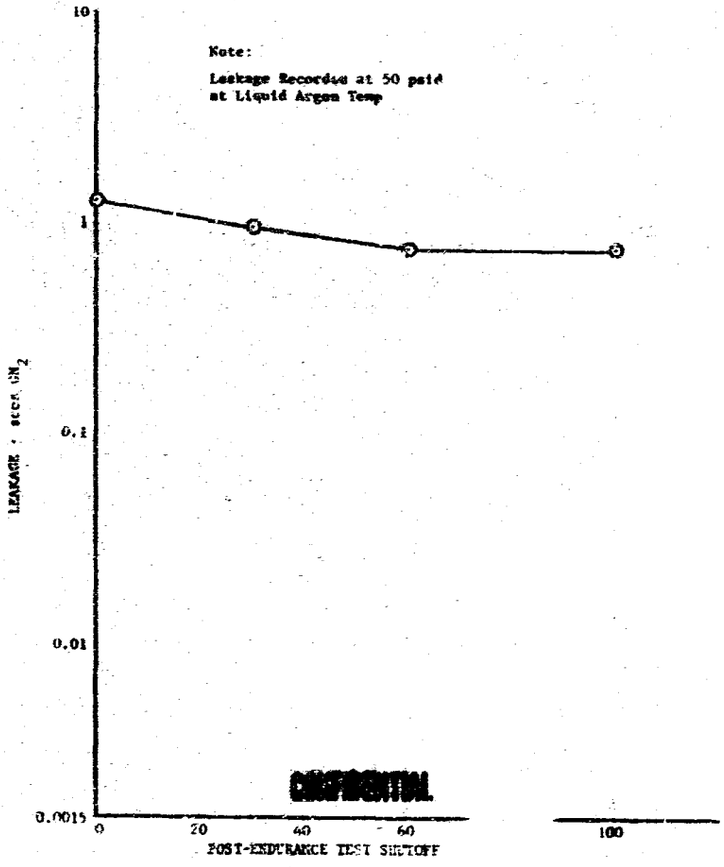

(U) Figure 452. Post-test Leakage, Rig F-33466-11 DFC 68889

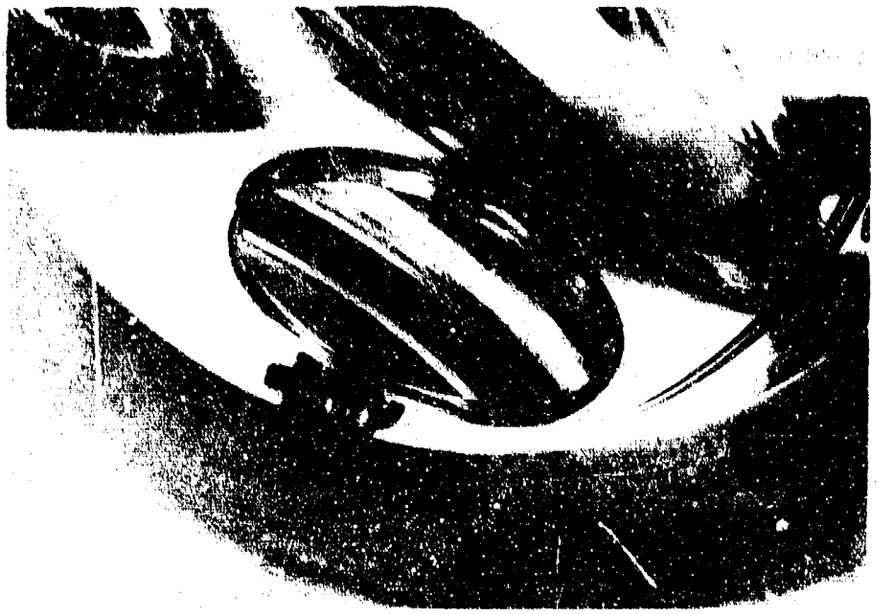

(U) Figure 453. Hoop Seal Wear, Rig F-33466-11 FE 80567

(U) Figure 454. Disk Seal Post-Test Condition, Rig F-33466-11 FE 80566

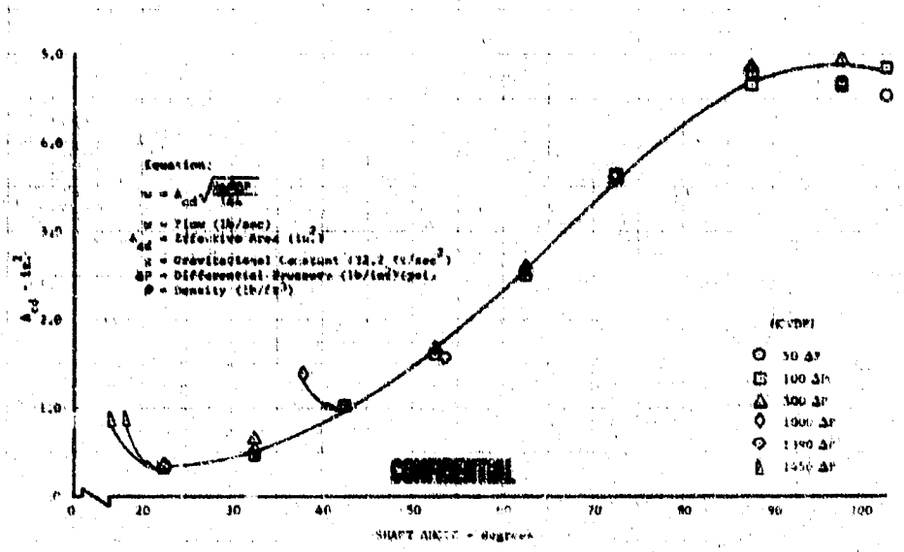

(U) Figure 455. Water Calibration Results Rig F-33466-11 DFC 68888

(U) Figure 456. Hoop Seal Surface Condition, Post-Test, Rig F-33466-11 FE 80770

(U) Figure 457. Hoop Seal Element Failure Rig F-33466-11 FE 80771

(U) Figure 458. Possible Cavitation Damage to Hoop Seal, Rig F-33466-11 FE 80978

(U) Figure 459. Post-Test, Shaft Seal Surface FE 80772
Rig F-33466-11

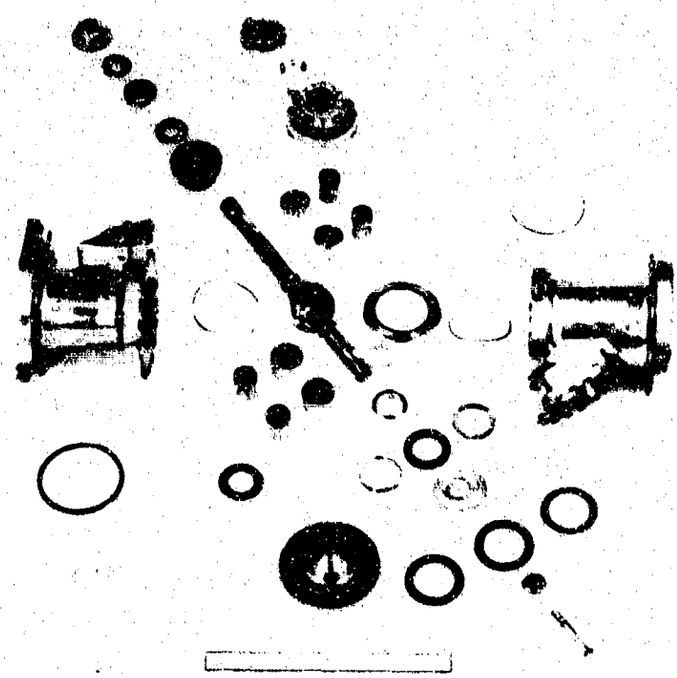

(U) Figure 460. Post-Test Teardown of Main Chamber Oxidizer Valve FE 80773
Rig F-33466-11

(2) Rig F-35106-8

(C) The valve was installed and tested on the B-22 stand. The ambient disk seal leakage prior to cycling the valve at 50 psid GN_2 was undetectable with 700-in.-lb torque applied to the shaft in the closed direction.

(C) The first 25% of the programmed shutoff cycles were performed with the valve submerged in liquid Argon. The valve was then allowed to warm to ambient temperature and the remaining 75% of the programmed shutoff cycles were completed at ambient temperatures. The valve was again submerged in liquid Argon and 100 shutoff cycles were completed. All cycles were performed at one cycle per second and with 50 psid nitrogen pressure across the closed valve shutoff seal. Shutoff seal leakage measurements at 50 psid were taken periodically during the test.

(U) Shutoff seal leakage during the endurance test is shown in Figure 461. Stable disk seal leakage during the cryogenic testing was observed approximately 15 minutes after the valve was closed. Figure 462 shows typical indicated leakage decay due to boil off in the discharge housing. Cryogenic leakage shown in Figure 461, was measured approximately 15 minutes after the valve was closed.

(C) Disk seal leakage versus shaft angle is shown in Figure 463. Post-test leakage at liquid argon temperature and 40 psid GN_2 is shown in Figure 464.

(C) Post-test ambient disk seal leakage at 50 psid GN_2 was 0.008 sccs with the valve at zero degrees. Inspection revealed that both the cam-actuated seal element and the shaft seal surface were in excellent condition as shown in Figures 465 and 466, respectively.

(U) Physical measurement of the disk angle with the valve in the closed position indicated the disk to be one degree from full closed.

(U) Post-test visual inspection was completed, photographs taken, and the valve was delivered to B-21 test stand for hydrostatic leak check and water calibration.

(C) A shutoff seal leakage test at 1300 psid water pressure indicated 13-sccs leakage prior to water flow calibration. The water calibration results are shown in Figure 467. Post-test shutoff seal leakage was greater than 80 sccs at 25-psid water pressure.

(U) Post-test inspection revealed seal damage as shown in Figure 468. An enlarged view of the damaged seal area is shown in Figure 469. The 10-micron filter just upstream of the valve inlet was inspected and no deterioration was found. All seal damage was on the portion of the seal that is downstream of the disk edge as shown in Figure 470.

(C) The appearance of the seal element indicates flow cavitation at the butterfly disk as the cause of the seal damage. The index of cavitation $(P_{in} - P_{out})/(P_{in} - P_{vapor})$ at all flow points of 1000 psid or more was greater than 0.85. Engine operating conditions produce less than the general index of incipient cavitation for a butterfly valve of 0.37.

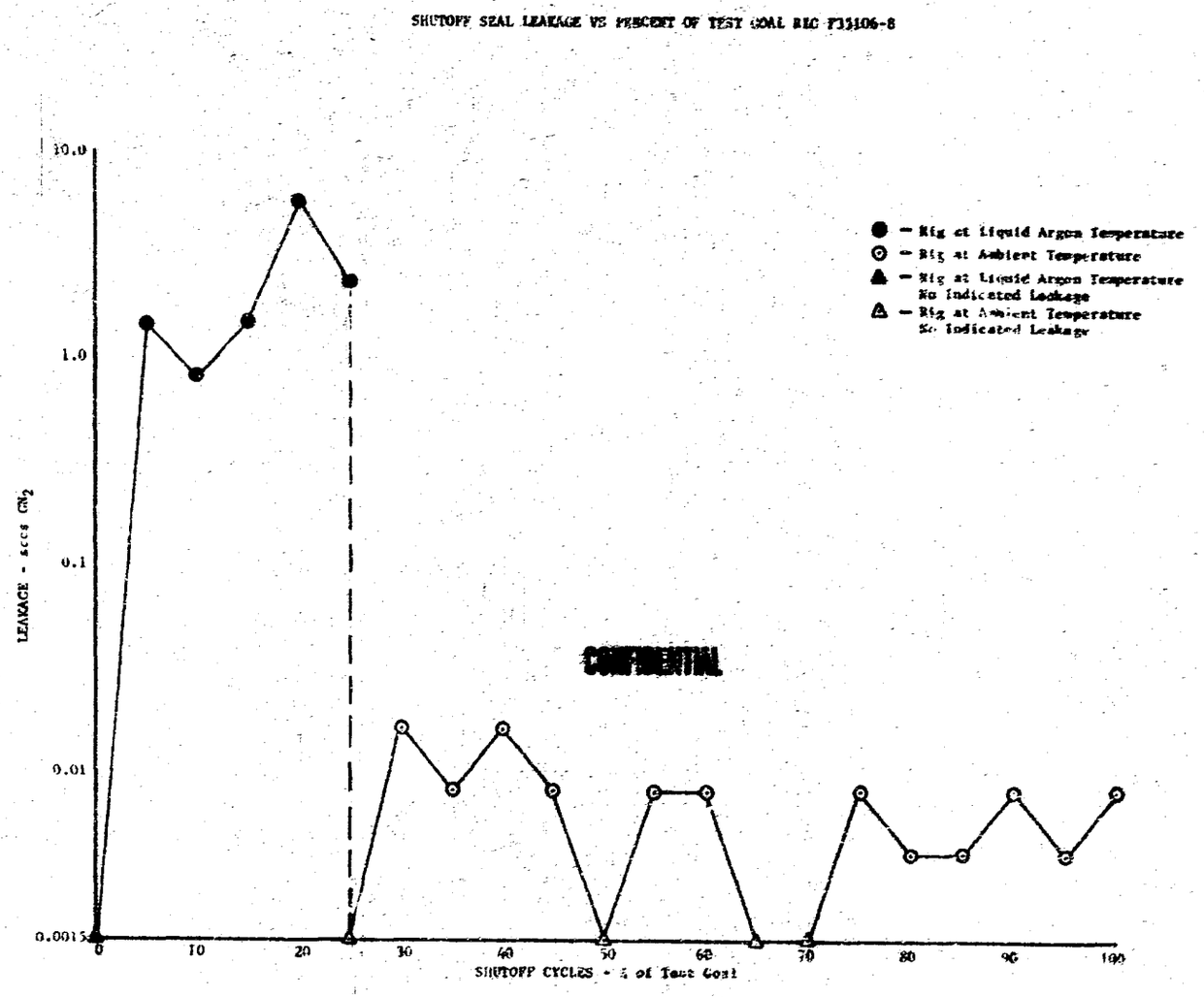

(U) Figure 461. Shutoff Seal Leakage vs Percent of Test Goal, Rig F-35106-8

DFC 68914

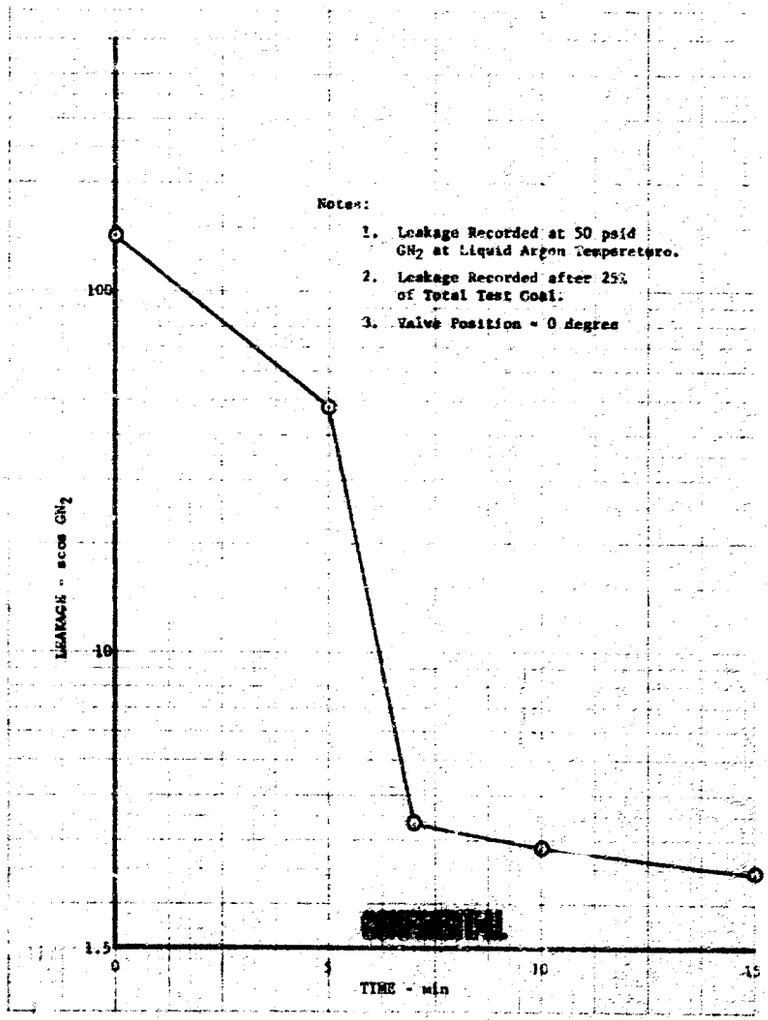

(U) Figure 462. Shutoff Seal Leakage vs Time, Rig F-35106-8 DFC 68915

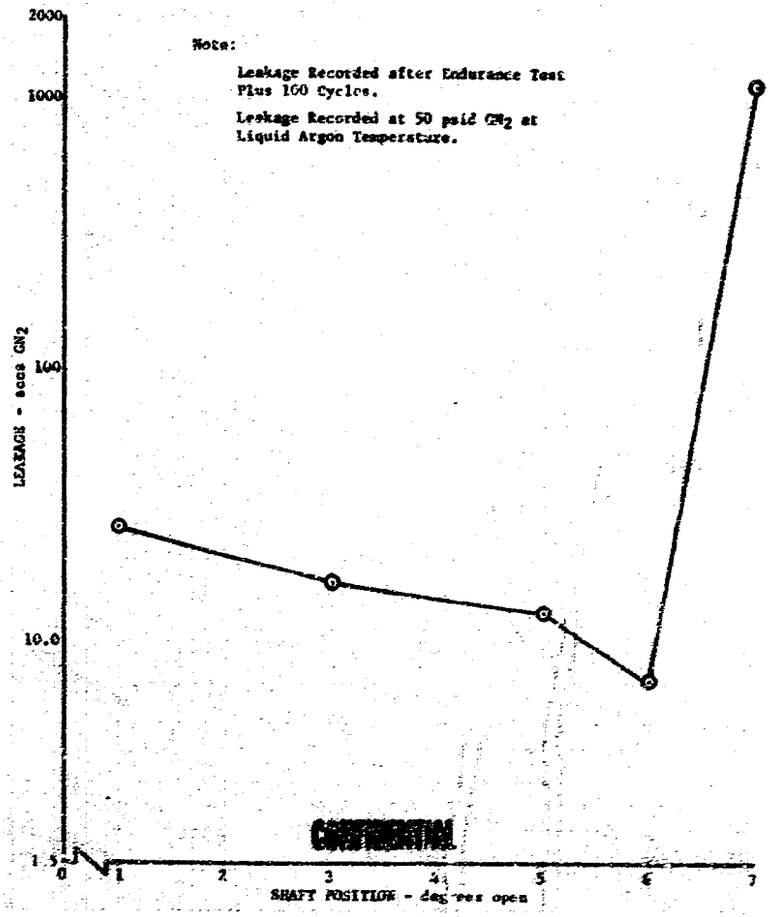

(U) Figure 463. Shutoff Seal Leakage vs Shaft Position Rig F-35106-8 DFC 68916

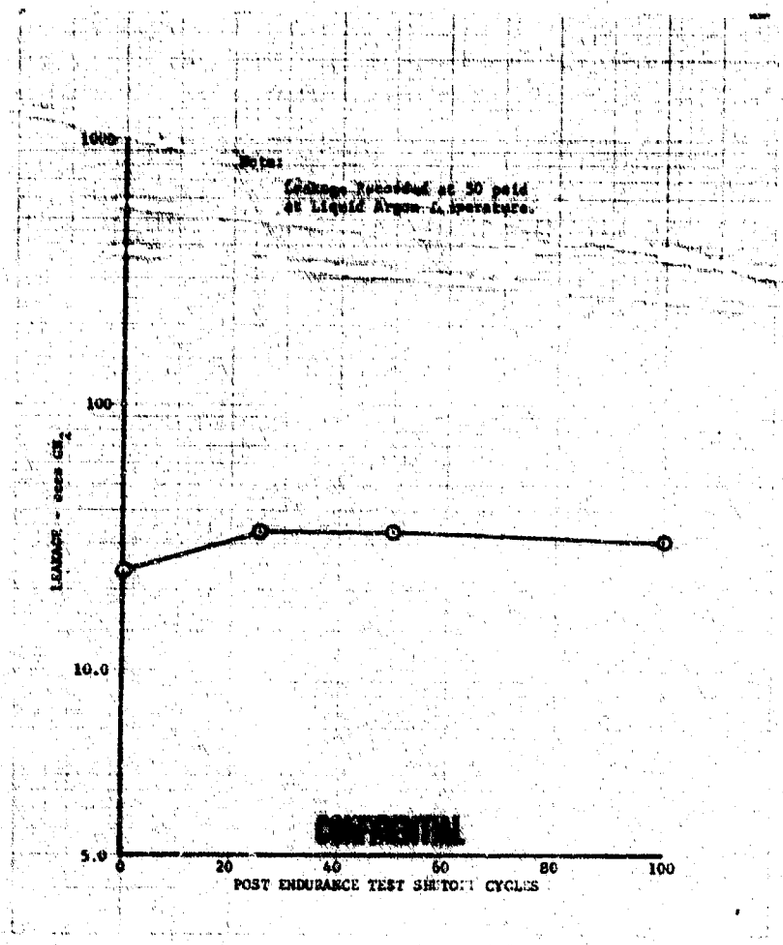

(U) Figure 464. Shutoff Seal Leakage vs Test Shutoff Cycles Rig F-35106-8

DFC 68917

(U) Figure 465. Shutoff Seal Wear Rig F-35106-8 FE 80692

(U) Figure 466. Seal Post-Test Condition Rig F-35106-8 FE 80694

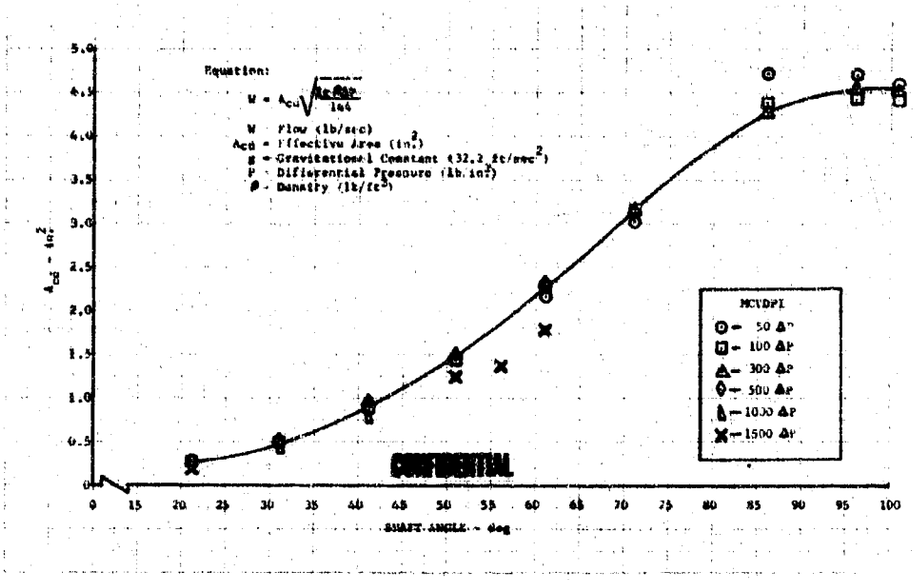

(U) Figure 467. Water Calibration Results DFC 68918
Rig F-35106-8

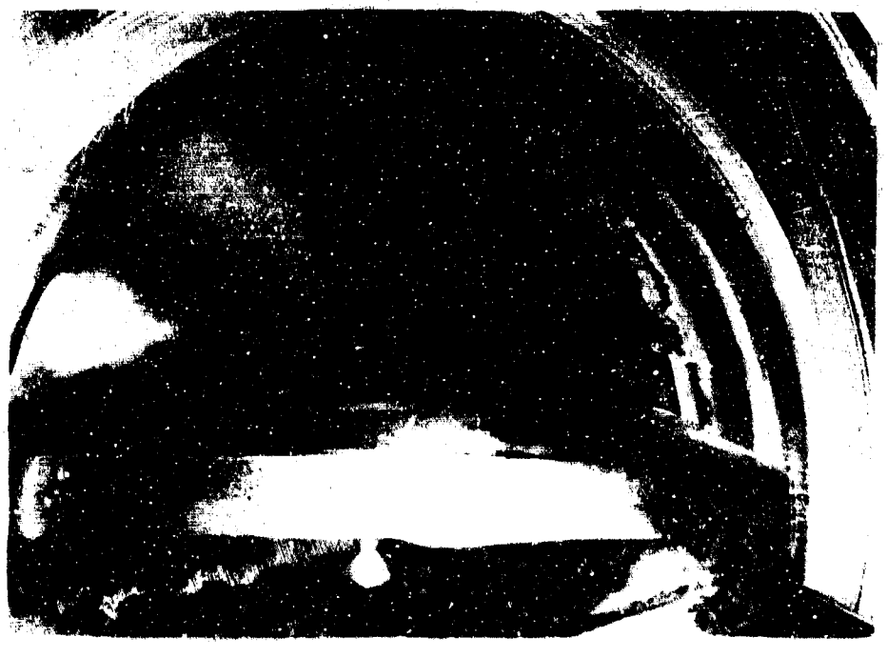

(U) Figure 468. Seal Element Damage After FE 80838
Water Calibration
Rig F-35106-8

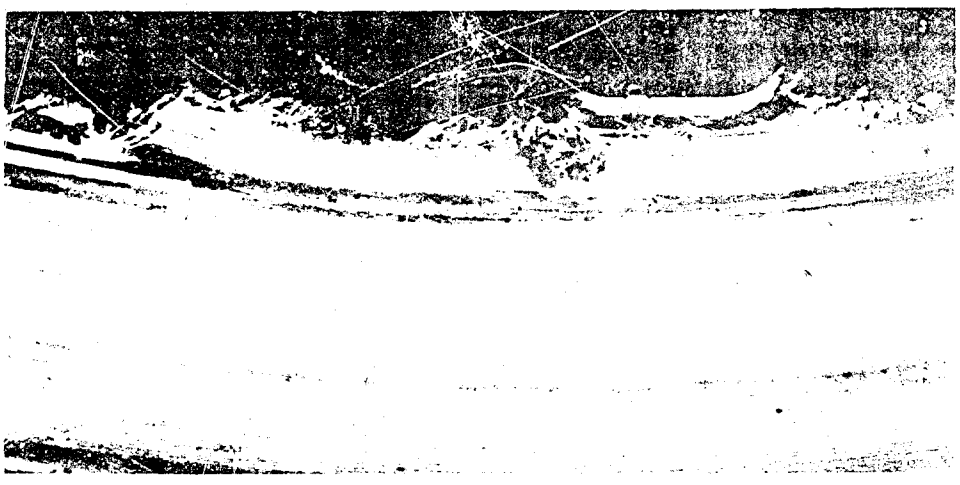

(U) Figure 469. Damaged Seal Element FE 80846
Rig F-35106-8

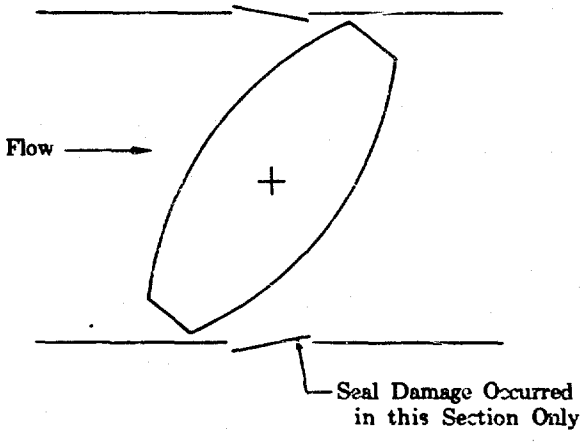

(U) Figure 470. Location of Seal Damage Area FD 25708

(U) Inspection of the seal support revealed cracks as shown in Figure 471. All slots on the damage side of the seal were cracked, but no cracks were apparent on the other side. The shaft seal surface was in good condition (Figure 472) but the driven cam was cracked adjacent to the lug contact point as shown in Figure 473. Figure 474 shows the post-test layout.

6. Vent Valves

Introduction

(U) The demonstrator engine requires fuel and oxidizer vent valves for engine conditioning prior to start and/or pump discharge bleed during shutdown. A common valve design is satisfactory for the three required locations (preburner dome vent, oxidizer pump discharge, and fuel pump discharge). A vent valve selection study was conducted to evaluate valve candidates that would satisfy the vent valve requirements and to select

the most suitable design. Ball valve, blade valve, and poppet valve, which are shown in figures 475, 476, and 477, design candidates were evaluated.

b. Conclusions and Recommendations

(U) Based on a point system, the ball valve design shown in Figure 475 received the highest rating from all evaluators. On this basis the ball valve type of design was selected for the fuel and oxidizer vent valves. A design layout is in process for this valve design requirement.

(U) Figure 471. Support Area Crack Rig F-35106-8 FE 80842

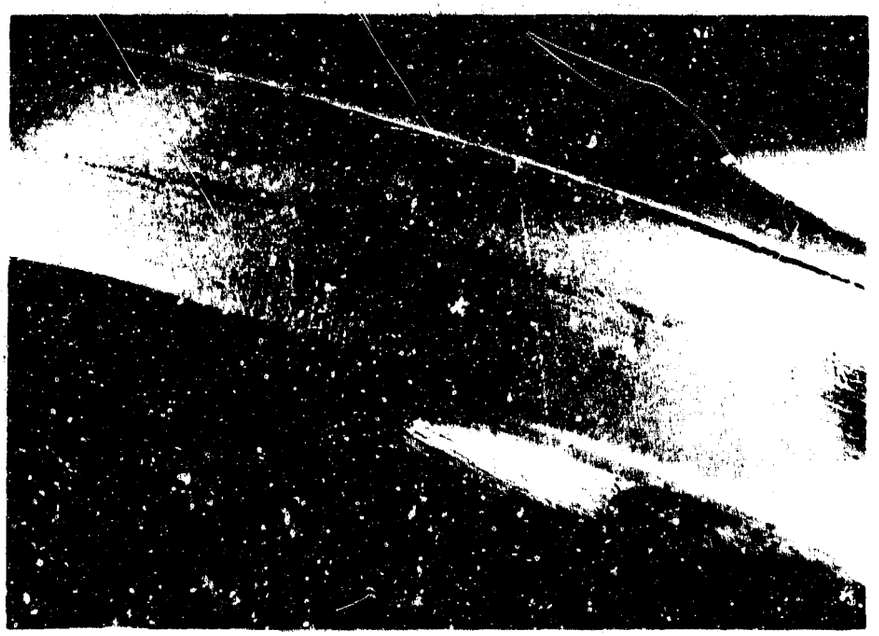

(U) Figure 472. Shaft Seal Surface Rig F-35106-8 FE 80851

(U) Figure 473. Crack in Cam Drive Rig F-35106-8 FE 80981

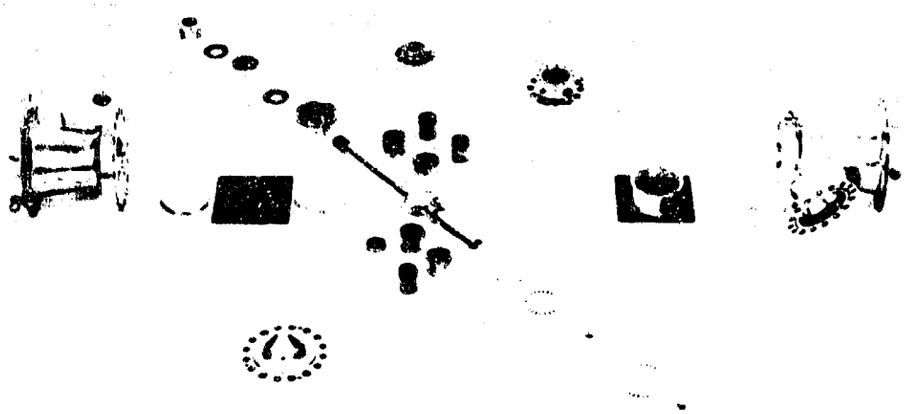

(U) Figure 474. Post-Test Parts Layout Rig F-35106-8 FE 80899

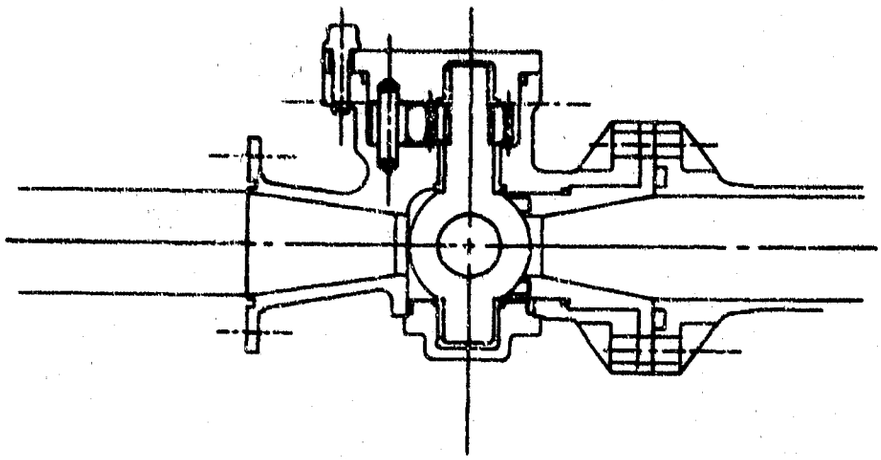

(U) Figure 475. Ball Valve Sketch FD 25603

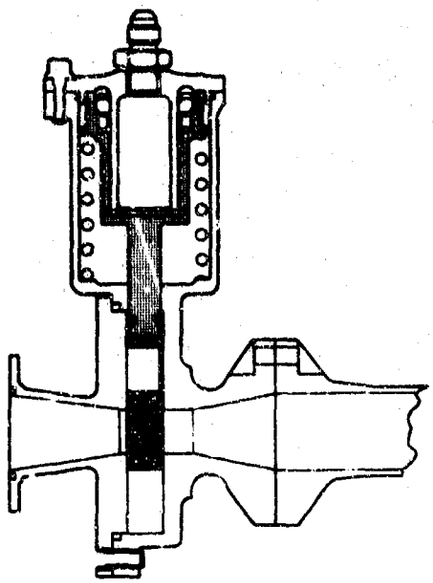

(U) Figure 476. Blade Valve Sketch FD 27667

c. Analysis

(U) The basic requirements for this valve were:

1. A positive shutoff seal
2. Two-position actuation (off-on)
3. Normally closed position requiring actuation pressure to remain open
4. A minimum effective area of 0.75 sq. in.

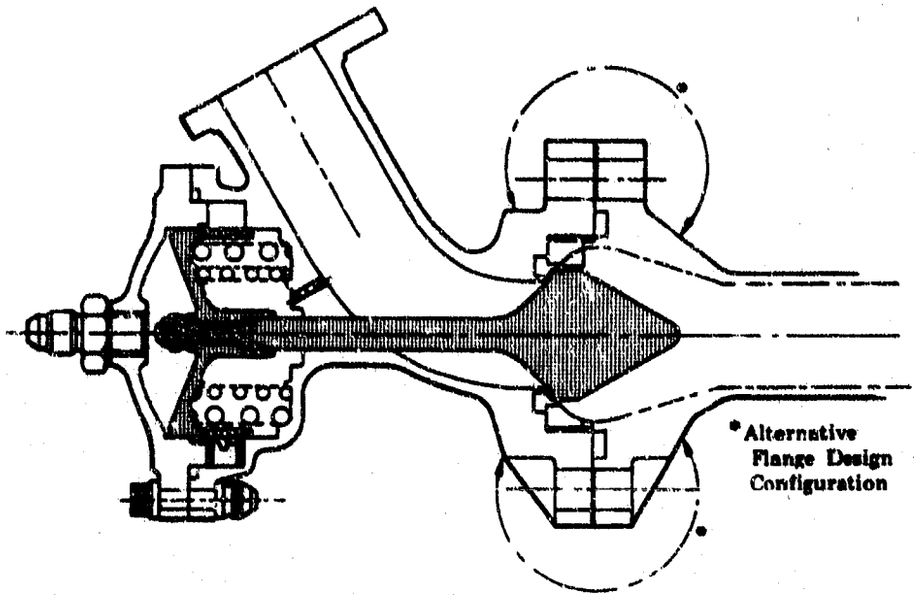

(U) Figure 477. Poppet Valve Sketch FD 27668

(U) A preliminary investigation revealed three valve types capable of fulfilling these requirements. These valve candidates; a poppet valve, a ball valve and a blade valve, were then subjected to a detailed study to determine their relative rank with respect to seal development requirements, weight, reliability, contamination tolerance and other selection criteria as shown in Table XLVI.

(U) At the conclusion of the study, a point rating system was established with a point weighting scale established as shown on Table XLVI. This weighting scale was established by averaging four independently selected scales, two from Design Engineering and two from Project Engineering.

(U) After the weighting scale was established, each valve type was assigned a number of points for each selection criterion. The valve type most satisfactorily meeting the requirements of each criterion was assigned the maximum number of points for that criterion, the other types receiving proportionately less.

(U) The ball valve offers an excellent combination of the following features:

1. Light Weight
2. Compact size - excellent packaging
3. Small seal diameters for both static and dynamic seals
4. Small size actuator
5. Resistance to dynamic seal contamination due to seal wiping action

(U) Table XLVI. Relative Development Ranking

Selection Criteria	Weighting Factor (Maximum Number of Points)	Poppet Valve	Ball Valve	Blade Valve
		75	85	90
Weight (Valve and High Pressure Flanges)	90	75	85	90
		75	85	90
		100	50	30
Shutoff Seal Development Required	100	100	70	70
		50	100	80
		11	50	14
Actuator Volume	50	11	50	14
		10	50	15
		14	50	34
Actuator Leakage Circumference	50	14	50	34
		15	50	35
		85	60	75
Reliability	85	85	70	50
		65	85	65
		20	50	40
Packaging	50	30	50	50
		50	35	40
		40	60	60
Ability to Combine with Adjacent Components	60	30	60	60
		40	60	60
		37	55	55
High Pressure Seal Diameter	55	37	55	55
		35	55	55
		45	25	35
Manufacturing Ease	45	45	40	40
		36	14	45
		35	15	25
Complexity	35	35	20	20
		35	7	25
		30	70	50
Contamination Tolerance	70	30	50	40
	___	21	56	35
		492	570	508
Total Points Possible	690	492	600	523
		432	599	551

7. Nozzle Coolant Valve

a. Introduction

(U) Coolant for the translating nozzle must be supplied during translation and while the nozzle is in the extended position. A shutoff valve, control orifice and feed mechanism is required.

b. Analysis

(U) Cycle analysis has defined the coolant flow requirements for the nozzle and a design selection study for the feed mechanism configuration is in process; however, no design effort on the valve and control orifice has been started.

8. Helium System

a. Introduction

(U) Helium will be used on the XLR129-P-1 engine for injector purges, oxidizer turbopump, helium dam seal, vent valve actuation, and liftoff seal actuation. A study is in process to define the optimum system operating pressure and to establish the solenoid design requirements.

b. Analysis

(U) Optimization of the helium system pressure will consider system weight, and helium consumption. In addition, any structural limitations of the system that may limit operating pressure will be considered.

(U) The preliminary pneumatic system flow is shown in Figure 478. An installation drawing of the system is being prepared to define line lengths, system weight, and system volume.

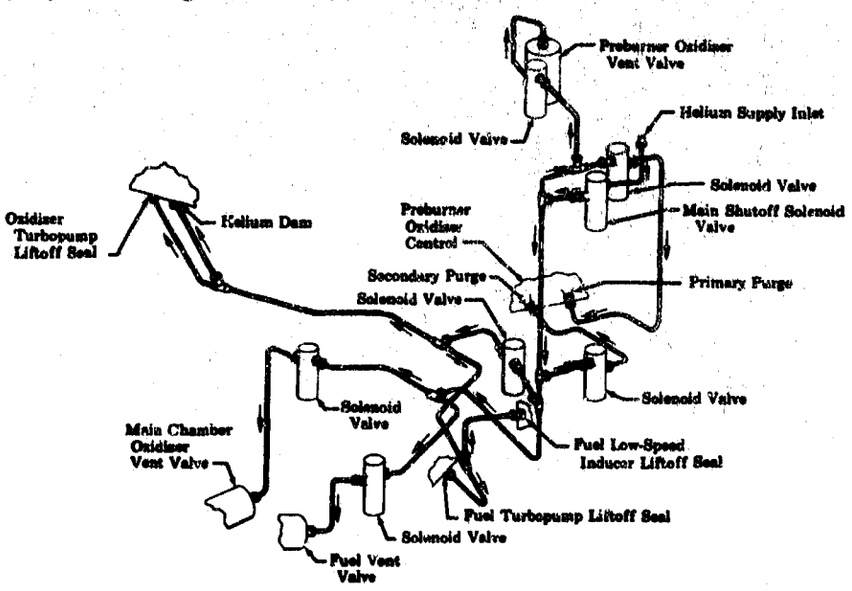

(U) Figure 478. Pneumatic System Flow FD 25604A

(U) The helium system includes a master solenoid to limit system leakage during coast, three vent valve solenoids, a liftoff seal and helium dam seal solenoid, and two preburner injector purge solenoids.

9. Static Seal Rig Design

a. Introduction

(U) A computer program for analysis of flange deflection and stress was developed under the supporting data phase of this contract. This program was used to analyze and optimize bolted flange coupling designs suitable to test static seals for the XLR129-P-1 engine.

b. Summary

(U) A study was made to select the lightest weight high-pressure fluid coupling from four typical flanged configurations. A concurrent study was made of commercial seals available for use at high pressures and cryogenic temperatures. Six seals capable of tolerating up to 0.002-inch total deflection were chosen as candidates for testing. A static seal test rig layout using a cantilevered flange coupling with progressive seal gland rework to allow testing of each of the six seal candidates was completed and released for detailing. Flange schemes to compensate for axial deflection, and seal schemes capable of tolerating relatively large flange deflections were also studied. Contact with the Battelle Memorial Institute was established, and a large (6-inch) aluminum coupling design for the "Bobbin" seal was received and analyzed.

c. Conclusions and Recommendations

(U) A finite element analysis showed that the cantilevered flange type coupling with 0.002-inch deflection is the most desirable configuration for a static seal rig from the standpoints of envelope and weight. Six face-type static seals were found to have deflection and sealing capability to meet the engine design goals according to the manufacturers.

(U) A finite element analysis of the Battelle Memorial Institute coupling design for the use of the AFRPL "Bobbin" seal indicated that it had moderate deflection at the seal, and was excessively bulky and heavy.

(U) It is recommended that six face-type seals be tested in the 0.002-inch deflection cantilevered flange seal rig. A seal rig capable of meeting the engine weight and envelope requirements should be designed for the AFRPL Bobbin seal.

d. Design Analysis

(C) The four basic types of bolted flanges chosen for investigation (Figure 479) were analyzed using the finite element technique. All were sized to provide zero deflection at the seal on a 5.00-inch inside diameter Inconel 718 (PWA 1010) fluid coupling under 7000 psia fluid pressure. This represented the maximum conditions of fluid pressure and fluid line inside

diameter foreseen for the XLR129-P-1. Inconel 718 (PWA 1010) was chosen as the flange material because of its high strength-to-weight ratio, its ductility at cryogenic temperature, and its compatibility with other major rocket engine components.

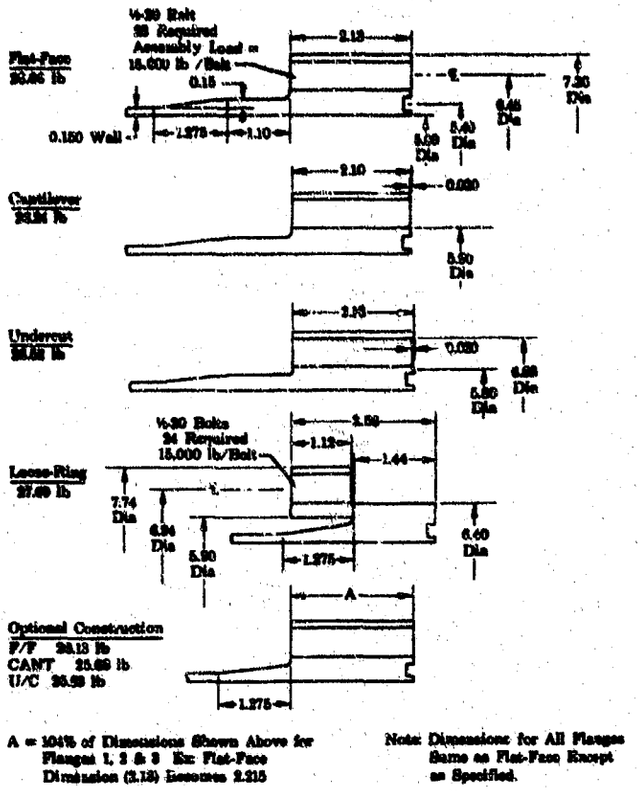

(U) Figure 479. Static Seal Rig Zero Deflection Flanges FD 25771A

(U) The variables that affect flange weight for any given seal deflection are: bolt circle diameter, flange thickness, bolt load, seal point diameter, taper height, taper length, and webs between bolt holes. Flange thickness, bolt circle diameter, and required bolt load have the largest influence on flange weight and the study concentrated on these factors. All of the factors except flange thickness and total bolt load were held constant during the analysis.

(U) The minimum bolt circle diameter was determined by minimum wrench clearance and was used for all but the loose-ring design where the bolt circle was limited by other geometric considerations such as minimum bearing surface and a taper height consistent with the other flange types. A bolt load of 15,000 lb/bolt was used throughout the analysis while the maximum permissible bolt load was 17,750 lb/bolt. The difference was used as an allowance for bolt bending.

(U) Stresses in the flange designs for zero deflection are not limiting and the size of the flanges shown in Figure 479 result from the deflection requirement. The rings for the loose-ring flange design are stress limited, however, and constitute about 50% of the flange weight. A trade-off study of bolt load versus flange thickness was made for the loose-ring but the flange weight was hardly affected by decreasing the bolt load. The loose-ring configuration shown in Figure 479 represents the smallest envelope size to provide for zero deflection.

(U) The flange weights shown in Figure 479 account for all of the weight outboard of a straight tube of 0.15-inch wall for a complete flange connection (two halves) including the weight of nuts and bolts. As indicated, all of the flanges have essentially the same weight, because for zero deflection the rotation of the flange hub must be approximately zero and the type of flange was found to have very little effect on the required hub size for zero rotation.

(U) The size and weight of these couplings was considered to be prohibitive for engine application, so a limited deflection (0.002 inch) analysis was initiated to take advantage of the claimed deflection capability of commercial seals. The flanges were then revised to produce a 0.002 inch deflection at the seal gland for the operating conditions specified above.

(U) A weight and size comparison for four couplings with total axial deflection at the seal point of 0.002 inch is shown in Figure 480. The cantilever flange proves to be the lightest while the undercut flange is the heaviest. The flat face flange was dropped from consideration because it was judged to have no advantage over the undercut flange. The disance from the theoretical pivot point to the sealing point was found to be a major influence on the flange size because very little bending occurs in the flange.

(U) An effort was then made to further reduce the flange weight by moving the pivot point as close to the sealing point as possible. This was accomplished on the cantilever flange by moving the bearing surface inboard of the seal cavity. The resultant additional weight reduction was 1 lb over the "conventional" cantilever flange as shown in Figure 480.

(U) Figure 481 shows the variation of weight of cantilever, undercut, and loose-ring flange couplings with increasing axial deflection. The cantilever flange shows the sharpest decline in weight of the three types as the allowable deflection is increased.

(U) The trade-off between the number of bolts and ribs on the backface of the flange was also considered. It was found that for a standard cantilever flange with seal point deflection of less than 0.0013 inch, it was more economical from a weight standpoint to use more bolts and no ribs as shown in Figure 481. Ribs are shown to be more beneficial above a 0.0013-inch deflection because the stiffness of the ribs and flange hubs are more nearly equal.

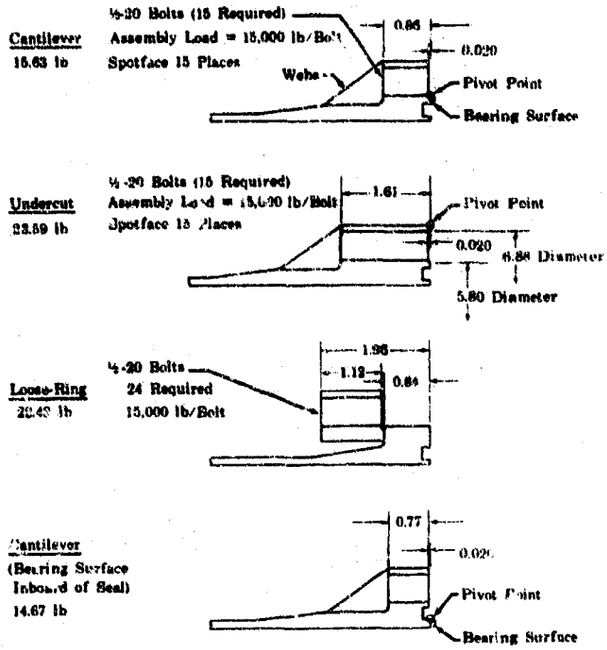

(U) Figure 480. Static Seal Rig 0.002 Deflection Flanges FD 25772

(U) The "conventional" cantilever flange design was chosen for the initial seal test rig design as shown in Figure 482. The rig may be subsequently reworked to the lighter configuration as shown in Figure 483.

(U) A major portion of the work accomplished involved a study of the types of commercial seals available and applicable to the test rig size and sealing environment. The static seals investigated were divided into two general classifications:

1. Face Seals - Those seals having sealing surfaces that are perpendicular to the bore of the joint and whose initial seating stress is obtained by axial compression or deformation of the seal as the joint is assembled.

2. Radial Seals - Those seals having sealing surfaces that are parallel to the bore of the joint and whose initial seating stress is obtained by a radial compression or deformation of the seal as the joint is assembled.

(U) A number of other cryogenic seals were investigated. Many were rejected on the basis of excessive physical size or other obvious deficiencies.

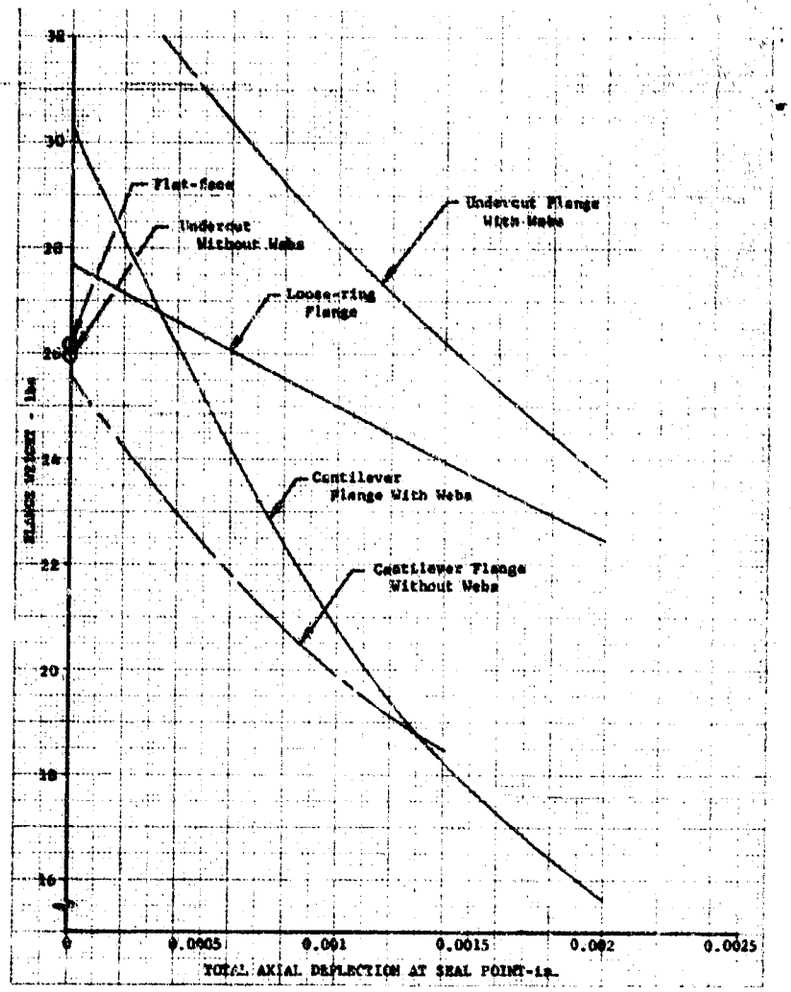

(U) Figure 481. Static Seal Rig Flange Weight vs Seal Point Deflection DF 68991

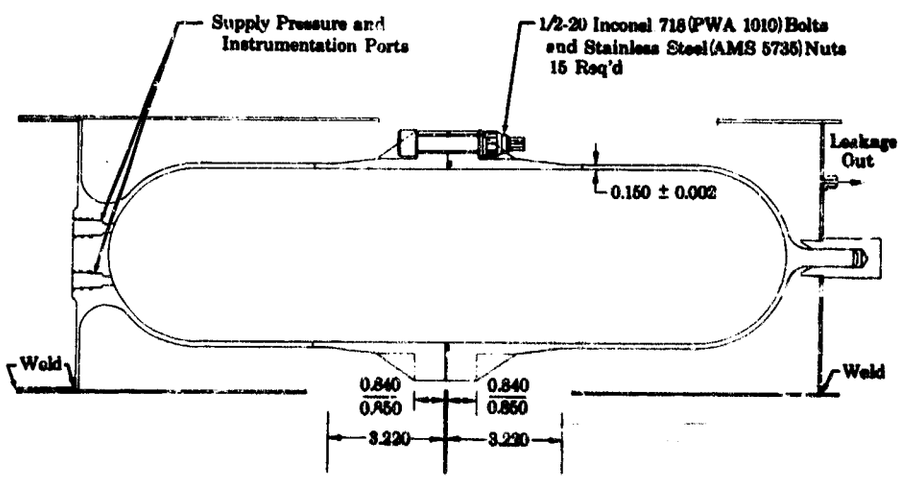

(U) Figure 482. Five-Inch Static Seal Rig FD 25,07A

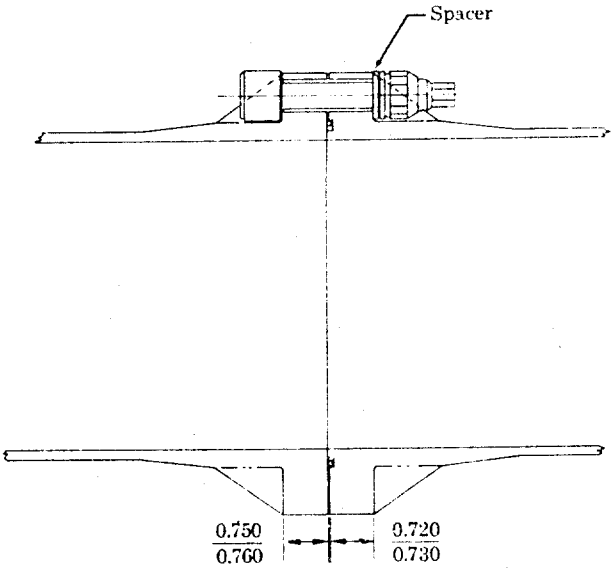

(U) Figure 483. Seal Gland Rework Static Seal Test Rig FD 25706A

(U) Six face-type seals were selected for detailed investigation and will be used in testing (Table XLVII, Group A). Seven other face seals and five radial seals (Table XLVII, Groups B and C) were investigated for consideration contingent on the performance of those in Group A. Of the seal candidates selected, all of the face type are pressure energized and all of the radial types are, or tend to be, pressure energized. A seal is said to be pressure energized when the force caused by the pressure of the contained fluid tends to increase the seal seating stress.

(U) For comparison purposes, both the face and radial seals were divided into three subgroups as follows:

1. Low deflection capability - 0.000 to 0.003 inch
2. Intermediate deflection capability - 0.003 to 0.010 inch
3. High deflection capability - above 0.010 inch.

(U) The seal deflection capability is the ability of the seal to adjust to the distortion or dimensional changes of flange faces upon which the seal seats without an excessive loss of sealing contact stress. This deflection capability can be considered to be in both the axial and radial directions. However, because of the assumed deflection characteristics of the joint flanges, the radial deflection characteristics become less significant than the axial deflection.

(U) The face seals were generally found to fall within the 0.000 to 0.010 inch (Groups A and B of Table XLVII). The radial type seals may offer higher axial deflection possibilities but pose other problems, among which are size and fit up problems. At the time of this report the Battelle bobbin seal had not yet been optimized in Inconel 718 for this application.

(U) Table XLVII. Applicable Commerical Seals

Size Category	Common Name	Manufacturer	Cross Section	Gland Dimension Width(in.)	Gland Dimension Depth(in.)	Seal Material	Vendor Recommended Seal Coating	Maximum Axial Deflection Capability	Remarks
Low Deflection Capability (Group A)	"V" Seal	Parker Seal Co.	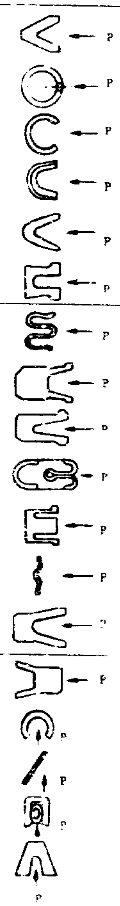	0.156	0.110	Inconel-X750	Teflon TFE	0.002	
	Metal "O" Ring	United Aircraft Product Co.		0.154	0.035	AISI 321	Teflon TFE	0.002	
	"C" Ring	Pressure Science Incorporated		0.119	0.116	Inconel-X750	Indium	0.002	
	Bi-Metal Gasket	Del Mfg. Co.		0.096	0.100	Inconel-X750	Teflon TFE	0.002	
	Apex Seal	Servotronics, Inc.		0.170	0.106	Inconel-X750	Lead	0.002	
	Omega Seal	Servotronics, Inc.		0.170	0.106	Inconel-X750	Lead	0.002	
Intermediate Deflection Capability (Group B)	"E" Ring	Pressure Science Incorporated		0.127	0.120	Inconel-X750	Indium	0.006	Has High Axial Defl. Cap. for Small Profile Seal
	K-Seal	Harrison Mfg.		0.235	0.125	Inconel-X750	Teflon TFE or Nickel-Lead	0.010	
	Naflex Seal	Navan Inc.		0.293	0.175	Inconel 718	Teflon TFE	0.003	
	Diverseal	W.S. [illegible] ban & Co.		0.488	0.230	Inconel or SST	None - Is Teflon Filled	N.A.	Maximum Operating Temperature is 500°F
	Spring Gasket	Donaldson Co., Inc.		0.194	0.[illegible]67	Inconel [illegible]	Silver	N.A.	
	Servoflex	The DSD Company		N.A.	N.A.	Inconel X	None	N.A.	Low Axial Defl. Capability Slender Profile
	Low-Load Seal	The Advanced Products Co.		0.169	0.058	Inconel 718	Indium Over Lead	0.005	Low Installation Load Required - 25 lb in.
Radial Seals (Group C)	Bobbin Seal	Battelle Memorial Institute		N.A.	[illegible]	Inconel 718	None	Per Seal Design	
	Radial "C" Ring	Pressure Science Incorporated		0.127	0.[illegible]	AISI 304	Indium	Per Flange Geometry	0.002 Maximum Radial Defl.
	Conoseal	Aeroquip Corp.		0.462	0.335	AISI 321	None	Per Flange Geometry	Vendor Quotes 0.042 Maximum Axial Deflection
	Bal-Seal	Bal-Seal Engr. Co.		0.127	[illegible]	Teflon TFE	None	Per Flange Geometry	* D.S Gland Finish Ready Max Temperature = 250°F
	Naco Seal	National Utilities Corp.		N.A	N.A	A-286	N.A.	Per Flange Geometry	Info Requested from Vendor Not Received 10-10-69

N.A. - Not Available

(U) The flange deflection compensation study showed that several schemes are feasible for flange deflections up to 0.020 inch. However, this deflection capability usually comes at the expense of a larger seal envelope and/or additional fabrication or maintenance problems.

(U) The three types of deflection compensation schemes shown in Figure 484 were analyzed. The deflection compensation capabilities were determined not only for those that could be contained in the small face seal envelope but also for the general case of larger envelopes. Figures 485 and 486 show deflection capability versus leg length and Figures 487 and 488 show the required maximum thickness versus leg length for the straight and tapered cantilevered beams, respectively, for three ranges of seal loads. Figure 489 shows type selection curves for straight and tapered beams versus leg length for the same range of required seal preloads. Note that Figure 489 is based upon equal maximum leg thicknesses. Figure 490 shows the deflection capability versus leg length for the flexible face seal support scheme.

e. Hardware Description

(U) The design of the seal rig flanges represents the results of flange trade-off studies for minimum weight flanges to meet the required leakage goals.

(U) The static seal rig shown in Figure 482 consists of a cylindrical pressure vessel approximately 20.0-inches long with a 5.00-inch inside diameter made in halves and joined together centrally with a flange having the cantilevered configuration. The pressure vessel, flanges and tie bolts are made of Inconel 718 (PWA 1010) material. Provisions were supplied to attach the vessel to a pressure source and to provide access for instrumentation. The vessel is surrounded by a cylindrical can that is sealed at both ends to act as a collector for measuring seal leakage rates. A scheme for reworking the seal gland to provide the proper gland configuration for each of the Group A seals to be tested was included.

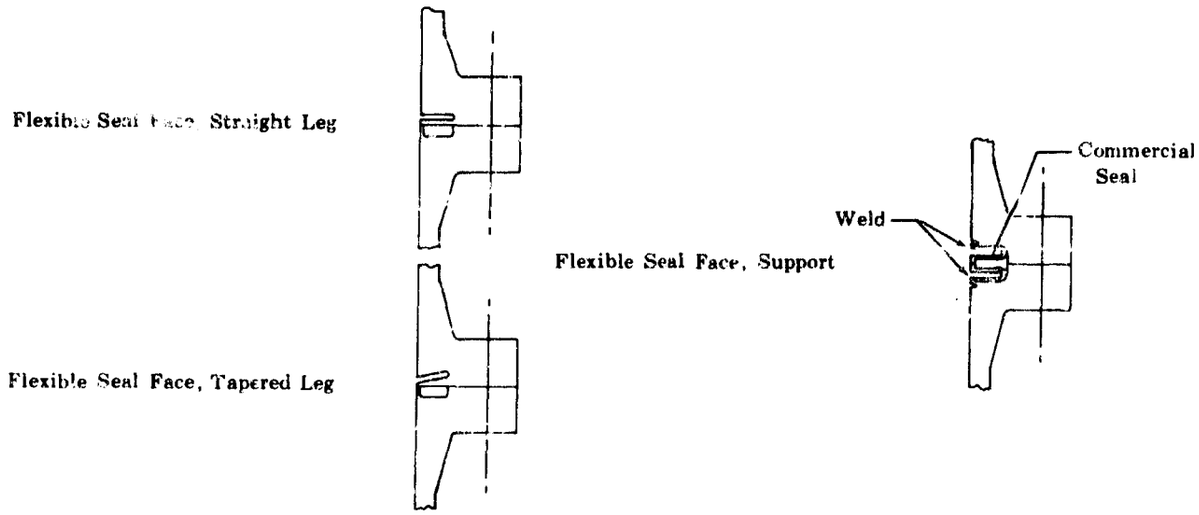

(U) Figure 484. Static Seal Rig Deflection Compensation Schemes FD 24773

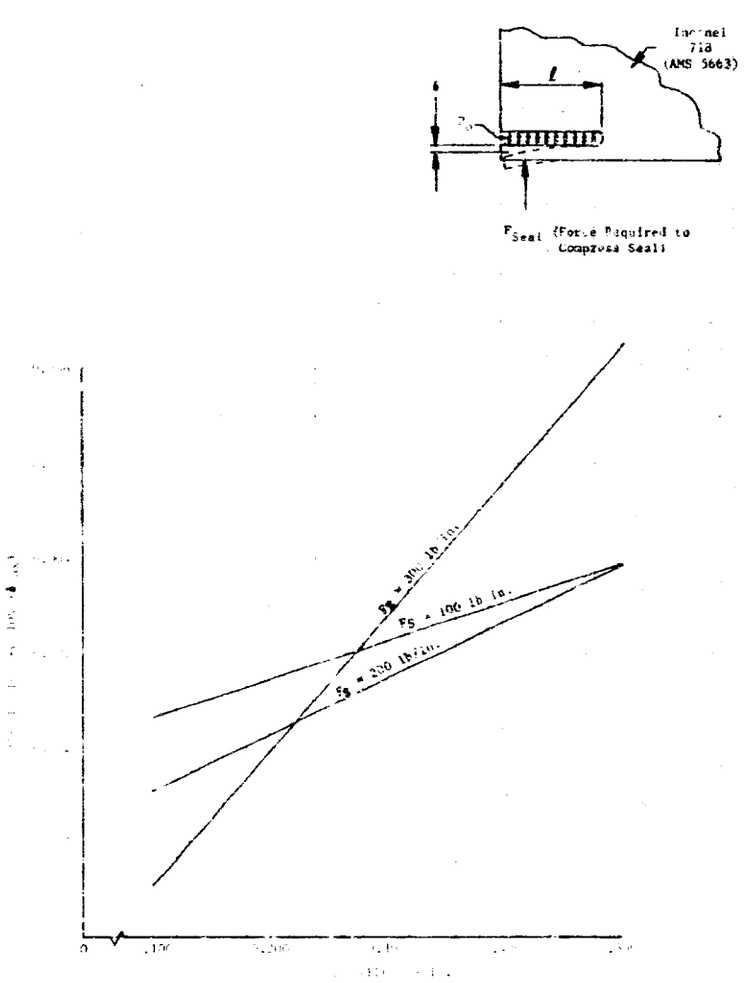

(U) Figure 485. Maximum Deflection vs Leg Length for Straight Cantilever Beam DF 68985

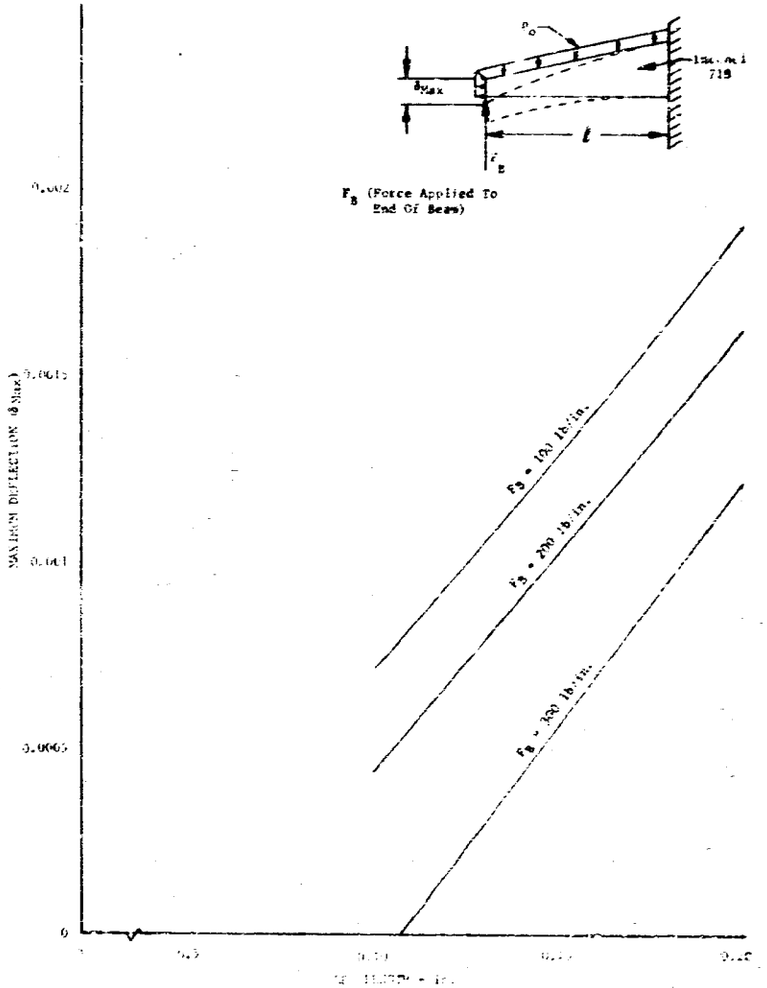

(U) Figure 486. Maximum Deflection vs Leg Length for Tapered Cantilever Beam DF 68987

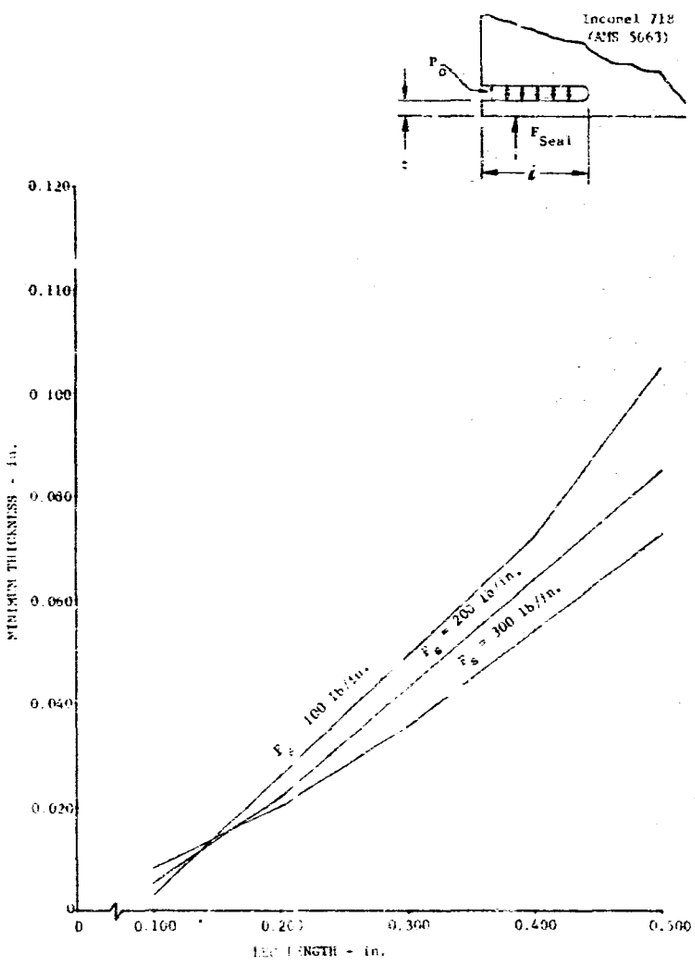

(U) Figure 487. Minimum Thickness vs Leg Length for Straight Cantilever Beam DF 68986

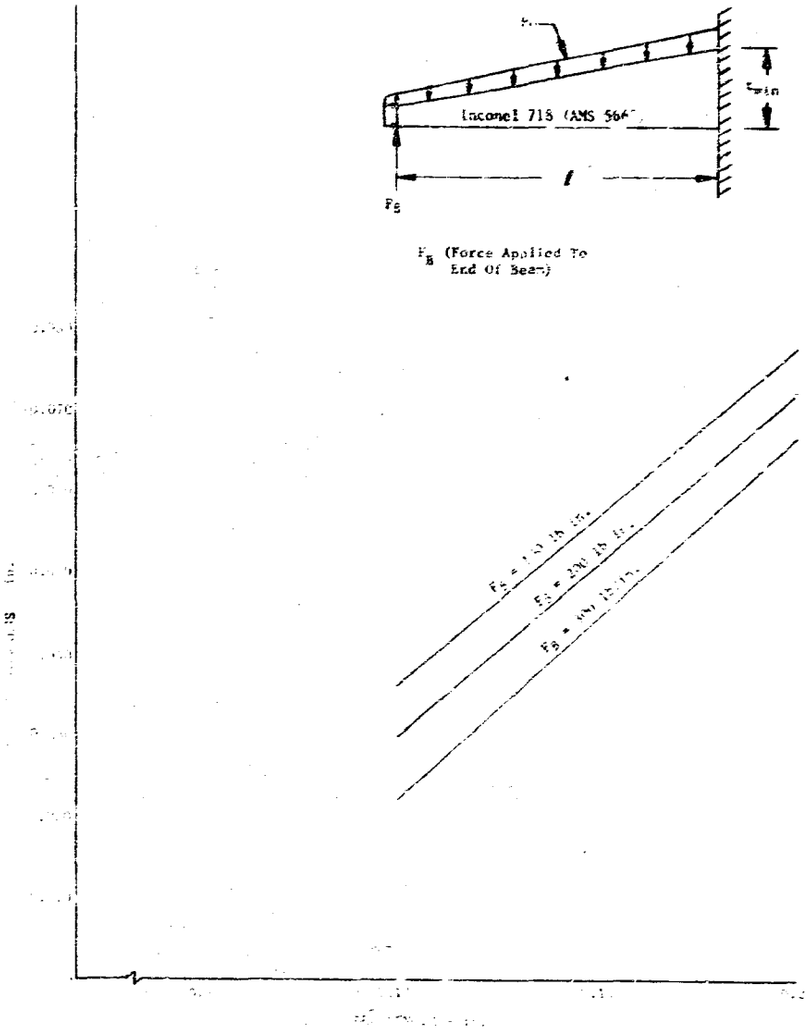

(U) Figure 488. Minimum Thickness vs Leg Length for Tapered Cantilever Beam DF 68988

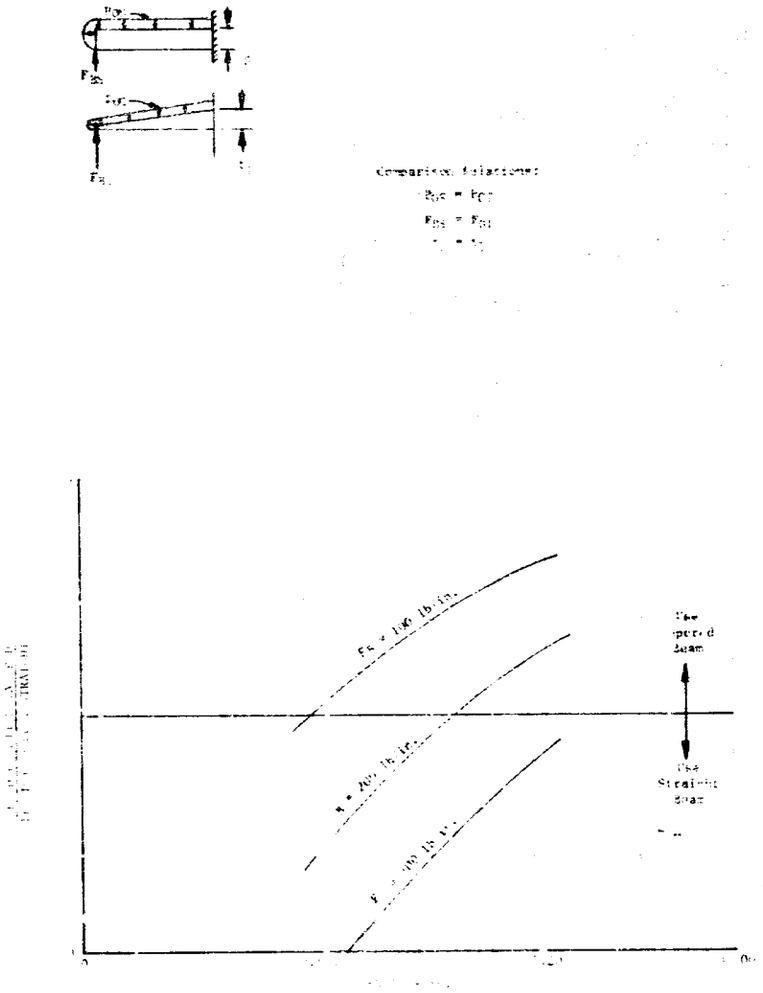

(U) Figure 489. Deflection Ratio (Tapered Leg to Straight Leg) vs Length DF 68989

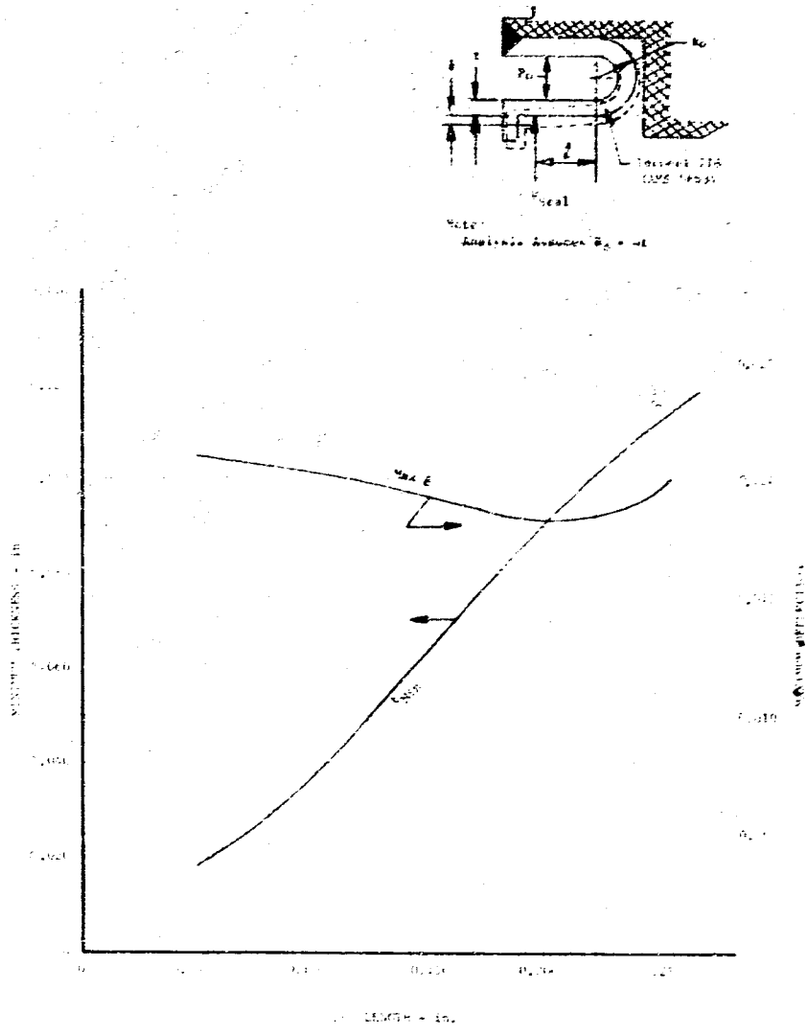

(U) Figure 490. Maximum Deflection and Minimum Thickness for Flexible Seal Support DF 68990

SECTION VI

TASK 1.3 - ENGINE INTEGRATION AND DEMONSTRATION

SECTION VI
TASK 1.3 - ENGINE INTEGRATION AND DEMONSTRATION

A. INTRODUCTION

(U) The XLR129-P-1 is a high pressure, reusable, oxygen/hydrogen rocket engine with a two-position exhaust nozzle. The objectives of this task are to design, fabricate, and demonstrate the performance and mechanical integrity of a 250,000 pound thrust engine using the staged-combustion bell-nozzle concept. The design and demonstration characteristics of the demonstrator engine are shown in Table XLVIII.

B. SUMMARY, CONCLUSIONS AND RECOMMENDATIONS

(U) The design requirements for the XLR129-P-1 engine are presented in Table XLIX. This table is based on cycle No. 6, which meets the demonstrator engine characteristics as defined in Table XLVIII. This cycle will be the basis for the design of the XLR129-P-1 engine.

C. CYCLE ANALYSIS

(U) The object of this analytical study was to establish an engine cycle to meet the demonstrator engine characteristics as defined by Table XLVIII. To assure that hardware designs would incorporate only those technologies that could reasonably be demonstrated within the scope of the program, demonstrated component performance for the major components was used to develop the engine cycle. Test data from the current program, Phase I and related high pressure engine component programs were used to define the component performance.

(U) Starting with the basic cycle as proposed at the beginning of the current program, six iterations were required to optimize the engine cycle. These iterations were dictated by engine operating limits, component hardware designs, desired operating characteristics, and engine envelope and/or packaging considerations. This sixth iteration (Cycle No. 6) is being used as the basis for the design of the XLR129-P-1 engine. Minor changes to this cycle will occur as the design of the engine proceeds and as components are developed. Major changes are not anticipated.

(C)(U) Table XLVIII. XLR129-P-1 Engine Characteristics

Item/Condition	Requirement
Nominal Thrust	250,000 lb Vacuum Thrust with Area Ratio of 166.1 244,000 lb Vacuum Thrust with Area Ratio of 75:1 209,000 lb Sea Level Thrust with Area Ratio of 35:1
Minimum Delivered Specific Impulse Efficiency	96% of Theoretical Shifting I_s at Nominal Thrust; 94% of Theoretical Shifting I_s during Throttling
Throttling Range	Continuous from 100% to 20% of Nominal Thrust Over the Mixture Ratio Range
Overall Mixture Ratio Range	Engine Operation from 5.0:1 to 7.0:1
Rated Chamber Pressure	2740 psia
Engine Weight (with 75:1 nozzle)	3520 lb (With Flight-type Actuators and Engine Command Unit) 3380 lb (Less Flight-type Actuators and Engine Command Unit)
Expansion Ratio	Two Position Booster-type Nozzle with Area Ratios of 35:1 and 75:1
Durability	10 Hours Between Overhauls, 100 Reuses, 300 Starts, 300 Thermal Cycles, 10,000 Valve Cycles
Single Continuous Run Duration	Capability from 10 Seconds to 600 Seconds
Engine Starts	Multiple Restart at Sea Level or Altitude
Thrust Vector Control	Amplitude: $\pm$7 Deg; Rate: 30 Deg/Sec; Acceleration: 30 Rad/Sec^2
Control Capability	$\pm$3% Accuracy in Thrust and Mixture Ratio at Nominal Thrust Excursions from Extreme to Extreme in Thrust and Mixture Ratio Within 5 Sec
Propellant Conditions	LO_2: 16 ft NPSH from 1 Atmosphere Boiling Temperature to 180°R LH_2: 60 ft NPSH from 1 Atmosphere Boiling Temperature to 45°R
Environmental Conditions	Sea Level to Vacuum Conditions Combined Acceleration: 10 g's Axial with 2 g's Transverse, 6.5 g's Axial with 3 g's Transverse, 3 g's Axial with 6 g's Transverse
Engine/Vehicle	No External to Engine except Normal Electrical Power and 1500 psia Helium from the Vehicle

(C)(U) Table XLIX. XLR129-P-1 Engine Operating Requirements

	100% Thrust r = 5.0	100% Thrust r = 6.0	100% Thrust r = 7.0	20% Thrust r = 5.0	20% Thrust r = 6.0	20% Thrust r = 7.0
Configuration						
Thrust, lb	244,000	244,000	244,000	48,800	48,800	48,000
Specific Impulse, sec	450	450	443	442	439	429
Envelope:						
Diameter, in.	68	68	68	68	68	68
Length: Nozzle Extended/Retracted, in.	132/80	132/80	132/80	132/80	132/80	132/80
Nozzle Area Ratio: Extended/Retracted	75/35	75/35	75/35	75/35	75/35	75/35
Fuel Flow, lb/sec	90.4	77.6	68.8	18.3	15.9	14.2
Oxidizer Flow, lb/sec	451.8	465.7	481.7	91.7	95.5	99.7
Total Propellant Flow, lb/sec	542.2	543.3	550.5	110.0	111.4	113.9
Main Burner Chamber						
Throat Total Pressure, psia	2805	2740	2676	552	537	526
Mixture Ratio (injector)	5.54	6.67	7.90	5.89	7.32	8.77
Specific Impulse Efficiency, %	96.8	97.0	96.9	96.4	96.1	96.0
Fuel Injector Pressure Loss, psi	161	130	120	16	16	17
Oxidizer Injector Pressure Loss, psi	822	913	984	40	42	46
Momentum Pressure Loss, psi	0.9	2.3	-1.7	9.4	7.8	7.3
Transpiration Coolant Flow, lb/sec	6.40	5.39	5.41	1.39	1.51	1.56
Throat Diameter, in.	7.68	7.68	7.68	7.68	7.68	7.68
Preburner						
Total Pressure, psia	4824	4367	4175	732	719	710
Mixture Ratio (preburner injector)	1.07	1.11	1.26	0.72	0.95	1.18
Temperature, °R	2015	2086	2326	1394	1796	2181
Fuel Injector Pressure Loss, psi	320	246	200	29	26	22
Oxidizer Injector and Control Valve Pressure Loss, psi	1101	981	566	533	596	635
Total Propellant Flow, lb/sec	155	136	126	23.0	21.4	20.4
Combustion Efficiency, %	100	100	100	100	100	100
Primary Nozzle						
Transpiration Supply Section:						
Coolant Flow, lb/sec	6.39	5.39	5.40	1.34	1.46	1.51
Coolant Inlet Pressure, psia	4903	4460	4516	1029	1116	1165
Coolant Inlet Temperature, °R	144	135	139	71	78	85
Coolant Pressure Loss, psi	76.9	62.1	63.7	11	12	13
Coolant Temperature Rise, °R	306	388	405	420	423	433
Preburner Supply Section:						
Coolant Flow, lb/sec	76	65	56	13.5	11.0	9.4
Coolant Inlet Pressure, psia	5293	4728	4468	770	752	738
Coolant Inlet Temperature, °R	141	133	140	71	77	82
Coolant Pressure Loss, psi	131	98	78	7	6	5
Coolant Temperature Rise, °R	42	51	57	55	70	84

(C)(U) Table XLIX. XLR129-P-1 Engine Operating Requirements (Continued)

	100% Thrust r = 5.0	100% Thrust r = 6.0	100% Thrust r = 7.0	20% Thrust r = 5.0	20% Thrust r = 6.0	20% Thrust r = 7.0
Two-Position Nozzle						
Coolant Flow, lb/sec	2.31	2.23	2.24	1.40	1.35	1.30
Thrust, lb	893	896	914	403	408	406
Fuel Turbopump						
Pump:						
Number of Pump Stages	2	2	2	2	2	2
Speed, rpm	48,043	44,477	44,220	19,650	20,947	21,933
Pressure Rise, psi	5542	4874	4911	991	1083	1136
Overall Efficiency, %	65.9	65.4	63.9	50.5	45.9	42.8
Impeller Tip Velocity (rms), ft/sec	2441	2261	2248	999	1065	1115
Temperature Rise, °R	91.1	82.5	87.1	24.4	31.7	38.2
Inlet Flow, lb/sec	91.3	78.5	69.7	18.7	16.3	14.6
Turbine:						
Number of Stages	2	2	2	2	2	2
Pressure Ratio	1.61	1.51	1.48	1.26	1.27	1.28
Inlet Temperature, °R	1986	2055	2292	1367	1760	2138
Inlet Pressure, psia	4766	4318	4129	726	712	703
Temperature Drop, °R	173	154	160	52.8	67.0	79.8
Mean Wheel Velocity, ft/sec	1468	1378	1370	609	649	679
Efficiency, %	75.4	75.2	75.0	63.5	62.7	62.3
Inlet Flow, lb/sec	111.5	97.3	90.0	16.5	15.4	14.6
Oxidizer Turbopump						
Pump:						
Number of Stages	1	1	1	1	1	1
Speed, rpm	25,263	23,263	22,369	10,099	10,290	10,400
Pressure Rise, psi	5737	5182	4603	1162	1204	1227
Efficiency, %	67.3	67.7	68.1	47.1	47.8	48.7
Impeller Tip Velocity, ft/sec	952	854	821	371	378	382
Temperature Rise, °R	35.0	31.1	27.4	10.4	10.7	10.7
Inlet Flow, lb/sec	630.6	535.7	548.1	127.0	131.4	135.9
Turbine:						
Number of Stages	2	2	2	2	2	2
Pressure Ratio	1.64	1.53	1.51	1.28	1.30	1.31
Inlet Flow, lb/sec	45.3	39.5	36.6	6.8	6.3	6.02
Inlet Temperature, °R	1986	2055	2292	1367	1760	2138
Inlet Pressure, psia	4782	4332	4141	727	714	705
Temperature Drop, °R	162.5	144	148	49	61	71
Mean Wheel Velocity, ft/sec	1131	1015	976	441	449	454
Efficiency, %	68.0	67.5	66.5	53.9	51.7	50.3

(C)(U) Table XLIX. XLR129-P-1 Engine Operating Requirements (Continued)

	100% Thrust r = 5.0	100% Thrust r = 6.0	100% Thrust r = 7.0	20% Thrust r = 5.0	20% Thrust r = 6.0	20% Thrust r = 7.0
Low-Speed Inducer						
Fuel Inducer:						
Flow Rate, lb/sec	90.4	77.6	68.8	18.3	15.9	14.2
Speed, rpm	19,777	17,846	16,908	6091	6094	6041
Pressure Rise, psi	90.2	94.7	108.9	25.0	29.0	31.0
NPSH, ft	60	60	60	60	60	60
Efficiency, %	80.0	79.2	77.3	48.5	42.9	38.7
Oxidizer Inducer:						
Flow Rate, lb/sec	451.8	465.7	481.7	91.7	95.5	99.7
Speed, rpm	5316	5221	5164	2008	2128	2236
Pressure Rise, psi	253	233	197	62	70	77
NPSH, ft	16	16	16	16	16	16
Efficiency, %	78.6	80.2	80.6	37.8	38.0	38.3
Fuel Low-Speed Inducer Turbine						
Pressure Ratio	1.38	1.34	1.36	1.37	1.40	1.41
Flow Rate, lb/sec	4.90	4.12	4.13	1.03	1.12	1.16
Speed, rpm	19,777	17,846	16,908	6091	6094	6041
Efficiency, %	60.5	59.0	56.9	28.3	27.1	26.0
Oxidizer Low-Speed Inducer Turbine						
Pressure Drop, psi	747	637	565	523	598	660
Flow Rate, lb/sec	371	393	411	81.4	84.3	87.9
Speed, rpm	5316	5221	5164	2008	2128	2236
Efficiency, %	51.9	51.1	50.2	34.1	33.8	33.8
Preburner Oxidizer Valve						
Inlet Pressure, psia	5885	5316	4707	1265.2	1314.8	1344.8
Inlet Temperature, °R	225.8	220.3	215.1	200.0	200.3	200.1
Exit Pressure, psia	5202	4664	4468	742.8	729.4	719.9
Flow, lb/sec	70.72	62.44	63.72	2.97	3.42	3.85
Overall Effective Area, $in.^2$	0.49	0.45	0.75	0.02	0.03	0.03
Main Chamber Oxidizer Valve						
Inlet Pressure, psia	5215	4735	4195	741.7	717.2	685.3
Inlet Temperature, °R	225.8	220.3	215.1	200.0	200.3	200.1
Exit Pressure, psia	3635	3663	3666	601.7	587.6	579.9
Flow, lb/sec	370.56	393.16	410.63	81.39	84.32	87.93
Overall Effective Area, $in.^2$	1.70	2.19	3.25	1.27	1.37	1.58

CONFIDENTIAL

(C)(U) Table XLIX. XLR129-P-1 Engine Operating Requirements (Continued)

	100% Thrust r = 5.0	100% Thrust r = 6.0	100% Thrust r = 7.0	20% Thrust r = 5.0	20% Thrust r = 6.0	20% Thrust r = 7.0
Preburner Fuel Valve						
Inlet Pressure, psia	5600	4956	5019	1061.5	1157.3	1212.28
Inlet Temperature, °R	138.7	130.1	135.12	70.84	78.5	85.32
Exit Pressure, psia	5300	4733	4472	770.2	751.7	738.0
Flow, lb/sec	81.29	69.69	60.84	15.41	12.88	11.21
Throat Effective Area, $in.^2$	3.44	3.44	1.93	0.70	0.52	0.43
Oxidizer Pressure Limit Valve						
Inlet Pressure, psia	6000	5412	4804	1266.8	1316.7	1346.9
Inlet Temperature, °R	225.8	220.3	215.1	200.0	200.3	200.1
Exit Pressure, psia	262	229.6	201	104.8	112.7	120.1
Flow, lb/sec	105.43	0.0	0.0	0.0	0.0	0.0
Overall Effective Area, $in.^2$	0.25	0.0	0.0	0.0	0.0	0.0

D. XLR129-P-1 ENGINE DESCRIPTION

(U) The staged-combustion, high-pressure demonstrator engine with a two-position bell-nozzle is a 250,000-lb thrust, throttleable, high-performance propulsion system. The operating envelope of thrust and mixture ratio is shown in Figure 491. The engine arrangement and a propellant flow schematic illustrating the principal flow paths are presented in Figure 492.

(U) Hydrogen and oxygen enter at the engine-driven low-speed inducers. The low-speed inducers minimize vehicle tank pressure requirements while maintaining high-speed main propellant pumps for high turbopump efficiencies. The low-speed fuel inducer is a single shaft unit with a high suction specific speed axial-flow inducer driven by a partial-admission, two-stage, hydrogen turbine. The low-speed oxidizer inducer is also a single shaft unit with a high specific speed axial-flow inducer driven by a partial admission, single-stage liquid oxygen turbine.

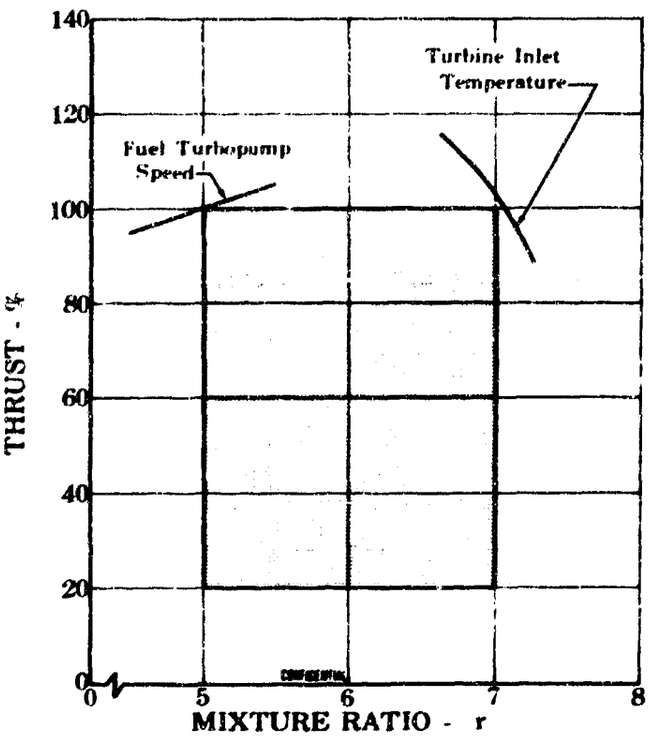

(U) Figure 491. Operating Range for XLR129-P-1 Engine FDC 25101

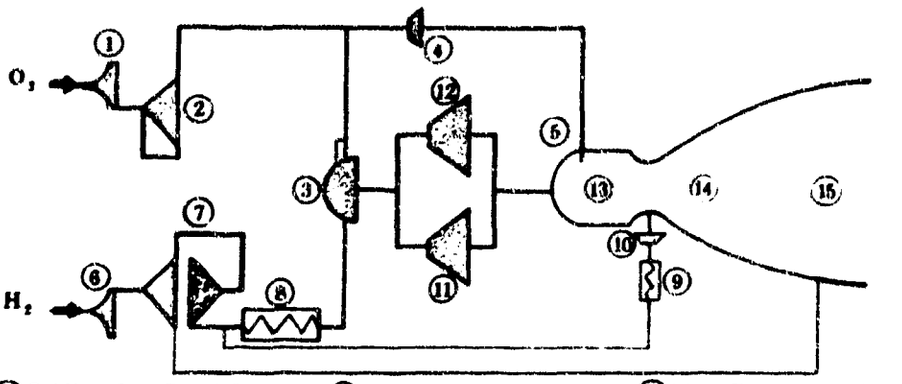

1. Oxidizer Low-Speed Inducer
2. Oxidizer Pump
3. Preburner
4. Oxidizer Low-Speed Inducer Turbine
5. Main Burner Injector
6. Fuel Low-Speed Inducer
7. Fuel Pump
8. Preburner Supply Heat Exchanger
9. Transpiration Supply Heat Exchanger
10. Fuel Low-Speed Inducer Turbine
11. Fuel Pump Turbine
12. Oxidizer Pump Turbine
13. Main Burner Chamber
14. Primary (Regeneratively Cooled) Nozzle
15. Two-Position Nozzle

(U) Figure 492. XLR129-P-1 Engine Propellant Flow Schematic FD 19362F

(U) The main fuel turbopump is a single shaft unit with two back-to-back centrifugal pump stages driven by a two-stage, pressure-compounded turbine. A double-acting thrust balance piston is provided between the pump and turbine.

(U) The oxidizer turbopump is a single shaft unit with a single, centrifugal pump stage driven by a two-stage, pressure-compounded turbine. A single-acting thrust balance piston is provided between the pump and turbine.

(C) The preburner injector consists of dual-orifice tangential slot swirler oxidizer injection elements with concentric fixed-area fuel injection. A preburner liquid oxygen valve is incorporated at the rear of the injector assembly to vary the total oxidizer flow rate to adjust engine power level and to adjust the relative flow of the primary and secondary elements. The preburner combustion chamber is an integral part of the transition case, which contains the turbine drive gas ducts and a cooled outershell. The main turbopumps are mounted to the transition case with a plug-in arrangement of the turbines for maintainability.

(C) The main burner injector consists of fixed-area, tangential slot swirler oxidizer injection elements arranged in radial spraybars. The fuel side (preburner combustion products after expansion through the turbine) is a fixed area design that directs fuel-rich gas flow through slot areas around the oxidizer injection elements and a porous faceplate to provide cooling. The combustion chamber wall is composed of a hydrogen cooled liner extending from the injector face through the throat region to an area ratio of about 5. The liner is composed of grooved copper wafers creating a porous transpiration cooling chamber liner.

(U) The nozzle, which attaches immediately downstream of the throat, is composed of two fixed regeneratively cooled sections and a retractable, low-pressure, dump-cooled section.

(U) The main fuel flow, which is pumped to system operating pressure levels by the main fuel pump, is ducted to cool the regeneratively cooled sections of the nozzle. The forward section is cooled with the majority of the fuel flow from the pump in a single pass heat exchanger. This flow exits from the nozzle and is ducted to the preburner. The regeneratively cooled rear section of the fixed nozzle is cooled with the remainder of the fuel flow in a two-pass heat exchanger. This flow is subsequently used as the working fluid to power the fuel low-speed inducer drive turbine and is then used to cool the porous main chamber walls.

(U) A small amount of fuel is ducted from the fuel pump interstage to cool the retractable nozzle skirt. This fuel is heated to high temperature in the skirt and expelled overboard through small nozzles at the nozzle exit plane. A valve is provided to shut off the flow when the secondary nozzle is retracted.

(U) After being pumped to system operating pressure, the oxidizer is divided between the preburner and the main chamber. The smaller portion of the flow is supplied to the preburner and is burned with the fuel. The resulting combustion products provide the working fluid for the main turbines, which are arranged in parallel. The turbine exhaust gases are rejoined and directed to the main burner injector.

(U) The main burner oxidizer flow provides the oxidizer low-speed inducer turbine working fluid and uses the available pressure drop between the main oxidizer pump discharge pressure and the main chamber pressure for the turbine power. The oxidizer flow is then injected into the main burner chamber and is mixed and burned with the fuel-rich turbine exhaust gases. The resulting combustion gas is then expanded through the bell-nozzle.

(U) The primary engine controls are located in the liquid oxygen supply lines to the preburner and the main chamber and in the liquid hydrogen supply line to the preburner.

E. XLR129-P-1 ENGINE ARRANGEMENT STUDY

1. Introduction

(U) The objective of this study was to determine the arrangement and effect of a spherical transition case on the overall engine configuration. The transition case serves as the engine center body for mounting the preburner and turbo-machinery. An arrangement was studied in which the main turbopumps and preburner were rotated upward and toward the engine centerline. This design was referred to as the canted design. A second arrangement was studied in which the main turbopumps and preburner are perpendicular to the engine centerline and in the same plane. This design was referred to as the coplanar design.

2. Summary, Conclusions and Recommendations

(U) Either the canted or coplanar designs can be reasonably packaged and no significant advantage is obtained from one design over the other. Selection of the transition case design should, therefore, be based on component structural requirements.

3. Design Description

(U) The ground rules governing the design layouts shown in Figures 493 and 494 were:

1. Engine diameter and length were not restricted.
2. The rear skirt must move forward so that its rear was flush with the rear of the primary nozzle.
3. The location of the inlets was optional.
4. Single preburner and separate turbines were used.
5. Three evenly-spaced jackscrews were used.

(U) Figure 493 with the canted case design does not represent an optimized design, but one which is a starting point for noting advantages, problem areas, etc. The items listed below summarize the more significant observations:

1. The engine low-speed inducers were moved forward with two major effects: the engine tends to become longer and the inlets are forward of the gimbal pad. Further study and/or use of banjo fittings might allow the low-speed inducers to go rearward.
2. The jackscrew supports or brackets on the rear translating skirt may have interference problems, especially if they are widened to overcome the moment problem at the base of the bracket. This problem would be relieved by not having the skirt come so far forward.
3. The cant angles on the transition case shown in Figure 493 are 20 degrees.
4. At station A.R. 11.75 there are four manifolds. With or without a mechanical joint, this area requires additional study to determine construction versus heat transfer considerations.
5. Line sizes were based on a design study of the Phase I (Contract AF04(611)-11401) mockup. Additional line size optimization appears warranted for new engine configurations.
6. The layout does not show or make provision for the supports of the low-speed inducers or the jackscrew front bearings.

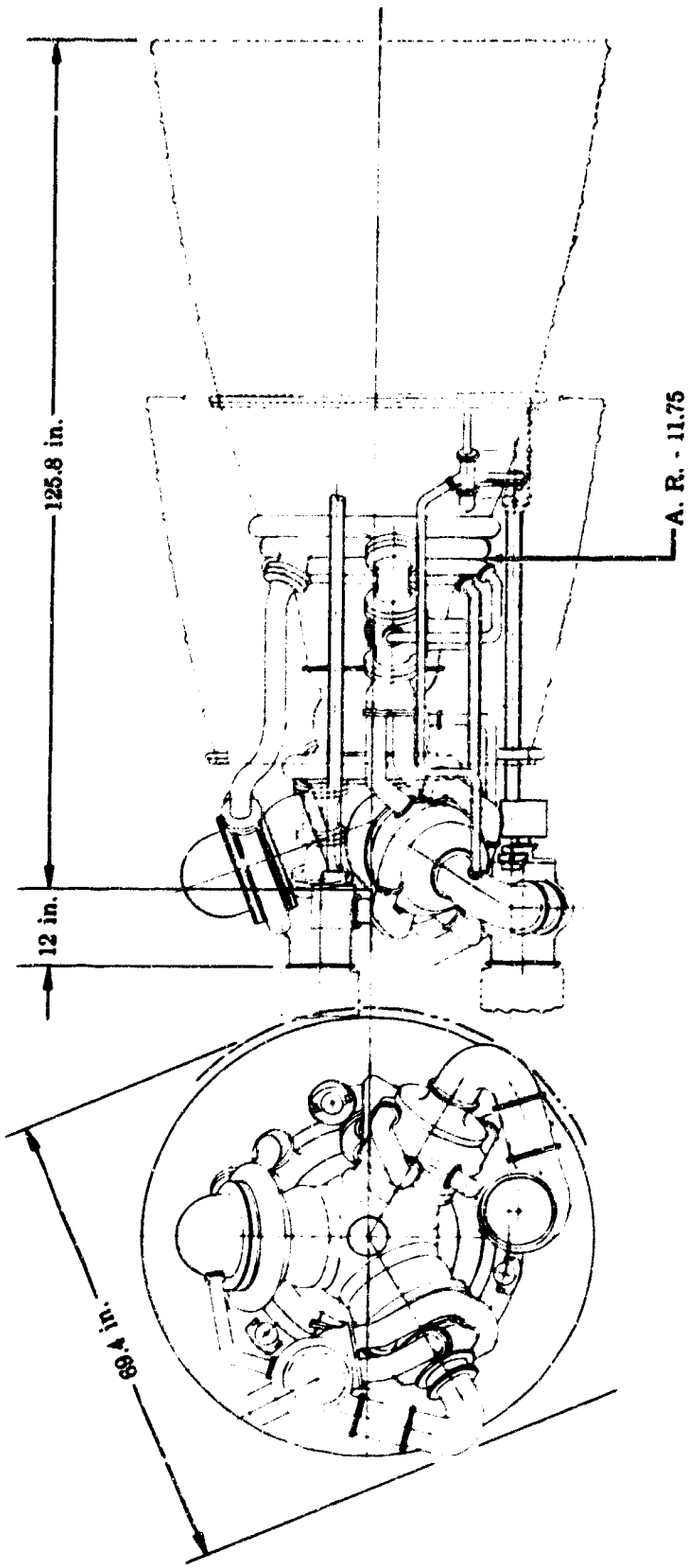

(U) Figure 493. Demonstrator Engine Components Arrangement with Canted Transition Case FD 25711A

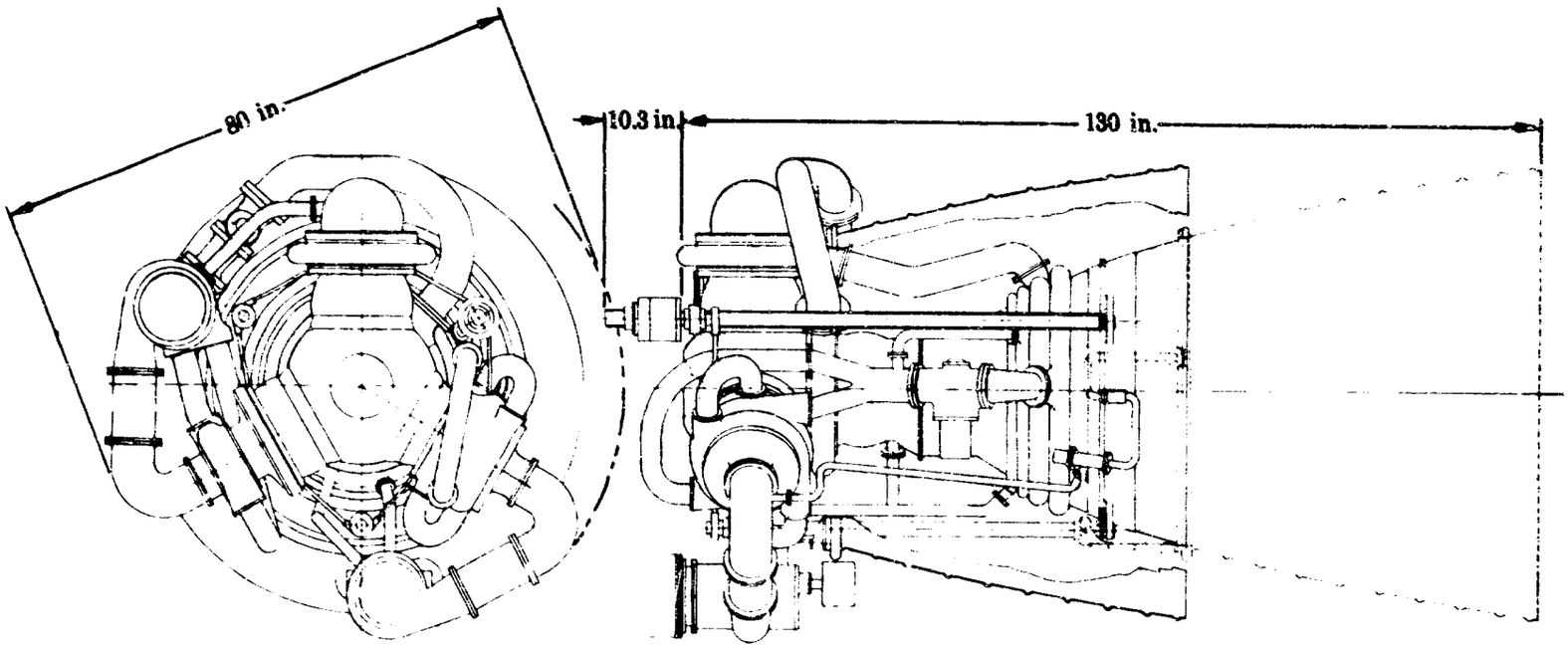

(U) Figure 494. Demonstrator Engine Components Arrangement with Co-planar Transition Case FD 25712A

(U) In general, the canted design appears to produce the lowest transition case weight and a smaller engine diametrical envelope, excluding the nozzle diameter. However, an increased engine length will also result with this configuration.

(U) Figure 494 represents the engine configuration with the coplanar transition case. The more significant observations for this configuration are:

1. A reduction in the size of the transition case as shown in Figure 494 is required to meet the desired diametrical envelope.

2. The coplanar arrangement of the main components produces the shortest engine length.

3. The routing of large high pressure plumbing is reasonable.

This engine arrangement appears to produce the most compact configuration.

F. XLR129-P-1 ENGINE PLUMBING STUDY

1. Introduction

(U) The objectives of the engine plumbing study were to compare the cycle sheet flow head loss with the calculated flow head loss based on a mockup plumbing configuration, determine if the mockup plumbing configuration can be fabricated into real hardware and derive ground rules required to govern material selection and fabrication, and make a fabrication feasibility study to define the configuration problem areas prior to initiating the major engine component design.

2. Summary, Conclusions and Recommendations

(U) The calculated head loss values used in the engine cycle balance are representative of the engine plumbing system.

(U) The material that appears most desirable for use in the plumbing lines is Inconel 718 (AMS 5589) because of its high strength and elongation. The use of castings for the plumbing lines is a possibility, however, castings generally have a lower fatigue and yield strength than wrought alloys, along with lower elongations. The use of bent tubes for the plumbing lines is another possiblity. All of the vendors contacted have had extensive experience in similar lower pressure aerospace plumbing.

3. Design Analysis

a. Head Loss Calculation

(U) The engine cycle sheet plumbing pressure drops were calculated based on an engine mockup constructed in Phase I (Contract AF04(611)-11401). The flow head loss calculations in the lines were based on the inside diameters government by Inconel 718 (AMS 5589) wall thickness requirements. The calculated head loss numbers were within the limitations of the engine cycle.

b. Material Selection

(U) Material selection must be a compromise that considers minimum weight, maximum strength and ease of fabrication. Table L compares relative line weights using several material selections. Flange weight is not included. Three of the materials proved to be undesirable because of the high weight and a large wall thickness requirements. These materials were Inconel 625 (AMS 5599), stainless steel (AMS 5654 and AMS 5735G).

(U) Table L. Plumbing Weight Summary

Material	Line Weight, lb
Inconel 718 (AMS 5589)	72
Inconel 625 (AMS 5599)	161
Stainless Steel (AMS 5735G)	105
Stainless Steel (AMS 5654)	282
A110 Titanium (AMS 4910)	57
6061 Aluminum (AMS 4082)	89

(U) A line with a large wall thickness displays the following disadvantages:

1. Bend forming is difficult.
2. Proper weld joints are difficult to make where thick walls must be joined.
3. Heavy walls increase line stiffness that may impose high assembly stresses on the flanges of mating components.

The Inconel 718 (AMS 5589) line affords a relatively thin wall and a low overall weight. Some disadvantages in fabrication with Inconel 718 (AMS 5589) must be considered in spite of the light weight advantage:

1. Inconel 718 (AMS 5589) must be heat treated to gain any increase in tensile strength.
2. Heat treating can reduce the ductility to half the original amount.
3. Unequal wall thinning along the circumference of a bend may be a problem.

(U) At cryogenic temperatures Inconel 718 (AMS 5589) would be preferable to Inconel 625 (AMS 5599) provided that Inconel 718 (AMS 5589 is not subjected to severe fabrication bends. Inconel 625 (AMS 5599) requires no heat treating and after bending only stress relieving is necessary. The ductility is preserved by the non-requirement of heat treating. Inconel 718 (AMS 5589) exhibits a higher yield strength than Inconel 625 (AMS 5599), although Inconel 625 (AMS 5599) can be obtained in the cold rolled condition with an elevated yield strength near that of Inconel 718 (AMS 5589). The cold rolled Inconel 625 (AMS 5599) is limited in

ormality and any welding will remove the cold work strength properties at the weld joint. Weld fabricated bends of Inconel 718 (AMS 5589) seems to be the logical choice of the nickel alloys.

(U) The second material choice based on light weight advantage is A-110 titanium (AMS 4910). Titanium should be limited to the fuel side of the plumbing because the oxidizer compatibility is questionable. A-110 titantium is weldable. Impact strength and elongation at cryogenic temperatures are not completely defined and behavior of the metal is not fully predictable.

(U) Stainless steel (AMS 5654) has ideal properties at cryogenic temperatures and is used extensively on the RL10 rocket engine. For the high pressure applications of this rocket engine, however, stainless steel (AMS 5654) is not a practical choice because of the required heavy wall thickness of the lines.

(U) Stainless steel (AMS 5735G) will allow a line wall thickness near that of A-110 titanium (AMS 4910). Stainless steel (AMS 5735G) has the advantage of an elongation capability that increases with decreasing temperature. Although weight and elongation factors look favorable, the weldability of stainless steel (AMS 5735G) is very poor, and it is not recommended for welding.

(U) Aluminum (AMS 4082) is applicable on the low pressure side of the oxidizer and fuel plumbing. The yield strength of the aluminum (AMS 4082) allows for a minimum commercial wall thickness to be employed. The combination of a think wall with a low density material makes aluminum (AMS 4082) a good choice. Aluminum has good weldability, machining, and forming properties. For high pressure plumbing, the aluminum is impractical because the heavy wall requirements in the lines would present fabrication problems.

(U) Waspaloy has strength properties similar to Inconel 718 (AMS 5589), but the formability is much lower.

c. Fabrication Considerations

(1) Fabrication of Bends from Half Sections

(U) Bends can be made by welding two half sections together where the turning radius of the bend is in the joining plane of the two sections. Dies to stamp out the half sections can be produced economically from steel. The turning radius of the half section and the outside diameter of the tube cross section can be held to a ratio of 1 to 1 for tubes ranging from 2-inch OD and up. Maintaining a 1 to 1 ratio of r/OD for tubes with an OD less than 2 inch is difficult. This difficulty arises because the wall thickness relative to the OD becomes proportionately larger as the OD of the tube becomes smaller. Fabrication of half sections for bends with a tube OD less than 2-inch and a relatively small turning radius can be accomplished by lathe turning two semi-toroidal sections from heavy plate. The semi-toroidal sections can be cut into required bend segment angle and joined by welding. This method is economically feasible where only a few parts are required.

(2) Castings

(U) Castings generally have lower fatigue and yield strengths along with lower elongations than wrought alloys. The fatigue strength of a casting can be increased by shot peening. This puts a residual compressive stress in the outer fibers that increases the tensile strength of the casting. Investment casting of the bend half-sections is another method of fabrication where the tube OD is less than 2 inches and the turning radius relatively small. This choice is governed by the number of parts required. Economic feasibility may not be applicable for less than 5 or 10 parts. A good material choice for the investment casting method is cast Inconel 718 (AMS 5383). This case alloy has a 0.2% yield strength of 110,000 psi and good elongation. A disadvantage of using Inconel 718 (AMS 5383) is that the desired properties of nickel cast alloys are hard to control and the porosity may be the only quality the casting vendor is willing to guarantee. The minimum wall thicknesses on investment castings can range from 0.030 to 0.080 inch, which is a suitable size requirement limit on most of the lines.

(3) Tubes

(U) Several tube vendors were contacted in the course of this study to ensure that the proposed engine plumbing would not be fabrication limited. Comments from interviews with the vendor representatives are included below.

(U) The most desirable method of fabricating a tube consisting of several bends is by direct bending provided that all of the limiting conditions are favorable. A bend location is preferable near the end of the tube. The unbent tube will have its end cut on an angle in the plane of the proposed bend. The angled cut will be pulled square with respect to the tube centerline during bending. This caused by the fibers along the inside of the bend being pushed back and the fibers along the outside of the bend being pulled forward. The free end is unrestrained and wall thinning will be held to a minimum.

(U) If the tube consists of several bends rather close together, the bends will present difficulties because of the restraint on the inner and outer fibers by the previous bend. Excessive wall thinning of the outside of the bend may result if the bend angle is too severe. A material like Inconel 718 (AMS 5589) must be bent in multiple stages per bend, consisting of alternate partial bending, removal from the die and anealing. The Inconel 718 (AMS 5589) has a tendency to work harden to a high degree, therefore, annealing during bending must be accomplished.

(U) The out-of-roundness of the tube cross section at the bend is held to a minimum because the die is reinstalled at each continuation stage in the bending after annealing. The diametrical reduction for a 4-inch ID tube may be 0.020 inch. This diametrical reduction decreases as the tube ID decreases. The Inconel 718 (AMS 5589) has the highest rate of elongation if it is bent in the annealed condition spec. (1975°F). Because the tube application is cryogenic, notch sensitivity will not be a problem.

APPENDIX

APPENDIX

A. GENERAL

(U) The roller bearings that will be used in the XLR129 fuel pump have two unique features.

1. The outer race is thin and is mounted so that it can flex under roller load, as shown in Figure 495.
2. There is a tight or negative fit between inner race, rollers, and outer race.

(U) The interaction of the parameters that affect the bearing loads are complex. Therefore, a computer program was written to provide answers to the following questions:

1. Where is the assembly (room temperature) negative internal fit absorbed?
2. How does the roller load change as the environment changes (temperature, rpm)?
3. What is the effect of an external bearing load on individual roller loads?

(U) This appendix is organized as follows:

1. The effects considered in analyzing the bearing
2. The nomenclature used in the program
3. The formulation or equations used in the program
4. A compilation of the program
5. A sample case.

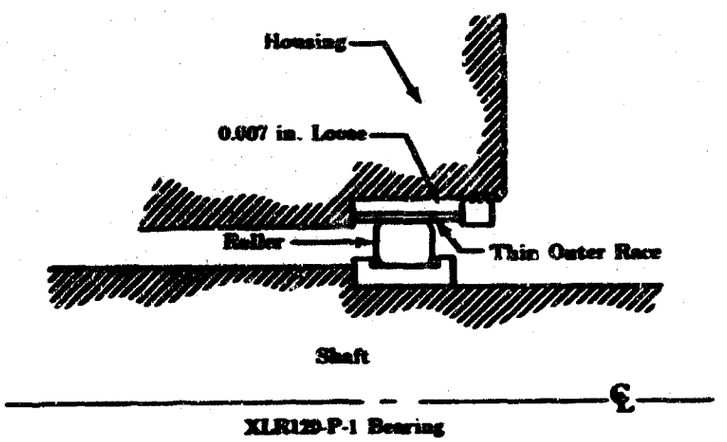

(U) Figure 495. Fuel Pump Bearing Concept FD 25497

1. Effects Considered in Analyzing the Bearing

(U) The effects that were considered in analyzing the bearing are as follows:

1. Outer Race
   a. Thermal growth - δ_8
   b. Hoop growth and axial crowning (Figure 496) - δ_9
   c. Race chording because load is local from each roller rather than uniform (Figure 497) - δ_{10}
   d. Hertz deflection (roller and outer race) (Figure 498) - δ_{11}
   e. Growth caused by axial loading - δ_{12}.
2. Roller
   a. Thermal growth - δ_7
   b. Deflection from load - δ_6
   c. Change in load inner to outer race because of rpm.
3. Inner Race
   a. Thermal growth - δ_{1a}
   b. Race diameter change caused by differing coefficients of expansion of the shaft and inner race. (Shrink fit is assumed.) - δ_{1b}
   c. Hoop growth from load - δ_2
   d. Bending growth or chording - δ_3
   e. Hertz deflection (roller and inner race) - δ_4
   f. Inner race deflection from rpm - δ_5.
4. Variation in load along roller axis because roller is offset on outer race (Figure 499) Note P_3 and P_4).
5. Redistribution of roller loads because of externally applied radial load (Figure 500).

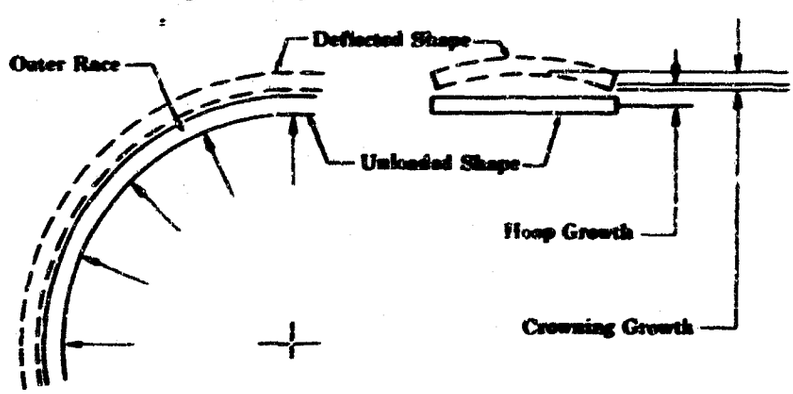

(U) Figure 496. Growth from Hoop and Crowning FD 25501

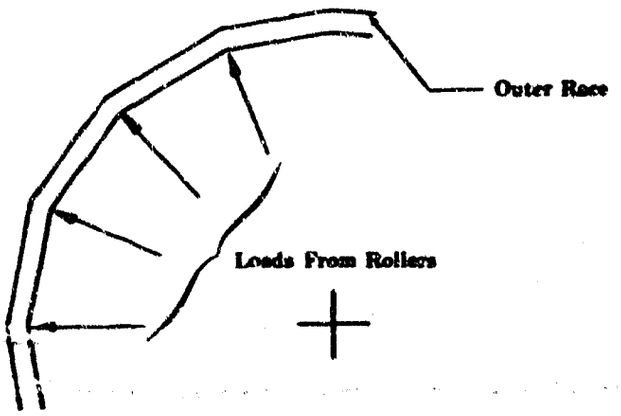

(U) Figure 497. Chording FD 25537

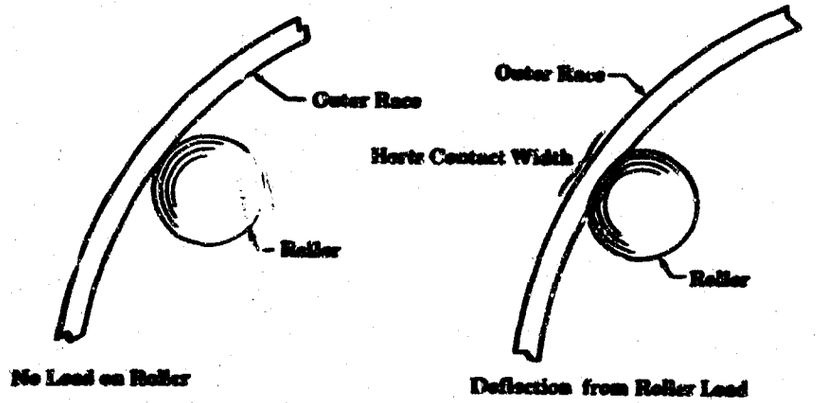

(U) Figure 498. Hertz Deflection FD 25538

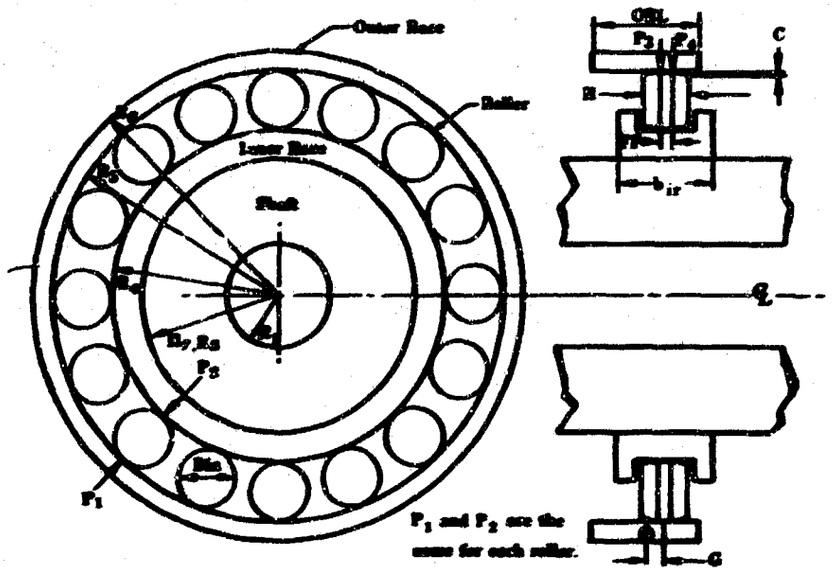

(U) Figure 499. Symmetrical Loading Rotation FD 25539

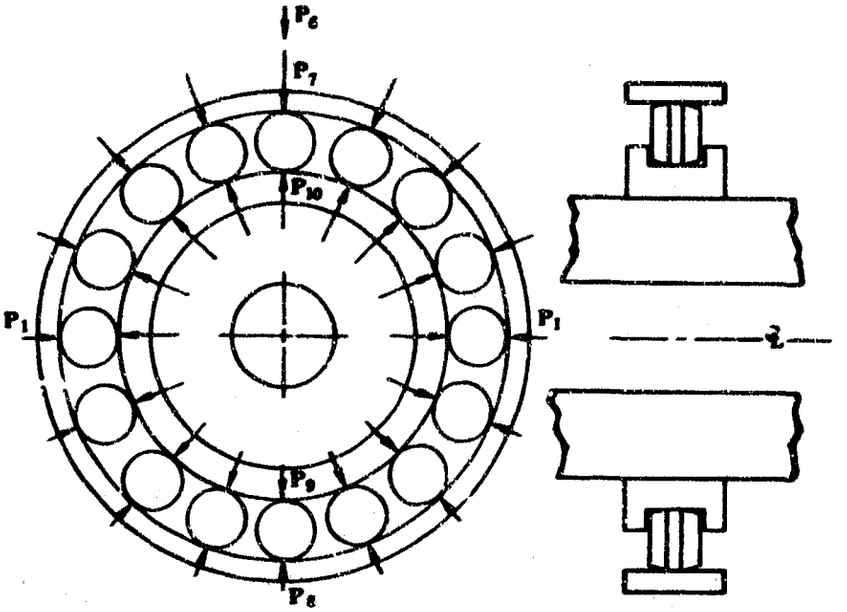

(U) Figure 500. Unsymmetrical Loading Notation FD 25540

2. The Nomenclature Used in the Program (See Figures 499 and 500.)

(U) Figure 501 shows the placement and sequence of the program input parameters. The following is a list of the nomenclature used:

1. Input Notations

NOC - Number of cases in fixed point, one card precedes each group of cases.

NOPT - 1 in fixed point uses δ_{12}
2 omits δ_{12}, which calculates change in outer race diameter due to axial pinch of carrier on race.

R_1 - Shaft inside radius (can be 0) - inches.

R_2 - Shaft outside radius - inches.

R_3 - Inner race inside radius - inches.

R_4 - Inner race outside radius - inches.

R_5 - Outer race inside radius - inches.

R_6 - Outer race outside radius - inches.

DIA - Roller diameter - inches.

ORL - Outer race length - inches.

FF - Roller crown length (flat) - inches.

G - Offset of center of roller relative to the center of the outer race - inches.

FIT - Radial negative internal clearance (built tight fit) - inches.
T_s - Shaft temperature - °F.
T_{ir} - Inner race temperature - °F.
α_s - Shaft coefficient of thermal expansion - inches/inch/°F.
α_{ir} - Inner race coefficient of thermal expansion - inches/inch/°F.
EE - Modulus of elasticity - pounds/inch^2.
T_D - Roller temperature - °F.
α_{or} - Outer race coefficient of thermal expansion - inches/inch/°F.
T_{or} - Outer race temperature - °F.
P_5 - Axial pinch load on outer race - pounds.
H - Roller length - inches.
P_1 (guess) - Guess at load from internal fit - pounds.
P_6 - Side load on bearing - pounds.
ΔP_7 (guess) - Guess at load redistribution from side load - pounds.
C - Crown height - inches.
XN - Number of rollers
μ - Poisson's ratio
b_{ir} - Inner race width - inches.
ρ - Inner race and roller weight density - pounds/inch^3.
rpm - Shaft speed - revolutions/minute.
α_D - Roller coefficient of thermal expansion - inches/inch/°F.

2. Output Notations

P_1 - Roller to outer race load with no side load, pounds.
P_2 - Roller to inner race load with no side load, pounds.
P_3 - Roller to race load at one end of crown - pounds/inch of circumference.
P_4 - Roller to race load at other end of crown - pounds/inch of circumference.
CF - Centrifugal force of 1 roller, pounds.
DEL - Loss in fit shaft to inner race because of thermals - inches.
B_1 - Roller to outer race circumferential contact width - inches.
B_2 - Roller to inner race circumferential contact width - inches.
Cage rpm - Cage rpm assuming no slippage of rollers to race.
D_1 - Inner race thermal deflection - inches.
D_2 - Inner race hoop deflection - no side load - inches.
D_3 - Inner race bending deflection - no side load - inches.

D_4 - Hertz deflection inner race and roller - no side load - inches.

D_5 - Inner race rpm deflection - inches.

D_6 - Roller deflection from load - no side load - inches.

D_7 - Roller deflection from thermals - inches.

D_8 - Outer race thermals - inches.

D_9 - Outer race hoop and crowning - inches.

D_{10} - Outer race bending - inches.

D_{11} - Hertz deflection, outer race to roller - inches.

D_{12} - Outer race Poisson deflection from axial load - inches.

B_{10} - Inner race contact width, most loaded roller - inches.

B_7 - Outer race contact width, most loaded roller - inches.

B_9 - Inner race contact width, least loaded roller - inches.

B_8 - Outer race contact width, least loaded roller - inches.

P_7 - Roller to outer race load on loaded side - pounds.

P_8 - Roller to outer race load on unloaded side - pounds.

P_9 - Roller to inner race load on unloaded side - pounds.

P_{10} - Roller to inner race load on loaded side - pounds.

DP_7 - Change in outer race to roller load on loaded side - pounds.

DP_8 - Change in outer race to roller load on unloaded side - pounds.

A_1 - Outer race hoop and crowning deflection loaded side - inches.

A_2 - Roller deflection from load on loaded side - inches.

A_3 - Inner race Hertz deflection, loaded side - inches.

A_4 - Outer race Hertz deflection, loaded side - inches.

B_1 - Outer race hoop and crowning deflection, unloaded side - inches.

B_2 - Roller deflection from load on unloaded side - inches.

B_3 - Inner race Hertz deflection, unloaded side - inches.

B_4 - Outer race Hertz deflection, unloaded side - inches.

PWA 10100 REV. 3-63

M038

FORTRAN CODING FORM

SHEET ____ OF ____

ANALYST ROLLER BEARING OUTER RACE DEFLECTION ENGINEER A. SCHULTZ/STEVENSON EXT ____

JOB NO. ____ COST CONTROL NO. ____

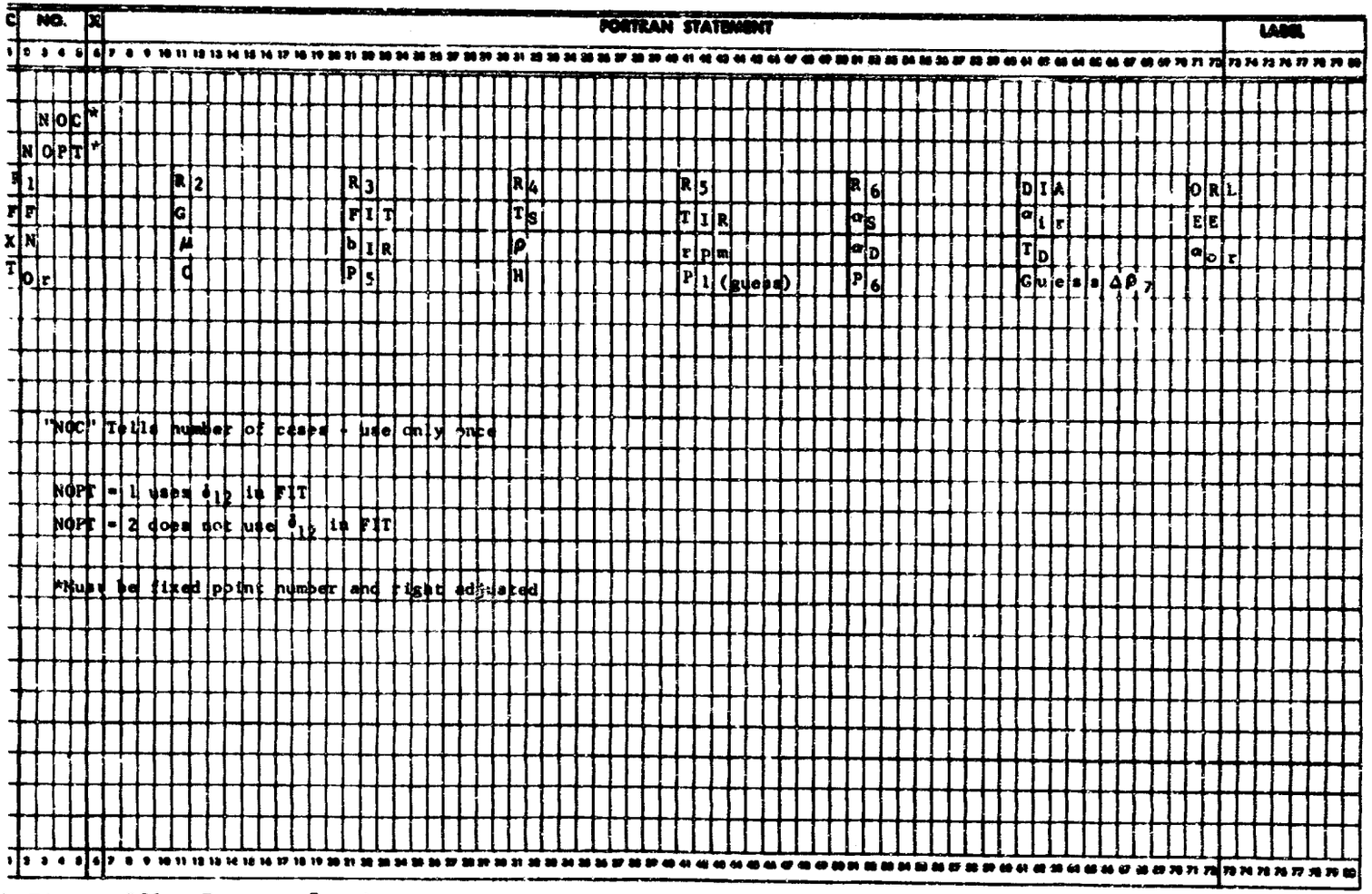

(U) Figure 501. Program Input

3. Formulation or Equations Used to Analyze the Bearing

a. Outer Race Deflection Terms

(1) Thermal Growth

$$\delta_8 = -R_5 \ \alpha_{or} \ (T_{or}-70) \tag{1}$$

(2) Hoop Growth from Radial Load and Axial Crowning
(Figures 496 and 500)
Note that the deflection under P_3 is the same as that under P_4

$$2\pi R_5 (P_3 + P_4) = XN \ P_1 \tag{2}$$

$$\lambda = \frac{1.285}{\sqrt{R_5 (R_6 - R_5)}} \tag{3}$$

$$\delta_9 = \frac{P_3 \ \lambda R_5^2}{EE(R_6 - R_5)} \left(\frac{1}{\text{Sinh}^2 \lambda ORL - \sin^2 \lambda ORL} \right) \Big[(\text{Cosh}^2 \lambda a + \cos^2 \lambda a)$$

$$(\text{Sinh } \lambda b \ \text{Cosh } \lambda b - \sin \lambda b \cos \lambda b) +$$

$$(\text{Cosh}^2 \lambda b + \cos^2 \lambda b) \ (\text{Sinh } \lambda a \ \text{Cosh } \lambda a - \sin \lambda a \cos \lambda a) \Big] +$$

$$\frac{P_4 \ \lambda R_5^2}{EE(R_6 - R_5)} \left(\frac{1}{\text{Sinh}^2 \lambda ORL - \sin^2 \lambda ORL} \right) \Big\{ 2 \ \text{Cosh } \lambda a \cos \lambda a$$

$$(\text{Sinh } \lambda ORL \cos \lambda e \ \text{Cosh } \lambda f - \sin \lambda ORL \ \text{Cosh } \lambda e \cos \lambda f) +$$

$$(\text{Cosh } \lambda a \sin \lambda a + \text{Sinh } \lambda a \cos \lambda a) \ \Big[\text{Sinh } \lambda ORL \ (\sin \lambda e \ \text{Cosh } \lambda f -$$

$$\cos \lambda e \ \text{Sinh } \lambda f) + \sin \lambda ORL \ (\text{Sinh } \lambda e \cos \lambda f -$$

$$\text{Cosh } \lambda e \sin \lambda f) \Big] \Big\} \tag{4}$$

also:

$$\delta_9 = \frac{P_4 \ \lambda R_5^2}{EE(R_6 - R_5)} \left(\frac{1}{\text{Sinh}^2 \ \lambda ORL - \sin^2 \ \lambda ORL} \right) \Big[(\text{Cosh}^2 \ \lambda e + \cos^2 \ \lambda e)$$

$$(\text{Sinh } \lambda f \ \text{Cosh } \lambda f - \sin \lambda f \cos \lambda f) + (\text{Cosh}^2 \ \lambda f +$$

$$\cos^2 \lambda f) \ (\text{Sinh } \lambda e \ \text{Cosh } \lambda e - \sin \lambda e \cos \lambda e) \Big] +$$

$$\frac{P_3 \ \lambda R_5^2}{EE(R_6 - R_5)} \left(\frac{1}{\text{Sinh}^2 \ \lambda ORL - \sin^2 \ \lambda ORL} \right) \Big\{ 2 \ \text{Cosh } \lambda f \cos \lambda f \ (\text{Sinh } \lambda ORL$$

$$\cos \lambda b \cosh \lambda a - \sin \lambda ORL \cosh \lambda b \cos \lambda a) + (\cosh \lambda f \sin \lambda f + \sinh \lambda f \cos \lambda f) \left[\sinh \lambda ORL (\sin \lambda b \cosh \lambda a - \cos \lambda b \sinh \lambda a) + \sin \lambda ORL (\sinh \lambda b \cos \lambda a - \cosh \lambda b \sin \lambda a)\right] \quad (5)$$

(3) Local Growth Because the Thin Race Chords Between Rollers (Figure 497)

$$\delta_{10} = \frac{3P_1(R_5 + R_6)}{2\,EE\,ORL\,(R_6 - R_5)^3}\left(\frac{2.12}{XN^{3.135}}\right) \quad (6)$$

(4) Hertz Deflection (Contact Deflection) Outer Race to Roller (Figure 498)

$$\delta_{11} = 4.36 \times 10^{-7}\,\frac{P_1 0.9}{FF^{0.8}} \quad * \quad (7)$$

(5) Radial Growth Due to Axial Loading

$$\delta_{12} = \frac{\mu P_5\left[R_5 - \left(\frac{R_6 - R_5}{2}\right)\right]}{EE\pi 2\;\; R_5(R_6 - R_5)} \quad (8)$$

b. Roller Deflection Terms

(1) Thermal Growth

$$\delta_7 = -\,DIA\,\alpha_D\,(T_D - 70) \quad (9)$$

(2) Deflection Under Load

$$\delta_6 = \frac{(P_1 + P_2)}{FF\;EE} \quad (10)$$

(3) Inner to Outer Race Load Variation Caused by rpm

$$P_1 = P_2 + \frac{\rho}{386}\left[rpm\left(\frac{R_4}{R_4 + R_5}\right)\,0.1045\right]^2$$

$$\left(R_4 + \frac{DIA}{2}\right)\left[\frac{FF\pi DIA^2}{4} + (H - FF)\left(\frac{DIA}{2} - C\right)^2\right] \quad (11)$$

---

*Roller Bearing Analysis, T. A. Harris, 1966

c. Inner Race Deflection Terms

(1) Thermal Growth

$$\delta_{1a} = -R_4 \alpha_{ir} (T_{ir} - 70) \tag{12}$$

(2) Growth From Change of Fit Between Race and Shaft Because of Thermal Expansion Coefficient Differences

$$\delta_{1b} = \frac{\left[\alpha_{ir}(T_{ir} - 70) - \alpha_s (T_s - 70)\right]}{R_2^2} \frac{\left(R_2^2 - R_1^2\right)\left(R_4^2 - R_2^2\right)}{\left(R_4^2 - R_1^2\right)} \frac{R_2^2 R_4^2}{\left(R_4^2 - R_2^2\right)} \tag{13}$$

(3) Hoop Growth From Load

$$\delta_2 = \frac{XNP_2}{EE\ 2\pi ORL} \left(\frac{R_1^2 + R_4^2}{R_4^2 - R_1^2} + \mu \right) \tag{14}$$

(4) Bending Growth or Chording Between Rollers

$$\delta_3 = \frac{3P_2 R_4^3}{EEB_{ir}\ (R_4 - R_1)^3} \left(\frac{2.12}{XN^{3.135}} \right) \tag{15}$$

(5) Hertz Deflection (Contact Deflection) Inner Race to Roller

$$\delta_4 = 4.36 \times 10^{-7} \frac{P_2^{0.9}}{FF^{0.8}} \tag{16}$$

(6) Growth From rpm of Shaft and Race

$$\delta_5 = \left(-\frac{R_4^3 \rho}{EE\ 386} \right) \left(\frac{rpm\ 2\pi}{60} \right)^2 \left(\frac{3 + \mu}{8} \right) \left(1 + \frac{2R_1^2}{R_4^2} - \frac{1 + 3\mu}{3 + \mu} \right) \tag{17}$$

d. Load Variation Along Roller Axis Because of Roller Offset on Outer Race (Defined in the Equation in Section 3.1b)

e. Redistribution of Roller Loads Because of Externally Applied Radial Load (Figure 500)

The load per roller changes to a sinusoidal distribution:

$$P_6 = P_1 + \Delta P_7 + 2\left(P_1 + \Delta P_7 \cos \frac{2\pi}{XN}\right) \cos \frac{2\pi}{XN} + 2\left(P_1 + \Delta P_7 \cos \frac{4\pi}{XN}\right) \cos \frac{4\pi}{XN} + 2\left(P_1 + P_7 \cos \frac{6\pi}{XN}\right) \text{etc} \text{ ---------- to } \cos \frac{\pi}{2}$$

$$+ P_1 - \Delta P_8 + 2(P_1 - \Delta P_8 \cos \frac{2\pi}{XN}) + 2(P_1 - \Delta P_8 \cos \frac{4\pi}{XN})$$

$$\cos \frac{4\pi}{XN} + 2(P_1 - \Delta P_8 \cos \frac{6\pi}{XN}) \cos \frac{6\pi}{XN} \text{ etc -------- to } \cos \frac{\pi}{2} \quad (18)$$

$$P_7 = P_1 + \Delta P_7 \quad (19)$$

$$P_8 = P_1 - \Delta P_8 \quad (20)$$

The increase in outer to inner race spacing on the side of the bearing being unloaded equals the decrease in spacing on the loaded side.

$$\frac{P_7}{P_1} \delta_9 + \frac{P_7}{P_1} \delta_6 + 4.36 \times 10^{-7} \frac{P_7^{0.9}}{FF^{0.8}} + 4.36 \times 10^{-7}$$

$$\frac{(P_7 - P_1 + P_2)^{0.9}}{FF^{0.8}} - \delta_4 - \delta_{11} - \delta_6 - \delta_9 =$$

$$\frac{P_8}{P_1} \delta_9 + \frac{P_8}{P_1} \delta_6 + 4.36 \times 10^{-7} \frac{P_8^{0.9}}{FF^{0.8}}$$

$$+ 4.36 \times 10^{-7} \frac{(P_8 - P_1 + P_2)^{0.9}}{FF^{0.8}} \quad (21)$$

4. Program Compilation

```
      1

//M048    30  1541101040T   E. STEVENSON                          PRTY=0
// P=0

LOG DRIVE   CART SPEC   CART AVAIL  PHY DRIVE
  0000        1111        1111        0000
*NAME M048 ROLLER BEARING OUTER RACE DEFLECTION -- HARRIS EQUATIONS
*NAME                   FORTRAN    A. SCHULTZ/STEVENSON
*IOCS(CARD,1132 PRINTER)
*ONE WORD INTEGERS
*LIST SOURCE PROGRAM
C
C     M048 ROLLER BEARING OUTER RACE DEFLECTION -- HARRIS EQUATIONS
C                       FORTRAN    A. SCHULTZ/STEVENSON
C
      READ(2,200) NOC
      DO 100 I=1,NOC
      READ(2,200) NOPT
  200 FORMAT (I5)
      READ(2,201) R1,R2,R3,R4,R5,R6,DIA,ORL,FF,G,FIT,TS,TIR,ALS,ALIR,EE,
     1  XN,XMU,BIR,RHO,RPM,ALD,TD,ALOR,TOR,C,PS,H,P1,P6,DP7
  201 FORMAT (8F10.0)
      WRITE(3,333)
  333 FORMAT (29X,'M048  ROLLER BEARING OUTER RACE DEFLECTION -- HARRIS
     1EQUATIONS'// )
      WRITE(3,300) NOPT,R1,R2,R3,R4,R5,R6,DIA,ORL,FF,G,FIT,TS
  300 FORMAT(' INPUT'/3X,'NOPT=',I2//9X,'SHAFT I.R.',10X,'SHAFT O.R.',7X
     1 ,'INNER RACE I.R.',5X,'INNER RACE O.R.',5X,'OUTER RACE I.R.',5X,
     2 'OUTER RACE O.R.'/6E20.6//8X,'ROLLER DIA.',6X,'OUTER RACE LENGTH'
     3  ,9X,'ROLLER CR. LENGTH',5X,'ROLLER OFFSET',6X,'NEG INTER CLEAR',
     4  5X,'SHAFT TEMP (F)'/6E20.6//)
      WRITE(3,301) TIR,ALS,ALIR,EE,XN,XMU,BIR,RHO,RPM,ALD,TD,ALOR
  301 FORMAT(5X,'INNER RACE TEMP(F)',3X,'SHAFT EXP COEFF',3X,'INNER RACE
     1 EXP COEFF',2X,'MODULUS OF ELAST',5X,'NO OF ROLLERS',6X,'POISSON''
     2S RATIO'/4E20.6,F16.0,4X,E20.6//6X,'INNER RACE WIDTH',8X,'DENSITY'
     3 ,13X,'SHAFT RPM',7X,'ROLLER EXP COEFF',7X,'ROLLER TEMP',9X,'OUTER
     4 RACE'/6E20.6/)
      WRITE(3,302) TOR,C,PS,H,P1,P6,DP7
```

```
  302 FORMAT (1H,'OUTER RACE TEMP',4F,'ROLLER CR. HEIGHT',3X,'AXIAL LOAD
     1 ON RACE',5X,'ROLLER WIDTH',7X,'PI (1ST GUESS)',12X,'P6'/6E20.6//
     2 7X,'DPT (1ST GUESS)'/E20.8 )
C
      FAC = 4.35E-7*FF**.8
      XBAR = 1.162713*ALOG(XN) - 2.512941
      XK = -2.855209 - 1.575424*XBAR + .5075836E-1*XBAR**2 - .626219E-2*
     1 XBAR**3
      XK = EXP(XK)
C
C     EQUATIONS TO DETERMINE RACE CROWNING
C
      T = R6 - R5
      F=(CRL-FF)/2.-C
      E=CRL-F
      A=(CRL-FF)/2.-G
      B=CRL-A
      XLMDA=1.285/SQRT(R5*T)
      XL=XLMDA*CRL
      XA=XLMDA*A

PAGE   2     11/11/66, MD

      XB=XLMDA*B
      XE=XLMDA*E
      XF=XLMDA*F
      HCXA=1./SQRT(1.-(TANH(XA))**2)
      HCXB=1./SQRT(1.-(TANH(XB))**2)
      HCXE=1./SQRT(1.-(TANH(XE))**2)
      HCXF=1./SQRT(1.-(TANH(XF))**2)
      HSXA=TANH(XA)*HCXA
      HSXB=TANH(XB)*HCXB
      HSXE=TANH(XE)*HCXE
      HSXF=TANH(XF)*HCXF
      HSXL=TANH(XL)/SQRT(1.-(TANH(XL))**2)
      HS2XL=HSXL**2
      SXA=SIN(XA)
      SXB=SIN(XB)
      SXE=SIN(XE)
      SXF=SIN(XF)
      SXL=SIN(XL)
      S2XL=SXL**2
      CXA=COS(XA)
      CXB=COS(XB)
      CXE=COS(XE)
      CXF=COS(XF)
      TPM=XLMDA*RE**2/(EE*T)
      XLT=1./(HS2XL-S2XL)
      T33M= 1.285*R5**1.5/(EE*T**1.5)
      T331 =  (HCXA**2+CXA**2)*(HSXB*HCXB+SXB*CXB)
      T332 =       (HCXB**2+CXB**2)*(HSXA*HCXA+SXA*CXA)
      T441 =       (HCXE**2+CXE**2)*(HSXF*HCXF+SXF*CXF)
      T442 =    (HCXF**2+CXF**2)*    (HSXE*HCXE+SXE*CXE)
      T33 = 1.285*R5**1.5/(EE*T**1.5)     *((HCXA**2+CXA**2)*(HSXB*HCXB+
     1  SXB*CXB)+(HCXB**2+CXB**2)*(HSXA*HCXA+SXA*CXA))
      T34 = TPM    *(2.*HCXA*CXA*(HSXL*CXE*HCXF-SXL*HCXE*CXF)+(HCXA*SXA+
     1  HSXA*CXA)*(HSXL*(SXE*HCXF-CXE*HSXF)+SXL*(HSXE*CXF-HCXE*SXF)))
      T44 = TPM*((HCXE**2+CXE**2)*(HSXF*HCXF+SXF*CXF)+(HCXF**2+CXF**2)*
     1  (HSXE*HCXE+SXE*CXE))
      T43 = TPM*(2.*HCXF*CXF*(HSXL*CXB*HCXA-SXL*HCXB*CXA)+(HCXF*SXF+
     1  HSXF*CXF)*(HSXL*(SXB*HCXA-CXB*HSXA)+SXL*(HSXB*CXA-HCXB*SXA)))
      TT =(T44-T34)/(T33-T43)
C
C     NON-MISALIGNED--SYMMETRICAL LOADING
C
      DPID = P2*ALIN*(TIP-TO.)
      DSOD = P2*ALS *.75 -TO.
      DEL = DPID - DSOD
      R1S = R1**2
      R2S = R2**2
      R4S = R4**2
      SR4R2 = R4S-R2S
      S4R1 = R4S-R1S
      P4 = EE*DEL*(R2S-R1S)*S4R2/(2.*R2S*R2*SR4R1)
      D1 = -R4*ALIN*(TIR-TO.) + 2.*P4*R2S*R4/(EE*SR4R2)
      D6 = -R4**3*[illegible]**2*.3*[illegible]*2.*[illegible] R4S-.1*.3*[illegible]
     1  (3.+[illegible]*.3552435E-5
      D7 = -D1A*ALIN*(TI-TO.)
```

```
  604 DP8 = P6/CONST - DP7
      P7 = P1 + DP7
      P8 = P1 + DP8
      P10= P7 - CF
      B10= 2.15*SQRT(P10*BRTY1)
      B7 = 2.15*SQRT(P7 *BRTY2)
      P9 = P8 - CF
      B9 = 2.15*SQRT(P9*BRT1)
      B8 = 2.15*SQRT(P8*BRT2)
      B1 = P8/P1*D9
      B2 = (P8+P9)/EF
      B3 = FAC * P9**.9
      B4 = FAC * P8**.9
      D89 = B1 + B2 + B3 + B4
      DP1 = D9 + D6 + D4 + D11
      DD89 = DP1 - D89
      D710 = DD89 + DP1
      A2 = (P7+P10)/EF
      A3 = FAC * P10**.9
      A4 = FAC * P7**.9
      DP77 = (D710 - A2 - A3 - A4)*P1/D9 - P1
      Y =  DP77 - DP7
      T1 = .001*DP7
      TST = Y
      IF (ABS(Y)-ABS(T1)) 610,610,600
  600 IF (IFLAG-1) 601,601,602
  601 X1 = DP7
      Y1 = TST
      DP7 = DP7 + SINC
      IFLAG = 2
      GO TO 604
  602 KOUNT = IFLAG - 1
      CALL ITRAL (X1,Y1,DP7,TST,KOUNT,ITEST,A1,B1)
      IFLAG = IFLAG + 1

PAGE   4    11/11/66  MD

      IF (IFLAG-50) 604,604,632
  632 WRITE(3,889)
      GO TO 111
  610 A1 = P7/P1*D5
      WRITE(3,322) B10,B7,B9,B8,P7,P10,P8,P9,DP7,DP8,D710,A1,A2,A3,A4,
     1 D89,B1,B2,B3,B4
  322 FORMAT (////12X,'B10',17X,'B7',18X,'B9',18X,'B8'/4E20.6//12X,'P7',
     1  17X,'P10',17X,'P8',18X,'P9',18X,'DP7',17X,'DP8'/6E20.6//12X,
     2  'D710',17X,'A1',18X,'A2',18X,'A3',18X,'A4'/5E20.6//12X,'D89',17X
     3  ,'B1',18X,'B2',18X,'B3',18X,'B4'/5E20.6  )
   50 WRITE(3,325)
  325 FORMAT (1H1)
  111 CONTINUE
      CALL EXIT
      END

FEATURES SUPPORTED
 ONE WORD INTEGERS
 IOCS

CORE REQUIREMENTS FOR FORTR
 COMMON       0  VARIABLES     312  PROGRAM    2994

 END OF COMPILATION
```

5. Sample Case

(C) This sample case is for a bearing with stainless steel (AMS 5640) rollers and races, a 0.0039 inch negative diametral internal clearance L/D = 1.00, single crown rollers, and a 1700 lb radial load. The program input and output are shown for this case and the data are plotted in Figure 502.

PAGE 1 10/02/68 M038

M038 ROLLER BEARING OUTER RACE DEFLECTION

Room Temperature (Assembly Conditions)
Speed = 0 rpm

INPUT
NOPT= 2

SHAFT I.R. 0.0000000E 00	SHAFT O.R. 0.1082700E 01	INNER RACE I.R. 0.1082700E 01	INNER RACE O.R. 0.1310000E 01	OUTER RACE I.R. 0.1[illegible]2000E 01	OUTER RACE O.R. 0.1862000E 01
ROLLER DIA. 0.4331000E 00	OUTER RACE LENGTH 0.4350000E 0[illegible]	ROLLER CR. LENGTH 0.3900000E 00	ROLLER OFFSET 0.0000000E 00	NEG INTER CLEAR 0.1950000E-02	SHAFT TEMP (F) 0.7000000E 02
INNER RACE TEMP(F) 0.7000000E 02	SHAFT EXP COEF 0.4900000E-05	INNER RACE EXP COEFF 0.4000000E-05	MODULUS OF ELAST 0.3125000E 08	NO OF ROLLERS 16.	POISSON'S RATIO 0.3000000E 00
INNER RACE [illegible] 0.9300000E 00	DENSITY 0.2800000E 0[illegible]	SHAFT RPM 0.0000000E 00	ROLLER EXP COEFF 0.4000000E-05	ROLLER TEMP 0.7000000E 02	OUTER RACE 0.4000000E-05
OUTER RACE TEMP 0.7000000E 02	ROLLER CR. HEIGHT 0.1[illegible]000E-02	AXIAL LOAD ON RACE 0.0000000E 00	ROLLER WIDTH 0.4331000E 00	P1 (1ST GUESS) 0.[illegible]E 04	P6 0.1700000E 04
DP7 (1ST GUESS) 0.2200000E 03					

OUTPUT

P1 0.6413450E 03	P2 0.6413450E 03	P3 0.46[illegible]219E 03	P4 0.4680180E 03	CF 0.0000000E 00	
DFL 0.[illegible]0000E 00	B1 0.1[illegible]E-01	B2 0.1260590E-01	CAGE RPM 0.0000000E 00		
D1 0.1000000E 00	D2 0.7254750E-04	D3 0.2302630E-07	D4 0.3838580E-03	D5 0.0000000E 00	D6 0.1360820E-03
D7 0.[illegible]0000E 00	D8 0.0000000E 00	D9 0.9480790E-03	D10 0.2401230E-04	D11 0.3030530E-03	K = 0.3496610E-03
B10 0.1252130E-01	B7 0.1444430E-01	B9 0.8476060E-02	B8 0.1043910E-01		
P7 0.8559600E 03	P10 0.8559600E 03	P8 0.4299190E 03	P9 0.4299190E 03	DP7 0.2142150E 03	DP6 0.2114430E 03
D710 0.2443410E-02	A1 0.1265810E-02	A2 0.1425190E-03	A3 0.4975240E-03	A4 0.4975240E-03	
DMR 0.1273420E-02	M1 0.6360720E-03	M2 0.9171620E-04	M3 0.2678160E-03	M4 0.2678160E-03	

CONFIDENTIAL

M038 ROLLER BEARING OUTER RACE DEFLECTION

INPUT
NOPT= 2

Cooldown to -410°F
Speed = 0 rpm

SHAFT I.R. 0.0000000E 00	SHAFT O.R. 0.108270E 01	INNER RACE I.R. 0.108270E 01	INNER RACE O.R. 0.131000E 01	OUTER RACE I.R. 0.174200E 01	OUTER RACE O.R. 0.186400E 01
ROLLER DIA. 0.433100E 00	OUTER RACE LENGTH 0.935000E 00	ROLLER CR. LENGTH 0.300000E 00	ROLLER OFFSET 0.000000E 00	NEG INTER CLEAR 0.195000E-02	SHAFT TEMP (F) -0.410000E 03
INNER RACE TEMP(F) -0.410000E 03	SHAFT EXP COEFF 0.490000E-05	INNER RACE EXP COEFF 0.400000E-05	MODULUS OF ELAST 0.312500E 08	NO OF ROLLERS 16.	POISSON'S RATIO 0.300000E 00
INNER RACE WIDTH 0.935000E 00	DENSITY 0.280000E 00	SHAFT RPM 0.000000E 00	ROLLER EXP COEFF 0.400000E-05	ROLLER TEMP -0.410000E 03	OUTER RACE 0.400000E-05
OUTER RACE TEMP -0.410000E 03	ROLLER CR. HEIGHT 0.100000E-02	AXIAL LOAD ON RACE 0.000000E 00	ROLLER WIDTH 0.433100E 00	P1 (1ST GUESS) 0.100000E 04	P6 0.170000E 04
DP7 (1ST GUESS) 0.220000E 03					

OUTPUT

P1 0.468203E 03	P2 0.468203E 03	P3 0.341669E 03	P4 0.341669E 03	CF 0.000000E 00	
DEL 0.467726E-03	U1 0.926284E-02	R2 0.105853E-01	CAGE RPV 0.000000E 00		
D1 0.302160E-02	D2 0.729621E-04	D3 0.166079E-07	D4 0.269187E-03	D5 0.000000E 00	D6 0.995834E-04
D7 0.831551E-03	D8 -0.334463E-02	D9 0.692713E-03	D10 0.175296E-04	D11 0.269187E-03	R = 0.349681E-03
R10 0.111876E-01	R7 0.129057E-01	R9 0.686757E-02	R8 0.792224E-02		
P7 0.683007E 03	P10 0.683007E 03	P8 0.257366E 03	P9 0.257366E 03	DP7 0.214804E 03	DP8 0.214838E 03
D710 0.196872E-02	A1 0.101091E-02	A2 0.145708E-03	A3 0.406229E-03	A4 0.406229E-03	
DP9 0.773215E-03	B1 0.380777E-03	B2 0.544749E-04	B3 0.168766E-03	B4 0.168766E-03	

CONFIDENTIAL

M038 ROLLER BEARING OUTER RACE DEFLECTION

INPUT

NOPT= 2

Speed = 20,000 rpm at -410°F

SHAFT I.R.	SHAFT O.R.	INNER RACE I.R.	INNER RACE O.R.	OUTER RACE I.R.	OUTER RACE O.R.
0.000000E 00	0.108270E 01	0.108270E 01	0.133480E 01	0.174200E 01	0.188200E 01
ROLLER DIA.	OUTER RACE LENGTH	ROLLER CR. LENGTH	ROLLER OFFSET	NEG INTER CLEAR	SHAFT TEMP (F)
0.433100E 00	0.935000E 00	0.300000E 00	0.000000E 00	0.195000E-02	-0.410000E 03
INNER RACE TEMP(F)	SHAFT EXP COEFF	INNER RACE EXP COEFF	MODULUS OF ELAST	NO OF ROLLERS	POISSON'S RATIO
-0.410000E 03	0.690000E-05	0.690000E-05	0.312500E 08	16.	0.300000E 00
INNER RACE WIDTH	DENSITY	SHAFT RPM	ROLLER EXP COEFF	ROLLER TEMP	OUTER RACE
0.935000E 00	0.240000E 00	0.200000E 05	0.600000E-05	-0.410000E 03	0.600000E-05
OUTER RACE TEMP	ROLLER CR. HEIGHT	AXIAL LOAD ON RACE	ROLLER WIDTH	P1 (1ST GUESS)	P6
-0.410000E 03	0.100000E-02	0.000000E 00	0.433100E 00	0.100000E 04	0.170000E 06
DP7 (1ST GUESS)					
0.220000E 03					

OUTPUT

P1	P2	P3	P4	CF	
0.496694E 03	0.439915E 03	0.962460E 03	0.362460E 03	0.247787E 02	
DFL	B1	B2	CAGE RPM		
0.467726E-03	0.897866E-02	0.110056E-01	0.854453E 04		
D1	D2	D3	D4	D5	D6
0.302166E-02	0.497623E-04	0.157943E-07	0.273414E-03	-0.400580E-04	0.999031E-06
D7	D8	D9	D10	D11	K = 0.349881E-05
0.831551E-03	-0.334463E-02	0.734266E-03	0.185965E-04	0.304974E-03	
B10	B7	B9	B8		
0.109536E-01	0.131723E-01	0.647931E-02	0.634935E-02		
P7	P10	P8	P9	DP7	DP8
0.711508E 03	0.654729E 03	0.285867E 03	0.229080E 03	0.214813E 03	0.210826E 03
D10	A1	A2	A3	A4	
0.201097E-02	0.105268E-02	0.145732E-03	0.391861E-03	0.421954E-03	
D89	B1	B2	B3	B4	
0.815353E-03	0.422949E-03	0.549267E-04	0.151982E-03	0.180447E-03	

CONFIDENTIAL

M038 ROLLER BEARING OUTER RACE DEFLECTION

INPUT
NOPT= 2

Speed = 35,000 rpm at -410°F

SHAFT I.R. 0.000000E 00	SHAFT O.R. 0.108270E 01	INNER RACE I.R. 0.108270E 01	INNER RACE O.R. 0.131000E 01	OUTER RACE I.R. 0.174200E 01	OUTER RACE O.R. 0.186200E 01
ROLLER DIA. 0.433100E 00	OUTER RACE LENGTH 0.350000E 00	ROLLER CR. LENGTH 0.300000E 00	ROLLER OFFSET 0.000000E 00	NEG INTER CLEAR 0.195000E-02	SHAFT TEMP (F) -0.410000E 03
INNER RACE TEMP(F) -0.410000E 03	SHAFT EXP COEFF 0.490000E-05	INNER RACE EXP COEFF 0.400000E-05	MODULUS OF ELAST 0.312500E 08	NO OF ROLLERS 16.	POISSON'S RATIO 0.300000E 00
INNER RACE WIDTH 0.935000E 00	DENSITY 0.280000E 00	SHAFT RPM 0.330000E 05	ROLLER EXP COEFF 0.400000E-05	ROLLER TEMP -0.410000E 03	OUTER RACE 0.400000E-05
OUTER RACE TEMP -0.410000E 03	ROLLER CR. HEIGHT 0.100000E-02	AXIAL LOAD ON RACE 0.000000E 00	ROLLER WIDTH 0.433100E 00	P1 (1ST GUESS) 0.100000E 04	P6 0.170000E 04
DP7 (1ST GUESS) 0.220000E 03					

OUTPUT

P1 0.555663E 03	P2 0.381778E 03	P3 0.405493E 03	P4 0.405492E 03	CF 0.173884E 03	
DEL 0.467726E-03	B1 0.836436E-02	B2 0.116406E-01	CAGE RPM 0.150229E 05		
D1 0.302160E-02	D2 0.431859E-04	D3 0.137070E-07	D4 0.240668E-03	D5 -0.122677E-03	D6 0.999993E-04
D7 0.831551E-03	D8 -0.334463E-02	D9 0.822112E-03	D10 0.208043E-04	D11 0.337360E-03	K = 0.349001E-03
B10 0.104567E-01	B7 0.137080E-01	B9 0.559551E-02	B8 0.917134E-02		
P7 0.770563E 03	P10 0.596678E 03	P8 0.344922E 03	P9 0.171037E 03	DP7 0.214099E 03	DP6 0.210740E 03
D710 0.209846E-02	A1 0.114005E-02	A2 0.145139E-03	A3 0.359712E-03	A4 0.492810E-03	
D89 0.301842E-03	B1 0.510318E-03	B2 0.550355E-04	B3 0.110334E-03	B4 -0.495536E-03	

NO3: ROLLER BEARING OUTER RACE DEFLECTION

INPUT

NOPT= 2

Speed = 48,000 rpm at -410°F

SHAFT I.R.	SHAFT O.R.	INNER RACE I.R.	INNER RACE O.R.	OUTER RACE I.R.	OUTER RACE O.R.
[illegible]	0.1037[illegible]E 01	0.1002[illegible]E 01	0.1[illegible]E 01	0.1742[illegible]E 01	0.1[illegible]E 01
ROLLER DIA.	OUTER RACE LENGTH	ROLLER CR. LENGTH	ROLLER OFFSET	NEG INTER CLEAR	SHAFT TEMP (F)
0.4391[illegible]E 01	0.9350[illegible]E 00	0.3[illegible]E 00	0.[illegible]E 00	0.1950[illegible]E-02	-0.4100[illegible]E 03
INNER RACE TEMP(F)	SHAFT EXP COEFF	INNER RACE EXP COEFF	MODULUS OF ELAST	NO OF ROLLERS	POISSON'S RATIO
-0.41[illegible]E 03	0.490[illegible]E-05	0.4[illegible]E-05	0.312500E 08	16.	0.3000[illegible]E 00
INNER RACE WIDTH	DENSITY	SHAFT RPM	ROLLER EXP COEFF	ROLLER TEMP	OUTER RACE
0.9350[illegible]E 00	0.2[illegible]E 00	0.480[illegible]E 05	0.4[illegible]E-05	-0.4100[illegible]E 03	0.4000[illegible]E-03
OUTER RACE TEMP	ROLLER CR. HEIGHT	AXIAL LOAD ON RACE	ROLLER WIDTH	P1 (1ST GUESS)	P6
-0.41[illegible]E 03	0.1[illegible]E-02	0.[illegible]E 00	0.4351[illegible]E 00	0.1[illegible]E 04	0.17[illegible]E 04
DP7 (1ST GUESS)					
0.22[illegible]E 03					

OUTPUT

P1	P2	P3	P4	CF	
0.633222E 03	0.3061[illegible]E 03	0.462091E 03	0.462091E 03	0.327045E 03	
DEL	B1	B2	CAGE RPM		
0.467726E-03	0.749054E-02	0.124265E-01	0.206028E 05		
D1	D2	D3	D4	D5	D6
0.302160E-02	0.346340E-04	0.109927E-07	0.197316E-03	-0.230734E-03	0.100202E-03
D7	D8	D9	D10	D11	K = 0.349681E-05
0.831551E-03	-0.334463E-02	0.936861E-03	0.237082E-04	0.379480E-03	
B10	B7	B9	B8		
0.977467E-02	0.143839E-01	0.418853E-02	0.101538E-01		
P7	P10	P8	P9	DP7	DP8
0.849421E 03	0.521375E 03	0.422780E 03	0.957350E 02	0.215198E 03	0.210441E 03
D710	A1	A2	A3	A4	
0.221379E-02	0.[illegible]E-02	0.146111E-03	0.315584E-03	0.493786E-03	
D89	B1	B2	B3	B4	
0.101393E-02	0.625509E-03	0.553083E-04	0.693031E-04	0.[illegible]E-03	

CONFIDENTIAL

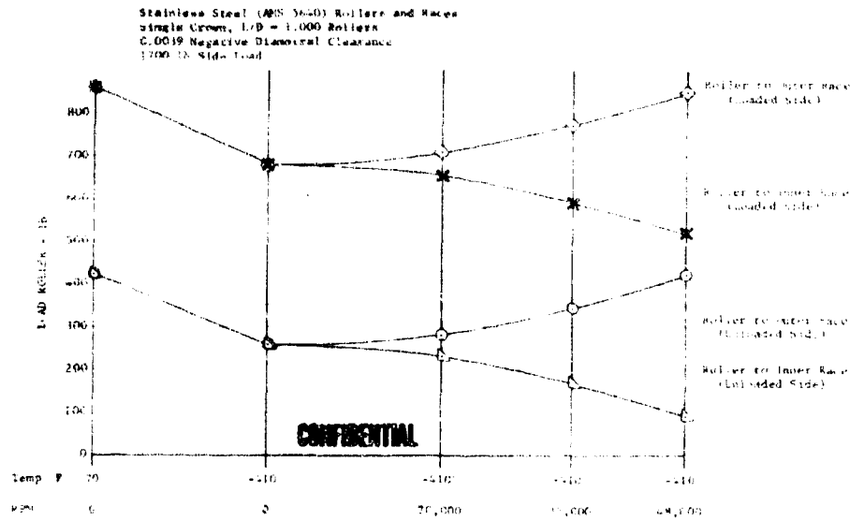

(U) Figure 502. Sample Case Data

DFC 70125
Sheet 1

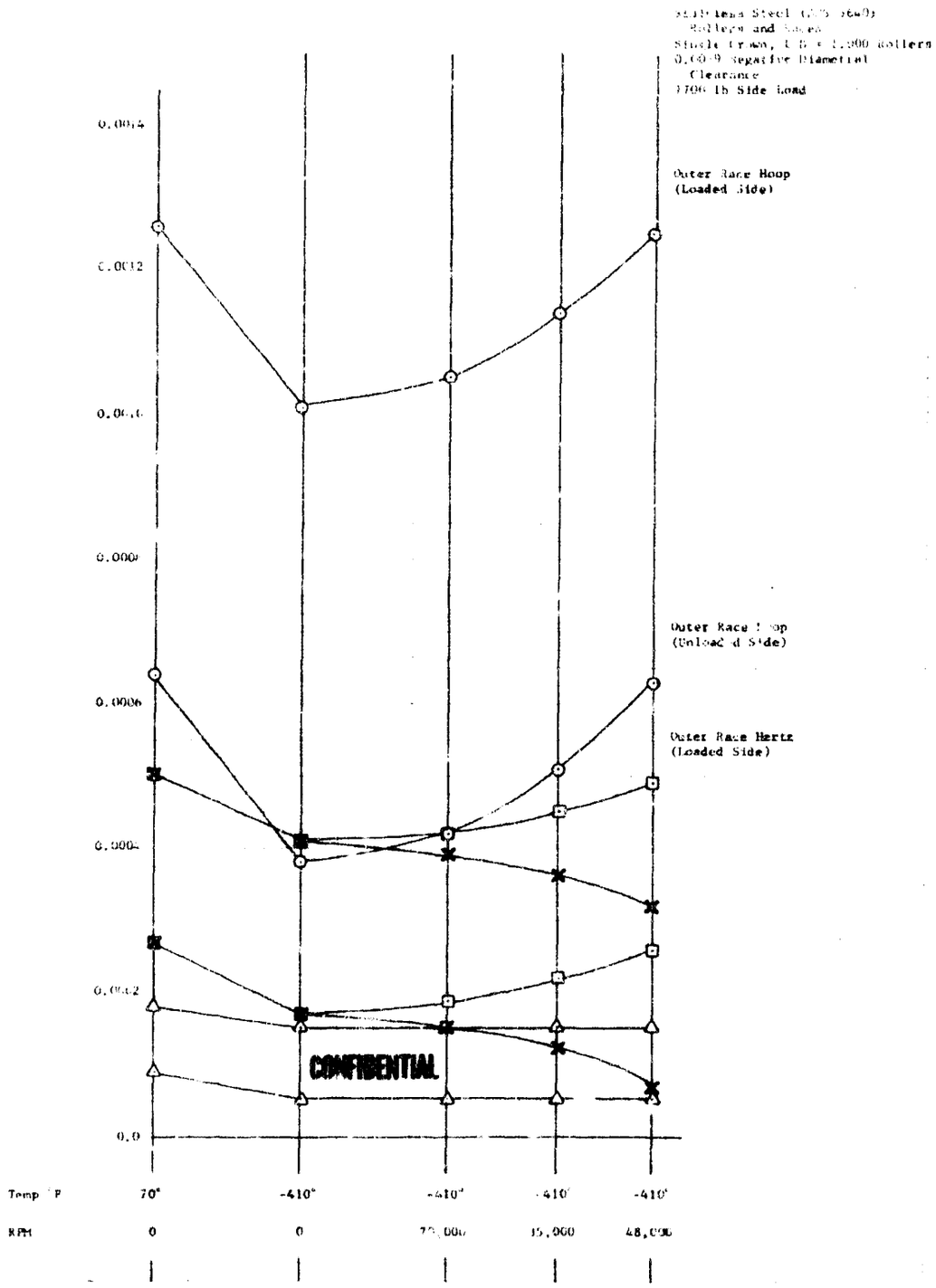

(U) Figure 502. Sample Case Data Concluded

DFC 70125
Sheet 2

Unclassified

Security Classification

DOCUMENT CONTROL DATA - R&D

(Security classification of title, body of abstract and indexing annotation must be entered when the overall report is classified)

1. ORIGINATING ACTIVITY (Corporate author) Pratt & Whitney Aircraft Division of United Aircraft Corporation Florida Research and Development Center	2a. REPORT SECURITY CLASSIFICATION Confidential 2b. GROUP 4

3. REPORT TITLE

Air Force Reusable Rocket Engine Program XLR129-P-1
First Annual Report

4. DESCRIPTIVE NOTES (Type of report and inclusive dates)

Annual Report, 6 November 1967 to 6 November 1968

5. AUTHOR(S) (Last name, first name, initial)

Atherton, Robert R.

6. REPORT DATE January 1969	7a. TOTAL NO. OF PAGES 563	7b. NO. OF REFS None
8a. CONTRACT OR GRANT NO. F04611-68-C-0002 b. PROJECT NO. 57X3600 2894703 c. P63681C 63408F d. S669800	9a. ORIGINATOR'S REPORT NUMBER(S) PWA FR-2972 9b. OTHER REPORT NO(S) (Any other numbers that may be assigned this report) AFRPL-TR-69-3	

10. AVAILABILITY/LIMITATION NOTICES In addition to security requirements which must be met this document is subject to special export controls and each transmittal to foreign governments or foreign nationals may be made only with prior approval of AFRPL(RPOR/STINFO) Edwards, California 93523

11. SUPPLEMENTARY NOTES	12. SPONSORING MILITARY ACTIVITY AFFTC Procurement Division (FTMKR-2) Edwards AFB, California 93523

13. ABSTRACT

The objective of this program is to demonstrate the performance and mechanical integrity of a 250,000-lb thrust reusable oxygen/hydrogen rocket engine designated the XLR129-P-1. The program, which is sponsored by the Air Force Rocket Propulsion Laboratory, is being accomplished at Pratt & Whitney Aircraft and consists of design, analysis, fabrication, and test of all the engine components and the complete demonstrator engine. This effort is the second phase of the Air Force Cryogenic Rocket Engine Advanced Development Program, Project 2 of Program Element 65048F. During the first year, experimental evaluation was conducted in the areas of a fixed fuel area preburner injector, hydrogen cooled roller bearings, compact pump inlets, lightweight nozzle fabrication techniques, and selected control valves. Under the fixed fuel area preburner injector evaluation, a new full-scale preburner injector was designed, fabricated, and tested that produced a uniform temperature profile suitable for use in the engine. Under the roller bearing durability tests, four bearing configurations surpassed the test duration goal at the design operating conditions. Under the pump inlet evaluation, an elbow type of inlet with turning vanes was selected for both the fuel and oxidizer turbopumps. Under the nozzle fabrication investigation, it was concluded that the internal corrugated type of construction was best for the two-position nozzle. Under the controls component tests, both a hoop shutoff seal and a cam-actuated shutoff seal have proven to be potentially feasible types of seals for use in the main chamber oxidizer valve, which is a butterfly valve. Also, pressure balance configurations of piston rings used in the preburner oxidizer valve have demonstrated acceptable wear leakage and actuator force characteristics. Under the Component Development Task, designs have been initiated for the preburner injector, main burner injector, main burner chamber, nozzles, transition case, fuel turbopump, oxidizer turbopump, fuel low-speed inducer, oxidizer low-speed inducer, and the control components. The demonstrator engine design has also been started.

DD FORM 1 JAN 64 1473

Unclassified

Security Classification

14 KEY WORDS	LINK A		LINK B		LINK C	
	ROLE	WT	ROLE	WT	ROLE	WT
Air Force						
Pratt & Whitney Aircraft, FRDC						
XLR129-P-1 Reusable Rocket Engine Program						
250K Oxygen/Hydrogen Demonstrator Engine						
Supporting Data and Analysis						
Fixed Fuel Area Preburner Injector						
Roller Bearing Durability Tests						
Pump Inlet Evaluation						
Nozzle Fabrication						
Controls Components						
Component Development						
Engine Integration and Demonstration						
Flight Engine						
Engineering Support						

INSTRUCTIONS

1. ORIGINATING ACTIVITY: Enter the name and address of the contractor, subcontractor, grantee, Department of Defense activity or other organization (*corporate author*) issuing the report.

2a. REPORT SECURITY CLASSIFICATION: Enter the overall security classification of the report. Indicate whether "Restricted Data" is included. Marking is to be in accordance with appropriate security regulations.

2b. GROUP: Automatic downgrading is specified in DoD Directive 5200.10 and Armed Forces Industrial Manual. Enter the group number. Also, when applicable, show that optional markings have been used for Group 3 and Group 4 as authorized.

3. REPORT TITLE: Enter the complete report title in all capital letters. Titles in all cases should be unclassified. If a meaningful title cannot be selected without classification, show title classification in all capitals in parenthesis immediately following the title.

4. DESCRIPTIVE NOTES: If appropriate, enter the type of report, e.g., interim, progress, summary, annual, or final. Give the inclusive dates when a specific reporting period is covered.

5. AUTHOR(S): Enter the name(s) of author(s) as shown on or in the report. Enter last name, first name, middle initial. If military, show rank and branch of service. The name of the principal author is an absolute minimum requirement.

6. REPORT DATE: Enter the date of the report as day, month, year, or month, year. If more than one date appears on the report, use date of publication.

7a. TOTAL NUMBER OF PAGES: The total page count should follow normal pagination procedures, i.e., enter the number of pages containing information.

7b. NUMBER OF REFERENCES: Enter the total number of references cited in the report.

8a. CONTRACT OR GRANT NUMBER: If appropriate, enter the applicable number of the contract or grant under which the report was written.

8b, 8c, & 8d. PROJECT NUMBER: Enter the appropriate military department identification, such as project number, subproject number, system numbers, task number, etc.

9a. ORIGINATOR'S REPORT NUMBER(S): Enter the official report number by which the document will be identified and controlled by the originating activity. This number must be unique to this report.

9b. OTHER REPORT NUMBER(S): If the report has been assigned any other report numbers (either by the originator or by the sponsor), also enter this number(s).

10. AVAILABILITY/LIMITATION NOTICES: Enter any limitations on further dissemination of the report, other than those imposed by security classification, using standard statements such as:

(1) "Qualified requesters may obtain copies of this report from DDC."

(2) "Foreign announcement and dissemination of this report by DDC is not authorized."

(3) "U. S. Government agencies may obtain copies of this report directly from DDC. Other qualified DDC users shall request through _____."

(4) "U. S. military agencies may obtain copies of this report directly from DDC. Other qualified users shall request through _____."

(5) "All distribution of this report is controlled. Qualified DDC users shall request through _____."

If the report has been furnished to the Office of Technical Services, Department of Commerce, for sale to the public, indicate this fact and enter the price, if known.

11. SUPPLEMENTARY NOTES: Use for additional explanatory notes.

12. SPONSORING MILITARY ACTIVITY: Enter the name of the departmental project office or laboratory sponsoring (paying for) the research and development. Include address.

13. ABSTRACT: Enter an abstract giving a brief and factual summary of the document indicative of the report, even though it may also appear elsewhere in the body of the technical report. If additional space is required, a continuation sheet shall be attached.

It is highly desirable that the abstract of classified reports be unclassified. Each paragraph of the abstract shall end with an indication of the military security classification of the information in the paragraph, represented as (TS), (S), (C), or (U).

There is no limitation on the length of the abstract. However, the suggested length is from 150 to 225 words.

14. KEY WORDS: Key words are technically meaningful terms or short phrases that characterize a report and may be used as index entries for cataloging the report. Key words must be selected so that no security classification is required. Identifiers, such as equipment model designation, trade name, military project code name, geographic location, may be used as key words but will be followed by an indication of technical context. The assignment of links, roles, and weights is optional.